"Se non é vero, è bene trovato."

Italian adage.

"ABSORPTION AND FLUORESCENCE STUDIES OF HOT PLASMAS USING TUNEABLE DYE LASERS"

A Thesis Submitted for the Degree of

DOCTOR OF PHILOSOPHY

in the

UNIVERSITY OF LONDON

by

CHARLES HUBERT SKINNER

Department of Physics
Imperial College of Science and Technology
South Kensington
London, S.W.7.

October 1974.

Acknowledgements

I would like to offer my deepest gratitude to Dr. D.D. Burgess for his supervision, help and encouragement during the course of this work.

I would like to thank Professor W.R.S. Garton for the use of his Laboratory and the many people who have helped during the course of this work. In particular I would like to thank Mr. S.J. Fielding for helpful discussions and assistance with the fluorescence experiment at Culham Laboratory, Dr. N.J. Peacock for his help and encouragement, Dr. K. Woodhouse for help with the theoretical sections, and Dr. Mark Eckart for many useful and stimulating discussions.

Thanks are due to Mr. C. Smith and Rita Mahon for the preliminary plasma diagnostic work on the linear pinch.

I would like to express my appreciation of the technical assistance of Mr. J.E.G. Wheaton, the patient instruction of Mr. M. Pimm in the student workshop, Mr. P. Dawson for technical assistance at Culham Laboratory and Mr. H. Yates for fabricating the Fabry Perot etalons.

I should like to thank Mrs. T. Wright for her care and attention in typing this thesis.

I also thank Culham Laboratory for financial support in the form of a Research Studentship.

Finally, I should like to thank my parents for their confidence and encouragement over the years.

THE COAXIAL DYE LASER

The output beam may be seen impinging on the card to the left. The atmosphere was filled with smoke to show up the laser beam.

This Thesis is Dedicated

to my Parents

ABSTRACT

An experiment is described in which neutral helium in the recombination phase of a linear pinch (electron density 10^{14} - 10^{15} cm^{-3}) was excited by a dye laser tuned to the 5876 Å 2^3P-3^3D transition. Complete details of the laser are given with particular attention to those aspects most important for scattering experiments. At 50 kW/cm^2 the light intensity inside the pinch was sufficient to saturate the helium transition. Time histories and spectral profiles of 5876 Å fluorescence are presented together with time histories of collision induced fluorescence from other transitions.

Similar experiments with the dye laser tuned to the 6678 Å 2^1P-3^1D transition and the Balmer α transition are described, the latter being with hydrogen replacing the helium in the linear pinch. Studies of the optical opacity of the plasma with simultaneous laser excitation are also described.

With the laser pulse lasting longer than the relevant collisional and radiative decay rates, relaxation effects in the time history of the fluorescence offer new possibilities for the measurement of collisional excitation rates to and from the levels interacting with the laser. Possible extensions of this technique to determine VUV 'A' values are described.

In a second experiment a dye laser operating at Hα (6563 Å) was set up to measure neutral hydrogen densities and temperatures in a large Tokamak plasma machine. A detailed account of the experimental set-up is given. Unfortunately due to the small number of shots allotted to the fluorescence experiment no results were obtained on the plasma.

Finally, a theoretical analysis of a new method of measuring magnetic field directions in a plasma machine is given. The method, based on the third Hanle effect, enables spatially resolved magnetic field measurements to be made by observation of the polarisation of the fluorescence produced under laser excitation.

Contents

Contents

Contents

Contents

Contents

Contents

CHAPTER I

INTRODUCTION

One of the major areas of expansion in post-war Physics has been in the field of Plasma Physics. This has been stimulated by the growing realisation of the limited extent of most fossil fuel reserves and in contrast, the possibility of virtually unlimited power from nuclear fusion. The advent of electronic computers has made it possible to solve numerically some of the complex theoretical problems involved in the understanding of the physics of highly ionised gases. On the experimental side, plasmas have been produced with temperatures in excess of one million degrees (Peacock et al. 1969) or with particle densities (4×10^{20} cm^{-3}) approaching that of a solid, (Peacock et al. 1973). The subject of Plasma Spectroscopy arose from need to measure the parameters of these extreme physical states. For a recent review of this subject see D.D. Burgess (1972). At first it was not possible to measure basic qualities such as temperature and density without appealing to theoretical considerations of plasma equilibrium. However a notable advance was made in 1963 when ruby lasers were used in a Thomson scattering experiment (Fünfer et al. 1963) and for the first time it was possible to make unambiguous spatially resolved measurements of the electron density and temperature and ion temperature (see - Kunze 1968) . Subsequent developments in laser technology especially in the field of frequency tuneable lasers have made possible a wide variety of experiments in atomic and molecular physics, see e.g. the review by

Demtröder (1973). In particular we mention the high resolution saturation spectroscopy study of the sodium D lines using a pulsed tuneable dye laser (Hansh et al. 1971). This technique enabled the natural line profile to be measured independent of the doppler effects with a resolution of 7 MHz! Dye lasers have also been used in studies of the upper atmosphere,(Gibson and Sandford (1972)),fluorescence from sodium atoms being detected from distances of up to 90 km. The high light intensities available from tuneable lasers have made it possible to substantially increase excited state populations, by tuning the laser wavelength into coincidence with the atomic transition wavelength and this has made possible absorption spectroscopy of excited states (see e.g. Bradley et al. 1973,and Carlsten et al. 1974).

In the field of plasma diagnostics Measures (1968) first discussed the application of tuneable lasers to the measurement of electron density and temperature of plasmas in what he termed "selective excitation spectroscopy". A subsequent experiment on a potassium plasma (Rodrigo and Measures 1973) confirmed this possibility but the interpretation of their results was complicated by non-ideal laser parameters. Dimcock et al. (1969) also discussed optical pumping techniques using tuneable dye lasers to measure density, ion temperature, electron temperature and ion drifts in barium or barium doped plasmas. He showed that the large value of the resonance fluorescence cross sections enabled measurements to be made of barium densities as low as 2.5×10^{3} cm^{-3}.

Collins et al. (1972) used a tuneable dye laser to optically pump a flowing helium afterglow excited by a microwave discharge. Analysis of the time history of the fluorescence yielded estimates for the cross section for excitation transfer between atomic levels by atom or electron collisions.

Burell and Kunze (1972a) have observed fluorescence in a low electron density (3×10^{12} cm^{-3}) helium plasma by using a dye laser tuned to the 4471 Å ($2^3P - 4^3D$) transition. They observed sensitised fluorescence on many other helium lines. By measuring the relaxation rate of the fluorescence after the laser pulse they deduced collision rates between excited states.

The potentialities of laser-plasma interactions in the study of plasmas are wide. Burgess et al. (1971) have suggested a new technique for the optical generation of plasma waves based on the coupling between electron plasma waves and optical photons by bound electrons. With laser powers above 30 Mwatt/cm^2 this Raman scattering process becomes self-stimulated and considerable enhancement of the plasma wave number density is possible. Burell and Kunze (1972b) have observed two photon absorption and stimulated Raman scattering on excited helium atoms by focussing simultaneously microwave radiation and the beam from a tuneable dye laser into a helium plasma. Both effects offer substantial advantages over previous techniques in the measurement of high frequency electric fields in plasmas, (see also Burell C.F. 1974, Ph.D. Thesis, Univ. of Maryland).

Laser scattering measurements provide information on local plasma conditions without any considerations of spatial averaging. It is possible to observe homogeneous spectral profiles independently of doppler effects by observing scattering in a foreward direction, as long as there are no velocity changing collisions in the lifetime of the excited state. This technique is complementary to the saturation spectroscopy described by Hansch et al.(1971).

At the time when this work was conceived (1971) tuneable laser technology was only a few years old and no plasma diagnostics experiments using tuneable lasers had been reported. At present, although tuneable

lasers have found many applications in experiments with low density plasmas and atomic vapours, no work has been done on plasmas with electron densities above 10^{14} cm^{-3}. In this thesis we report the first fluorescence experiment on a plasma with electron densities in the region 10^{15} cm^{-3}.

This work was begun in order to pursue experimentally a new method of measuring magnetic field directions in large toroidal plasma machines. (Burgess, D.D. to be published). Because of the strictly limited machine time available for scattering experiments on large plasma devices, a small pilot experiment was set up using the recombination phase of a linear pinch as a plasma source, to check simple ideas about plasma saturation. In the event, through reasons beyond our control, the large scale experiment was unsuccessful while the pilot experiment yielded several unexpected and interesting results which demonstrate new possibilities for the measurement of collision cross sections and 'A' values.

After the review of tuneable lasers in the next chapter the thesis divides into two main sections. In the first fluorescence experiments on the 5876, 6678 Å lines in helium, and the Balmer alpha line in hydrogen are described. Full details of the coaxial dye laser used are given. Measurements of the change in optical opacity during laser excitation are also described.

In the second section a fluorescence experiment on a large toroidal plasma machine is described. A new method for measuring the magnetic field direction is discussed in the light of the fluorescence results observed previously for the particular case of a hydrogen plasma.

CHAPTER II

TUNEABLE LASERS

In this chapter we describe the essential features of flashlamp pumped dye lasers and then briefly review other types of dye lasers and other tuneable lasers.

There are several published reviews of dye lasers, e.g. Schaefer (ed.) 1973, De Michelis 1971, Mobzrichter and Schawlow 1970, Snavely 1969, Sorokin 1969, and an extensive bibliography was given by Magyar (1974).

Interestingly, the first discovery of dye laser emission was made accidentally by Sorokin and Lankard (1966) whilst studying stimulated Raman effects. Subsequently there has been an explosive growth of the subject and the many different types of dye lasers now available have had a considerable impact on fields such as optics, spectroscopy and metrology.

Flashlamp Pumped Dye Lasers

Principles of dye laser operation

Fig. 2.1 shows a typical energy level diagram of an organic dye molecule. Each level is composed of several vibrational and rotational sub-levels which in the presence of interactions with the dye solvent merge into a quasi continuum.

The first step in the laser process is light absorption by ground state molecules exciting them to the higher vibrational and rotational levels of the first singlet state ((A) in Fig.2.1). The molecules then relax by fast (10^{-12} sec) radiationless transitions to the lowest level of the first singlet state (B). Lasing action takes place between this state and the upper sub-levels of the ground state (C). Once in the ground state molecules relax

FIGURE 2.1

RHODAMINE 6G MOLECULAR STRUCTURE

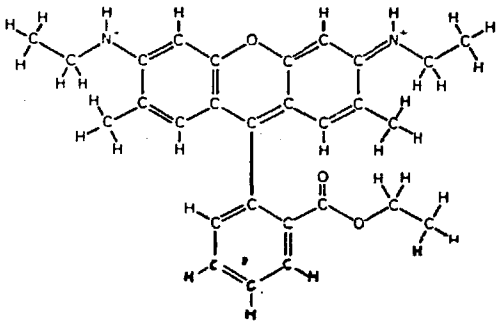

Energy Level Diagram of Typical Dye Molecule

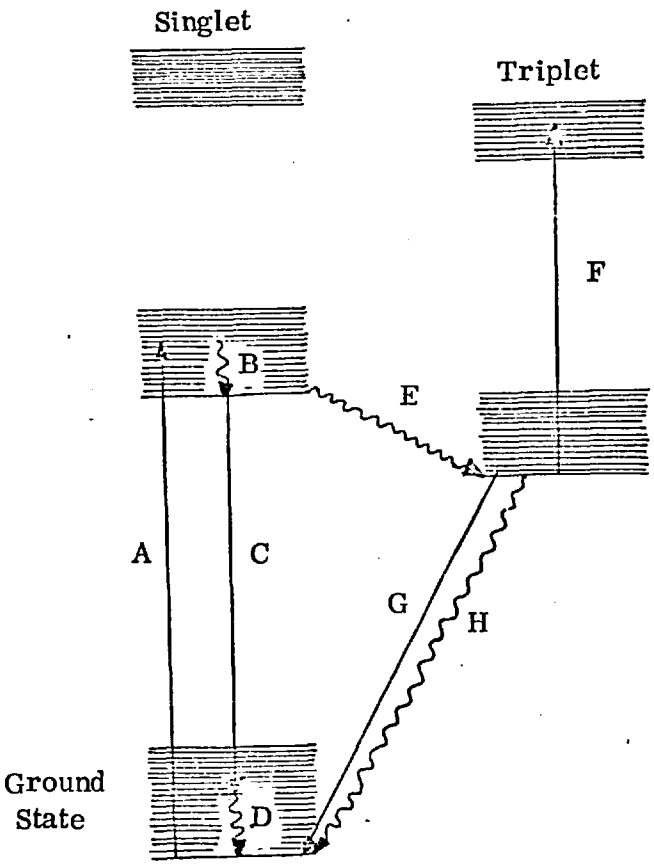

radiative transitions

radiationless transitions

very quickly to the lowest sub-level (D) thus a high population inversion is maintained between the first singlet state and the upper levels of the ground state.

Excited molecules can also make a slower (10^{-8} sec) radiationless transition to the triplet system (E). As the lifetime of the lowest triplet state is long (10^{-7} - 10^{-4} sec) a substantial number of atoms can build up in this state. This has a deleterious effect on lasing action because of (i) the reduction in the number of atoms able to participate in the lasing process and (ii) additional losses caused by absorption to higher triplet states (F). This is only important in flashlamp pumped dye lasers where the pumping pulse ($\cong 1$ μS) is longer than the intersystem crossing time. Considerable effort was expended in the early stages in producing flashlamps with as short a pumping pulse as possible (e.g. Sorokin et al.(1968)). Subsequently it was realised that dissolved oxygen or other substances, e.g. cyclooctatetraene, greatly reduced the triplet state life time and permitted long pulse or even CW operation of dye lasers.

Coaxial Flashlamp Pumped Dye Lasers

The first flashlamp pumped dye lasers were of the coaxial type with the pumping discharge filling an annular region around the dye cell (Fig.2.2). This design permits very rapid optical pumping of the dye with a high intensity flashlamp pulse of about half a microsecond duration. The basic design was improved by Furomoto and Ceccon (1969) who obtained an efficiency of 0.5% using a flashlamp of annular width 0.5 mm filled with Xenon. Experiments with these types of lamps by the present author revealed however that they had a short lifetime limited by flashlamp fracture, and in Chapter III a new way of overcoming this difficulty is described. Very high energies and powers

FIGURE 2.2

FLASHLAMP OF SOROKIN ET AL. (1968)

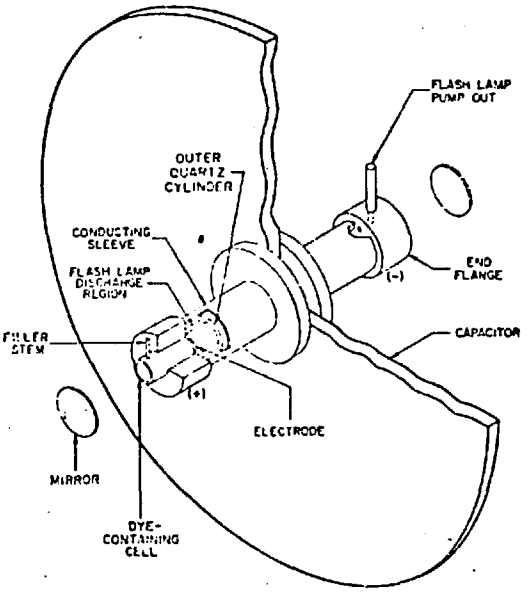

The dye is circulated in the inner quartz tube. The lamp is self-fired by reducing the air pressure in the space between the inner and outer quartz tubes.

FIGURE 2.3

CONFOCAL DYE LASER

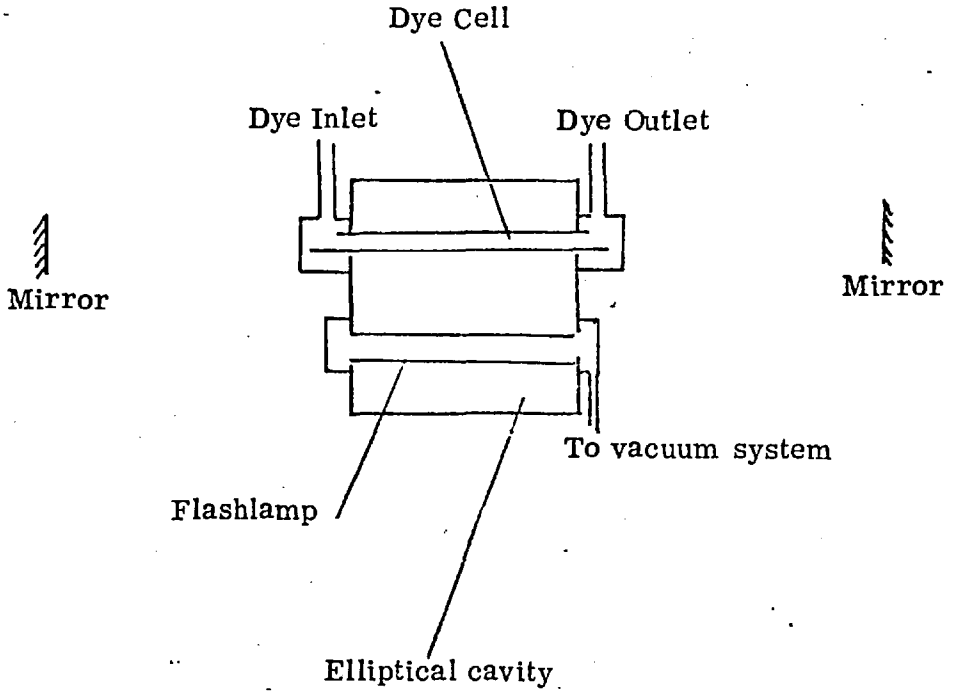

have been achieved using coaxial flashlamps: 110 Joules, 5.5 Mwatts being reported by Baltakor et al (1973), and 6.8 Joules, 11 Mwatts by Bunkenberg (1972).

Confocal Flashlamp Pumped Dye Lasers

An alternative type of flashlamp is shown in Fig.2.3. A linear flashlamp and dye cell are placed at the foci of a highly reflective elliptical cavity. The poorer optical coupling between the flashlamp and dye cell leads to a decreased efficiency (typically 0.2%) compared to coaxial designs. The intrinsically higher inductance of the flashlamp circuit in confocal systems limits the maximum output power attainable. The highest output energy and power using linear flashlamps was achieved by Anliker et al (1972), who used eight flashlamps completely surrounding the dye cell to obtain an energy output of 12 Joules with a peak power of 2.4 Mwatts. The efficiency of this laser (1.2%) is the highest reported for flashlamp pumped dye lasers. However experiments by Fielding (private communication) with a very similar laser failed to duplicate these results.

Laser Pumped Dye Lasers

Several kinds of lasers have been used to optically pump organic dyes, e.g. ruby lasers, Sorokin et al (1966); frequency doubled ruby or neodymium lasers, Schaefer et al (1967); nitrogen lasers, Lankard et al (1969); argon ion lasers, Peterson et al (1970); Krypton lasers, Yarborough (1974); and mode locked helium neon lasers, Runge (1971). Because the pumping radiation is usually at the same wavelength as the dye molecule absorption band laser pumped dye lasers have much higher efficiencies (20% - 50%) than flashlamp pumped dye lasers. The active region of the dye cell can be very small ($< 1\ mm^2$) and hence these lasers have a much lower beam divergence than flashlamp pumped dye lasers.

Continuous (CW) dye lasers pumped by argon ion or krypton lasers are commercially available[+] covering the wavelength range 4200 - 7800 Å. Another CW dye laser with a more limited wavelength range is available commercially[*] with a bandwidth of less than 30 MHz. Mode-locking of both pulsed (Schmidt et al. 1968) and CW (Dienes et al. 1971) dye lasers has been reported, output pulses of the order of 10^{-12} sec. being produced.

Spectral Output of Dye Lasers

The outstanding feature of dye lasers is the possibility of tuning the spectral output over a wide range of wavelengths in the visible and near visible regions of the spectrum. Recent improvements in laser dyes (Drexhage 1973, 1974) have produced dyes which operate in the regions 4600-5600Å and 6500-7500Å with the previously unequalled efficiency of rhodamine 6G (see also Marling et al. 1974). The total wavelength range covered by pulsed dye lasers is 3400-12000 Å. The spectral output is usually controlled by an optical filter placed inside the laser cavity which only transmits a small fraction of the dye fluorescence band. Diffraction gratings have been used in this way for low energy pulsed dye lasers (Sorokin et al. 1968). At high (> 50 mJ) output energies this method is unsuitable as gratings become damaged by the intense radiation in the laser cavity and an alternative system using Fabry Perot etalons becomes preferable (Bradley et al. 1971). Gale (1973), using three etalons, achieved single mode operation of a flashlamp pumped dye laser with a spectral bandwidth of 4 MHz.

The spectrally narrowed laser output has a bandwidth less than the passive bandwidth of these filters typically by a factor of 10-20. The output

+ Coherent Radiation Ltd.

* Spectra Physics Ltd.

spectra of pulsed dye lasers sometimes changes with time during a single pulse, this is termed "chirp". Chirp has been observed even in a flashlamp pumped dye laser with an output bandwidth of 0.5 Å. (Magyar 1972). Magyar also reported a spatial dependence of the laser output in time. Chirp does not seem to be capable of a simple theoretical explanation and it is clearly important for many laser applications to ensure that it is not seriously affecting the results. (See also Atkinson et al. 1973).

Laser Divergence

In most applications to date dye lasers have simply been used as very high intensity light sources. For this it is not simply the often quoted total output energy that is important but the laser brightness or the intensity per unit solid angle. Most lasers have a divergence of a few milliradians or less. However, the divergence of flashlamp pumped dye lasers is much higher, typical values being in the range 5 - 15 milliradians. This is due to several reasons. With a high gain per unit length the dye solution produces a substantial amount of amplified spontaneous emission. Thermal and mechanical effects combine to make the dye column less than perfectly homogeneous. Also it is impossible to completely remove all small particles from the dye solution and these act as scattering centres. Quite often in practice the highest laser brightness is obtained at conditions other than those which give the maximum energy. The laser divergence is commonly measured by photographing the far field laser intensity distribution and the figure usually quoted is related to the diameter of the beam at half intensity (Furomoto et al. 1969; Avizonis et al. 1967). For flashlamp pumped dye lasers this can lead to serious error in estimates of the laser brightness as the beam diameter at half intensity is only a measure of the laser brightness

when the laser output is in the form of a limited number of radial modes. This is not the case for most flashlamp pumped dye lasers as a substantial fraction of the light is emitted at angles which could not sustain a radial mode (see Plate I). The laser brightness or energy output per unit time per unit solid angle can only be measured with a calorimeter for the case of flashlamp pumped dye lasers, using for example the arrangement described on Page 43.

The laser divergence in general changes as a function of time during the laser pulse. In coaxial flashlamp pumped dye lasers an inwardly propagating radial shock wave is generated by the flashlamp discharge, the resulting optical distortion of the dye solution scatters the laser beam at highly divergent angles finally terminating laser action completely. (Ewanizky 1973). The time dependence of the divergence of a dye laser pumped by a coaxial pinched discharge was studied by Alekseev et al. (1972). He found the divergence was dependent on three factors (i) deflection of the beam through thermal lensing effects, (ii) inhomogeneities in the dye solution caused an ultrasonic shock wave, (iii) diffraction of laser radiation in the grating formed by ultrasonic waves generated as a result of vibrations in the quartz dye cuvette.

A novel way of obtaining the low divergences of laser pumped dye lasers without the expense of a solid state laser was described by Fielding (1974). The beam from a flashlamp pumped dye laser was used to pump a second dye cell. Because of the small size of the active region in the second dye cell the divergence was reduced to 2.7 milliradians, an overall gain in brightness of x 40.

Other Tuneable Lasers

The total coverage in wavelength from different tuneable lasers now spans from 1260 Å to 300 μm with only a few ever decreasing gaps in between, see e.g. the review by Colles et al. (1973) and Hansch (1972). In the infra-red region tuneable spin flip Raman lasers (Dennis et al. 1972) semiconductor diode lasers (Hinkley 1972) and parametric oscillators (Hanna et al. 1973) are already finding important applications, e.g. in the detection of molecular polutants (Hinkley 1972). Tuneable infra-red radiation has also been produced by difference frequency generation using a dye laser and ruby laser, (Dewey et al. 1971). There is currently much research being done in the field of tuneable UV lasers. Tuneable UV radiation has been generated from visible frequency dye lasers by frequency doubling techniques (Kuhl et al. 1972). Even shorter wavelengths $\sim$1800 Å have been generated by Sorokin et al. (1974) by mixing the radiation from two dye lasers in strontium vapour. Harris et al. (1973) have observed stimulated emission at 1260 Å from xenon and argon excimers+ pumped by multiphoton absorption of laser radiation. Previously the possibility of vacuum ultra-violet lasers had seemed unlikely as the ratio of spontaneous to stimulated emission increases as the frequency cubed. However, the high efficiency ($\simeq$ 25%) reported by Harris et al. indicates that relatively high power lasers are possible in the VUV region. In the coming years it seems highly likely that even shorter wavelength lasers will be produced (see e.g. Hodgson et al. 1974) and many novel and important applications will be discovered.

+ An excited dimer formed by the association of excited and unexcited molecules, which in the ground state would remain dissociated.

CHAPTER III

THE COAXIAL DYE LASER

In the initial stages of this work dye laser technology was still in a comparatively undeveloped state and it was not clear which of the various systems available was most suited to plasma diagnostic applications. As two coaxial dye laser flashlamps were available on loan from Harvard College Observatory, it was decided to investigate these with particular regard to the properties such as reproducibility, reliability, etc., of most importance in plasma diagnostics.

The flashlamps were based on the design of Furomoto et al (1969). They incorporated a central quartz tube through which dye was circulated surrounded by a larger concentric quartz tube. The annular region between the two quartz tubes was sealed off by epoxied ring electrodes and was filled with xenon at a pressure of about 50 torr. When the laser was fired a 0.3 M.F.D., 25 kv capacitor was discharged through the annular region providing a pulse of very intense illumination in the central dye column. A population inversion built up in the dye and with two suitably placed mirrors lasing action occurred. To obtain a high laser output power the laser was designed with the lowest possible inductance. However the resulting high density current pulse meant that the flashlamp was loaded with a severe mechanical shock each time it was fired. Because of this the two H.C.O. flashlamps had very short lives, each lasting less than 20 shots.

Improved Coaxial Flashlamps

To overcome this problem a new flashlamp was designed incorporating 'O' ring seals in place of the epoxy. This had two advantages (i) broken quartz tubes could easily be replaced without needing to discard the whole flashlamp,

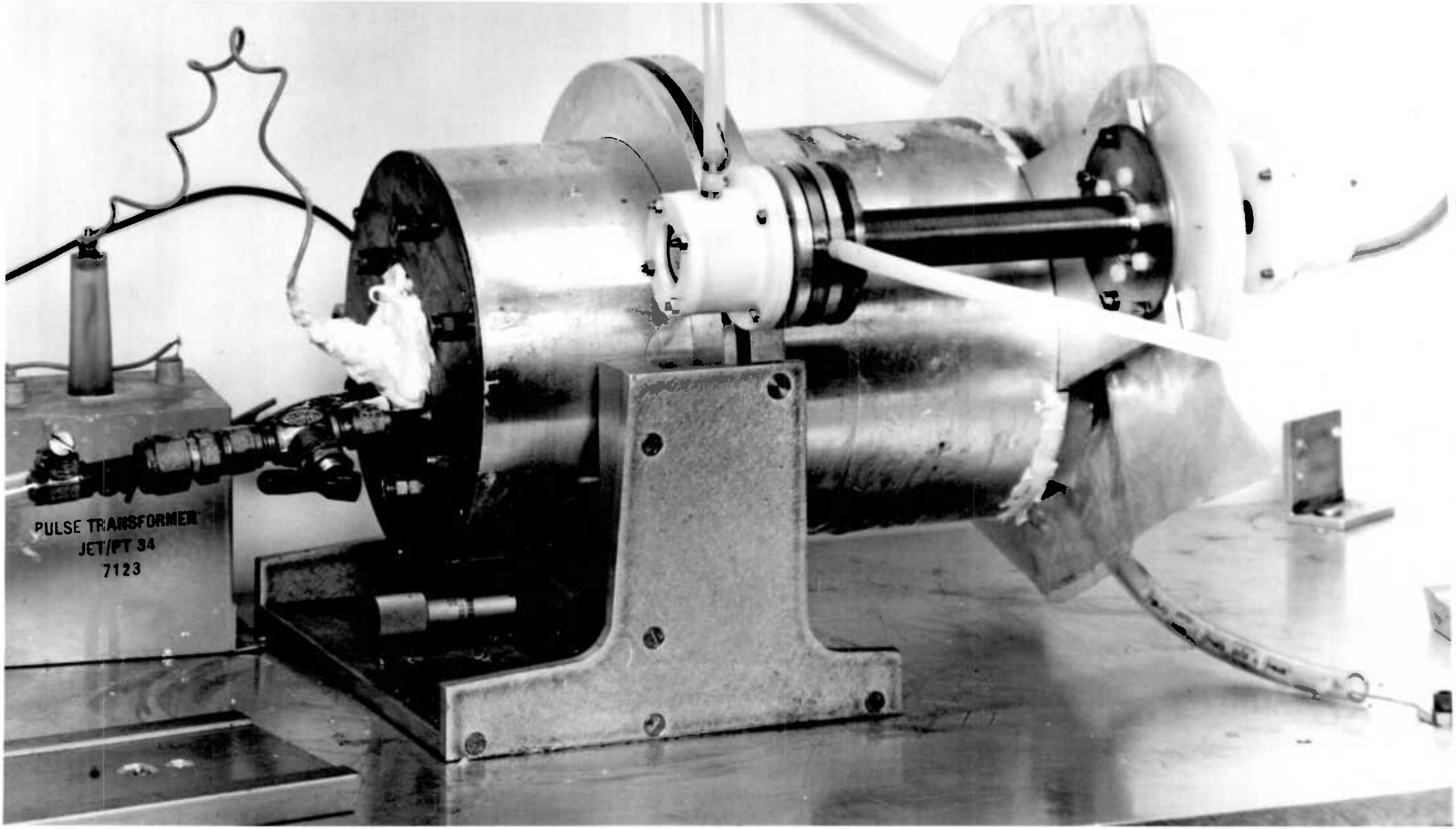

PLATE II - THE COAXIAL DYE LASER

PLATE III - THE COAXIAL DYE LASER (PARTLY ASSEMBLED)

FIG. 3.1 COAXIAL LASER

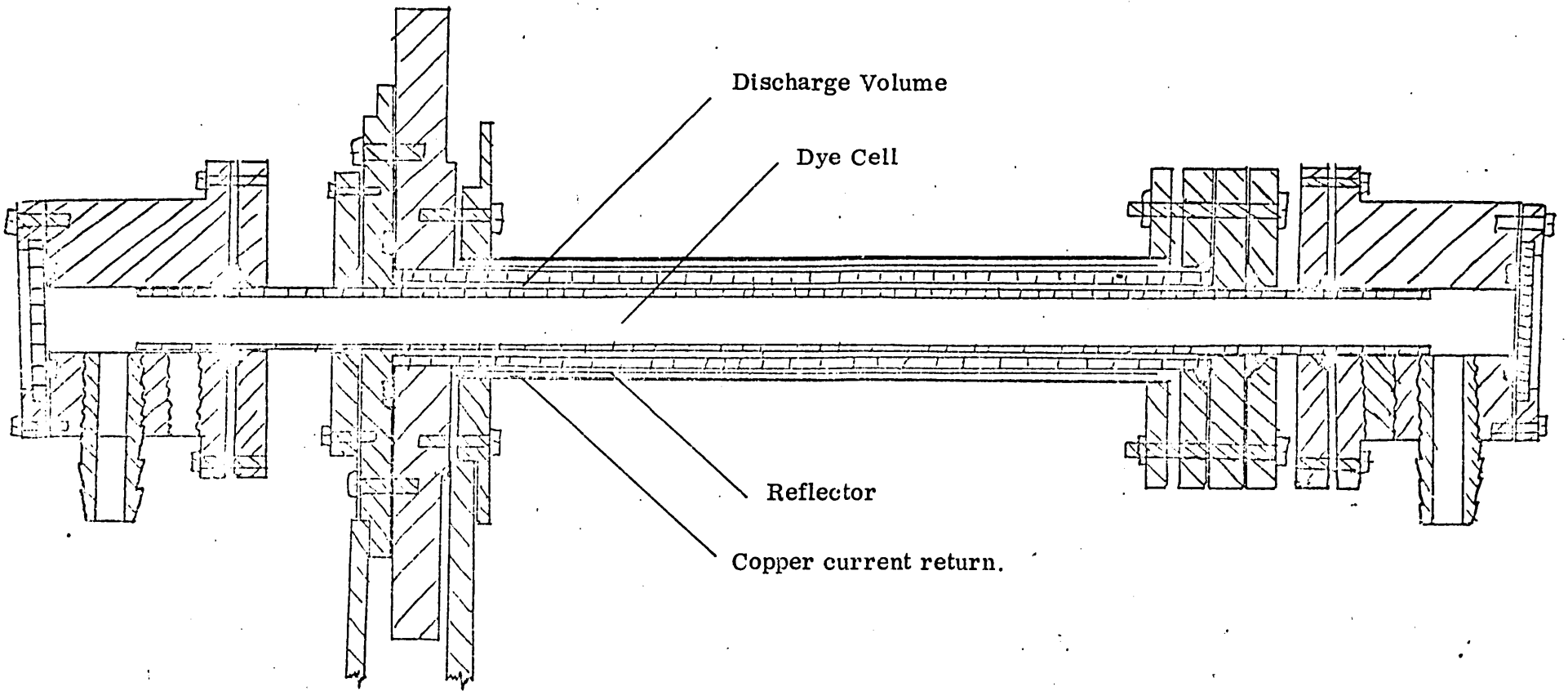

● 'O' ring. Quartz tubes. Plastic (PTFE or Nylon) Metal (Stainless Steel, Brass or Aluminium).

and (ii) the 'O' rings provided a cushioning effect against the mechanical shock and rendered the flashlamp less likely to fail in the first place. A diagram of the flashlamp is shown in Fig.3.1, and photographs on P. 3, 26, 27. Page 3 shows a colour photograph of the laser in action. At this stage after two years of continuous operation not a single flashlamp has failed due to the mechanical shock of the discharge at energy loadings upto 94 J. The design should be suitable for even higher energies provided the thickness of the quartz tubes is scaled appropriately (see e.g. Ferrar 1969).

The electrical driver unit was similar to that used by Furomoto (1969). A pancake type low inductance pressurised spark gap switch was mounted on the end of a 0.3 M.F.D. 25 kv capacitor. The capacitor was charged by a 25 kv, 50 mA power supply and when the spark gap was triggered upto 94 J of electrical energy was discharged through the laser flashlamp. The spark gap was triggered by a high voltage pulse from a trigger circuit via a pulse transformer (Fig.3.2). Although the rise time of the trigger pulse was 1 μ S with careful adjustment of the spark gap pressure the jitter in the laser timing could be reduced to less than 100 nS shot to shot (Plate VI, P.141).

Different size flashlamps were tried of 12 and 50 cm length and 0.5 and 1 mm annular gap. Of these the 0.5 mm gap 12 cm long combination gave the highest energy output (Table 3.1) and the following results refer to this flashlamp.

Dynamic Flashlamp Behaviour

Because the upper lasing level in the dye molecule has a short lifetime, typically 5 nS (De Michelis 1971) no energy storage in the active medium is possible, unlike the case of Q switched ruby lasers, and the chief factor governing laser power is the speed with which the electrical energy in the capacitor can be discharged in the flashlamp. For high powers a system with the lowest possible inductance is necessary. A short pumping

FIG. 3.2 LASER TRIGGER CIRCUIT

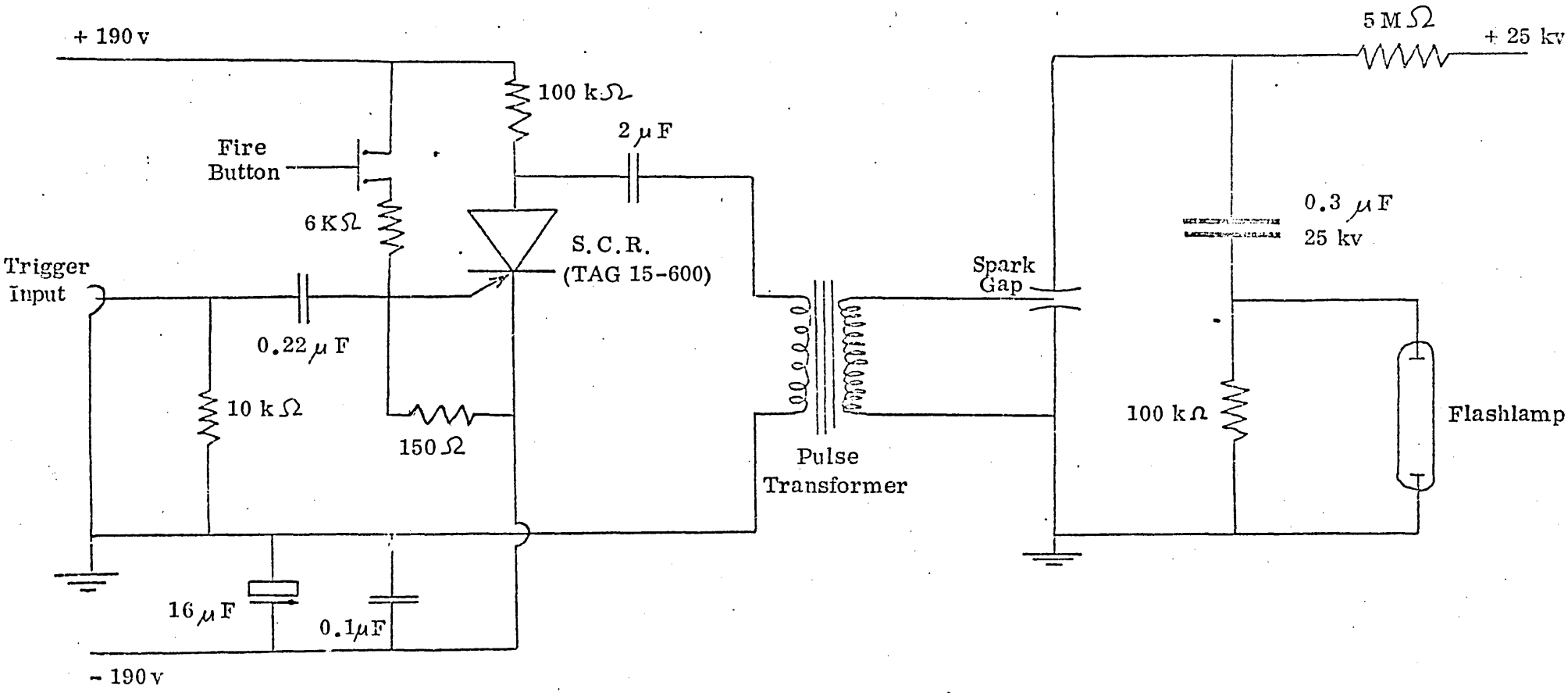

pulse also increases the laser efficiency through reduced triplet state losses. The dynamic behaviour of the flashlamp was therefore studied. The time histories of the flashlamp current and light emitted were similar with a 250 nS rise and full width half maximum (F.W.H.M.) duration of 600 nS (Plate VI). The inductance of the capacitor and spark gap was measured by replacing the flashlamp with a shorting block. From the period of oscillation of the current the inductance was calculated to be 26 ($\pm$1) nH. Including the theoretical inductance of the flashlamp, the total system inductance was found to be 38 nH. At the highest voltage settings the current time history became slightly over damped. Assuming the flashlamp to be critically damped at voltage settings just less than the above values, the calculated rise time of a system with the above capacitance and inductance is $t_r = (LC)^{\frac{1}{2}} = 106$ nS, much less than the value observed in practice. The difference is due to the time varying nature of the flashlamp resistance (a function of the degree of ionisation of the gas), and indicates that the current rise time is limited by the rate at which this resistance is reduced and not by the flashlamp inductance. Hence to increase laser power further it would be more profitable to develop higher voltage systems rather than seek to reduce the inductance since (i) the threshold voltage at which ionisation begins to occur is reached sooner for higher voltage systems with the same rise time, and (ii) above threshold the higher electric field strengths reached would accelerate the increase in ionisation.

Flashlamp Spectrum

The flashlamp spectrum in the visible region showed a continuum overlaid by weak emission lines.

TABLE 3.1

Flashlamp Performance

Flashlamp	Annular Flashlamp Width	Flashlamp Length	Duration (F.W.H.M.) of Flashlamp Light	Duration of Laser Pulse	Energy Output 79 J Input 25% Reflectivity Output Mirror 50 torr Xe pressure
(i) H.C.O.	0.5 mm	12 cm	Unrecordable due to flashlamp fracture		
(ii)	0.9 mm	12 cm	1500 nS	150 nS	110 mJ
(iii)	0.94 mm	50 cm	1200 nS	-	75 mJ
(iv)	0.56 mm	12 cm	600 nS	300 nS	305 mJ
(v) EPL laser (SUA9) For comparison (Chapter XVI)			15 μS	1.4 μS	1.1 J for 1000 J Input

Flashlamp Fill Pressure

The flashlamp was evacuated to approximately 0.01 torr with a rotary pump and then filled with xenon before use. Air was tried as a filling gas but it gave very irreproducible results with a lasing threshold at an input energy double that for the case of xenon. The optimum xenon pressure was found by measuring the laser energy output at different filling pressures over the range 4 - 110 torr, maximum energy output being obtained in the region 40 - 80 torr for capacitor voltages of both 20 and 23 kv. A pressure of 50 torr was chosen as the normal operating pressure.

Dye Preparation

The laser was initially run broadband with a solution of rhodamine 6G in ethanol being continuously circulated through the central quartz tube. Dye laser performance is very sensitive to dye contamination and to avoid this problem the only materials in contact with the dye solution were glass, stainless steel and P.T.F.E. The performance depended markedly on the purity of the dye, the best results for rhodamine 6G being obtained with dye supplied by Kodak. An output energy of 420 mJ was achieved at 92 J electrical energy input. Over many tens of shots however the performance deteriorated, probably due to photodecomposition of the dye, thermal lensing effects as the dye temperature increased, and the presence of microscopic air bubbles in the dye solution. Changing to a new solution of dye improved the performance but the previous 420 mJ could not always be achieved. Filtering the dye before use or using ultrapure solvents made no difference. It was only after an on-line dye filter[+] was installed that high energies could

[+] Whatman Filter supplied by Reeve Angel Scientific Ltd., Gaunt Street, London, SE1 6BD.

be consistently achieved. The on-line filter is thought to improve laser performance by removing the air bubbles produced by the shock wave due to the discharge (Bunkenberg 1972, Hirth et al. 1973). The dye concentration used was not critical, best results being obtained in the region of 80 mg/litre using ultrapure methanol * as a solvent.

The dye cresyl violet + was also used both on its own and in a mixture with rhodamine 6G. Best results were obtained using a solution of 60 mg each of cresyl violet and rhodamine 6G in one litre of "ultrar" methanol, the solution being filtered through a sintered glass filter (pore size 2μ) ** before use. The maximum energy output obtained with this mixture was 175 mJ untuned.

Flashlamp Reflector

Various reflecting materials were wrapped around the flashlamp to find the optimum reflecting material.

TABLE 3.2

Reflecting Material	Energy Output mJ
Al cooking foil shiny side inward	80
" " " dull (unlaquered) side inward	120
Al coated mylar	65
MgO deposited by burning Mg ribbon	50
Black paper	12

* "Ultrar" methanol supplied by Hopkins & Williams, Chadwell Heath, Essex.

\+ B.D.H. Chemicals Ltd., Poole, Dorset.

** Jobling & Co. Ltd., Wear Glass Works, Sunderland.

Part of the variation is due to dye deterioration but it is clear that the optimum reflector is the dull side of ordinary cooking foil. The result with black paper shows that the dye is optically thin to the flashlamp radiation.

Reproducibility

A solid state photodiode (Motorola MRD510) placed so as to pick up stray light from the laser was used to provide a permanent monitor of the laser output. The reproducibility of the total (wavelength integrated) laser output was measured by firing the laser at a constant repetition rate (of 4 per minute) and superposing the time histories of the laser light from many shots on the same photograph. The traces coincided well giving a reproducibility better than 5%.

Laser Mirrors

The variation in the laser energy with different output mirror reflectivities was measured.

TABLE 3.3

Output Mirror Reflectivity	Laser Energy mJ
16%	67
25%	110
65%	90

The 25% reflectivity mirror was an uncoated sapphire resonator. As this was expected to produce some wavelength dependent structure in the laser spectrum (acting as a Fabry Perot) it was replaced for the fluorescence experiments by a broadband dielectric mirror of reflectivity 30%.

Laser Efficiency

Above threshold the energy output increased linearly with the energy input and showed no sign of saturation at high energies.

FIGURE 3.3 LASER EFFICIENCY

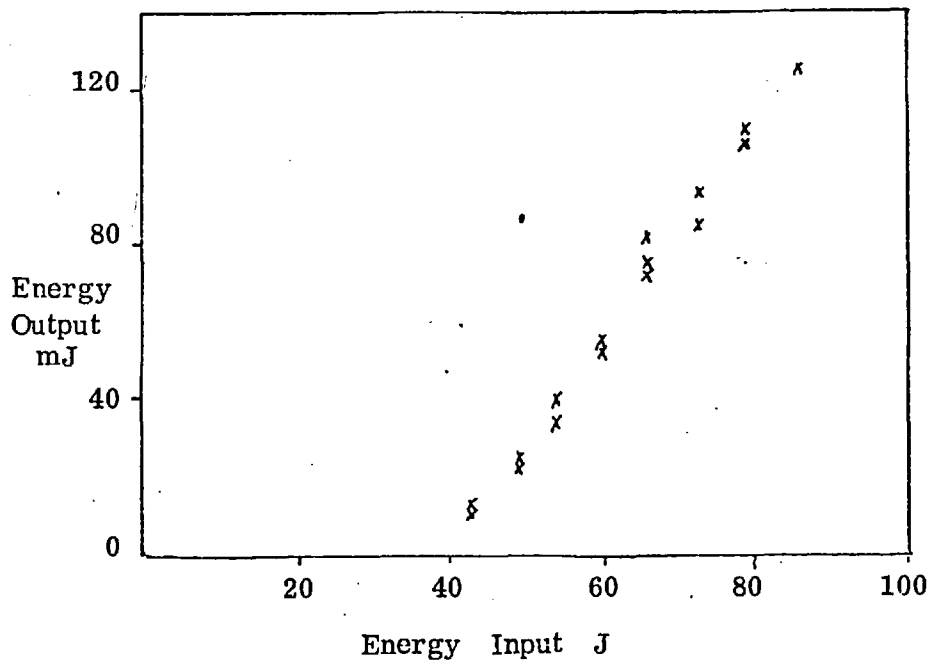

The laser pulse length increased from 220 → 300 nS with increasing energy.

FIGURE 3.4 LASER DURATION

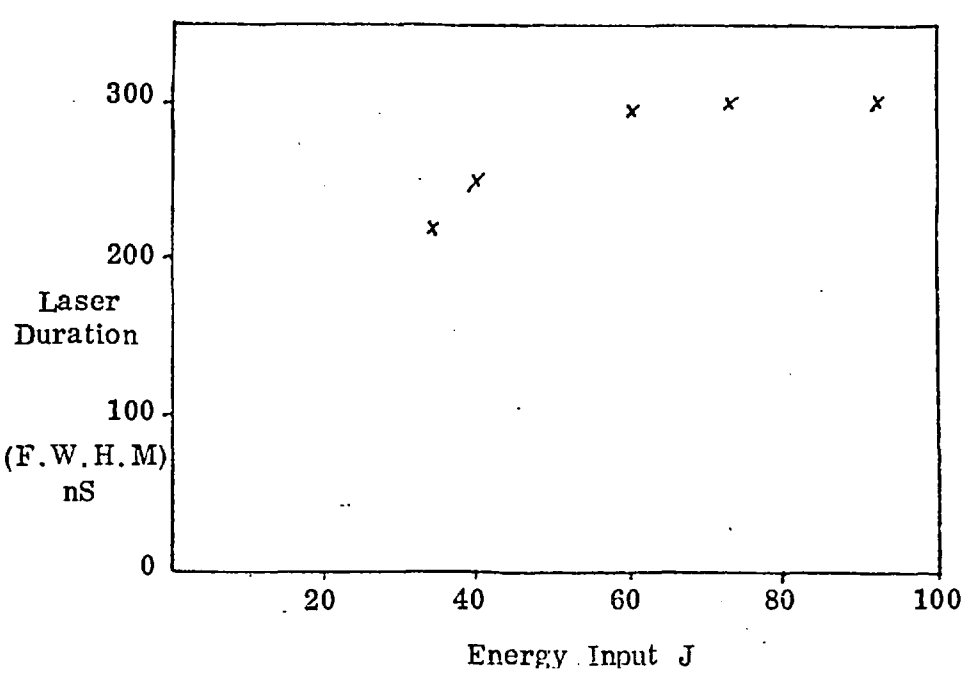

The maximum energy of 420 mJ obtained corresponded to a peak power (untuned) of 1.4 Megawatts, an energy conversion efficiency of 0.45%.

Laser Wavelength Tuning

Without mirrors the dye does not lase but emits a broad band of fluorescence which, for rhodamine 6G, extends from 5730 - 6100 Å. With mirrors aligned so that lasing action takes place but without tuning elements the laser emits light over a band, 5920 - 6000 Å for rhodamine 6G, 6480 - 6530 for cresyl violet. It is possible to tune this output band by varying the dye concentration. However this reduces the output energy and at low dye concentrations the performance deteriorates very rapidly in the order of 10 - 20 shots.

A diffraction grating was used to tune the laser over a limited range 5800 - 5900 Å. However without a specially constructed precision mount it was very difficult to line up. A wide gap poor quality Fabry Perot etalon was inserted into the cavity. This split the previous untuned broadband into about 15 lines about 5 Å apart. With an optical filter in the laser cavity the laser emitted a line approximately 20 Å wide at 5880 Å with a 60% energy reduction compared to the untuned case.

A specially constructed Fabry Perot etalon was then purchased.* This was of the optically contacted type with permanently stable alignment (Bradley et al. 1971). The gap between the reflecting surfaces was 6 μm wide. The plates were polished to a flatness of $\lambda/40$ and had a broadband dielectric coating of 70% reflectivity over the region 5700 - 6700 Å. With the etalon in the laser cavity the energy output was reduced by 35% compared

* I.C. Optical Systems Ltd., Franklin Road, London SE20.

to the untuned case but was spectrally narrowed to a line of width (F.W.H.M) 2.2 Å.

The laser output wavelength could be conveniently changed by rotating the Fabry Perot with respect to the laser axis. The tuning range was 5770 - 6010 Å using rhodamine 6G, 6380 - 6660 Å with cresyl violet; both at the optimum dye concentration. These wavelength ranges can be extended somewhat by changing the dye concentration. These measurements were recorded photographically using a spectrograph.

Laser Chirp

For a fluorescence experiment it is important for there to be no systematic frequency shifts (chirps) during the course of a laser pulse. The apparatus described in Chapter IV was used to check this. A black card was positioned in the laser beam and light scattered from this was collected, dispersed with a monochromator and detected with a photomultiplier. A double beam Tektronix 551 scope was used to display this, wavelength resolved, signal together with a wavelength integrated signal from a photodiode picking up stray light. The second signal was used as a time marker By scanning the monochromator across the laser line a picture of the time and wavelength dependence of the laser was built up over a series of shots. The results are shown in Fig.3.5. The laser spectrum becomes more concentrated near the central wavelength as the time in the pulse progresses. In other words the laser duration is shorter in the line wings. Atkinson et al. (1973) have computed theoretical estimates of spectral line widths of flashlamp pumped dye lasers. They solve numerically rate equations for molecular state populations and mode photon densities including the effects of intersystem crossing to triplet states. The predicted line width narrows during

FIG. 3.5 LASER CHIRP

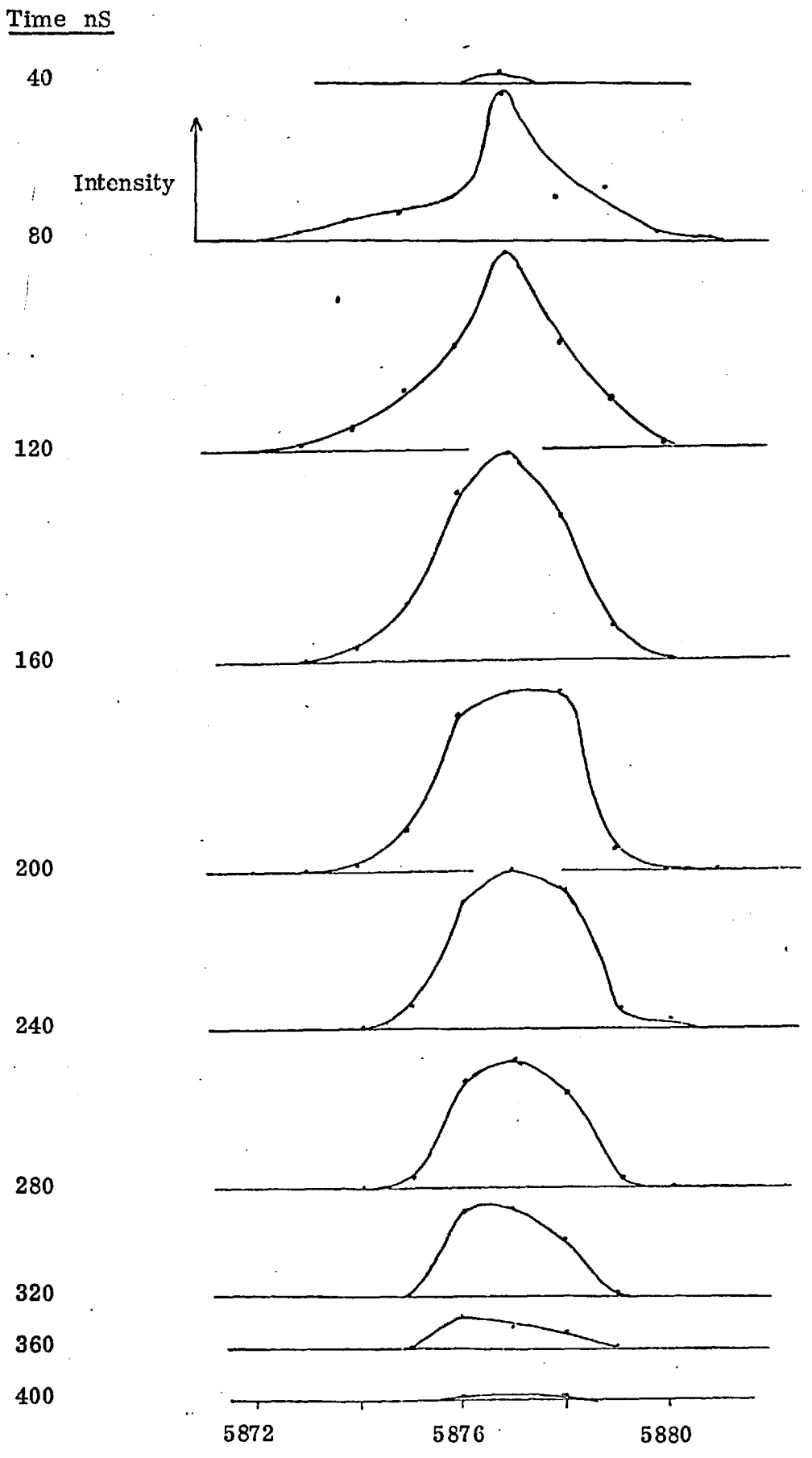

the laser pulse in a way very similar to the present results.

No systematic frequency shifts in the laser spectrum were observed. A high resolution scan over the central 2.5 Å (corresponding to 10 times the line width (F.W.H.M.) of the He 5876 Å line in the fluorescence experiment) showed a smoothly varying spectrum.

Laser Polarisation

In the early stages of the experimental work the windows at the end of the dye cell were Brewster angled to produce a polarised output. However when it became clear that a second dye laser which also had Brewster windows was only partially polarised (Chapter XVI), the windows of the coaxial laser were changed to ones nearly perpendicular to the laser axis. They had a one degree angle to the normal to avoid any possibility of them forming a laser cavity. This greatly eased alignment problems. With these windows the laser polarisation was found to be completely random.

Divergence

The outstanding advantage of lasers over conventional light sources is high brightness. This is inversely proportional to the square of the laser divergence expressed in radians.

The divergence of the laser was studied by various methods:

(1) A burn pattern was formed when the laser beam hit a piece of exposed polaroid film. The pattern was approximately the same size at different distances from the laser but decreased in intensity with increasing distance.

(2) The radial intensity distribution in the laser beam was measured at two distances from the laser by placing a variable iris in front of a calorimeter. The results are shown in Fig.3.6.

FIGURE 3.6 LASER RADIAL INTENSITY DISTRIBUTION

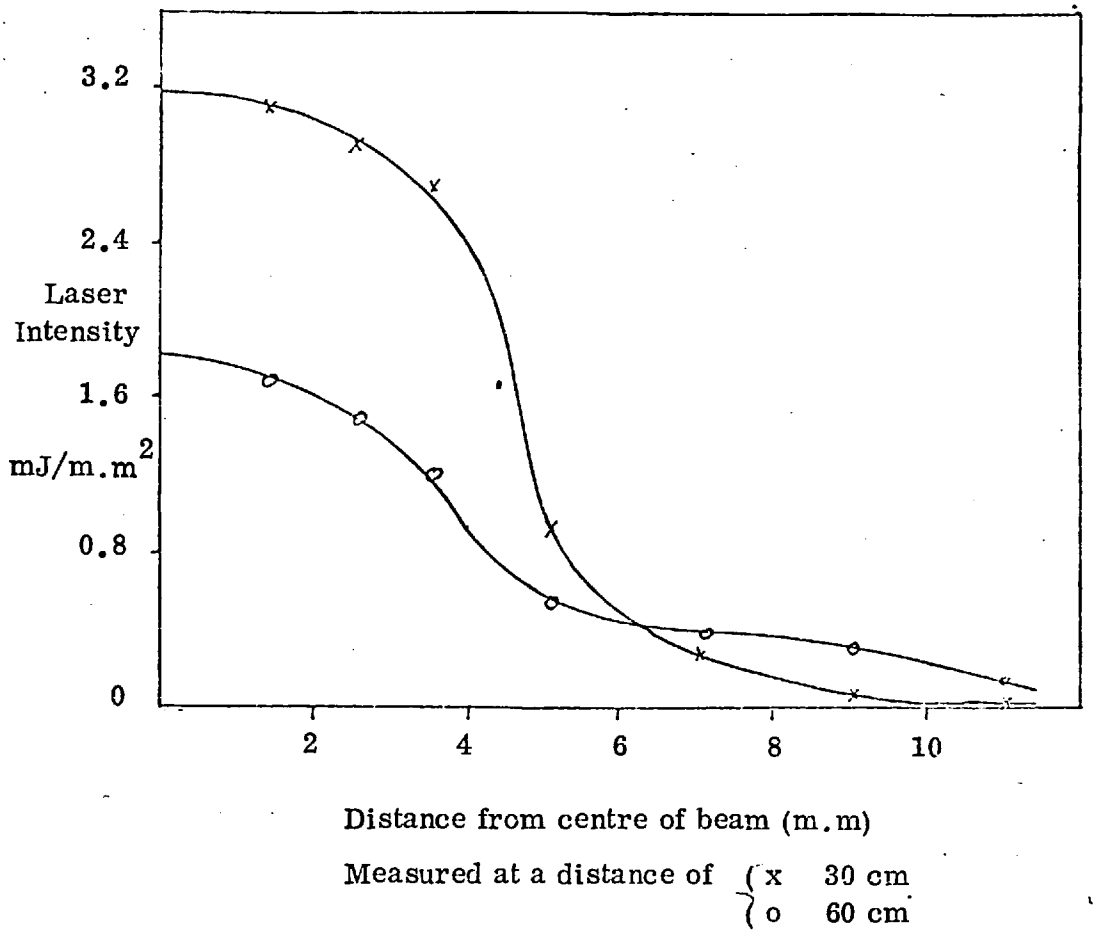

(3) The energy incident on the 1" diameter sensitive area of a calorimeter 1 metre away from the laser was measured as a function of laser cavity length. It was found that cavity lengths of 45 - 90 cm gave 40% higher energy into this area than a 35 cm cavity, although the 35 cm cavity gave the highest total energy

(4) The laser output beam was photographed by recording the scattered light from a matt black card. The distance of the card from the laser was varied and the following features were found :

(i) A central bright spot staying the same size but getting fainter as the distance from the laser was increased.

(ii) The central spot was surrounded by a dark region.

(iii) Surrounding this dark region there was an area of diffuse illumination of increased brightness.

A measurement of the divergence including all three regions gave a value of 20 milliradians half angle full beam. This is to be compared with the theoretical diffraction limit on the divergence of the system of only 0.05 milliradians and the maximum angle of light that can pass through the dye cell without deflection, 40 mradians half angle. Removal of the 100% rear reflector on the laser cavity showed that regions (ii) and (iii) were not due to superradiance. These regions appear to be due to a type of axial mode involving reflection from the dye cell wall, as shown in Fig.3.7.

FIGURE 3.7 OFF AXIS LASER MODES

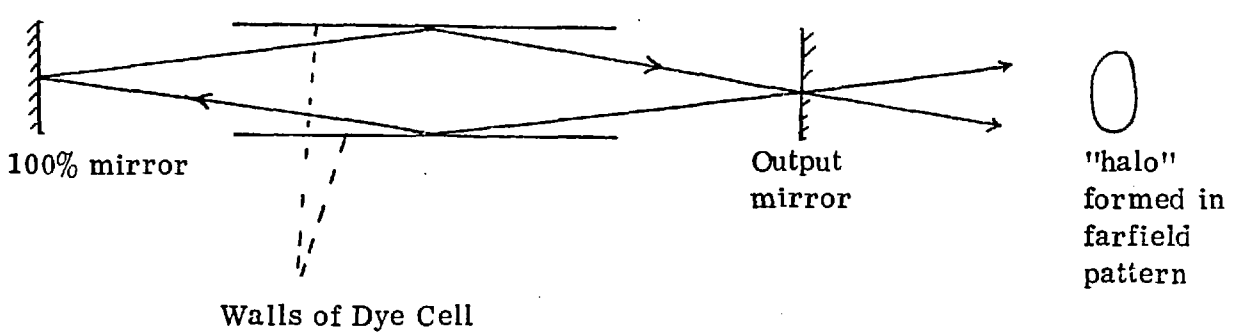

At the angles of incidence involved the reflection coefficient of the walls of the dye cell is 75% so that the losses involved in these modes are not prohibitively large. The predicted angle on this explanation at which the "halo" would be expected to diverge from the axis is in good agreement with its observed size.

To check this hypothesis a wire spiral was fitted inside the dye cell in order to produce large losses in any modes involving reflection from the dye cell walls. This caused the large halo to disappear, but a substantial amount of light outside the central axial spot remained. Quantative comparison of the energy output in the different modes was impossible because insertion of the wire also reduced the power output of the laser in the central axial mode as it absorbed a substantial part of the flashlamp illumination.

Laser Brightness

The brightness of the laser was measured directly by using a lens in conjunction with a variable iris and calorimeter. With the iris in the focal plane of the lens (Fig.3.8) the light emitted at varying angles was measured by recording the energy passing through the iris when it was set to different apertures.

FIGURE 3.8 MEASUREMENT OF LASER BRIGHTNESS

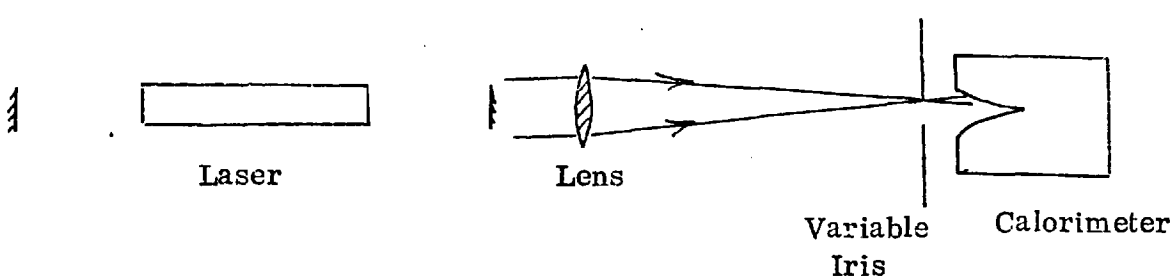

FIG. 3.9 LASER BRIGHTNESS

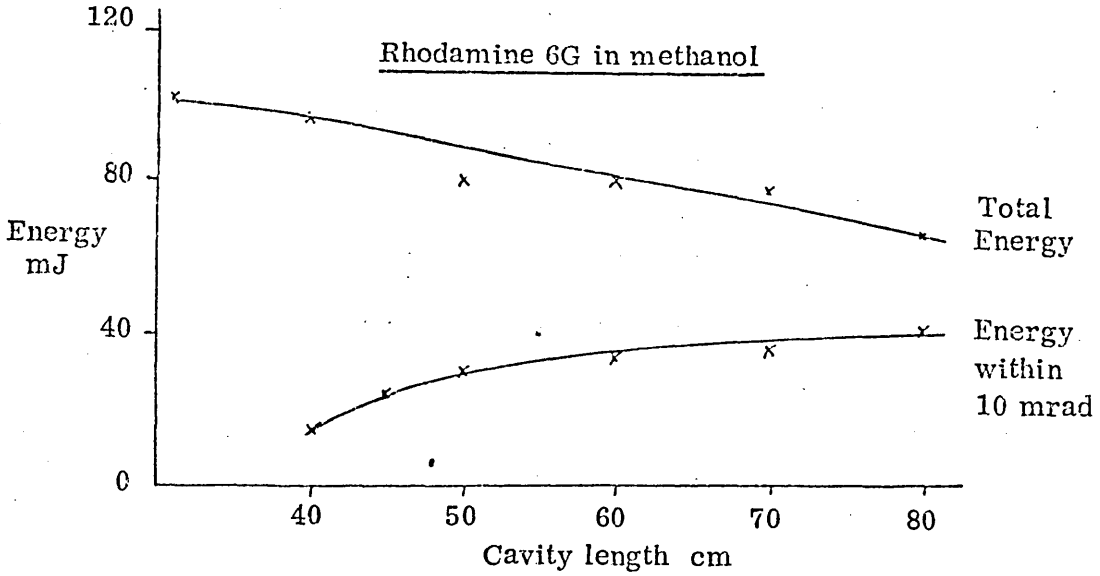

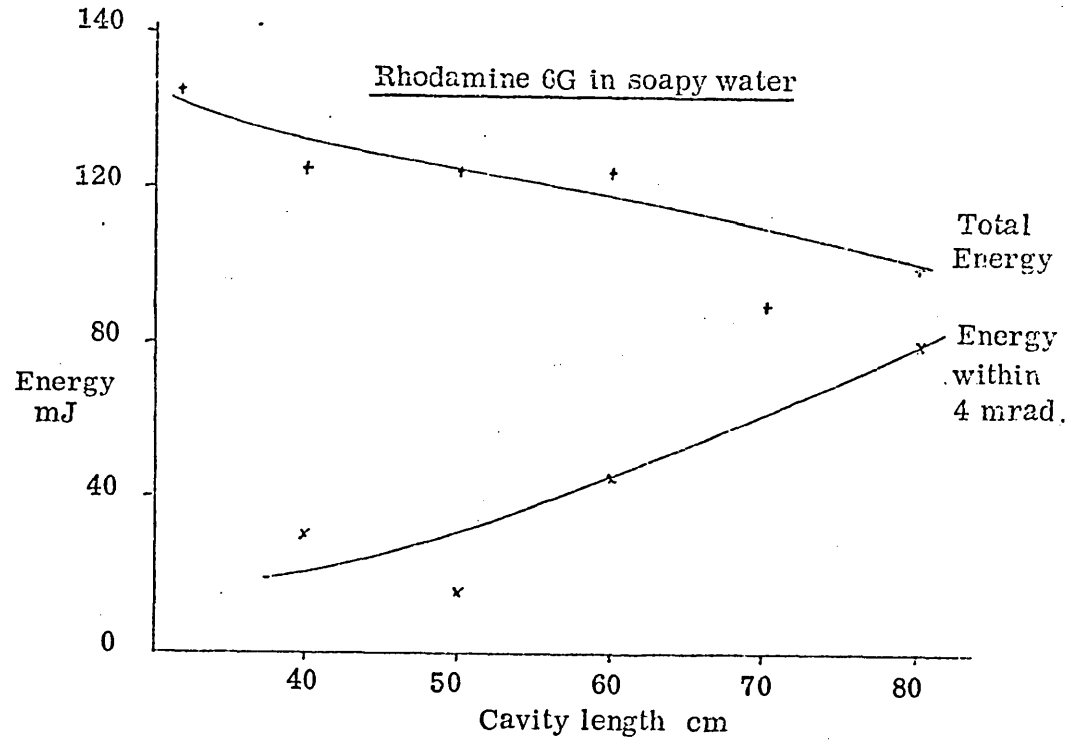

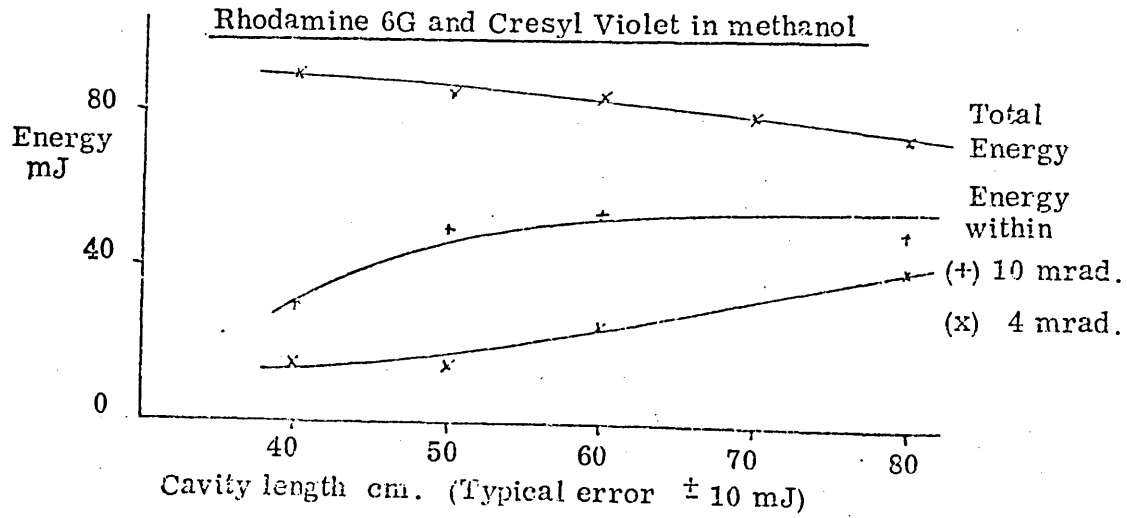

Results were obtained for rhodamine 6G and also a mixture of cresyl violet and rhodamine 6G using a solvent of either alcohol or soapy water.

For multi-mode lasers the divergence should always decrease on increasing the laser cavity length. However if the total output energy decreases still faster there is a net loss in brightness. The total energy inside a given solid angle was measured as a function of laser cavity length. (Fig.3.9). For both rhodamine 6G and the cresyl violet/rhodamine 6G mixture the laser brightness increased with increasing cavity length even though the total energy output went down. The half energy full angle divergence for an 80 cm cavity was 8 mradians. The results for rhodamine 6G in soapy water were substantially better. The solvent was distilled water with 10% by volume of a liquid soap known as Ammonyx L.O. added. This solvent is used in CW dye lasers. Because of its higher thermal conductivity the inhomogeneities caused by heating effects are much reduced. (In fact CW dye laser operation has not been reported for alcohol solutions of dyes). In the coaxial laser with an 80 cm cavity 90% of the total laser energy was emitted inside a full angle of 4 milliradians, an increase in brightness of a factor of 16 compared to the case of alcoholic solutions.

The position of the absorbtion and fluorescence bands of the dye molecule is influenced by solvent interactions. The bands in rhodamine 6G dissolved in soapy water are shifted to longer wavelengths compared to alcoholic solutions. The fluorescence experiment required a laser operating at 5876 Å and a solution of rhodamine 6G in soapy water would only lase at this wavelength at a reduced concentration. This caused a decreased laser output energy and a rapid dye deterioration. A solution of rhodamine 6G in

alcohol was retained for the fluorescence experiment.

The mixture of rhodamine 6G and cresyl violet in soapy water was tried but it barely lased with an extremely low energy and so was unuseable. Table 3.4 shows the normal operating conditions for the laser.

TABLE 3.4

Normal Operating Conditions for Laser

Flashlamp fill pressure	50 torr
Input electrical energy	38 J
Total output energy	50 - 100 mJ
Laser duration	250 - 300 nS
Cavity length	80 cm
Divergence (half energy full angle)	8 mrad.
Dye: rhodamine 6G in ultrapure methanol continuously circulated	80mg/litre
Laser line width (with Fabry Perot)	2.2 Å (F.W.H.M.)
Laser mirrors -	
(i) 5 M radius of curvature 99% reflectivity over range :	5700-6700 Å
(ii) plane 30% reflectivity over range :	5700-6700 Å

A confocal flashlamp pumped dye laser is described in chapter XVI

CHAPTER IV

THE HELIUM FLUORESCENCE EXPERIMENT

Description of the Apparatus

The experiment essentially involved illuminating a plasma of excited helium atoms with a laser and recording the fluorescence produced. The coaxial dye laser used for this experiment has been described in Chapter III. The recombination phase of a linear pinch was used as a source of excited helium atoms. This plasma source has been much used for lineshape studies (e.g. Burgess and Cairns 1970, 1971; Burgess and Mahon 1972; Mahon, Lee and Burgess 1973). The electron density N_e, and temperature T_e, are accurately known both from the measurements in the papers cited above and from spatially resolved Thomson scattering measurements along the discharge axis. (Mahon, R. Ph.D. thesis, University of London 1973, and Smith, C. unpublished). The variation of N_e and T_e with time is shown in Fig.4.1. Thomson scattering measurements along the pinch axis at distances of 3, 10, 35 cm (centre) from one electrode gave the same value for the electron density to within the experimental error (15%).

The discharge vessel was a quartz tube 70 cm long with an internal diameter of 5 cm. Electrical energy was supplied by a 1 μF capacitor. The capacitor voltage was set at 20 kv and the discharge was initiated by a -25 kv pulse applied to the trigger pin of a series spark gap. With a 2 Ω series resistor the current had a critically damped time history. The discharge current, as monitored by a Rogowski coil, reached a peak of 5 kA in 2 μS, and became negligably small after 6 μS. The usual pinch fill pressure was 0.45 torr, the gas being continuously flowed through the

FIGURE 4.1

LINEAR PINCH PARAMETERS

THOMSON SCATTERING RESULTS

(Helium 0.45 torr)

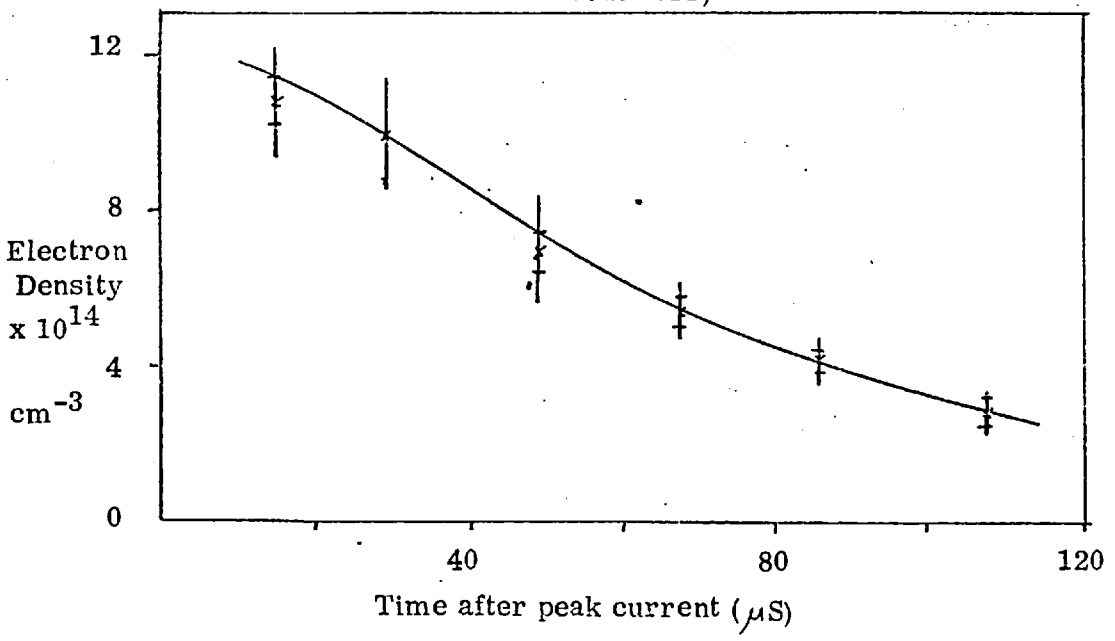

Absolute values relative to value at 30 μ S measured to be 1.0 x 10^{15} cm^{-3} ± 15%. Relative accuracy indicated by horizontal strokes.

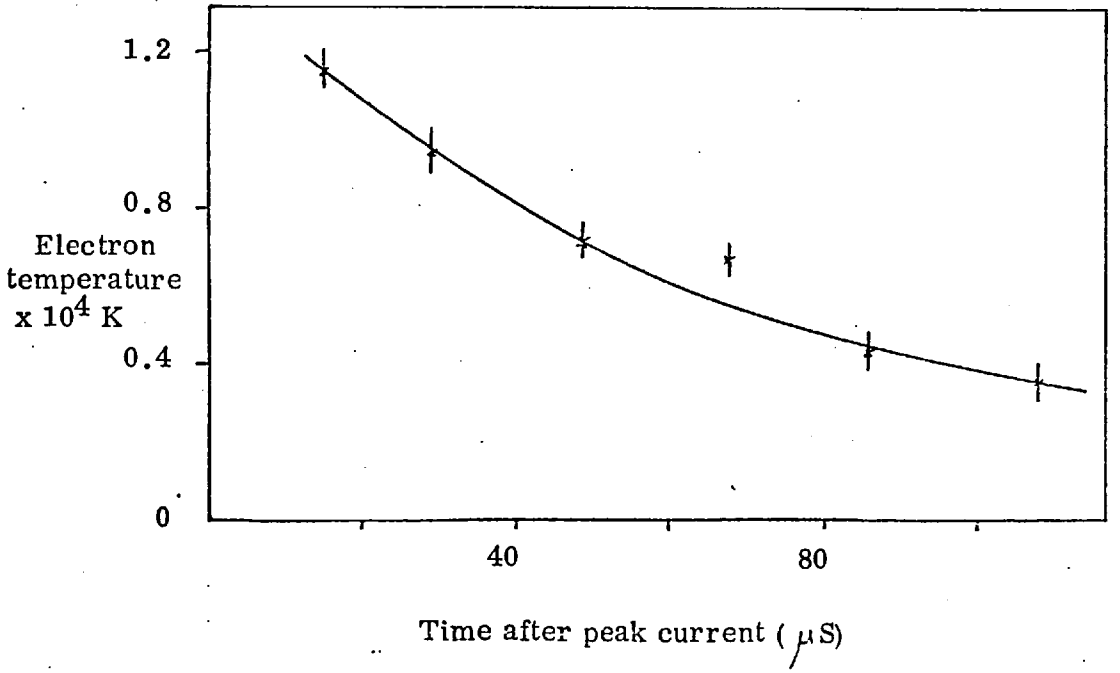

discharge tube. The shot to shot plasma reproducibility, as gauged by the time histories of the light output for both line and continuum emission, was better than the shot noise on the traces which was typically of the order of 3%.

The light from the pinch was imaged on to the entrance slit of "Monospek 1000" Czerny Turner monochromator. The grating used was 10 cm square blazed at 7500 Å and had 1200 lines per mm. The dispersion was 8 Å per mm.

The detector was an RCA C31034 photomultiplier normally run at 1200 volts cathode E.H.T. The signal lead from the photomultiplier was terminated with a 50Ω load.

Optical Arrangement

The optical arrangement is shown in Fig.4.2. Because the fluorescence and laser beam are at the same wavelength but are many orders of magnitude different in intensity it is necessary to take particular care to avoid stray light problems. An OB10 blue glass aperture and beam dump, developed for Thomson scattering experiments, were used for this reason. The aperture limited the laser beam inside the pinch so that reflections at the walls were prevented and the beam dump ensured very little light was scattered back into the pinch. An aluminium mirror directly beneath the centre of the pinch reflected light emitted at approximately 90° to the pinch axis to a 5 cm diameter quartz lens. This provided a 2x demagnified image of the plasma at the entrance slit of the monochromator. The axis of the pinch was imaged along the length of the slit so that the light detected came from a narrow region along the pinch axis. The collected light over-filled the grating thus ensuring the maximum detection efficiency.

FIGURE 4.2 EXPERIMENTAL SET-UP

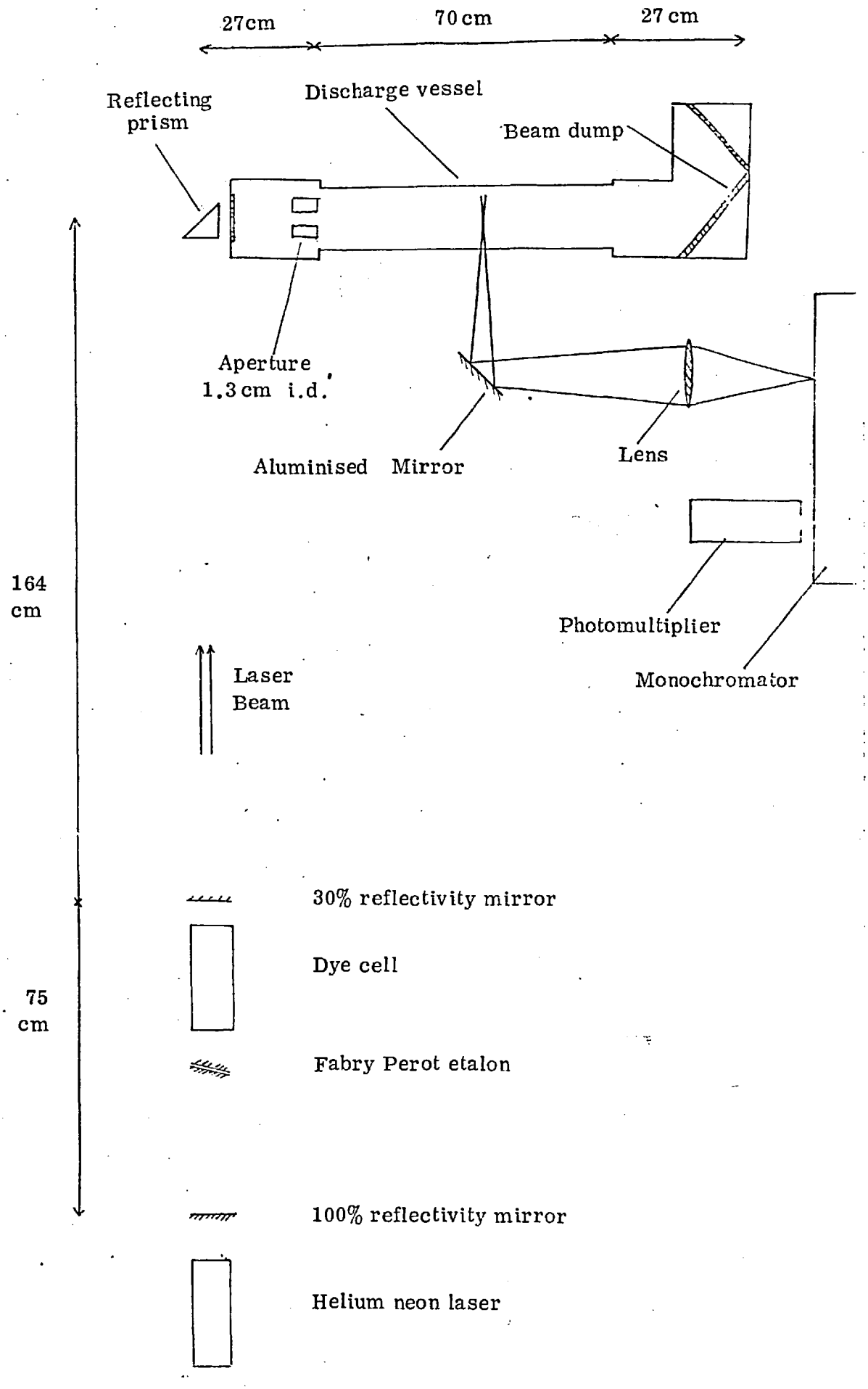

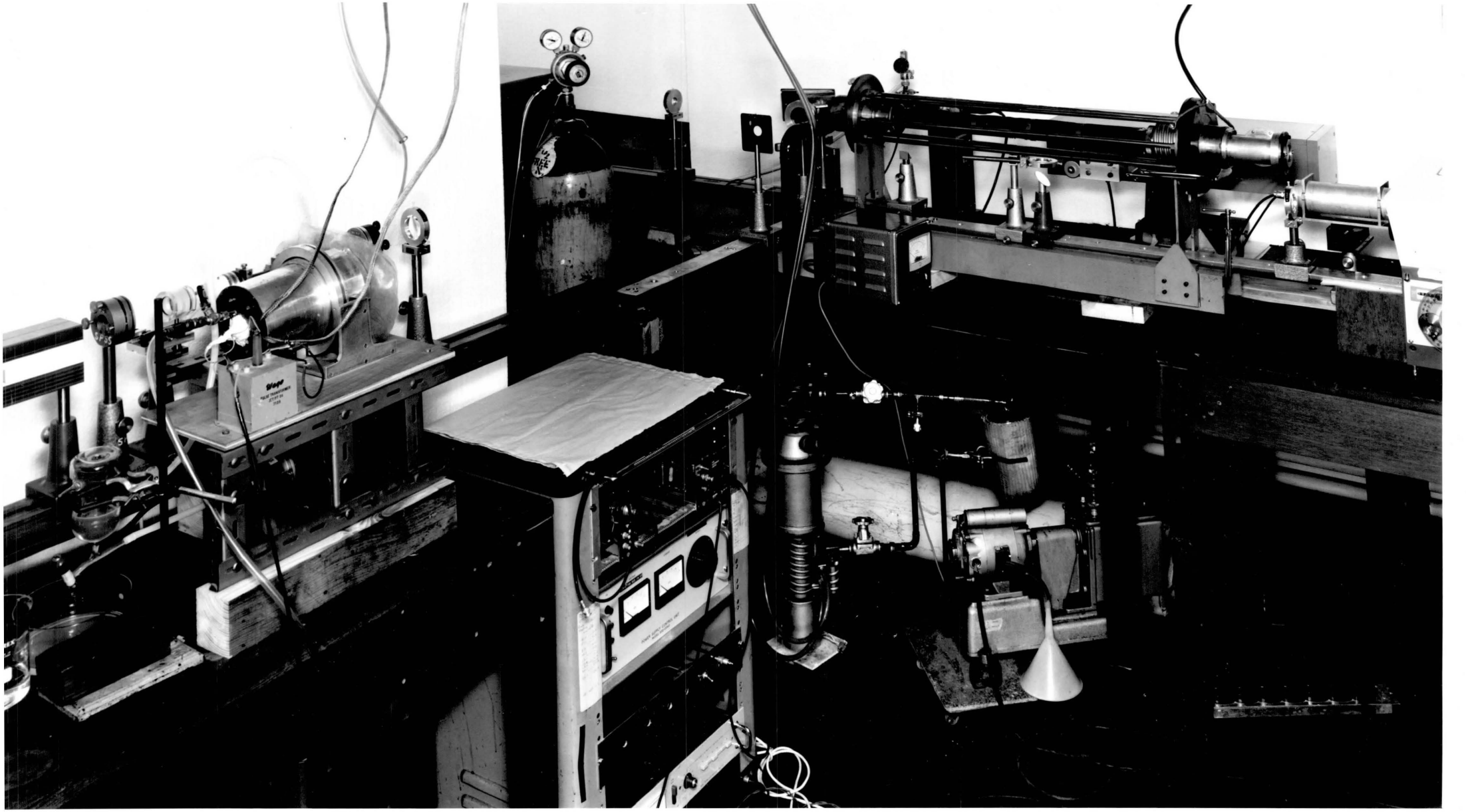

PLATE IV - THE FLUORESCENCE EXPERIMENT

The dye laser may be seen to the left. The linear pinch is on the right.

The design of the laser input optics was aimed at producing a sharply defined region of uniform illumination down the length of the pinch. Because the plasma is radially homogeneous at least in the central 2 cm (Mahon, Ph.D. thesis, University of London 1973) the signal/background ratio can be maximised by illuminating as large an area of the plasma as possible within the limits imposed by stray light considerations.

Spatial Variation of Laser Intensity

The spatial variation of the laser intensity was investigated in situ by placing a black card inside the pinch at 45^{o} to the pinch axis. Laser light scattered from the card was collected and dispersed in the monochromator. By limiting the height of the entrance slit of the monochromator to 1.0 mm a picture of the spatial variation of the laser intensity across the pinch could be built up by moving the black card along the axis of the pinch (Fig.4.3). The monochromator sampled the central 1 $\mathring{A}$ of the laser spectrum. The most uniform illumination was obtained with no lenses at all in the laser beam (Fig.4.4). The width of the illumination was 1.4 ($\pm$ 0.1) cm measured out to 20% of peak intensity. This corresponded to the internal diameter of the blue glass aperture, also of 1.4cm. The variation in the intensity of the laser beam was 50% in the central region. This was to be expected as the burn pattern formed when the laser beam hit a piece of exposed polaroid film next to the output mirror revealed that the laser intensity was not uniform across the width of the dye cell. In particular the edges of the dye cell, being closer to the flashlamp, emitted more intense light than the centre.

Laser Reproducibility

The reproducibility of the small part (in space and wavelength) of the laser output recorded in this way was worse than the reproducibility of the total.

FIGURE 4.3 - SPATIALLY RESOLVED LASER INTENSITY

Experimental Set-up

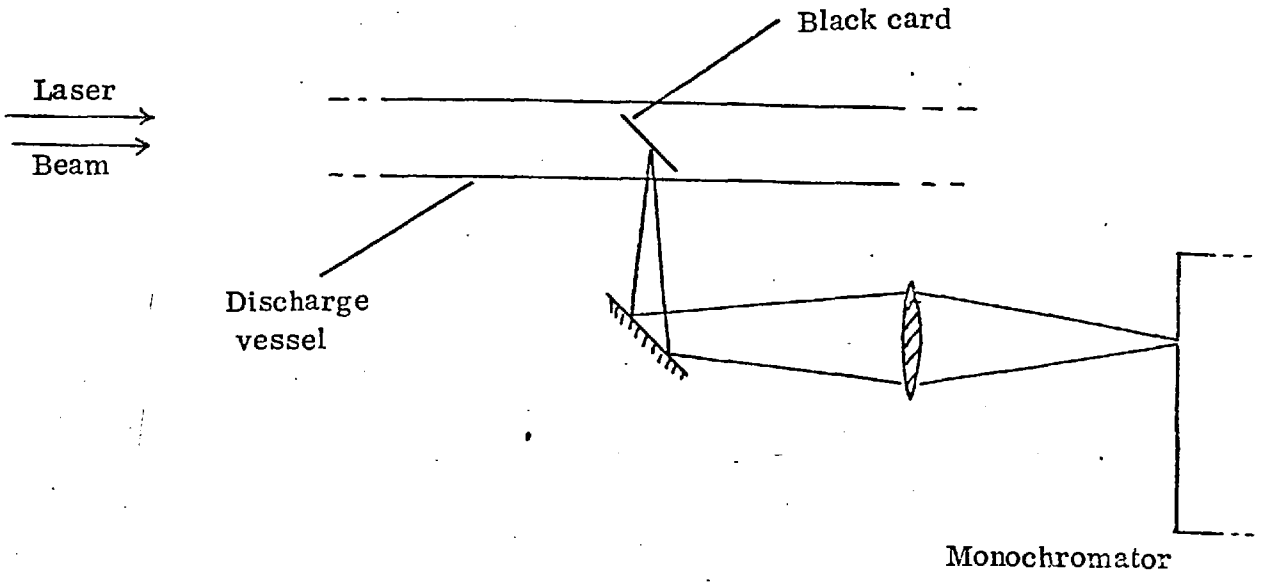

FIGURE 4.4 - SPATIAL INTENSITY DISTRIBUTION

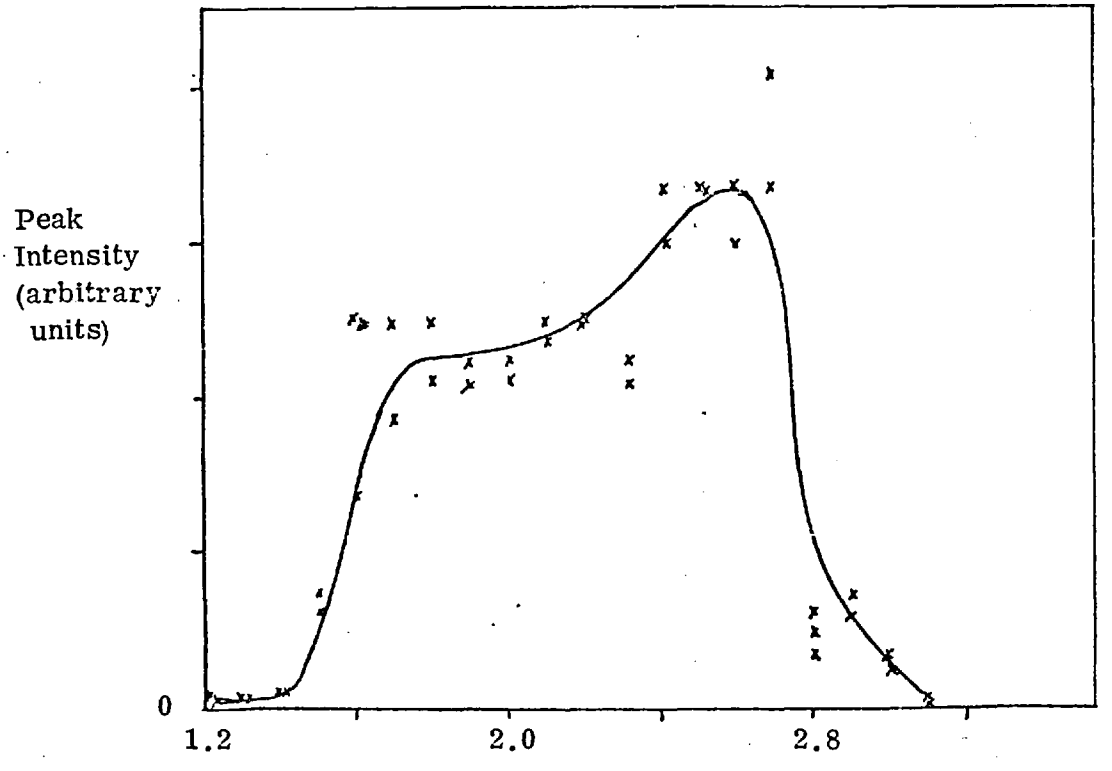

With the monochromator entrance slit height and width set so that the scattered laser light detected was that part in space and wavelength responsible for the fluorescence the reproducibility was found to be about $\pm 10\%$. (Plate VI.) The variation in the laser pulse length(F.W.H.M.) measured in the same way was found to be 3%. At least part of the variation is thought to be due to a variation in the laser beam direction caused by thermal lensing effects in the dye. As discussed in Chapter VI, when the laser saturates the helium transition the fluorescence produced is virtually independent of variations of the laser intensity in time and space. All that is required for unambiguous results is for the laser intensity to be sharply delimited, i.e. have a large $\frac{dI}{dx}$ and $\frac{dI}{dt}$ at the point where the intensity, I, is just sufficient to saturate. The laser intensity distribution inside the plasma was further modified by optical depth effects - this is discussed in Chapter XI.

Photomultiplier Linearity

The linearity of the photomultiplier was checked by recording the pinch emission and fluorescence at different monochromator entrance slit widths. The entrance slit was subsequently set at about half the value at which non-linear effects first appeared.

Optical Transfer Efficiency

The proportion of the total energy output of the laser that passed through the pinch was measured by replacing the beam dump in the pinch with a calorimeter and comparing the energy recorded with the energy measured directly in front of the laser. The transfer efficiency was found to be 30%. Thus a total laser energy of e.g. 100 mj in a pulse of F.W.H.M. 250 nS produced a total intensity of $\frac{100 \times 10^{-3} \times 0.3}{250 \times 10^{-9}}$ = 120 kilowatts inside the pinch.

Total area illuminated = $\pi \left(\frac{1.4}{2}\right)^2$ = 1.54 cm

Power density inside pinch = $\frac{120}{1.54}$ = 79 kilowatts cm^{-2}

The laser power in the pinch for the fluorescence experiments was normally in the region 30 - 80 kwatts cm^{-2}.

Electrical Setup

The design requirements were twofold (i) to trigger the pinch, laser and oscilloscopes at precisely defined times, and (ii) to ensure the signal from the photomultiplier suffered from a minimum of electrical pick-up. Two oscilloscopes were used, a Tektronix 551 dual beam 30 MH_Z oscilloscope and a 7704 single beam 160 MH_Z oscilloscope. The 7704 instrument had facilities for displaying a delayed sweep using a second time base. As the laser pulse length was shorter by a factor of about 10^{-3} than the plasma lifetime, fluorescence could be studied under different plasma conditions by varying the timing of the laser with respect to the pinch. After some initial problems with pick-up, etc., the basic sequence of events was fixed as follows :

1) The pinch was manually triggered, the discharge occurring at a random delay of a few microseconds (μS) after this.

2) The pinch current pulse detected by a Rogowski coil triggered and was displayed on the 551 oscilloscope.

3) The gate output from the 551 oscilloscope triggered an external delay unit. After a controlled delay this produced two simultaneous output pulses - (i) a TTL pulse triggered the 'A' time base of the 7704 oscilloscope, and (ii) a higher voltage pulse (12v) triggered the laser trigger unit.

4) After a fraction of the sweep of the 7704 'A' time base the internal delaying facilities were used to trigger the 'B' time base at a higher sweep rate.

5) The laser fired and the photomultiplier signal was displayed on the 7704 oscilloscope.

With careful adjustment of the spark gap pressure and charging voltage the jitter in time of the laser could be reduced to 50 nS.

The delay unit was calibrated by displaying the laser monitor signal together with the pinch current on the 551 oscilloscope.

Initially the photomultiplier signal suffered from a high level of electrical pick-up. This took the form of a 30 MH_Z oscillation produced by the laser spark gap and it seemed impervious to all the traditional methods of reducing pick-up, e.g. screened boxes, removal of earth loops. However the insertion of a 5 MΩ series resistor into the laser H.V. charging lead greatly reduced the pick-up indicating that the interference was coming from this. The loss in speed in charging the laser capacitor was of no consequence as only a low repetition rate was required.

Lining-Up Procedure

Before the experimental runs the apparatus was prepared in the following way:

A helium neon laser beam was arranged so that it passed exactly down the axis of the pinch. The dye cell, mirrors and Fabry Perot etalon were then positioned centrally in the laser beam and the mirrors aligned using multiply reflected spots. The dye laser beam was thus exactly coincident with the helium neon laser beam. This method is much more accurate than the procedure of observing the position of the laser burn marks necessary with lasers incorporating rooftop prisms or gratings. A small neon probe light was then inserted into the centre of the pinch and the longitudinal position of the collection lens adjusted so that a sharp image of the probe light was formed on the monochromator entrance slit. A second,

helium neon laser with co-linear beams was positioned inside the monochromator so that the beam was on axis between the centre of the entrance slits and the collimating mirror. This second beam passed through the collection system in the reverse direction to usual and intersected the first helium neon laser beam from the dye laser. By placing a piece of paper at the pinch centre it was simple to adjust the transverse position of the collection lens so that the two beams intersected exactly ensuring the optical system was lined up to an accuracy of less than a millimetre.

After this the pinch was evacuated with a double stage rotary pump and the oscilloscopes and photomultiplier power supply turned on. After allowing at least an hour warm-up time the gas supply to the pinch was turned on and the supply rate adjusted to give the correct pressure. The pinch was fired about 100 times to remove any remaining impurities in the discharge vessel. The wavelength setting of the monochromator was set to the centre of the desired line by using a helium lamp for most of the lines as the wavelength shifts produced by the plasma were negligible. Stray light, measured by firing the laser but not the pinch, was undetectable under normal conditions. However by raising the cathode voltage of the photomultiplier. from 1200 to 1700 volts stray light could be observed. This was used as a convenient way to tune the laser exactly to the same wavelength as the atomic transition. Leaving the monochromator fixed the Fabry Perot in the laser cavity was adjusted until the stray light was at a maximum. The photomultiplier cathode voltage was then returned to 1200 volts.

The laser energy was frequently monitored during an experimental run with a calorimeter.

CHAPTER V

PRELIMINARY FLUORESCENCE RESULTS

This chapter is primarily devoted to a description of the dye laser induced fluorescence of the 5876 Å 2^3P-3^3D transition in helium obtained as discussed in Chapter IV. The basic form of the results is shown in Plate V. Photograph 1 shows the time dependence of the current in the discharge, and the 5876 Å emission. Photograph 2 shows the laser intensity as a function of time, sampled in wavelength and space to correspond to that part of the laser beam actually producing the fluorescence as described on P.52 . It can be seen that the laser duration was much shorter than the plasma recombination phase. Photographs 3-5 show the 5876 Å plasma emission with and without the laser at various times in the afterglow. The trace of the 5876 Å emission without the laser shows that plasma conditions are very close to being constant on a time scale of the order of the laser duration. The form of the plasma emission with the laser was not as expected from simple ideas about equalisation of level populations. The fluorescence rose rapidly to a peak and then decayed exponentially to an enhanced plateau value finally reverting to the previous value at the end of the laser pulse. The exponential decay rate was observed to decrease with decreasing electron density. By recording the fluorescence on a fast time scale it was possible to accurately measure the decay rate from peak to plateau. This was done with the laser being fired over a wide range of delay times corresponding to different electron densities. The results are shown in Fig.5.1. The fluorescence was also studied at a reduced laser power, and in this case it more closely followed the variation of the laser intensity in time (Photograph 6). The emission from other transitions was also monitored (Fig.5.2).

PLATE V - PRELIMINARY FLUORESCENCE RESULTS

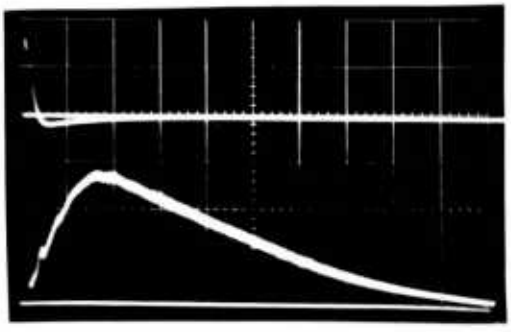

1. 20 μs/cm
Upper: Current trace.
Lower: 2^3P-3^3D 5876 Å light.
50 mV/cm (3 shots)

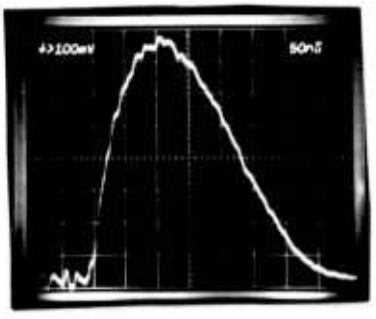

2. Laser Intensity.
(That part of laser beam producing the fluorescence).

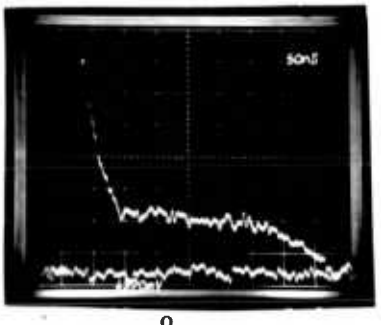

3. 5876 Å light.
(i) with laser.
(ii) without laser.
Delay after peak current .. 30 μs.

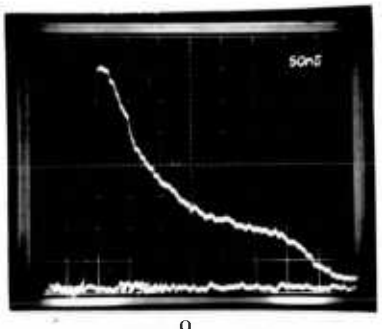

4. 5876 Å light.
(i) with laser.
(ii) without laser.
Delay after peak current . . 60 μs.

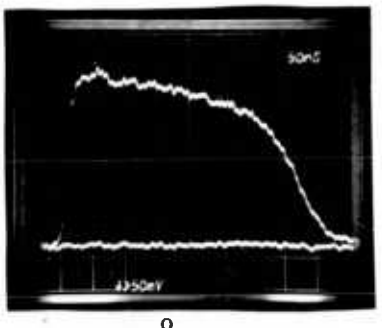

5. 5876 Å light.
(i) with laser.
(ii) without laser.
Delay after peak current .. 100 μs.

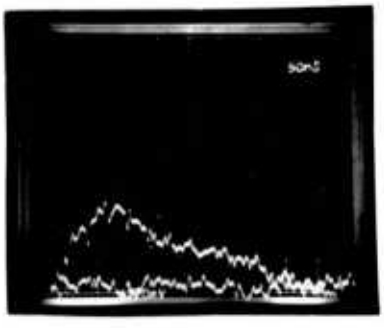

6. As 3. But laser power reduced from 40 kW/cm^2 to 4 kW/cm^2.
Same voltage scale.

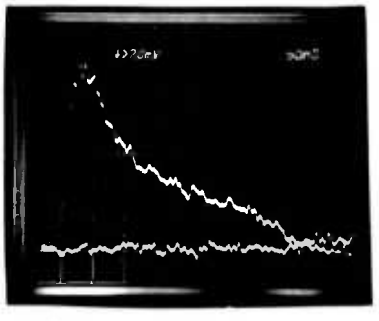

7. Sensitised fluorescence on 2^1P-3^1D 6678 Å.
60 μs Delay.

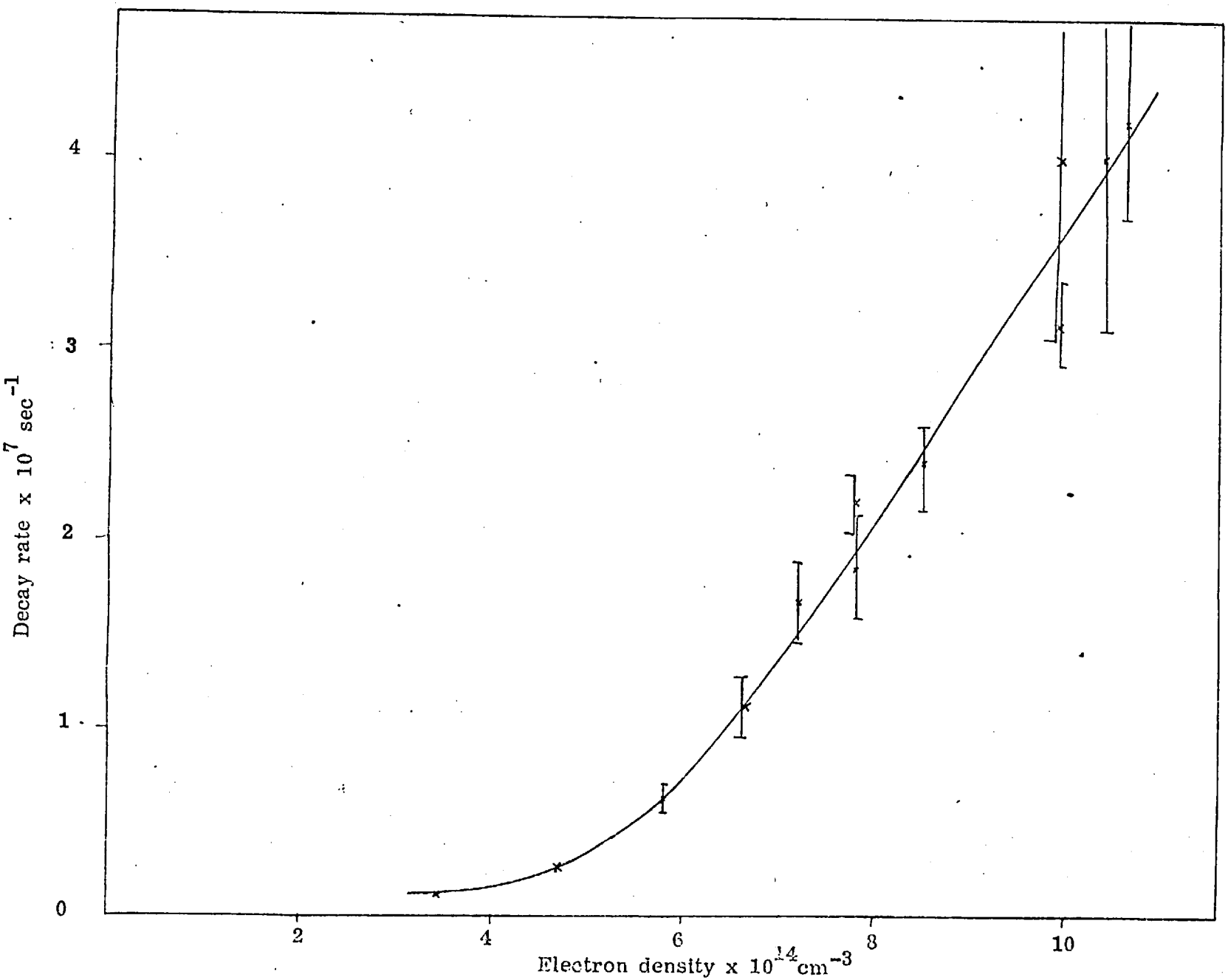

FIGURE 5.1 - FLUORESCENCE DECAY RATE (Based on Thomson scattering electron density measurements)

Photograph 7 shows the emission from $3\,^1D - 2\,^1P$, 6678 Å during laser excitations of the 5876 Å transition. This "sensitised fluorescence" shows a very similar time history to the 5876 Å results. Similar results were observed on all the $n = 3$ or 4 to $n = 2$ transitions. Emission from transitions between $n = 5$ or 6 and $n = 2$ was unaffected by the laser. These results prompted a reconsideration of the processes occurring in resonance fluorescence. It was soon realised that the fluorescence traces were showing relaxation effects in the atomic level populations after their equilibrium had been disturbed by the laser and that these results demonstrated new possibilities for the measurement of collision rates and radiative transition probabilities. The simple mathematical model devised to account for these results is described in the next chapter.

FIGURE 5.2 HELIUM ENERGY LEVEL DIAGRAM

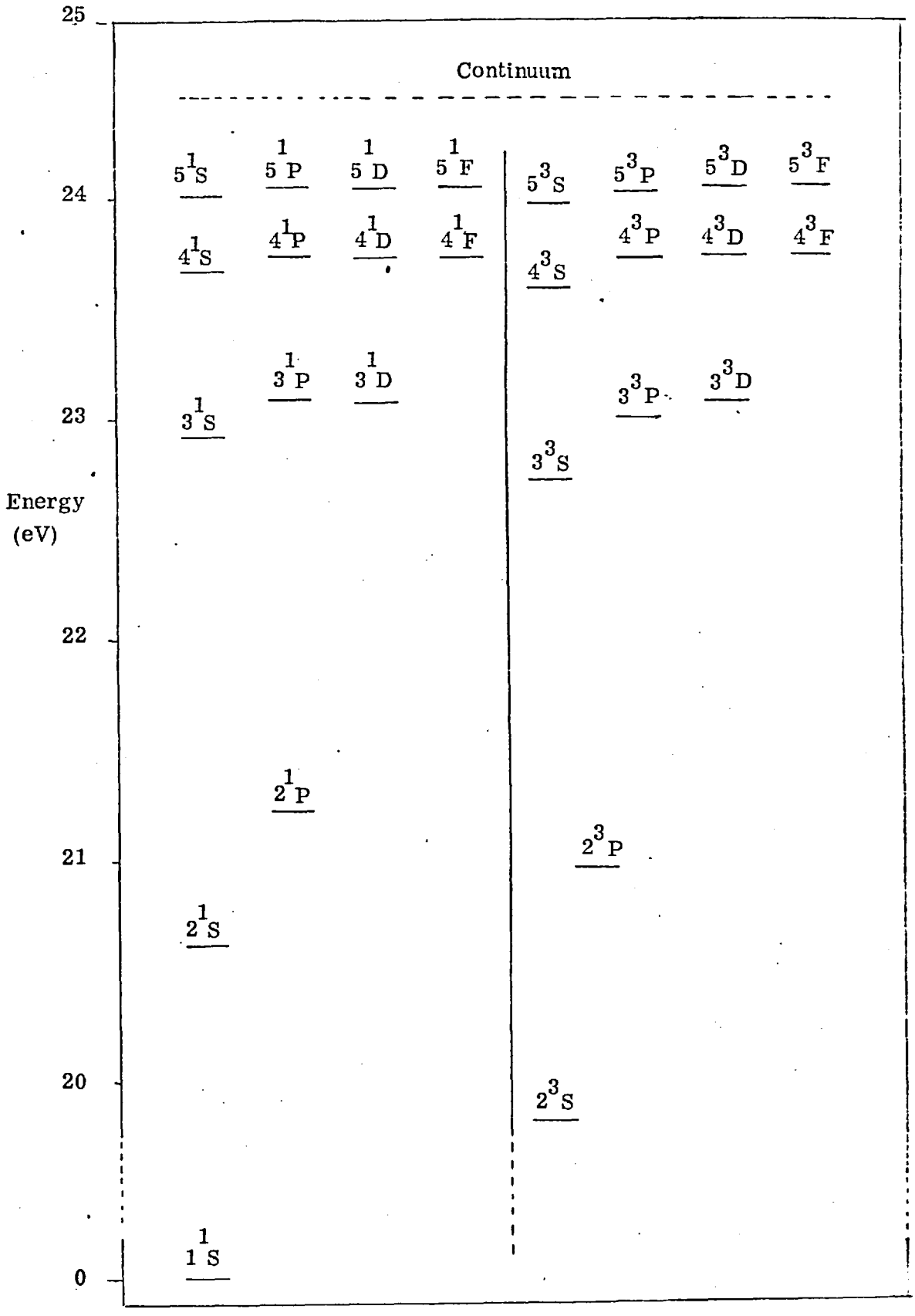

Helium Energy Levels 2^1S — 5^3F (with 1^1S shown not to scale)

CHAPTER VI

THEORETICAL CONSIDERATIONS - TWO OR THREE LEVEL ATOMS

In this chapter the basic theory of laser scattering from two and three level atoms is described. New possibilities for the measurement of collision rates and A-values are discussed. We discuss first the form of the fluorescence expected from a two level atom.

I) Laser Scattering from Two Level Atoms

With conventional low power light sources fluorescence can be described by a simple linear scattering equation.

Fluorescence = Cross section x Intensity input.

However, this no longer holds when the incident light intensity becomes sufficiently high that the stimulated emission probability becomes comparable to the spontaneous emission probability. In this case the level populations tend to become "equalised" or saturated, i.e. are in the ratio of their statistical weights. As the fluorescence is proportional to the excited state population it is clearly limited by this and a situation arises where ever increasing input light intensities do not lead to a corresponding increase in the fluorescence. This intensity level is easily achieved by pulsed lasers. Rayleigh scattering is subject to exactly the same limitation but here the laser intensity required to produce the same scattered flux is much higher than the case of resonance fluorescence.

Laser Power Required for Saturation

(i) Collision rate $\ll$ Radiative Transition Rate.

Mitchell and Zemansky (1934) give the following relation between the stimulated and spontaneous emission probabilities.

$$\frac{A_{21}(\nu)}{B_{21}(\nu)} = \frac{2 h \nu^3}{c^2}$$

where $B_{21}(\nu)$ is the stimulated emission probability at frequency ν in terms of the intensity (assumed isotropic) per unit solid angle per unit frequency interval of unpolarised light. The other symbols have their usual meanings. This leads to :

$$\frac{B_{21}(\lambda)}{A_{21}(\lambda)} = \frac{\lambda^5}{8 \pi c^2 h}$$

where $B_{21}(\lambda)$ is now in terms of the total intensity at wavelength λ, $I(\lambda)$. For the case where $I(\lambda)$ is constant over the atomic line this equation can be integrated to give the total stimulated emission probability W_{21},

$$\frac{W_{21}}{A_{21}} = \frac{\lambda^5 I}{8 \pi c^2 h \Delta\lambda_\ell}$$

where I is now the <u>total</u> light intensity and $\Delta\lambda_\ell$ is the bandwidth of the laser light. We define the intensity, I_{sat}, needed at the saturation threshold, in the absence of collisions by the condition $W_{21} = A_{21}$,

$$I_{sat} = \frac{8 \pi c^2 h \Delta\lambda_\ell}{\lambda^5}$$

(The corresponding formula in Seigman (1971), p.224, appears to be in error by a factor of 3/2)

for $\lambda = 5876 \text{ Å}$ and $\Delta\lambda_\ell = 2.2 \text{ Å}$.

$$I_{sat} = 471 \text{ watts cm}^{-2} \qquad 6.1$$

Note that this is independent of the oscillator strength, atomic line width and neutral atom density.

The intensity of the fluorescence essentially reflects the upper state population and this may be determined by rate equations. We define the population difference, $\Delta N(t)$, by

$$\Delta N(t) = n_1 - \frac{g_1}{g_2} n_2$$

where n_1 and n_2 are the lower and upper state populations and g_1, g_2 their statistical weights. These states are connected by collisional transitions at rates E_{12}, E_{21} and radiative transitions at rates A_{21}, W_{21} and W_{12}.

FIGURE 6.1

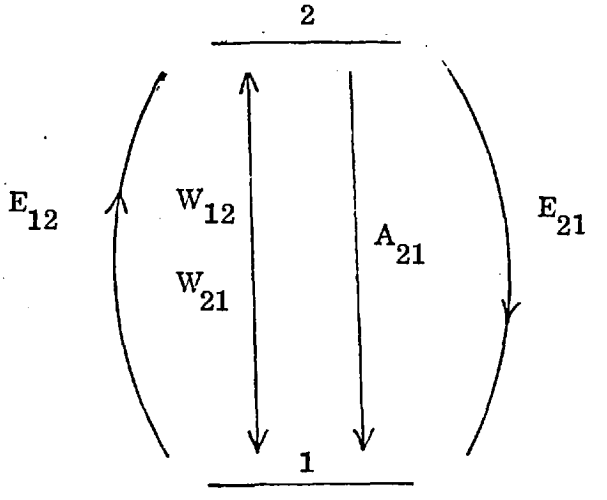

At $t < 0$ we take W_{21}, W_{12} = zero and then $\Delta N(t)$ is at an equilibrium value, ΔN_o.

$$t < 0 \qquad N(t) = \Delta N_o$$

At $t = 0$ we switch the laser on and W_{12}, W_{21} instantaneously assume constant values.

$\Delta N(t)$ is given by

$$\frac{d}{dt} \Delta N(t) = -(E_{21} + E_{12} + A_{21})(\Delta N(t) - \Delta N_o) - W_{21}(1 + \frac{g_2}{g_1}) \Delta N(t)$$

with a solution

$$N(t) = \Delta N_\infty - (\Delta N_o - \Delta N_\infty) \exp -\left\{E_{12} + E_{21} + A_{21} + (1 + \frac{g_2}{g_1}) W_{21}\right\} t$$

where

$$\Delta N_\infty = \frac{\Delta N_o}{1 + \frac{(1 + g_1/g_2) W_{12}}{E_{12} + E_{21} + A_{21}}} \qquad 6.2$$

The steady state solution is plotted in Fig. 6.2 for the case $g_1 = g_2$. We define the saturation threshold by the condition

$$W_{21} = E_{12} + E_{21} + A_{21} \qquad 6.3$$

For the case $A_{21} >> E_{12} + E_{21}$ and say $g_1 = g_2$ this value of W_{12} gives :

$$\Delta N_\infty = \frac{1}{3} \Delta N_o$$

i.e. the population difference is reduced to one-third of its previous equilibrium value.

(ii) Collision Rate $\gtrsim$ Spontaneous Radiative Transition Rate

In this case $E_{12} + E_{21} \gtrsim A_{21}$. The saturation threshold condition is given by equation 6.3. To our knowledge a value of the collisional quenching rate E_{21} for the He $2^3P - 3^3D$ transition is not available in the literature. However an upper limit may be obtained from the calculated Stark line width. The Stark line width cannot be smaller than

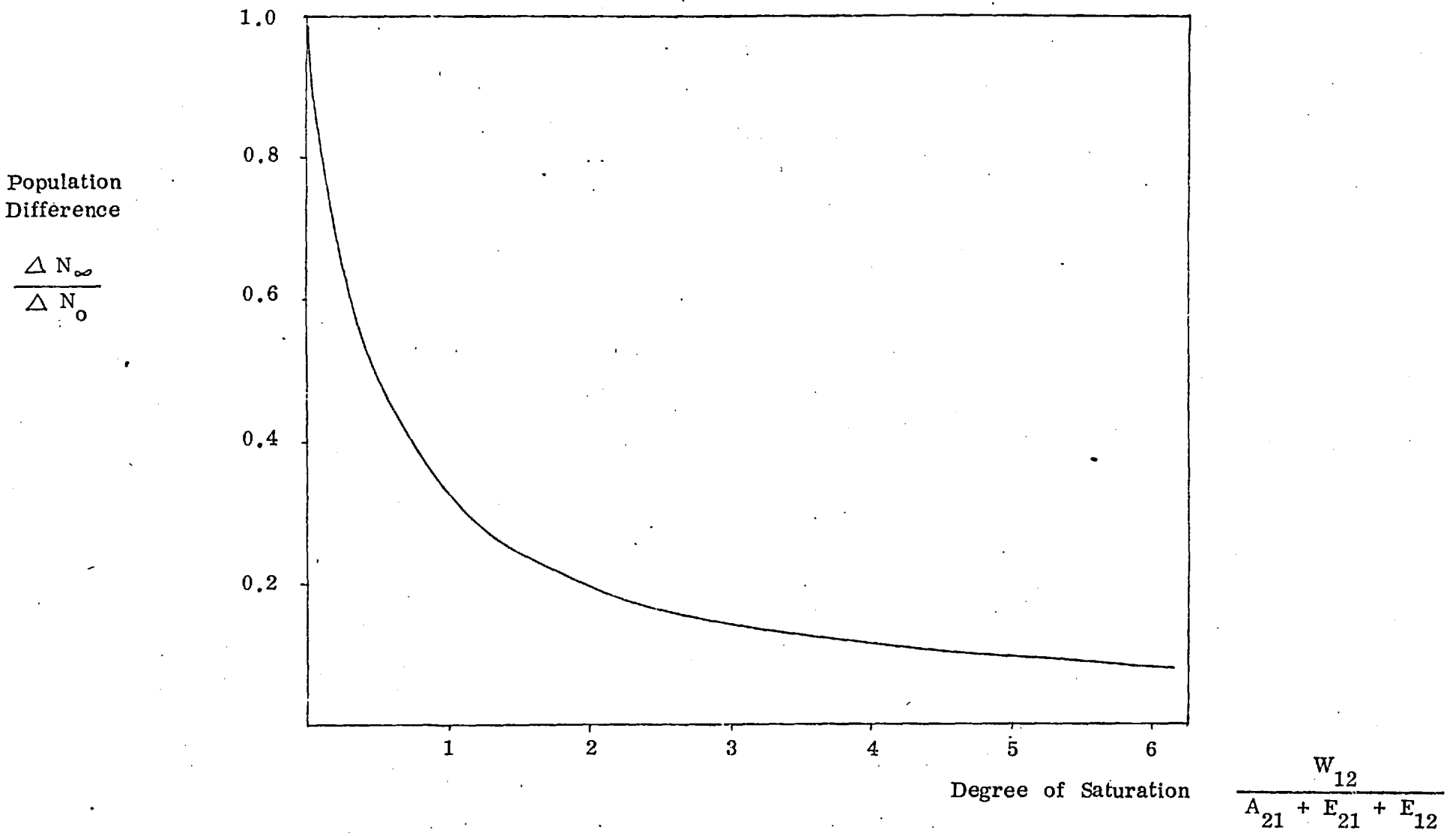

FIGURE 6.2 - STEADY STATE POPULATION DIFFERENCE AS A FUNCTION OF THE DEGREE OF SATURATION

the total (elastic + inelastic) collision frequency. Griem (1964) gives a value of 0.186 Å for the (half) half Stark width of the $2^3P - 3^3D$ transition at an electron density, $n_e' = 10^{16}\ cm^{-3}$ and electron temperature T_e of 10^4 K. In our conditions : $n_e = 10^{15}\ cm^{-3}$, $T_e = 10^4$ K, the (half) half width in angular frequency units is

$$0.186 \times 10^{-10} \times \frac{n_e}{n_e'} \times \frac{2\pi c}{\lambda^2}$$

$$= 1.015 \times 10^{10}\ sec^{-1}$$

According to Sobelman (1972, P.387) this corresponds to the total collision frequency. From detailed balance considerations we estimate the collisional excitation rate to be

$$E_{12} = E_{21} \frac{g_2}{g_1} \exp(-\frac{\Delta E}{kt})$$

$$= \frac{1}{5} E_{21}$$

which is negligible in the present approximation. The upper limit on the saturation condition is therefore

$$W_{12} = A_{21} + E_{21}$$

$$= 0.706 \times 10^8 + 1.015 \times 10^{10}$$

$$= 145 \times A_{21}$$

From equation 6.1

$$I_{sat} = 145 \times 471$$

$$= 68 \text{ kilowatts } cm^{-2}$$

In practice because the major part of the total collision frequency is due to elastic collisions, and collisions between sublevels, the intensity required to saturate is likely to be much less than the above value.

The two level model does not predict any relaxation effects during the laser pulse and is inadequate to describe the observed fluorescence. We now discuss the effects of including a third level in the analysis.

II. Laser Scattering from Three Level Atoms

In this model there is a third level in addition to the two levels interacting with the laser. Before the laser is turned on these levels are in some kind of equilibrium coupled by collisional and radiative processes. When the laser is turned on it redistributes the atoms in levels one and two and the net rate of transfer from levels one and two level three is changed. The levels then reach a new equilibrium in which the total population in levels one and two may be considerably different to that originally.

This may be described by the following simple mathematical model:

Three level model with arbitrary laser intensity

Assume the population of the third level is sufficiently large so that it is unperturbed by changes in the populations of the other two so that there is a constant supply of atoms from level three to levels one and two at rates C_1 and C_2 respectively. C_1 and C_2 include both collisional and radiative processes. The transfer rates per atom (collisional and radiative) from levels one and two to level three are similarly D_1 and D_2. E_{21} and E_{12} are the collisional rates per atom between levels one and two. W_{12}, W_{21} and A_{21} are the usual radiative rates.

FIGURE 6.4

THREE LEVEL MODEL

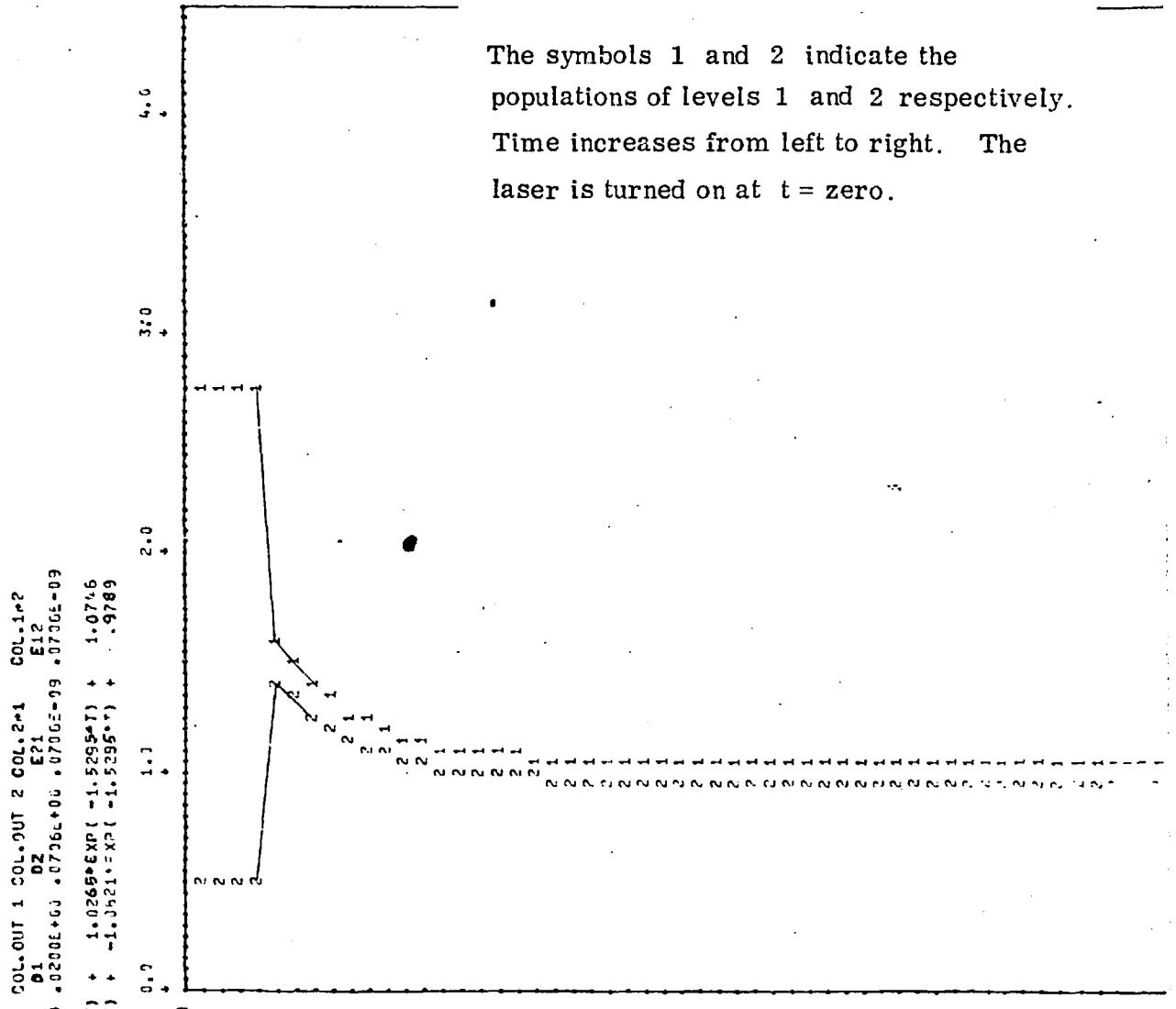

The symbols 1 and 2 indicate the populations of levels 1 and 2 respectively. Time increases from left to right. The laser is turned on at t = zero.

FIGURE 6.3

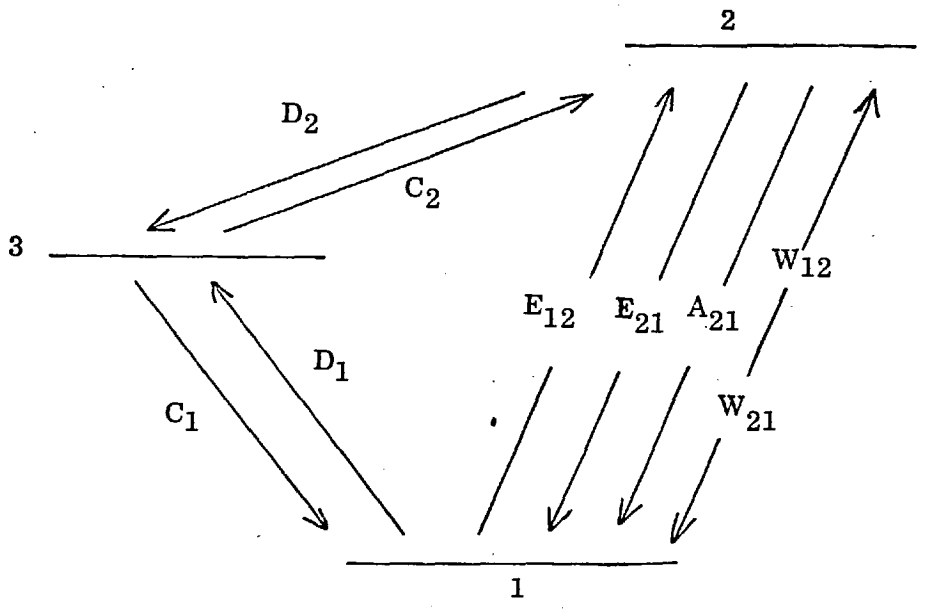

The general solution for the case where the laser intensity in time takes the form of a step function is deduced in Appendix 2. It takes the form -

$$n_2(t) = P.\exp(Lt) + Q.\exp(Mt) + R \qquad 6.4$$

$$n_1(t) = S.\exp(Lt) + U.\exp(Mt) + V \qquad 6.5$$

where P, Q, R, S, U, V are functions of the rates A_{21}, W_{12}, W_{21}, C_1, C_2, D_1, D_2, E_{21}, E_{12}. A similar solution was derived by Measures (1968) in the context of localised plasma diagnostics. Equations 6.4 and 6.5 were plotted with the aid of a computer for various values of the rate coefficients. Fig.6.4 shows one solution which is similar to the observed time history of the fluorescence. The dynamics of the physical processes involved may be easily visualised with the aid of a water tank model (Fig.6.5).

In the case where $D_2 > D_1$ opening the valve between tanks one and two leads to an initial rise in the level of two followed by a fall caused by the increased rate out of one and two taken together.

FIGURE 6.5 - WATER TANK MODEL

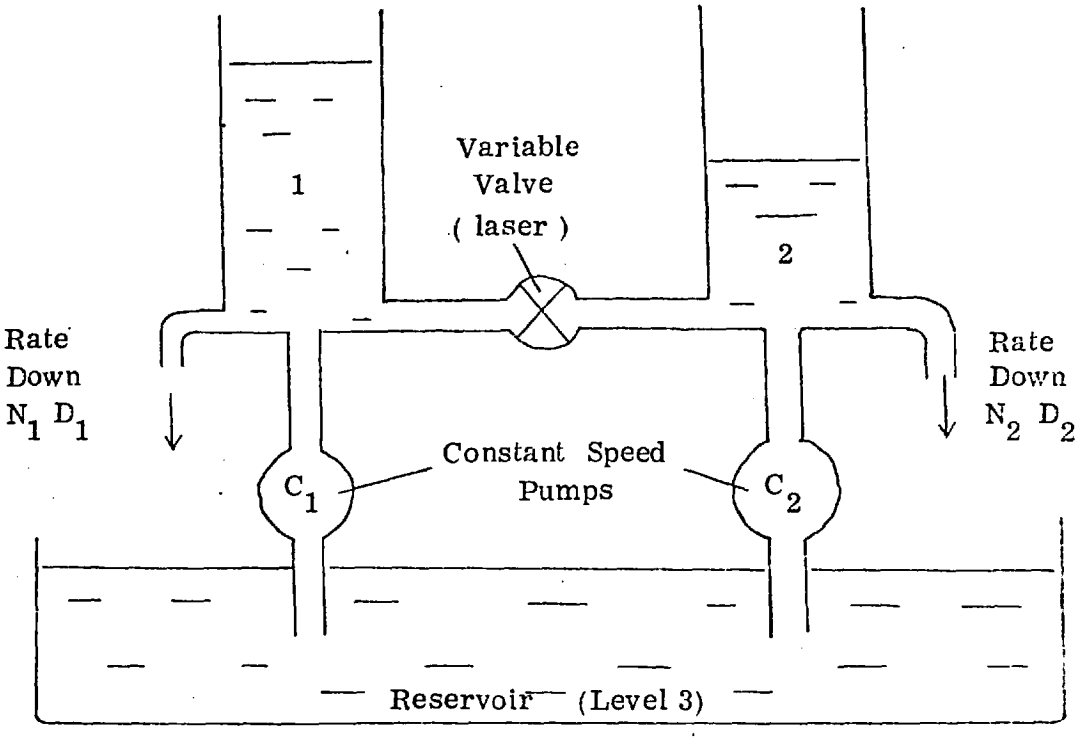

Three Level Model with Laser above Saturation Intensity

The analysis may be much simplified if the laser intensity is sufficient to equalise the populations of levels one and two. Let the laser be turned on at $t = 0$ and instantaneously rise to a value sufficient to saturate the transition. Note that this does not require a very carefully shaped laser pulse provided the saturation intensity is reached rapidly since further variations in intensity for $I > I_{sat}$ do not then alter the populations of levels one and two. Note also one important distinction from other excitation methods whether beam foil, optical or otherwise in that so long as the laser remains on the excitation and decay rates between levels one and two do not enter into the analysis thus simplifying interpretative problems. Let the level populations before the laser is turned on be N_{10} and N_{20}. Then consider the equilibrium situation under the laser illumination for the joint system of the two levels one and two.

$$t < o \qquad C_1 + C_2 = N_{10} \cdot D_1 + N_{20} \cdot D_2 \tag{6.6}$$

$$t > o \qquad N_1(t) = \frac{g_1}{g_2} \; N_2(t) \tag{6.7}$$

We define $$g = \frac{g_1}{g_2}$$

$$\frac{d}{dt} \left(N_1(t) + N_2(t) \right) = C_1 + C_2 - N_1 D_1 - N_2 D_2$$

$$\frac{d}{dt} \; N_2(t) \; (1 + g) = C_1 + C_2 - N_2 (g \cdot D_1 + D_2)$$

with the solution

$$N_2(t) = \left[\frac{N_{10} + N_{20}}{1 + g} - \frac{C_1 + C_2}{g \cdot D_1 + D_2} \right] \exp - \left[\frac{g \cdot D_1 + D_2}{1 + g} \right] t + \frac{C_1 + C_2}{g \cdot D_1 + D_2} \tag{6.8}$$

Using equation 6.4 this may be written -

$$N_2(t) = \left[\frac{(N_{10} - g.N_{20})\ (D_2 - D_1)}{(1+g)\ (g.D_1 + D_2)}\right] \exp - \left[\frac{g.D_1 + D_2}{1+g}\right] t + \frac{C_1 + C_2}{g.D_1 + D_2} \qquad 6.9$$

Hence the fluorescence has two possible forms. If $D_2 > D_1$ the intensity rises very rapidly from the initial background level corresponding to N_{20} to a peak value and then decays exponentially with a time constant determined by both D_1 and D_2 levelling out at a new steady enhanced value for as long as the laser remains on. Or if $D_2 < D_1$ after the initial rise the fluorescent intensity continues rising to a new equilibrium plateau value . (With the exception of lasers, $N_{10} - g\,N_{20}$ is always positive in practice.) In either case the following information is available from a single time history of the fluorescence. The height of the initial spike against the background gives the ratio of the initial populations, $\frac{N_{20}}{N_{10}}$. The exponential decay gives the combined decay rates out of the two levels weighted by their statistical weights since with the laser on decays from one level effect the population of the other level. The final equilibrium gives the ratio of the decay rates determined from the exponential decay to $\frac{C_1 + C_2}{N_{20}}$. Combination of these values with the initial equilibrium equation 6.6 then yields separately D_1, D_2, $\frac{N_{20}}{N_{10}}$, and $\frac{C_1 + C_2}{N_{20}}$.

New Possibilities for Collision Rate Measurement

In discussing the implications of the above analysis one should first point out that the decay of fluorescence radiation has long been used to measure

total decay rates whether collisional or radiative for the upper state of the fluorescing transition and with the advent of high power tuneable dye lasers such measurements have become possible on relatively hot dense plasmas (e.g. Kunze and Burell, 1971). The classical use of fluorescence relies on a short excitation pulse and therefore dye laser systems pumped by ruby, neodymium, or N_2 lasers, or mode locked flashlamp pumped dye lasers, have attracted much attention. However, from the above analysis it is clear that it is unnecessary to use a short pulse since decay rates can still be deduced just as easily from the relaxation of the fluorescence with the laser still on and indeed much more information is then obtained since the fluorescence also yields the decay rate of the lower state of the pumped transition.

In many cases it should be possible to deduce for example the A-value of a VUV resonance line for instance in the first ionisation stage in a coronal plasma by pumping on a visible transition out of the first excited state and thus determining D_1. Previous plasma measurements have not permitted the determination of A-values as opposed to collisional excitation rates for high ionisation stages (for which coronal equilibrium usually applies). Conversely, this technique allows determination of collisional de-excitation rates from first excited states to ground in high density LTE plasmas where spectroscopic measurements normally yield only A-values. The technique also provides information on collisional excitation rates via $C_1 + C_2$.

We now examine the limits on the validity of this model.

Validity of Three Level Model

I. Third Level Population

The population of the level not interacting with the laser is assumed to be sufficiently large that the supply rates C_1 and C_2 may be assumed

constant. For most cases this will be satisfied if the third level corresponds to the ground state or continuum. In the present case these have populations $\times 10^4$ higher than the 2^3P state (Cairns 1970).

II. Very High Laser Intensities

In the quantum theory of particles and fields the total Hamiltonian may be written in two parts corresponding to the radiation field and the particle (see, e.g. Griem 1964). The second part is split into two terms, one independent of the electromagnetic field and one term containing the interaction with light. The last term is considered small and perturbation theory is applied to the time dependent Schroedinger equation to derive the form of the radiative transition probabilities. However at a sufficiently large laser intensity the interaction term will no longer be small and simple concepts like stimulated and spontaneous emission will need correction. We now estimate the laser intensity at which this effect will become important. To avoid lengthy calculations based on quantum field theory we use practical criteria in order to calculate an order of magnitude estimate of the laser intensity required. One possible criterion is to calculate the point at which the electric field due to the laser becomes equal to the electric field between the nucleus and electron, i.e.

$$\frac{1}{4\pi\epsilon_o}\ \frac{e}{a_o^2} = \left(\frac{2P}{\epsilon_o c}\right)^{\frac{1}{2}}$$

where P is the laser intensity in watts m^{-2}

ϵ_o permittivity of free space

a_o bohr radius

e electron charge

c velocity of light

The condition is

$$P = \frac{c}{2} \frac{e^2}{(4\pi)^2 \varepsilon_o a_o^4}$$

$$= \frac{3 \times 10^8 \times (1.6 \times 10^{-19})^2}{32\pi^2 \times 8.85 \times 10^{-12} \times (5.29 \times 10^{-11})^4}$$

$$= 3.5 \times 10^{20} \text{ watts m}^{-2}$$

$$= 10^{16} \text{ watts cm}^{-2}$$

A less demanding criterion is to calculate the laser intensity at which the dynamic Stark shift is equal to the energy spacing between the atomic levels. Bradley (1969) measured a stark shift of $0.075\ \text{cm}^{-1}$ on the potassium 7699 Å line at a laser intensity of 25 Mwatts cm^{-2}. This stark shift is proportional to the square of the electric field (i.e. is linearly proportional to the laser intensity) and is inversely proportional to the energy difference of the two states in the transition. The laser intensity at which a stark shift of 5876 Å is produced in the 5876 Å transition may be extrapolated from the above figures:

$$\text{Laser intensity} = 25 \times 10^6 \times \frac{7699}{5876} \times \frac{\left(\frac{1}{5876 \times 10^{-8}}\right)}{.075}$$

$$= 10^{13} \text{ watts cm}^{-2}$$

This is 9 orders of magnitude above the laser intensity in the fluorescence experiment and clearly the standard quantum theory is valid. (Of course a much lower laser intensity (10^9 watts cm^{-2}) would shift the atomic line to a wavelength at the edge of the laser spectrum and so cause considerable complications). However, in practice the laser intensity is far below this value. For an account of the laser-atom interaction at ultra high ($>10^{17}$ watts/cm^2) laser intensities see Geltman et al. (1974).

III Laser Coherence Effects

In the three level theory outlined above the coherent nature of the laser illumination was not taken into account. McIlrath and Carlsten (1972) have examined the conditions in which laser excitation of atomic systems may be considered as a simple two-body process. They conclude that as long as the dephasing time of the atomic system is sufficiently short coherence effects of the kind discussed by Dicke (1954) and Arecchi et al. (1970) do not occur and the laser-atom interaction reduces to a two-body collision. The dephasing time is the average time an atom remains in the quantum state to which it has been excited by the laser. This time must be short compared to the time required for the laser to equalise the relevant atomic level populations. In the present case the dephasing time is given by the electron impact line width which is comparable to the total stark width of 10^{10} sec^{-1}, corresponding to a time of 10^{-10} sec. The time taken to equalise the level populations is the fluorescence rise time of 1.5×10^{-8} sec. Clearly in the present case the effects of the laser coherence are negligible. (See also P.97).

Theory of Absorption at High Light Intensities

The fluorescence is dependent on the local laser intensity at the point observed in the plasma. The laser intensity in the plasma is a function of the absorption coefficient. The intensity is given by the equation of radiative transfer:

$$\frac{dI}{dx} = -KI + j \qquad (6.10)$$

where K is the effective absorption coefficient (including stimulated emission)

j is the intensity of the spontaneous emission.

In general j and K are functions of I and an exact solution is difficult to obtain. In the next chapter we describe experimental measurements of the intensity of the laser beam observed after transmission through the plasma. The geometry of the experimental set up allows us to make some simplifying assumptions regarding the spontaneous emission term in the radiative transfer equation. At laser intensities far below saturation the spontaneous emission intensity is unaffected by the laser as the laser does not significantly perturb the level populations. We may subtract the spontaneous emission from the total intensity observed and the solution for the laser intensity alone yields an exponential decay with distance.

At laser intensities in the region of the saturation threshold and above, the observed intensity is dominated by the laser. The energy absorbed from the laser beam reappears as spontaneous emission and as kinetic energy from inelastic collisions involving the laser excited state. Even if all the energy is re-emitted as spontaneous emission only a small fraction (10^{-3} in the present case) is emitted in the direction of the laser beam and hence does not contribute significantly to the intensity observed. We therefore neglect the term j in equation (6.10). Spontaneous emission is not entirely neglected as it is implicit in the definition of K. For a finite value of K, with steady state plasma conditions, the energy lost from the laser beam must reappear as spontaneous emission; the essential point is that most of this is not observed in the direction of the laser beam.

$$\frac{dI}{dx}(x,\nu) = K(\nu)\ I(x,\nu)$$

where $K(\nu)$ the absorption coefficient is given by: (Griem 1964, P.173) :

$$K(\nu) = k(\nu)\left[1 - \frac{g_1}{g_2} \times \frac{N_2}{N_1}\right] \qquad (6.11)$$

$k(\nu)$ is the small signal absorption coefficient for the low temperature ($g_1 N_2 \ll g_2 N_1$) case.

$$k(\nu) = 2\pi^2 r_o c f_{21} N_1 L(\omega) \tag{6.12}$$

with r_o classical electron radius.

f_{21} oscillator strength.

N_2 (N_1) the upper (lower) state population.

g_1 (g_2) the upper (lower) statistical weight.

$L(\omega)$ the normalised line shape.

We use the result

$$\Delta N_\infty = \frac{\Delta N_o}{1 + \frac{(1 + \frac{g_2}{g_1}) W_{21}}{E_{12} + E_{21} + A_{21}}} \tag{6.2}$$

here ΔN is the population difference

$$\Delta N = (N_1 - \frac{g_1}{g_2} N_2)$$

The subscripts o and ∞ correspond to $t < o$ before the laser is turned on and t with the laser on. We use a two level model with $N_1 + N_2$ constant and N_{20} = zero.

$$\frac{\Delta N_\infty}{\Delta N_o} = \frac{N_{1\infty} - g_1/g_2 \; N_{2\infty}}{N_{10}}$$

$$= \frac{N_{1\infty} - g_1/g_2 \; N_{2\infty}}{N_{1\infty} + N_{2\infty}} \tag{6.13}$$

Combining equations 6.2 and 6.13 we have

$$1 - \frac{g_1}{g_2} \frac{N_{2\infty}}{N_{1\infty}} = \frac{1}{1 + I} \tag{6.14}$$

where I is the laser intensity expressed in dimensionless units :

$$I(x) = \frac{W_{21}(x)}{E_{12} + E_{21} + A_{21}}$$

$I(x)$ is also known as the degree of saturation. From equation (6.14)

$$K(\nu) = \frac{k(\nu)}{1 + I(x)}$$

$$\frac{dI(x)}{dx} = \frac{I(x)}{1 + I(x)} \; k(\nu)$$

The solution at $x = L$ is given by

$$\int_{I_{in}}^{I_L} \frac{1 + I(x)}{I(x)} = - \int_{o}^{L} k(\nu)\, dx$$

$$\ln \frac{I_L}{I_{in}} + I_L - I_{in} = - k(\nu) L \qquad (6.15)$$

In the limit $I \ll 1$ the equation becomes

$$\ln \frac{I_L}{I_{in}} = - k(\nu) L$$

the standard small signal result for the case where I does not include spontaneous emission. For $I > 1$ we have

$$I_L - I_{in} = - k(\nu) L$$

a linear fall of intensity with distance. This is due to the energy lost by spontaneous emission. As there is no simple analytic solution to the complete equation (6.15) it was necessary to substitute various trial values of I_{in}, I_L in the equation and a graph was plotted of those values which fitted to better than 1%. A solution was plotted for the case of small signal optical depths ($k(\nu) L$) of 14, 5 and 1.4. (Fig. 6.6).

The solution for optical depth = 1.4 is discussed in Chapter XII. The case for optical depth = 14 corresponds to the 5876 Å transition at delays of

FIGURE 6.6

THEORETICAL LASER TRANSMISSION

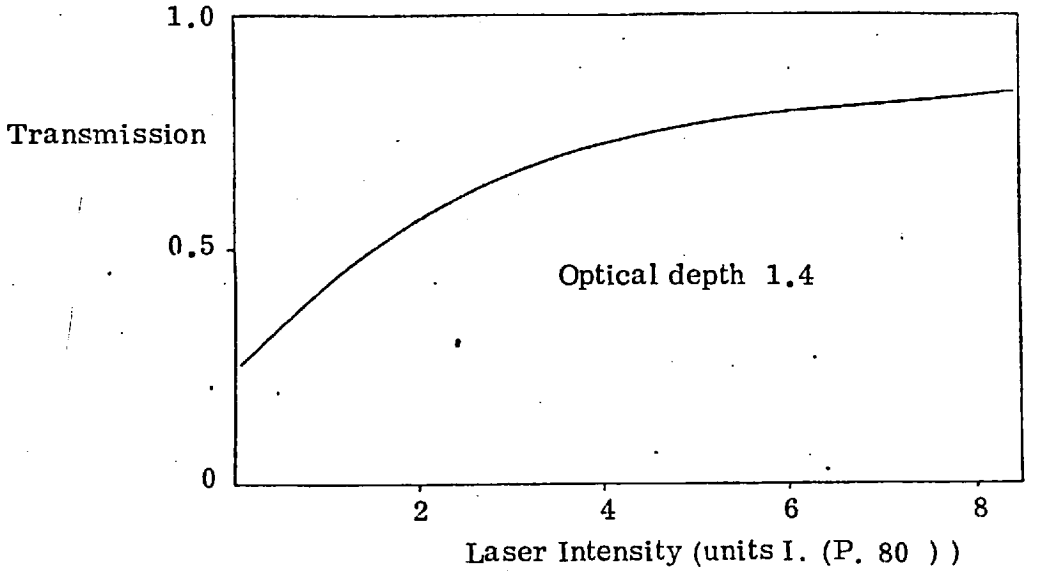

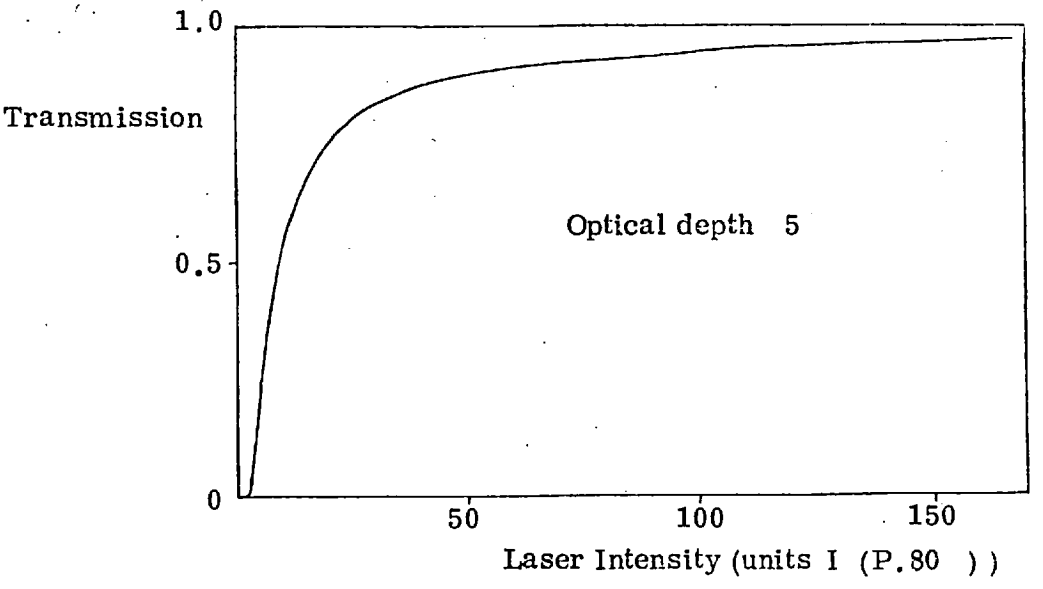

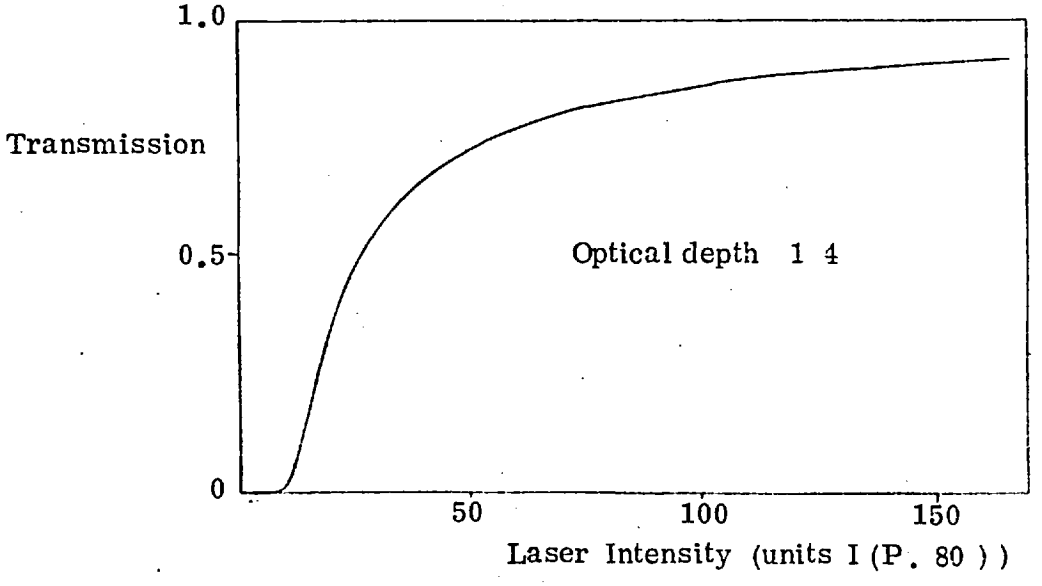

30 and 60 μS and $k(\nu) = 5$ to a delay of 100 μS after peak current (Chapter XI).

This theory suffers from several limitations. First it is only applicable to a two level atom in the presence of a constant laser intensity. In practice the presence of additional atomic levels and the finite laser duration will lead to departures from this model. In addition, equation 6.2 is only valid if the laser spectrum is constant over the atomic line. This will only be a good approximation when the laser transmission is high, i.e. the laser intensity is above saturation. On the other hand for the case where the laser intensity is below saturation equation 6.2 has little effect on the solution (equation 6.15) and so in general equation 6.15 is valid for laser intensities above or below saturation but not in the region of the saturation threshold. An exact general solution is difficult to obtain but it is hoped that the above model is of assistance in visualising the physical processes occurring. Fortunately, in practice, laser intensities above saturation are not difficult to attain.

CHAPTER VII

EXPERIMENTAL MEASUREMENTS OF THE DEGREE OF SATURATION

The most straightforward method of estimating the "degree of saturation" is to record the fluorescence over a range of laser intensities. Above saturation the fluorescence should be more or less independent of the laser intensity. In the present case this picture is complicated by optical depth considerations.

Fluorescence as a Function of Laser Intensity

Fluorescence traces were recorded over a range of laser intensity. This was done at delay times of 30, 60 and 100 μS. Figs. 9.1 and 9.2 show a plot of the peak intensity (and plateau intensity for the 30 μS case) and the duration of the fluorescence as a function of laser intensity. With increasing laser intensity the fluorescence intensity first rises rapidly and then becomes relatively insensitive to further increases in laser intensity. At low laser intensities the fluorescence duration (F.W.H.M.) tends to a value of 300 nS corresponding to the laser duration, the fluorescence resembles the shape of the laser pulse and the "spike" observed at high intensities is no longer apparent (Plate V). The fluorescence intensity in the plateau region is less dependent on the laser intensity than the fluorescence peak.

These results suggest that at the intensities normally used in the fluorescence measurements the laser intensity is sufficient to saturate the transition. However a quantative assessment must take into account the opacity of the 5876 Å transition.

FIGURE 7.1 - FLUORESCENCE AS A FUNCTION OF LASER INTENSITY

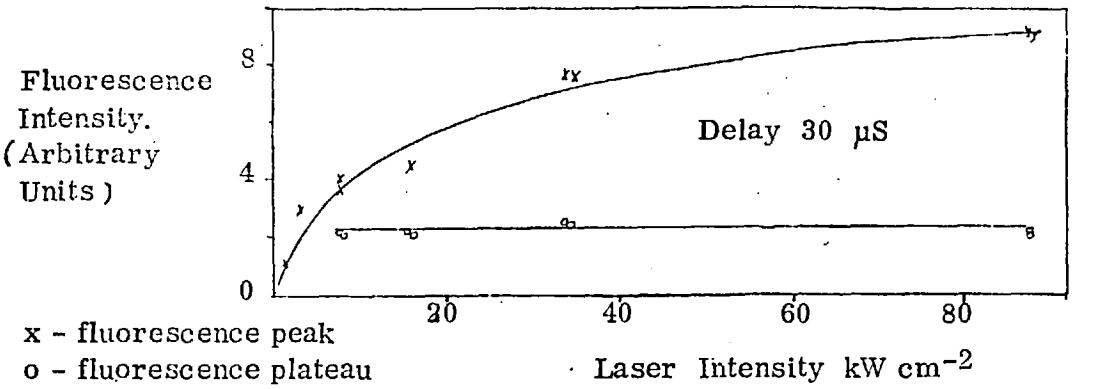

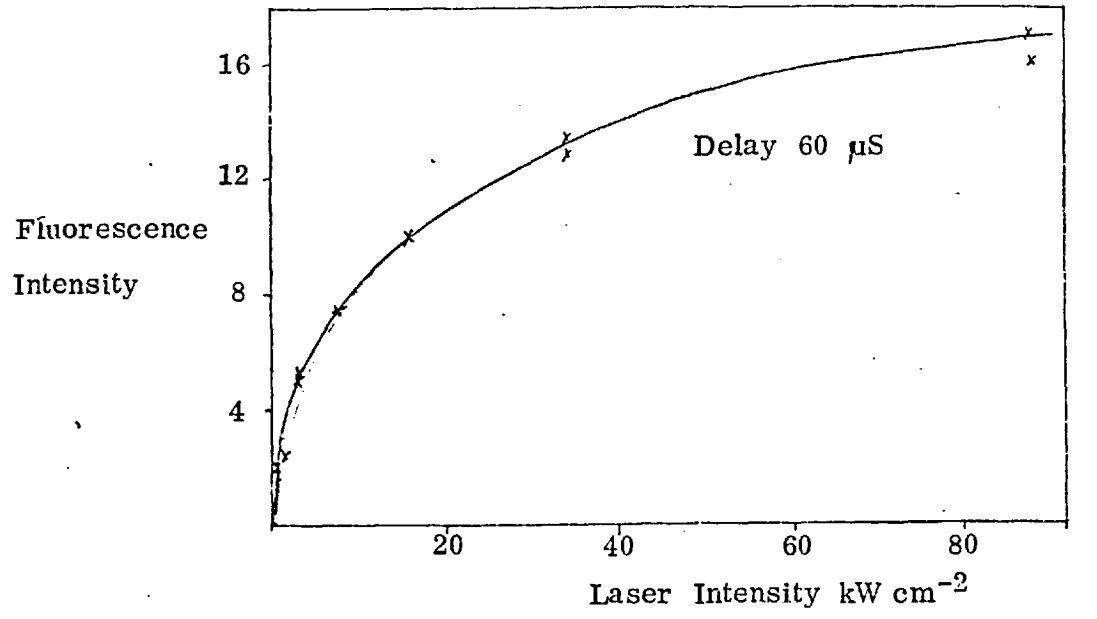

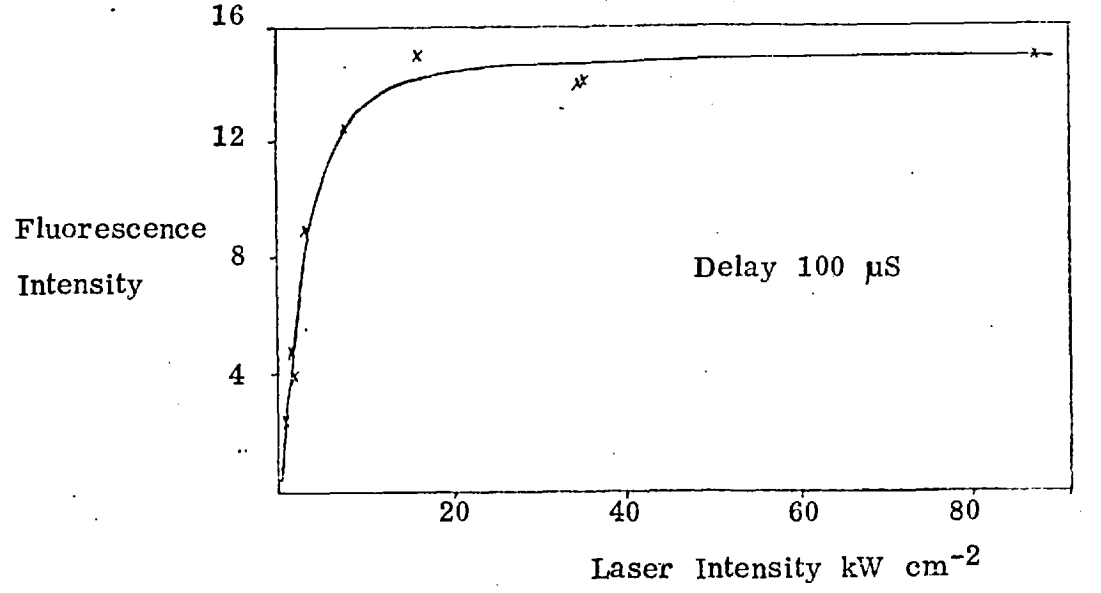

FIGURE 7.2 - FLUORESCENCE DURATION AS A FUNCTION OF LASER INTENSITY

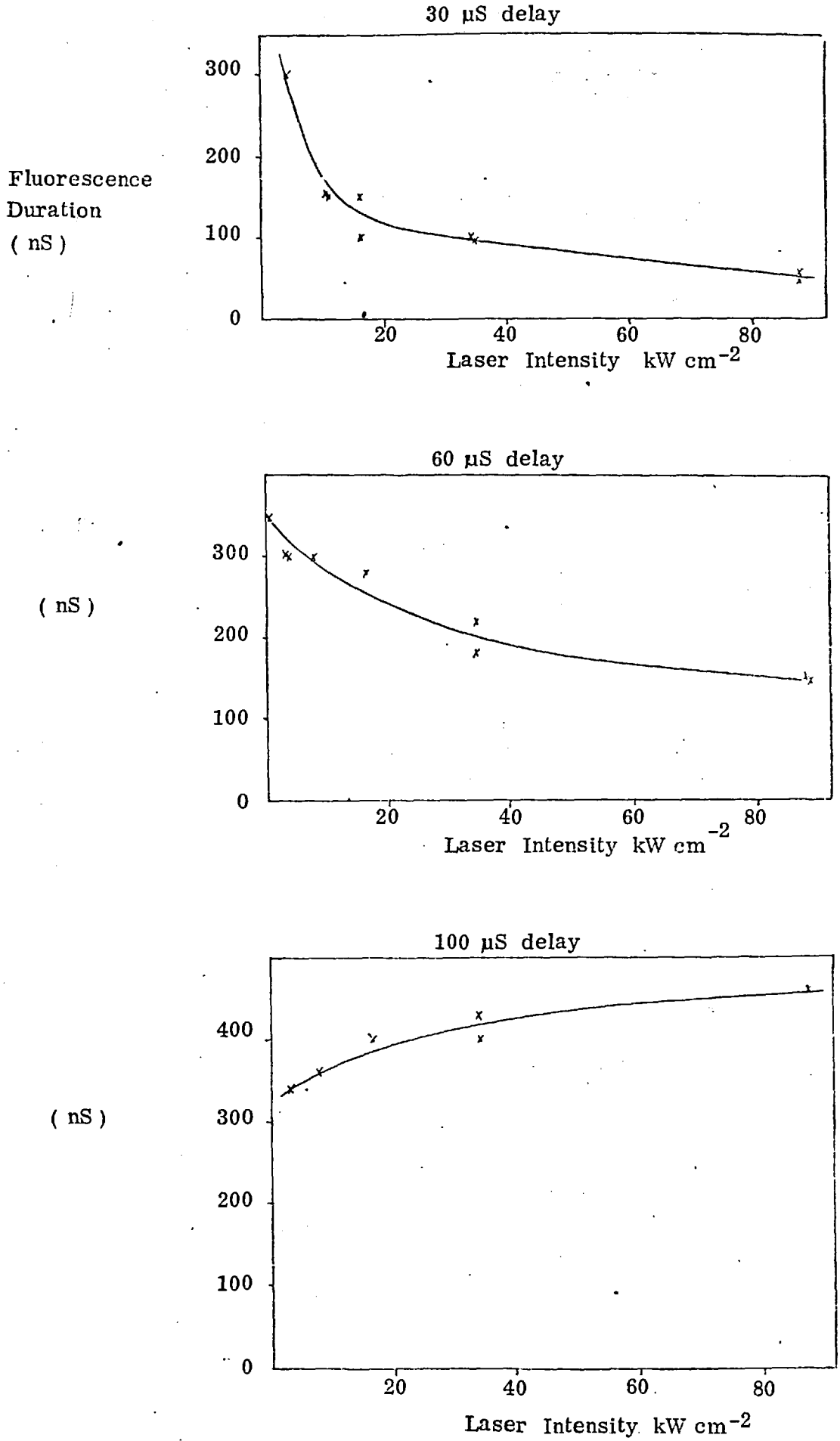

5876 Å Transition Optical Depth

A simple absorption experiment revealed that, in the absence of the laser illumination, the optical depth, sampling the central 0.3 Å of the line, was 1.0 across the 5 cm diameter of the discharge. This corresponds to an optical depth of 14 along the 70 cm long axis of the discharge.

Laser Transmission

The transmission of the laser beam by the plasma was measured under a range of plasma conditions. ' A quartz window was substituted for the beam dump and the monochromator position changed so that it viewed light emerging down the pinch axis. The optical arrangement used by Mahon (Ph.D. thesis 1973) was adopted for this (Fig. 7.3).

Figure 7.3 - Collection Optics used in Laser Transmission Experiments.

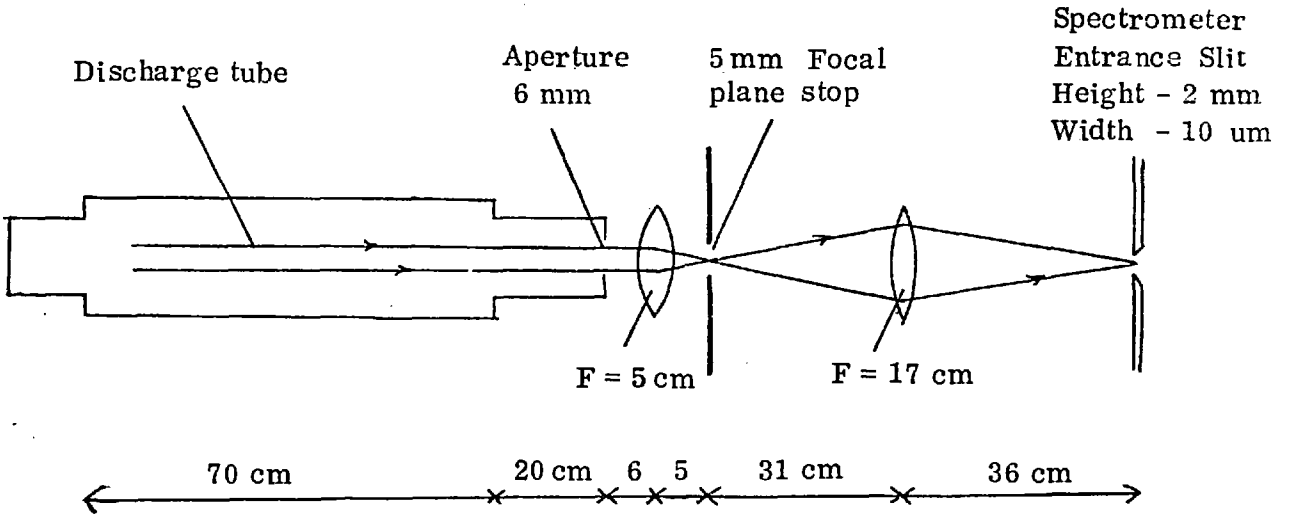

The monochromator slits were set so that the instrumental width (F.W.H.M.) was 0.18 Å to isolate the absorption from the surrounding laser continuum. The instrument function was measured using the Cd 5145 Å line and no light was detected beyond 0.3 Å from line centre. Neutral density filters were

placed before and after the pinch to control the laser intensity inside the pinch and also to prevent overloading of the photomultiplier. The peak transmitted laser intensity was measured at different delay times. Fig.7.4 shows the laser transmission as a function of laser intensity. The time history of the laser intensity also changed on transmission through the plasma. The overall shape remained the same but the F.W.H.M. duration was reduced by up to 50 nS, the largest reductions occurring at low laser powers. By triggering the oscilloscope time base with the signal from the laser monitor photodiode and comparing the transmitted laser time history with and without the plasma it could be seen that this reduction originated both at the beginning and end of the laser pulse.

Estimate of the Degree of Saturation

Comparison of the theoretical and experimental results, Figs.6.6 and 7.1, lead to an estimate of the degree of saturation (I), (P.80) corresponding to the experimental laser intensity. In this way a power level of 40 kW cm^{-2} can be seen to correspond to :

I = 53 at 30 μS delay.

50 " 60 μS "

33 " 100 μS "

It is surprising at first to find the degree of saturation higher at earlier times in the recombination phase when the collisional quenching rate should be high. However the present treatment is only valid for two level atoms. As we have seen the observed fluorescence indicates that the presence of other levels cannot be ignored. The fluorescence decay observed at delays of 30 and 60 μS is due to the loss of atoms from the levels interacting with the laser, to the third level. This will clearly lead to a reduction in the

FIGURE 7.4 - EXPERIMENTAL LASER TRANSMISSION

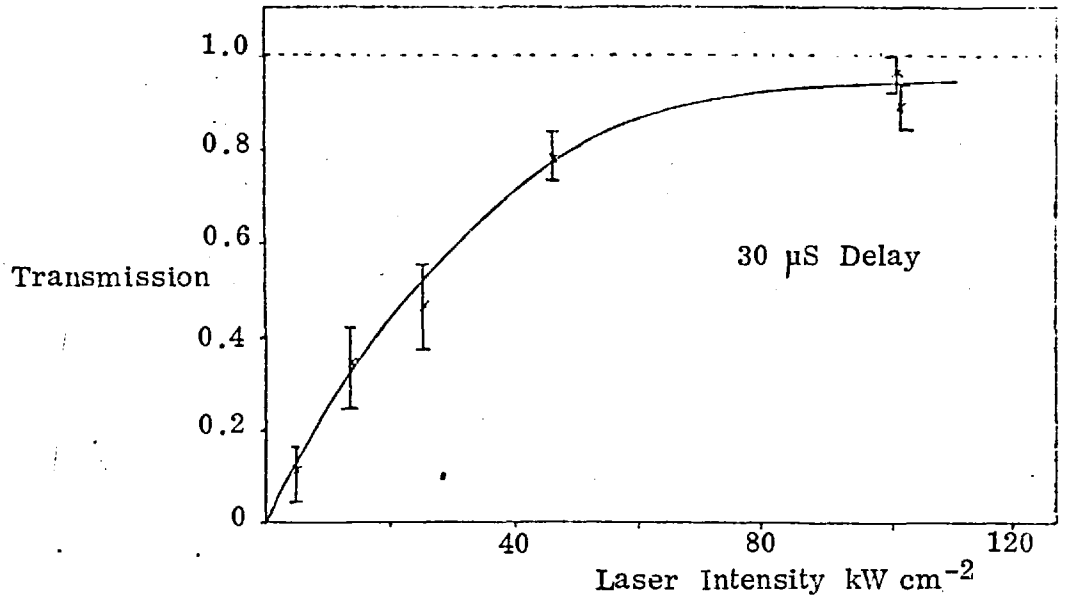

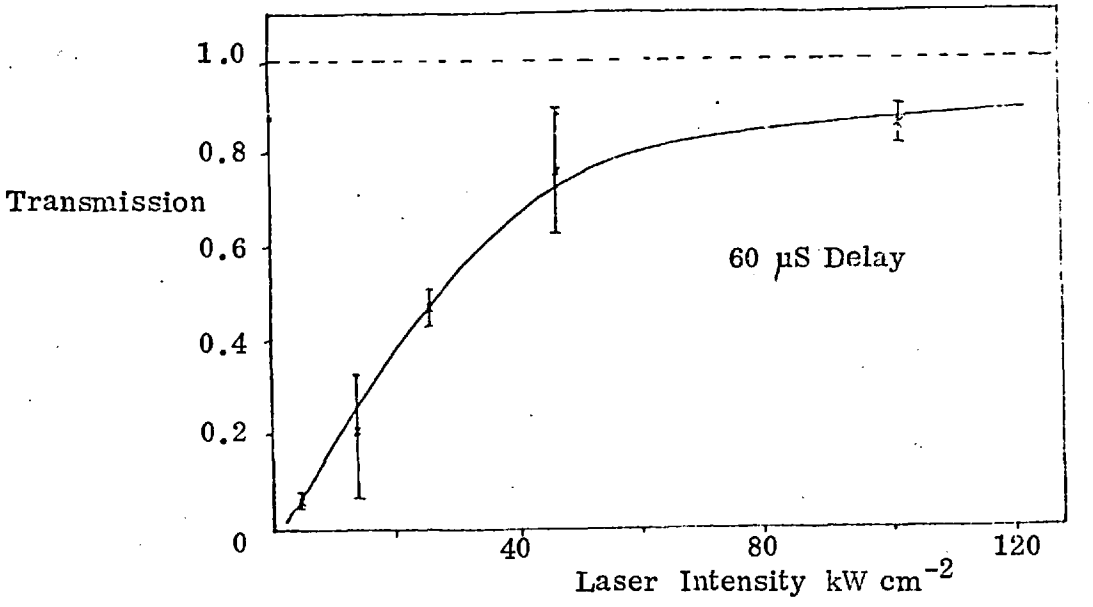

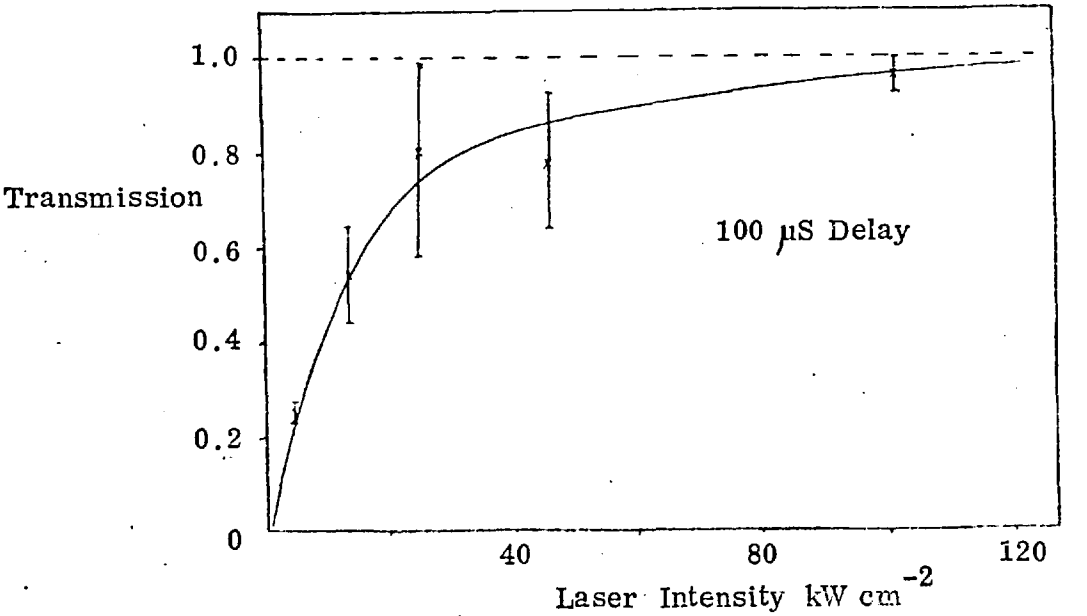

absorption experienced by the laser and is the reason for the high values of the estimated degree of saturation at early times. This is true even if the laser is below saturation. Here the small upper state population has little effect on the absorption. Loss of atoms from the levels interacting with the laser will lead to a reduction in the absorption due to the reduced lower state population.

At 100 μS delay there is little fluorescence relaxation and the two level model is valid. Taking the value $I = 33$ as being essentially correct we estimate the degree of saturation at earlier times by assuming the quenching rate to be proportional to the electron density. This gives a value of $I = 11$ and $I = 22$ at 30 μS and 60 μS delay respectively.

Time Dependent Effects

In addition there will be other time-dependent effects because it takes a finite time for the laser to change the level populations. A rough estimate of this time may be made in the following way. At the instant the laser is turned on (assumed to be a step function in time), but before the level populations have changed, the distance, y, the laser beam travels before it is reduced to the saturation threshold value is given by

$$y = \frac{\ln (I)}{k(\nu)}$$

We assume that inside this region the laser is unattenuated and calculate the time needed to change the level populations (roughly given by $\frac{1}{2 W_{12}}$ for large W_{12}). Assume that this time must elapse before the laser intensity can penetrate to the next region from y to $2y$ where the same process will be repeated. In this way the time delay experienced by the laser beam in travelling a distance, L, may be estimated as

$$T_{delay} = \frac{L}{y} \quad \frac{1}{2 W_{12}}$$

For our case : $L = 70$ cm, $I = 10$, $k(\nu) = 0.2\ \text{cm}^{-1}$, $\frac{1}{2W_{12}} \leqslant 0.7$ nS and the maximum delay is 5 nS. As we have seen the delays experienced were larger than this. The explanation arises from the saturation process emphasising the peak in the laser intensity time history and in addition the relaxation effects already discussed, reducing the absorption during the laser pulse. The delay in the laser rise at 60 μS delay was longer than the delay at 30 μS, supporting this contention.

Laser Intensity inside the Plasma

The change in the laser beam due to the plasma at the point in space where the fluorescence is observed will, of course, be only about half of the changes described above. In fact, for the laser intensities normally used in the fluorescence experiments the reduction in laser pulse length and intensity was at worst only 10% at this point. In view of the fact that the saturation factor was at least 10 this could have very little effect on the fluorescence.

In addition to reducing the rise and fall times of the laser the absorption will also affect the edges of the laser beam leading to a spatial intensity distribution that is even more well defined than that given on Fig.4.4.

Finally, it should be noted that the above model does not take into account the wavelength variation in the laser intensity caused by the absorption. The theoretical degree of saturation worked out above will need adjustment due to enhanced contributions to W_{12} from the line wings where the laser absorption is less. The experimental value of the degree of saturation arried at with the existing graphs will therefore be an over-estimate. As the absorption at line centre for the laser intensity used in the calculation of I was only 30% this does not add significantly to the existing uncertainties.

In conclusion

1) The high optical depth of the 5876 Å transition causes severe attenuation of the peripheral low intensity regions of the laser spatial intensity distribution, increasing the degree of collimation of the laser beam. It also attenuates the leading and trailing edges of the laser time history slightly shortening the laser pulse.

2) The small absorption of the central part of the laser beam leads to slightly reduced fluorescence intensity. The amount of this absorption is reduced by relaxation effects in the atomic level populations.

3) The laser intensity used in the fluorescence experiments corresponds to a degree of saturation of at least 10 and the simplified model of the fluorescence described on Page 73 is a very good approximation to the experimental conditions.

CHAPTER VIII

FURTHER FLUORESCENCE RESULTS

Preliminary fluorescence results were described in Chapter V. In this chapter we describe further experiments designed to reveal all the experimentally accessible aspects of the fluorescence.

Geometric Effects

To explore the possibility of any unexpected geometric effects the area in the pinch illuminated by the laser was changed by adjusting a variable iris immediately in front of the pinch. Over a range of plasma conditions (30, 60, 100 μS delay) the fluorescence intensity proved to be proportional to the illuminated volume as expected (Fig. 8.1). This is also further evidence for the homogeneous nature of the plasma.

Spectral Distribution of the Fluorescence

To obtain the optimum signal to noise ratio the monochromator slit width was normally set at 100 μ.m. giving an instrument function of width 1 Å (F.W.H.M.). The predicted line width of the 5876 Å transition is 0.3 Å (F.W.H.M.) and so the observed fluorescence originated from the whole 5876 Å line.

To obtain the spectral distribution of the emission and fluorescence of the 5876 Å line the slits were narrowed to 10 μm. Previous work had shown this to give an instrument function of width 0.18 Å (F.W.H.M.). However, it was later discovered that the exit slit jaws had become misaligned and the instrument width was then measured to be 0.27 Å. This was subsequently corrected but in this experiment the instrument width was 0.27 Å (F.W.H.M.). The spectral distribution of the fluorescence was obtained using three different techniques by varying the monochromator wavelength setting and/or the laser wavelength.

FIGURE 8.1 - FLUORESCENCE INTENSITY v. ILLUMINATED VOLUME

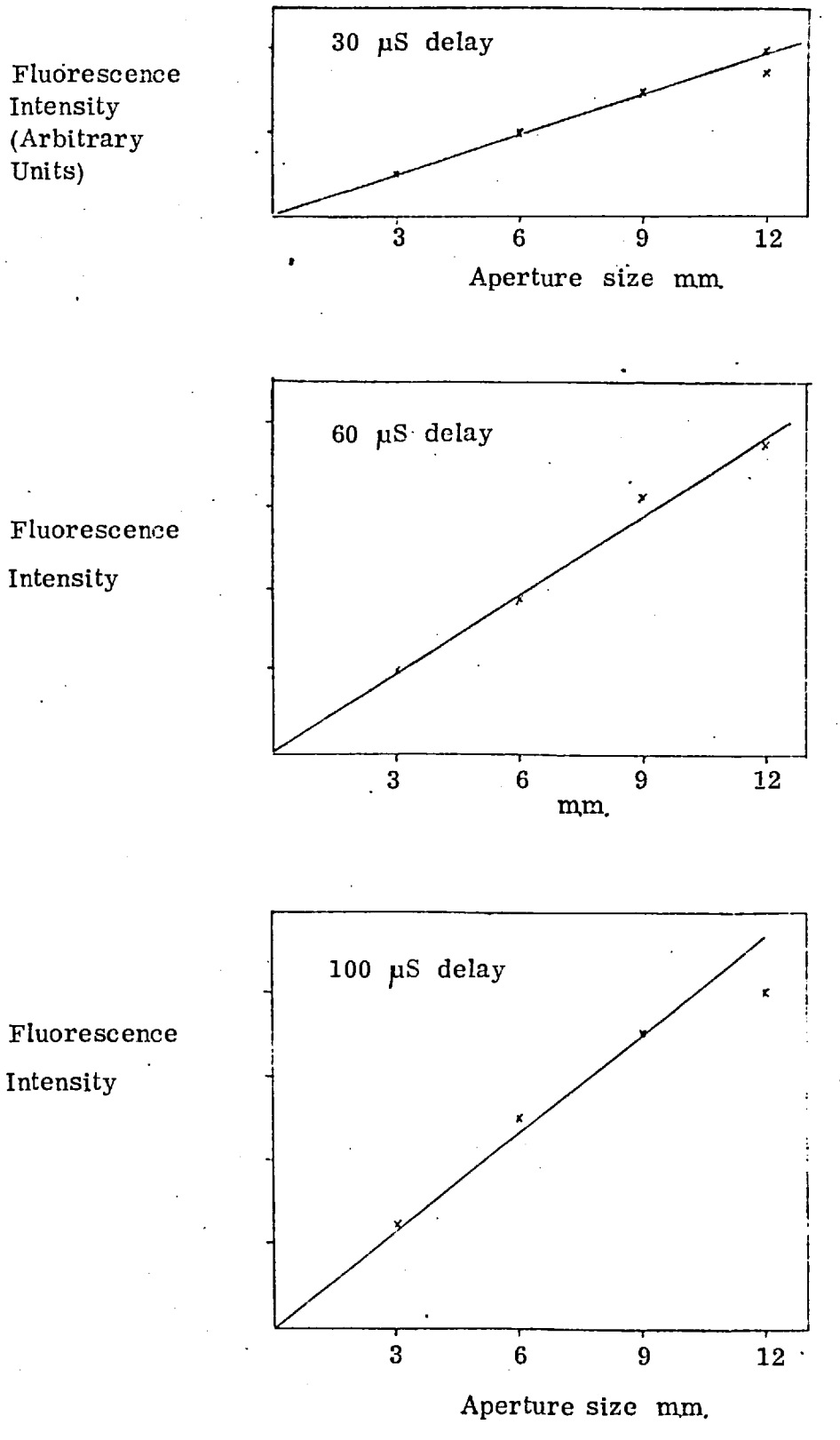

Method (i)

The monochromator setting was left fixed at line centre while the laser wavelength was scanned across the line. A line profile was obtained on a shot to shot basis. This is really another form of the fluorescence v. laser intensity experiment (P. 84). The experiment was done at a 100 μS delay time. The line profile obtained (Fig. 8.2) had a F.W.H.M. of 7 Å as compared to the width of the laser spectrum of 2.2 Å F.W.H.M. confirming that the laser intensity was above the saturation threshold. In the line wings the fluorescence had a shorter duration corresponding to the lower laser pulse length in the line wings.

Method (ii)

The monochromator wavelength setting was varied leaving the laser wavelength fixed at line centre.

Method (iii)

The monochromator wavelength setting and the laser wavelength were simultaneously scanned across the 5876 line, the wavelength setting of both being equal at any one time. A line profile was obtained on a shot to shot basis.

Methods (ii) and (iii) yielded the same results. This was expected as the fluorescence is produced by the centre of the laser line where the intensity is relatively independent of wavelength. The fluorescence was also compared to the ordinary emission profile at 100 μS delay and the two were found to be identical (Fig. 8.3). (These line profiles have not been deconvolved with the instrument function). A scan across the fluorescence line at 30 μS delay also revealed no large scale wavelength dependence in the time history of the fluorescence.

The 5876 Å line is predominantly doppler broadened with a calculated (whole) half width of 0.23 Å at 30 μS delay ($n_e = 10^{15} cm^{-3}$, $T_e = 1$ eV).

FIGURE 8.2 - FLUORESCENCE LINE PROFILE : METHOD (i)

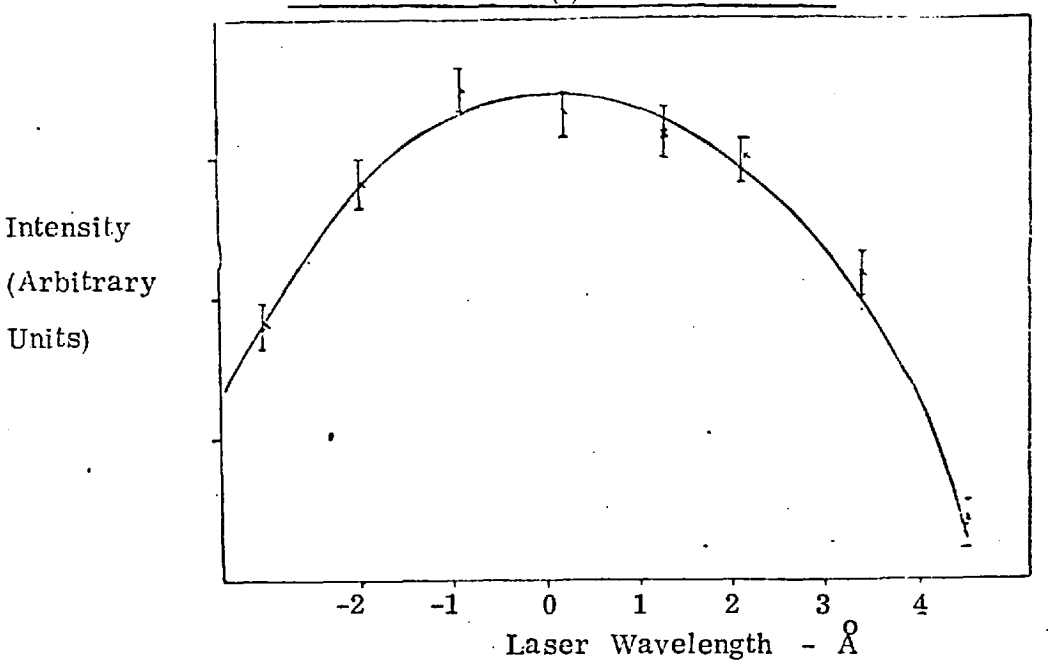

FIGURE 8.3 - FLUORESCENCE LINE PROFILE : METHOD (ii)

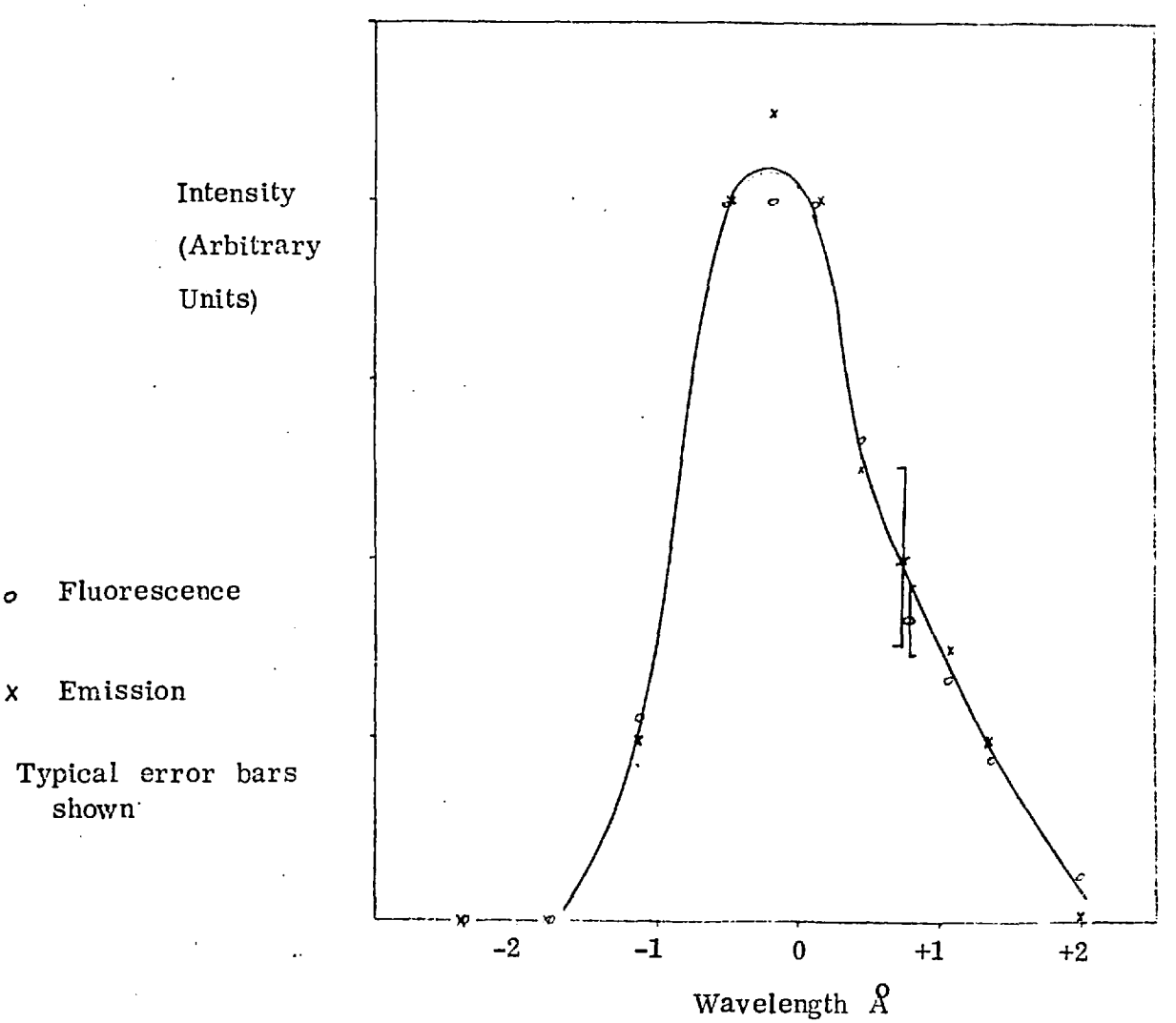

The calculated (whole) half stark width for the same conditions is 0.037 Å (Griem 1964). Under these circumstances no difference in the emission and fluorescence line profiles was expected but it is noteworthy that the signal to noise ratio for the fluorescence is $2\frac{1}{2}$ times better than for the emission line profile.

The 5876 Å line has fine structure with the main components in two groups 0.37 Å apart. In a helium lamp the longer wavelength component is about 10% of the intensity of the other component. This accounts for the slight asymmetry in the line profiles.

The Polarisation of the Fluorescence

The degree of polarisation of the fluorescence was measured by interposing "polaroid" polarising filters in the fluorescence collection optics. The polarisation produced by reflection at the aluminised mirror (Fig.4.2) was corrected for by measuring the apparent degree of polarisation in the light from a helium lamp. No sign of polarisation (< 5%) was detected in the fluorescence. Even though the laser is of random polarisation the fluorescence might be expected to be polarised as it is observed in a direction at 90^{o} to the laser beam and the laser cannot excite a dipole whose axis is in line with the direction of the laser beam. The absence of any polarisation in the fluorescence implies a high rate of depolarising collisions. This confirms that the dephasing time, as discussed by McIlrath and Carlsten (1972), is short enough to enable us to neglect any effects due to the coherent nature of the laser illumination.

Fluorescence "After Effects"

As may be seen in Plate V, the emission intensity at the end of the laser pulse does not always coincide with the value of the emission recorded in the absence of the laser illumination. In some

cases this may be simply due to a small degree of irreproducibility in the plasma emission. However by observing the fluorescence traces with the oscilloscope set to high voltage sensitivity but long time scales it was observed that the plasma emission did not always regain its original value immediately after the laser pulse. For delay times in the 60 - 80 μS range it remained enhanced by about 4% of the peak fluorescence value for a few hundred nanoseconds. The absence of this effect at other delay times showed that it was not due simply to electrical pickup. This phenomena will be discussed in Chapter XI.

Fluorescence Plateau

Even at early delay times it was observed (Plate V) that in the plateau region the fluorescence intensity was not quite constant. This is not predicted in the three-level theory of Chapter VIII where the plateau region is reached with a time constant given by the decay rates out of levels one and two and no subsequent changes occur until the end of the laser pulse. This effect will be discussed in Chapter XV.

Fluorescence as a Function of Neutral Helium Density

To determine if the fluorescence relaxation was due to resonance radiation and hence was a function of optical depth, some experiments were done at a reduced neutral helium density.

The first experiment tried was to run the pinch in a mixture of hydrogen and helium at the normal fill pressure. In this way it was hoped to reduce the helium density whilst keeping the electron density comparable to the case for a pure helium plasma. However in practice very little helium was excited and this method had to be abondoned. This effect is not well understood but is probably due to the lower ionisation potential of hydrogen limiting the

electron energy to a value below that needed to excite the helium.

To avoid this problem the pinch was run at a much reduced fill pressure .055 torr instead of 450 torr. At this pressure the plasma lifetime was reduced by half and the irreproducibility increased to as much as 50% at late times in the afterglow. However, both direct and sensitised fluorescence was observed of the same form as the previous results. The corresponding shapes occurred at different delays as listed below.

Fill Pressure		
0.055 torr	0.450 torr	
Delay Time		Fluorescence Shape
9 μS	8 μS	No fluorescence
16	27	Distinct spike
20	45	Concave fall
25	80	Straight fall
30	100	Convex fall
35	150	Step function
40	200	Step function

The next step was to measure the electron density of the .055 torr plasma.

Measurement of Electron Density At Reduced Initial Gas Pressure

This is difficult experimentally at the expected densities of around 10^{14} cm^{-3}. Here the Thomson scattering signal would be small, and Ashby Jephcott techniques (Mahon. Thesis 1973) would produce only a fraction of a fringe for the whole time variation.

The only practical way is to measure the Hβ profile using a small trace, 0.01%, of hydrogen in the plasma. An emitter follower with a 2 μS integration time was used to amplify the photomultiplier signal. The optical

arrangement used is on P.87. Because of the low signal/noise ratio and the increased plasma irreproducibility only rough estimates of the electron density could be made. Using the tables of Hill (1964) :

Pressure 0.055 torr

Delay Time	N_e
15 μS	2.5×10^{14} ($\pm$ 50%)
30 μS	1×10^{14} "

Because of the experimental uncertainties in the electron density it is difficult to make a causal link between the fluorescence relaxation and the neutral helium density.

n = 3 Sublevel Populations

The intensities, I, of all the n = 3 → n = 2 transitions were recorded using the arrangement of Fig.4.2. The wavelength dependence of the photomultiplier sensitivity and monochromator efficiency was measured with a tungsten standard lamp. The relative intensity emitted by the n = 3 → n = 2 transitions was obtained by correcting the recorded intensity for the wavelength dependence of the photomultiplier/monochromator efficiency, $\mathcal{E}$. The number of photons emitted per unit time for each transition was calculated by multiplying the emitted intensity by a factor proportional to the wavelength of the transition. In the absence of radiation trapping the n = 3 sublevel relative populations are given by the number of photons emitted per unit time divided by the appropriate statistical weight and radiative transition probability :

$$\text{Sublevel population} \propto \frac{I \times \lambda}{g_k \times A_{ki} \times \mathcal{E}}$$

In all but one case the optical depth of the n = 3 → n = 2 transitions was less than 0.3. For the 5876 Å transition the optical depth was 0.9 across

the diameter of the discharge and this accounts for the lower apparent population of the 3^3D sublevels. The monochromator instrument width was at least 3x the atomic line width for these measurements and thus corrections due to the different line profiles of the $n = 3 \rightarrow 2$ transitions were not necessary.

TABLE 8.1

Upper State	Wavelength Å	Optical Depth (P.145)	Sublevel Population Relative Units
3^3D	5876	0.9	8.8 ± 7%
3^3P	3888	0.3	14 "
3^3S	7065	.05	39 "
3^1D	6678	0.1	16 "
3^1P	5016	.05	18 "
3^1S	7281	.05	38 "

Even for the optically thin lines the sublevel populations are not equal indications that the levels are not in L. T. E.

Quantative Fluorescence Intensities

The intensity of the emission and peak fluorescence was recorded as a function of delay time for several transitions. The level of the total emission originating from the region illuminated by the laser was calculated by multiplying the total emission by a geometric factor of 1.4/5 (P.52). Fig.8.3 shows the intensity of the local emission and fluorescence as a function of electron density. The intensity of the emission and sensitised fluorescence from all the $n = 3$ and 4^1D, 4^3D levels was also recorded. Adjustments of the monochromator slit width enabled a satisfactory signal/noise ratio to be obtained for each transition. The enhancement of the emission during

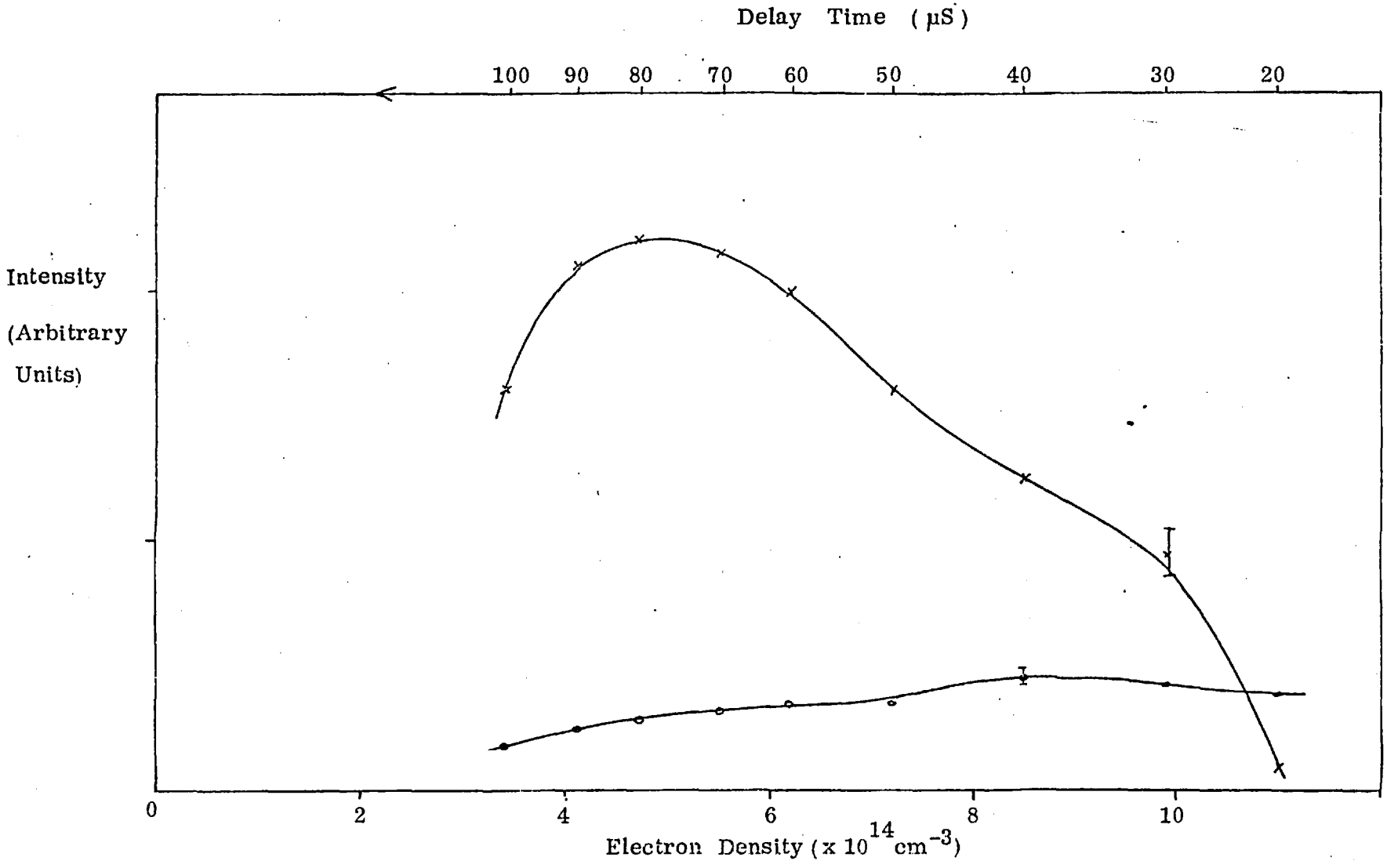

FIGURE 8.3 - EMISSION AND FLUORESCENCE INTENSITY

the laser pulse was calculated as follows :

$$\text{Enhancement} = \frac{\text{Peak Fluorescence Intensity}}{(1.4/5.0)\ \text{Emission Intensity}} + 1$$

To enable comparison to be made of the relative enhancement of a transition at different delay times, compared to the enhancement of the 5876 Å transition we also show figures normalised to the 5876 Å results.

TABLE 8.2

Fluorescence Enhancements

Delay Time		30 μS	60 μS	100 μS	30 μS	60 μS	100 μS
Wavelength Å	Upper Level				(normalised)		
5876	3^3D	3.3	6.7	9.8	100	100	100
"		2.0 *			60 *		
3888	3^3P	2.8	5.9	9.0	85	88	92
7065	3^3S	1.5	3.7	6.8	45	55	69
6678	3^1D	1.5	2.7	4.6	45	40	47
5016	3^1P	1.3	3.1	4.6	39	46	47
7281	3^1S	1.73	2.9	5.0	52	43	51
4471	4^3D	1.0	1.95	2.0	30	29	20
4921	4^1D	1.0	1.56	1.7	30	23	17

* These values are the enhancements in the plateau region.

The experimental uncertainty in the unnormalised $\frac{\text{fluorescence}}{\text{local emission}}$ value is 10%. Care is needed in interpreting the normalised enhancement figures as for instance the value of 30 for the 4471 Å transition

at 30 μS delay means that no increase in emission was recorded in the presence of the laser illumination. As we are calculating the ratio of the emission intensity with and without the laser it is not necessary to take differing A values, etc. into account to calculate the relative population enhancements.

The overall pattern may be described as follows. The population enhancement of the 3^3P level is almost equal to the enhancement of the 3^3D level directly excited by the laser. The n = 3 singlet level populations show roughly half the enhancement of the 3^3D level. The 4^1D and 4^3D population enhancement is approximately one-fifth the 3^3D enhancement. The value of the normalised enhancements increase with the delay time. This is unexpected as it was considered that the lower electron density at long delay time would result in lower excitation transfer rates.

Sensitised Fluorescence Rise Time

The rise time of the fluorescence observed at 100 μS delay time in the 5876 Å, 6678 Å and 5016 Å transitions was measured. The rise time in all three cases was 20 ± 4 nS. This shows that the collisional transfer time between the n = 3 levels was less than 20 nS even at the lowest electron densities (10^{14} cm^{-3}) used in the fluorescence experiments.

Effect of Finite Laser Rise Time on Fluorescence Relaxation

The finite laser rise time will have greatest influence on the observed fluorescence relaxation time for the case of a high electron density when the two times are comparable. On a typical fluorescence trace observed at an electron density of 10.6×10^{14} cm^{-3} the exponential decay rate to the fluorescence plateau was measured in the period 20 - 40 nS after the start of the laser pulse. From Plate V, photograph 2, it may be seen that the

laser intensity reaches the saturation threshold (1/10 of the peak intensity) 10 nS after the start of the laser pulse. In the period 20 - 40 nS after the start of the laser pulse, the laser intensity increases from 6 to 8x the saturation threshold value. Fig.7.1 shows that an increase in laser intensity of 6 - 8 times the saturation threshold value leads to an increase of 10% in the peak fluorescence intensity but has no effect on the fluorescence intensity in the plateau region. The effect of this change in laser intensity on the fluorescence decay rate (measured in the region between the peak and plateau) will therefore be less than 10%. As the experimental uncertainty in measuring the short relaxation times at these high electron densities is approximately 10% this effect is negligible. For the rest of the range of electron densities used in the fluorescence experiment this effect is even smaller.

CHAPTER IX

POSSIBLE DECAY PROCESSES - I. RADIATION

Although we have established the suitability of the three level model for the present case we have not so far assigned specific atomic states to levels one, two and three, or identified the nature of the decay process involved.

On the basis of the sensitised fluorescence results (P.61) we will, for the moment, assign level one to all the $n = 2$ states and level two to all the $n = 3$ and $n = 4$ states. This assumption will be discussed further in Chapter XI.

The possible routes of decay are

1) Decay to the ground state,

2) Decay to the high n levels,

3) Decay to the continuum,

by

A) Radiative transitions.

B) Electron collisions.

C) Normal atom collisions.

D) Excited atom collisions.

E) Helium ion collisions.

F) Ionised helium molecule collisions.

G) Collisions with impurities.

In this chapter we discuss radiative decay to the ground state, and photoionisation.

Radiative Decay to the Ground State

The three possible transitions are

		A_{21} ($\times 10^8$ sec^{-1})	τ (nS)
$2^1P - 1^1S$	584 Å	17.99	0.5559
$3^1P - 1^1S$	537 Å	5.66	1.767
$4^1P - 1^1S$	522 Å	2.46	4.065

Here τ is the atomic lifetime not the decay time for a plasma of excited atoms. The plasma decay time is related to the atomic lifetime by the optical depth of the atomic transition. We calculate the optical depth from the ground state atom number density and the line width.

Helium Density

As the density of doubly ionised helium atoms is extremely small the neutral atom density may be obtained using the gas laws. For a pressure of 0.45 torr and room temperature this gives a total helium density of 1.59×10^{16} cm^{-3}. Subtracting the helium ion density (equal to the electron density) gives a neutral helium density of 1.5×10^{16}cm. This is for a delay time of 30μS but the density changes little at other delay times.

584 Å LINE WIDTH

i) Resonance Broadening

Griem (1964) gives the following relation for resonance broadening

$$\omega_\alpha = 3\pi \left(\frac{g_1}{g_2}\right)^{\frac{1}{2}} \left(\frac{e^2 f}{4\pi \varepsilon_o \omega m}\right)$$

where

ω_α is the (half) half width in angular frequency units.

$g_1(g_2)$ the lower (upper) statistical weight.

e, m, electron charge and mass.

ε_o dielectric constant of vacuum.

ω angular frequency of the transition (for resonance lines only).

f oscillator strength.

N atom number density.

For the present case this gives:

$$\omega_\alpha = 1.2 \times 10^8 \text{ radians sec}^{-1}$$

$$= 2 \times 10^{-6} \text{ Å}$$

ii) Stark Broadening

Estimates of stark broadening parameters for neutral helium are given by Griem et al (1962). At an electron density of 10^{15} cm^{-3} the predicted electron impact (half) half widths are

584 Å	16.2×10^{-6} Å
537 Å	433×10^{-6} Å
522 Å	1780×10^{-6} Å

iii) Doppler Broadening

The normalised line shape for the case of doppler broadening is given by

$$L(\omega) = \frac{1}{\Delta\omega_D (\pi)^{1/2}} \exp - \left(\frac{\omega - \omega_o}{\Delta\omega_D}\right)^2$$

where $\Delta\omega_D = \frac{\omega_o v_m}{c}$

v_m the most probable speed $= \left(\frac{2kT}{m}\right)^{\frac{1}{2}}$

For the 584 Å transition

$\omega_o = 3.23 \times 10^{16}$ radians sec^{-1}

m = 4 x proton mass = 3.75×10^9 eV

kT_{atom} = 1 eV at 30 μS delay (Cairns Thesis 1970),

giving a doppler width of

$= 7.45 \times 10^{11}$ radians sec^{-1}

The doppler (half) half width $= (\ln 2)^{\frac{1}{2}} \Delta \omega_D$

$= 6.21 \times 10^{11}$ radians sec^{-1}

$= 1.12 \times 10^{-2}$ Å

Clearly for the 584 Å and also 537 Å and 522 Å transitions, doppler broadening is dominant. From equation 6.10 the absorption coefficient at the centre of a doppler broadened line (assuming a large population difference) is

$$k(\omega_o) = \frac{2\pi r_o \, c \, f_{21} \, n_1}{\Delta \omega_D \, (\pi)^{1/2}}$$

in the present case this gives

$$k(584\text{ Å}) = 5.23 \times 10^{4} \text{ m}^{-1}$$

Radiation Trapping

Because of the large amount of reabsorption the lifetime of excited atoms in the plasma is much longer than the simple radiative transition time. The problem of the imprisonment of resonance radiation has been treated extensively in two articles by T. Holstein (1947, 1951). He shows that a simple diffusion approach to the problem is inadequate. This is because of the impossibility of defining a mean free path for a photon due to the variation in absorption coefficient over the atomic line. He shows that the frequency spectrum of the radiation emitted by a given volume element is proportional to the absorption coefficient for the case of doppler and pressure broadening. (L. T. E. considerations are not sufficient here as the radiation leaks out through partially reflecting walls.)

Holstein obtains the result that, for the optically thick case, the excited atoms decay as $\exp - (\frac{g\,t}{\tau})$

where τ is the radiative lifetime

g is the escape factor equal to the reciprocal of the number of emissions and absorptions of a photon prior to its escape from the plasma.

The value of g depends on the line shape. Holstein gives the following results for a cylindrical geometry (radius R)

A - Doppler Broadening

$$g = \frac{1.60}{k_D R \, (\pi \ln k_D R)^{\frac{1}{2}}} \qquad 9.1$$

B - Impact Broadening

$$g = \frac{1.115}{(\pi \, k_L R)^{\frac{1}{2}}} \qquad 9.2$$

where k_D or k_L is the absorption coefficient at line centre.

The radiation escape process may be understood roughly by considering that only radiation emitted far out in the line wing where $k(\omega)R \leqslant 1$ may escape, and the radiative transition probability must be multiplied by the probability that emission will occur in this region to obtain the effective decay rate. The applicability of result A or B for a line both doppler and impact broadened is determined by the form of the line shape in the region $k(\omega)R \cong 1$.

First for a doppler broadened 584 Å transition we work out the point on the line wing where $k_D(\omega)R = 1$. The doppler broadened absorption coefficient is

$$k_D(\omega) = \frac{C}{\Delta\omega_D (\pi)^{1/2}} \exp - \left(\frac{\omega - \omega_o}{\Delta\omega_D}\right)^2 \qquad 9.3$$

where ω_o is the angular frequency at line centre, and C is given by the integral absorption relationship

$$C = \int k(\omega) \, d\omega = \frac{\lambda_o^2 \, N \, g_2 \, \gamma}{8 \pi \, g_1}$$

where γ is the radiative emission probability.

In our case, $k_D(\omega_o) = 5.23 \times 10^2 \text{ cm}^{-1}$

$$R = 2.5 \text{ cm}$$

$$k_D(\omega_o) R = 1.31 \times 10^3$$

$k_D(\omega')$ will equal 1 at the point where

$$\exp - \left(\frac{\omega' - \omega_o}{\Delta\omega_D}\right)^2 = \frac{1}{1.31 \times 10^3}$$

$$\omega' - \omega_o = 2.68 \, \Delta\omega_D$$

$$= 2.00 \times 10^{12} \text{ rad.sec}^{-1}$$

For the impact broadened case we need to work out the absorption coefficient at line centre considering all the atoms to be stationary.

$$k_L(\omega) = C \frac{\gamma}{\pi} \frac{1}{(\omega - \omega_o)^2 + \gamma_L^2} \qquad 9.4$$

here γ_L is the (half) half width in angular frequency of the impact broadened Lorentzian line. By comparison with equation 9.3 we see that

$$k_L(\omega_o) = \frac{\Delta\omega_D}{(\pi)^{\frac{1}{2}} \gamma_L} k_D(\omega_o)$$

for our case the impact (half) half width is 1.62×10^{-5} Å. (Page 108)

$$\gamma_L = 8.95 \times 10^8 \text{ angular frequency}$$

$$k_L(\omega_o) R = 6.15 \times 10^5$$

using $k_L(\omega) R = k_L(\omega_o) R \frac{\gamma_L^2}{(\omega - \omega_o)^2 + \gamma_L^2}$

we get for the case $(\omega' - \omega_o) = 2 \times 10^{12}$ rad.sec^{-1}

$$k_L(\omega' - \omega_o) R = 0.123$$

So we see that the absorption at the point in the line wing where the radiation escapes is controlled primarily by doppler broadening.

The escape factor g is hence given by equation 9.1.

$$g = \frac{1.6}{1.31 \times 10^{3} (\pi \log 1.31 \times 10^{3})^{\frac{1}{2}}}$$

$$= 2.57 \times 10^{-4}$$

and radiation lifetime $\frac{\tau}{g} = 2.16 \mu S$

If the escape had been controlled by a Lorentzian line shape we apply equation 9.2. i.e.

$$g = \frac{1.115}{(\pi \ k_L(\omega_o) R)^{\frac{1}{2}}}$$

$$= 8.02 \times 10^{-4}$$

radiation lifetime = $0.693 \mu S$

The stark widths of the transitions 3^1P and 4^1P to 1^1S are much higher. Using exactly the same procedure as above we determine the radiation lifetime. The results are summarised in the Table 9.1

From consideration of the value of $k_L(\omega' - \omega_o)R$ it can be seen that for the $3^1P - 1^1S$ transition the choice between the doppler and impact case is uncertain. For the $4^1P - 1^1S$ transition the impact broadening formula is preferable. The excitation decay time is a function of electron density and temperature as reflected in changes in optical depth. The decay time at long delay times should be increased as the line width will be reduced while the ground state level population remains approximately unchanged. It is clear that a more rigorous treatment using Voigt profiles is needed for accurate results especially for the $3^1P - 1^1S$ case. (See e.g. Bieberman et al.).

TABLE 9.1

Transition	$2^1P - 1^1S$	$3^1P - 1^1S$	$4^1P - 1^1S$
Wavelength	584 Å	537 Å	522 Å
τ	0.55 nS	1.77 nS	4.1 nS
$\Delta\omega_D$	7.45×10^{11}	8.1×10^{11}	8.33×10^{11}
$k_D(\omega_o)R$	1.31×10^{3}	321	128
$(\omega' - \omega_o)$	2.0×10^{12}	1.95×10^{12}	1.83×10^{12}
γ_L	8.95×10^{8}	2.83×10^{10}	1.23×10^{11}
$k_L(\omega_o)R$	6.15×10^{5}	5.18×10^{3}	4.89
$k_L(\omega' - \omega_o)R$	0.123	1.09	2.2
g Doppler Broadening	2.57×10^{-4}	1.17×10^{-3}	3.2×10^{-3}
g Impact Broadening	8.02×10^{-4}	8.74×10^{-3}	2.84×10^{-2}
Excitation Lifetime (Doppler)	2.16 μS	1.51 μS	1.27 μS
Excitation Lifetime (Impact)	0.69 μS	0.202 μS	0.143 μS

Symbols defined in the text.

In general the above results will be an underestimate of the decay time for in the present case the radiation is excited only in the centre of the plasma.

The excitation lifetime ranges from 5-60 times longer than the observed fluorescence decay time and it is clear that radiative transitions to the ground state are not a major factor in the decay of the fluorescence.

Photoionisation

One possible decay route for excited atoms is by photoionisation by the intense laser radiation. Dunning et al. (1974) have used a molecular beam apparatus in conjunction with a dye laser to determine absolute cross sections for the photoionisation of helium 3^1P, 4^1P, 5^1P, 3^3P, 4^3P, 5^3P atoms excited optically from the $2^{1,3}S$ metastable levels. The photoionisation cross section for each of these states is determined at the wavelength used for its excitation from the metastable state. In order to calculate an ionisation rate for the 3^3D level we assume that the 3^3D photoionisation cross section is approximately the same as the values given by Dunning et al. for the 3^1P and 3^3P states, i.e. $\simeq 10^{-17} cm^{-2}$. The total laser energy transmitted through the pinch is typically 15 mJ corresponding to 5×10^{16} photons at 5876 Å. Thus in a laser pulse (typically 250 nS duration) the average number of ions produced per atom is $5 \times 10^{16} \times 10^{-17} = 0.5$ corresponding to an ionisation rate of $2 \times 10^6 sec^{-1}$. This rate is 20x slower than the observed fluorescence decay rate and hence photoionisation processes cannot account for the observed fluorescence relaxation.

CHAPTER X

POSSIBLE DECAY PROCESSES II COLLISIONS

Collisional transfer is a strong possibility for the explanation of the observed decay in the fluorescence. In this chapter we explore the possible routes of collisional transfer and estimate collision rates for the various processes. For this we need cross sections and we first briefly review some previous papers in this field. The experimental papers fall into four main groups.

(a) Excitation of helium with an electron beam of energy above the excitation threshold.

(b) Excitation by optical pumping with conventional light sources.

(Both (a) and (b) measure the excitation rate by monitoring the radiation from visible helium transitions).

(c) Excitation with an electron beam near the excitation threshold - obtaining the cross section by measuring the flux of slow electrons produced in the collisions.

(d) Excitation with two electron beams. The first electron beam excites an atomic beam to a metastable level and the second ionises the metastable atoms. From measurements of the ion flux an ionisation cross section for metastable atoms can be deduced.

(a) Electron Beam Experiments (far above threshold).

Papers in this group include Lees (1932), Thieme (1932) and Gabriel and Heddle (1960). It was realised early on (Lees and Skinner (1932)) that various secondary processes have to be taken into account in the interpretation of the results of these experiments, viz.

(i) imprisonment of resonance radiation,

(ii) collisional excitation transfer - atom-atom collisions producing transfer between levels of the same principal quantum number, in particular transfer between singlet and triplet systems, e.g.

$$He\,(1^1S) + He\,(n^1P) \longrightarrow He\,(n^3D) + He\,(1^1S),$$

(iii) radiative cascade processes. (See also Phelps (1958)).

(b) Optical Pumping Experiments

Collisional transfer processes have also been studied by optical pumping techniques using conventional light sources to excite helium atoms from metastable states in a helium plasma, viz. Maurer and Wolf (1934, 1940); Bakos and Szigeti (1968); Teter and Robertson (1966); and Wellenstein and Robertson (1972). Wellenstein and Robertson measure cross sections for electron and atom collisions, taking account of associative ionisation :

$$He\,(3^1D) + He\,(1^1S) \longrightarrow He_2^+\,(^2\Sigma_u^+) + e$$

There is however disagreement between the above papers for the value of the collisional transfer cross sections probably due to uncertainties regarding radiative cascade processes (see van Raan et al. 1974), the worst example being the cross section for $4^1P - 4^1D$ transfer by atom collision, estimates ranging from 67×10^{-15} (Wolf and Maurer, 1940) to 0.28×10^{-15} cm^2, (Bakos and Szegeti, 1967).

(c) Electron Beam Experiments (near threshold)

Maier-Leibnitz (1935) measured the attenuations of the flux of an electron beam passing through a helium collision chamber as a function of incident electron energy and hence deduce collision cross sections. They found a peak cross section for excitation of the 2^3S level by electron collision of 3.7×10^{-18} cm^2 $\pm$ 20%. Similar experiments have been reported by Schulz and Fox (1957); Fleming and Higginson (1964); and Brongersma et al. (1969)

with less than a factor of two disagreement on the exact value of the cross section. Brongersma et al. (1972) use a double retarding potential difference method to obtain high resolution graphs of the variation of 2^3S and 2^1S excitation cross sections near threshold, with incident electron energy. They normalise their results with the absolute value for the 2^3S cross section given by Brongersma et al. (1969).

(d) Double Beam Electron Excitation Experiments

Vriens et al. (1968) reported an experiment in which two electron beams intersected an atomic helium beam. The first electron beam excited the atoms into the 2^1S and 2^3S states and the second beam ionised these atoms. By detecting the flux of ions produced it was possible to measure the energy dependence of the ionisation cross sections of the 2^1S and 2^3S states of helium. Long et al. (1970) in a similar experiment, measured the absolute electron impact ionisation cross section of He (2^3S) atoms. Above threshold the cross section rises with increasing electron energies up to about 8 eV. From 8 eV - 16 eV (the limit of experimental measurement) the cross section is fairly constant at 6.5×10^{-16} cm^2 $\pm$ 30%. Schearer-Izumi et al. (1974) describe a similar experiment and compare the relative cross sections they obtain with those of several other workers revealing some disagreement in the energy dependence of the cross sections. They also describe an increase in the electron impact excitation function for the case of the (first) exciting electron beam energy of 23 eV and above. They interpret this increase as being caused by an increased contribution to the ion flux due to the ionisation of helium atoms in higher excited states but are unable to assign cross sections to specific states.

Theoretical Work

Burke et al. (1969), and Oberoi and Nesbet (1973) have presented theoretical estimates of the excitation cross section near threshold. Their calculations successfully predict the resonances in the cross section found experimentally by Brongersma et al. (1972) but are about 50% larger in absolute magnitude than the experimental results. The discrepancy may be due to an error in the normalisation of the experimental results. Burke et al. (1969) also estimate cross sections for electron scattering by the $n = 2$ levels. The cross sections range from 10^{-16} cm^2 - 10^{-13} cm^2. The results are only partially in agreement with the experimental results of Neynaber et al. (1964).

Recent Experiments using Dye Lasers

Collins et al. (1972a) describe an experiment in which a dye laser is used to study excitation transfer in a flowing helium afterglow. The beam from a flashlamp pumped coaxial dye laser was frequency doubled to 2945 Å and used to excite the 5^3P state of helium by optical pumping from the 2^3S metastable level. The neutral helium density was 10^{16} - 10^{18} cm^{-3} and electron density 10^{10} - 10^{12} cm^{-3}. They interpret the observed decay of 2945 Å fluorescence (decay time~33 nS) as being due to de-excitation through neutral atom collisions and direct radiative decay from the 5^3P level. They mention no correction due to the finite fall time of the laser which is especially important as they are operating below saturation. Also they do not take into account the additional possibilities for radiative decay through collisional transfer to other $n = 5$ levels and subsequent radiation, which would drastically affect their results.

In a subsequent paper Collins et al. (1972b) study the rotational relaxation of molecular helium. They observed spiking behaviour in the fluorescence

at high laser powers similar to the present results. They suggest that this is due to cooperative phenomena of the kind discussed by Arecchi et al.(1970) but do not present any justification for this assertion. Arecchi considered the coherent interaction of a radiation field with an assembly of otherwise independent two level systems. He treated the case of the atoms which have been prepared in a properly phased super-radiant (Dicke, 1954) state in the vacuum of photons. By comparing the enhanced spontaneous emission rate for an assembly of N atoms and the limit on the size of this assembly, also a function of the enhanced emission rate, he obtains a maximum value for N, (N_c) if all the atoms are to cooperate in super-radiant emission and also a corresponding maximum super-radiant emission rate, γ_c.

$$N_c = \left(\frac{2A}{\lambda}\right)\left(\frac{c\rho}{\gamma}\right)^{\frac{1}{2}}$$

$$\gamma_c = \tfrac{1}{2}\left(c\,\rho\,\gamma\,\lambda^2\right)^{\frac{1}{2}}$$

where A is the area of the (cylindrical) sample

ρ atom number density

γ the spontaneous emission rate of an isolated atom.

To compare this to the case of Collins et al. we assume an excited state population density of 10^{11} cm^{-3} (based on their stated metastable population density of 10^{12} cm^{-3}). With $\gamma = 3 \times 10^6$ sec^{-1}, $\lambda = 2945$ Å, we calculate a value of γ_c of 1.5×10^9 sec^{-1}. It is difficult to see how a high spontaneous emission rate would produce the spiking behaviour of the fluorescence observed by Collins et al. Also, as in fact the observed fluorescence is used to determine collision rates it is unlikely that the dephasing collision rate discussed by McIlrath et al. (1972) (see P.78), is small enough to allow the production of a super-radiant state. Finally, it should be noted that it is not necessarily the case that coherent laser illumination

produces a "Dicke" super-radiant state and, in fact, the treatment of Arecchi et al. specifically excludes the presence of an external radiation field and so is not directly applicable to problems of laser induced fluorescence.

Similar considerations may be used in reference to the present experiment and it is clear that coherence effects play no part in the observed fluorescence decay.

Burell and Kunze have described a fluorescence experiment on a cold helium plasma with a laser pumped dye laser tuned to the 4471 $\mathring{A}$ $2^3P - 4^3D$ transition. The plasma conditions were helium number density 5×10^{16} cm^{-3} and electron number density 3×10^{12} cm^{-3}. With a short duration laser pulse (11 nS F.W.H.M.) they observed relaxation in the fluorescence and sensitised fluorescence at the end of the laser pulse on several helium lines. They observed transfer between singlet and triplet systems at the same rate (3×10^8 sec^{-1}) as transfer within the triplet system but are unable to assign this specifically to electron or atom collisions.

Present Experiment

To relate the published cross sections to the present experiment we deduce the value of the collision rates from the relation

$$W = \int_v N_{v,dv}\, \sigma_v\, v\, dv \qquad (13.1)$$

where W is the total collision rate per atom;

v speed of the incident particle;

σ_v cross section at incident speed v;

$N_{v,dv}$ number density of atoms with speeds in the range $v \rightarrow v + dv$.

Collisions with Ground State Helium Atoms

Wellenstein et al. (1972b) report a cross section of 4.5×10^{-16} cm^2 for associative ionisation :

$$He\,(3^3D) + He\,(1^1S) \rightarrow He_2^+ + e$$

In this case all the atoms can participate and $\int N\sigma v dv = N_{total}\sigma\ v_{average}$. As the atom (and electron) velocity distributions are Maxwellian the average atom speed is given by

$$v_{avr} = \left(\frac{8}{\pi}\ \frac{kT}{m}\right)^{\frac{1}{2}}$$

For a temperature of 1 eV $v_{avr} = 7.81 \times 10^5$ cm/sec. The neutral helium density is 1.5×10^{16} cm^{-3} (P.107). The collision rate is therefore 5.3×10^6 sec^{-1}. This is too slow to account for the observed fluorescence relaxation (Fig.5.1).

Exchange Collisions

These are collisions of the type

$$He'\,(1^1S) + He\,(2^3S) \rightarrow He'\,(2^3S) + He\,(1^1S)$$

Evans et al. (1969)gives a cross section for this process of 1.4×10^{-15} cm^2. The collision rate may be estimated in the same way as above to be 1.6×10^7 sec^{-1}. This process of course does not lead to any reduction in the number of excited atoms and will have no effect on the fluorescence.

To our knowledge there are no other published cross sections for processes involving neutral atoms that would deplete the $n = 2,3,4$ levels in helium. Collisions with other excited atoms are not expected to be significant as the densities are so low ($\sim 10^{11}$ cf 10^{15} electron density). The same argument applies to collisions with helium ions. In general, the rates for atom-atom and atom-ion collisions are much smaller than the rates for electron collisions

for plasmas having a degree of ionisation exceeding a few percent (Cooper, 1966). We now consider electron collisions.

Electron De-excitation to the Ground State

As described earlier there have been several experimental and theoretical estimates of the electron excitation cross section from the ground state to $n = 2$, with some disagreement over the absolute magnitude. In order to get a collision rate we arbitrarily choose the theoretical estimates of Oberoi and Nesbet (1973) and approximate their detailed cross sections by a step function.

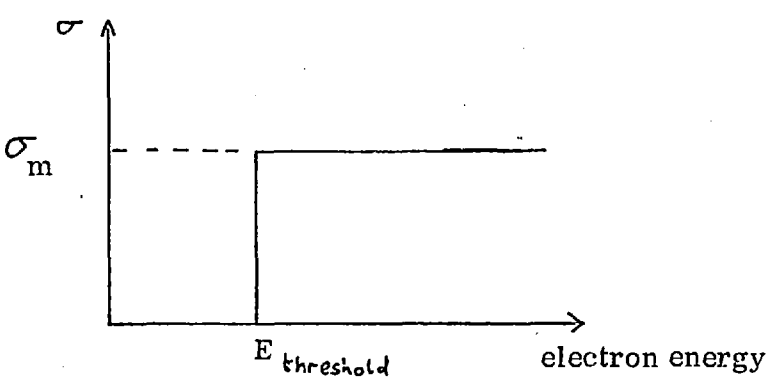

We take the threshold to be 20 eV and σ_m for each transition as :

Transition	σ_m
$1^1S - 2^1S$	1.5×10^{-18} cm^2
$1^1S - 2^3S$	3×10^{-18}
$1^1S - 2^1P$	1×10^{-18}
$1^1S - 2^3P$	0.5×10^{-18}

We estimate the total excitation rate by using -

$$W = \int_{v = v_{threshold}}^{\infty} \sigma_m \; N(v) \; v \; dv \qquad (10.1)$$

and use the principle of detailed balance to obtain the de-excitation rate.

For a maxwellian velocity distribution (Sears, 1952) -

$$\frac{d\,N(v,dv)}{N_{total}} = \frac{4}{(\pi)^{\frac{1}{2}}}\left(\frac{1}{v_m}\right)^{3/2} v^2 \exp -\left(\frac{v}{v_m}\right)^2 dv$$

where v_m is the most probable speed.

$$v_m = \left(\frac{2\,k\,T}{m}\right)^{\frac{1}{2}}$$

Substituting this in (13.1) we have

$$\text{Excitation rate} = \frac{4\,N\,\sigma}{(\pi)^{\frac{1}{2}}} \int_{v_{thresh}}^{\infty} \frac{v^2}{v_m^3} \exp -\left(\frac{v}{v_m}\right)^2 v\,dv$$

With the substitution

$$y = \frac{v}{v_m}^2$$

and $y = A$ when $v = v_{threshold}$

this becomes

$$\text{Excitation rate} = \frac{4\,N\,\sigma\,v_m}{(\pi)^{\frac{1}{2}}\,2} \int_{A}^{\infty} y \exp^{-y} dy$$

integrating by parts

$$= \frac{2}{(\pi)^{\frac{1}{2}}} N\,\sigma\,v_m \left[\exp - A^2\right](A^2+1)$$

$$A = \frac{v_{thresh}}{v_m}^2 = \frac{E_{thresh}}{\frac{1}{2}\,m\,v_m^2} = \frac{E_{thresh}}{k\,T}$$

$$\text{Excitation rate} = \frac{2}{(\pi)^{\frac{1}{2}}} N\,\sigma \left(\frac{2kT}{m}\right)^{\frac{1}{2}} \left(\frac{E_{thresh}}{kT} + 1\right) \exp -\left(\frac{E_{thresh}}{kT}\right) \quad (10.2$$

We obtain the de-excitation rate by detailed balance considerations -

$$\text{De-excitation rate} = \frac{g_1}{g_2} \exp\left(\frac{E}{kT}\right) \text{excitation rate}$$

$$= \frac{2}{(\pi)^{\frac{1}{2}}} N\,\sigma \left(\frac{2kT}{m}\right)^{\frac{1}{2}} \left(\frac{E_{thresh}}{kT} + 1\right) \frac{g_1}{g_2} \qquad (10.3)$$

In the present case

g_2 = 16 (the sum of the statistical weights of the n = 2 levels)

g_1/g_2 = 1/16

N_e = 10^{15} cm^{-3}

k T = 1 eV

E_{thresh} = 20 eV

σ the excitation

cross section = 6×10^{-18} cm^{-3}

the de-excitation rate (n = 2 → n = 1) = 5.28×10^{5} sec^{-1}.

As $E_{thresh}/kT \gg 1$ the rate scales as $\frac{N_e}{T_e^{\frac{1}{2}}}$ to a good approximation. We calculate the de-excitation rate over the range of electron densities and temperatures observed for the pinch (Fig. 4.1). The de-excitation rate is shown as a function of electron density in Fig. 10.1.

It can be seen that the decay rate is 50x too low to account for observed relaxation of the fluorescence (Fig.5.1). During the pinch lifetime N_e is roughly proportional to T_e (Fig.4.1), so that the de-excitation rate scales approximately as $N_e^{\frac{1}{2}}$. Even if the cross sections of Oberoi and Nesbet were in error the dependence of the collision rate with N_e would still be in disagreement with the form of the experimental results. Theoretical estimates of the 4^3S and 3^3S excitation cross sections (Mathur et al. 1974) indicate that the de-excitation rate from the n = 3 and n = 4 levels to the ground state is lower than the n = 2 → ground rate. We conclude that collisional de-excitation by electron impact is not responsible for the observed fluorescence relaxation.

FIGURE 10.1 - COLLISIONAL DE-EXCITATION RATE BY ELECTRON IMPACT OF THE n = 2 LEVELS IN HELIUM

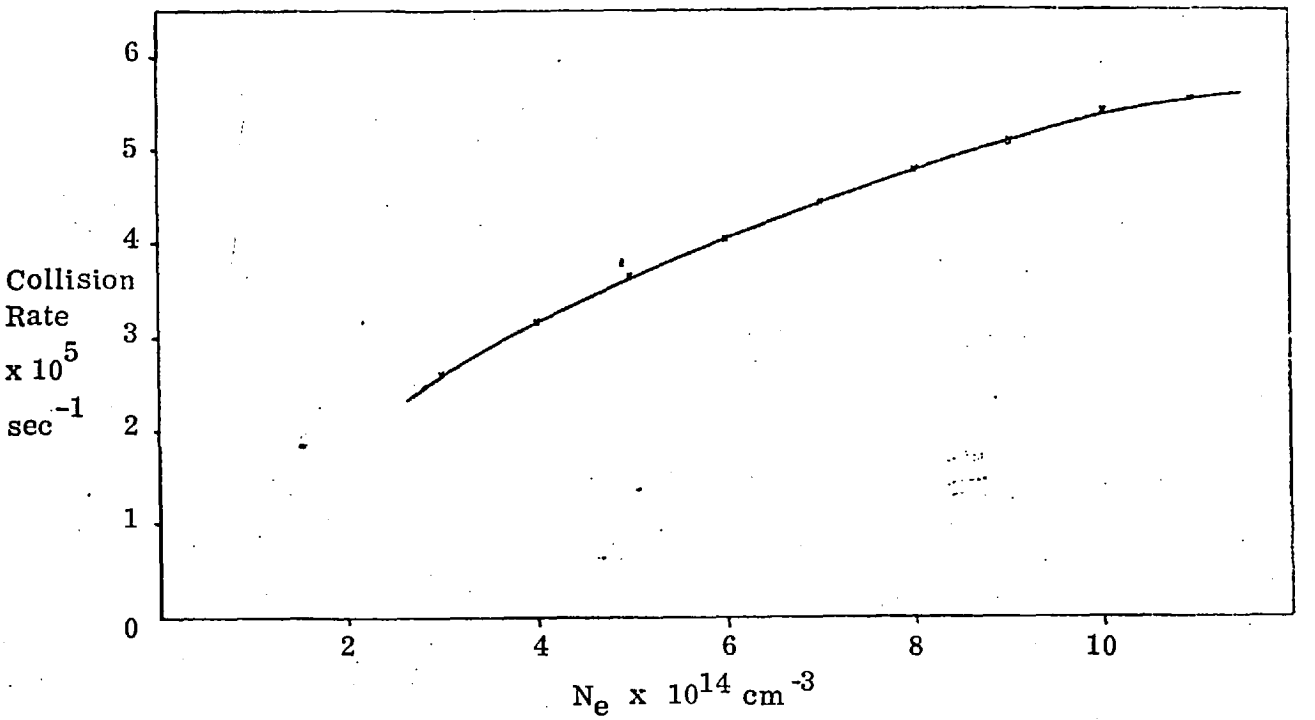

FIGURE 10.2 - COLLISIONAL IONISATION RATE BY ELECTRON IMPACT OF n = 3 AND 4 LEVELS IN HELIUM

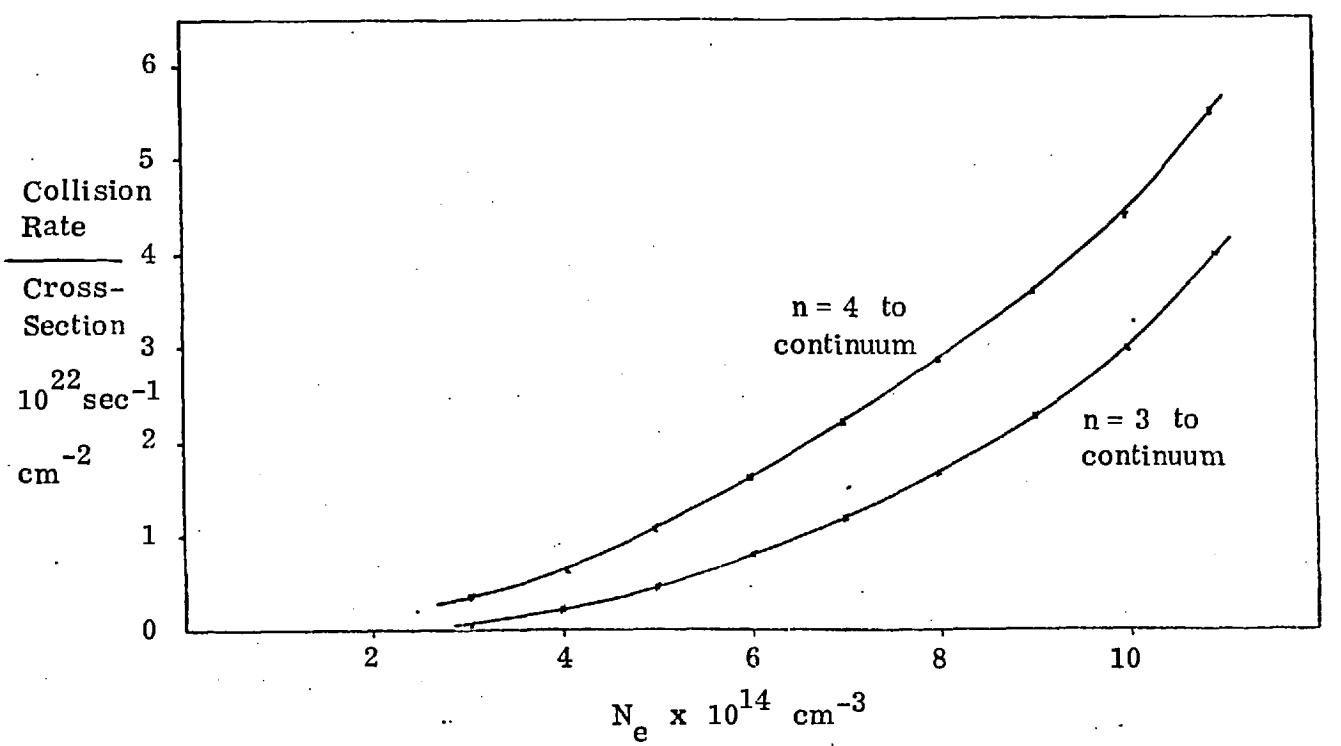

Collisional Ionisation

Before using various theoretical estimates to determine the collision rate we need to determine the ionisation potential, taking into account the lowering of the ionisation potential of an atom due to interactions with the rest of the plasma. Cooper (1966) gives the relation :

$$\Delta E_I = e^2/\rho_D$$

where ρ_D, the Debye length is given by :

$$\frac{kT_e}{\rho_D^2} = 4\pi e^2 N_e$$

In the present case $N_e = 10^{15}$ cm^{-3}, $kT_e = 1$ eV, $\rho_D = 2.18 \times 10^{-5}$ cm and $\Delta E_I = 6.6 \times 10^{-3}$ eV. This is a totally negligible correction. The average (weighted by the statistical weights) ionisation potential for the n = 2, 3 and 4 levels in helium, E_n, is (Martin, 1973)

	E_n	
n = 2	3.812 eV	(6.11×10^{-12} ergs)
n = 3	1.563 eV	(2.5×10^{-12} ergs)
n = 4	0.868 eV	(1.39×10^{-12} ergs)

Seaton (1964) gives the following relation for the rate coefficient for ionisation of ions in the solar corona

$$q_i(X^{+m}) = 2.0 \times 10^{-8} \frac{\zeta}{E_n^2} T^{\frac{1}{2}} 10^{-\left(\frac{5040}{T} E_n\right)} N_e \text{ sec}^{-1}$$

where ζ is the number of electrons in the shell from which the ionisation takes place -

E_n is the ionisation potential in eV

T is the temperature in ^oK

In our case for $k T = 1$ eV, $T = 1.16 \times 10^4$ °K

and $E_n \simeq 1$ eV for $n = 3$ electrons

$\int = 36$ for $n = 3$

this gives a rate of 2.8×10^{10} sec^{-1}. This is much too high to be compatible with the present results. It suggests any increase in the $n = 3$ level would be transferred to the continuum on a timescale of 3×10^{-11} sec. We conclude that the rate given by Seaton does not apply to the $n = 3$ and 4 excited states of neutral helium.

Hinnov et al. (1962) in calculating recombination coefficients, derive a formula for ionisation from excited levels using the classical Thomson relation (J.J. Thomson, 1924).

$$d_s^2 = e^4 \frac{1}{E} \left(\frac{1}{E_s} - \frac{1}{E}\right) \qquad (10.4)$$

where d_s^2 is the impact parameter

e electron charge

E incident electron energy

E_s energy transferred to atom

Hinnov gives an ionisation rate of

$$\frac{4}{5} \pi e^4 \left(\frac{2}{\pi m k T}\right)^{\frac{1}{2}} \frac{N_e}{E_n} \exp\left(-\frac{E_n}{kT}\right) \qquad (10.5)$$

In the present case E_n is given on P.126, $kT_e = 1$ eV, $T = 1.16 \times 10^4$ K; and the predicted ionisation rate is

ionisation rate		
	1.01×10^7 sec^{-1}	$n = 2$
	23.4×10^7	$n = 3$
	84.2×10^7	$n = 4$

From Equation 6.9 it may be seen that the higher ionisation rate for the $n = 3$ and 4 levels compared to $n = 2$ is consistent with the fact that the observed fluorescence decayed (cf. the de-excitation rates to ground

state, P.124). The decay rate predicted by Eqn.6.9 is $\frac{(g_1/g_2)\,D_1 + D_2}{1 + (g_1/g_2)}$ where D_1 and D_2 are loss rates for atoms in the lower and upper levels interacting with the laser. With the above figures for the ionisation rate the predicted decay rate (taking all the $n = 2$ levels as the lower levels and all the $n = 3$ and 4 levels as the upper level) is 5×10^8 sec^{-1}. This compares to the observed decay rate (Fig.5.1) at $N_e = 10^{15}$, $kT_e = 1$ Ev of 3.1×10^7 sec^{-1} ($\pm$ 7%). The disagreement is not too surprising in view of the rudimentary nature of the approximation used (Eqn.10.4).

Published Ionisation Cross Sections

As mentioned on P.117, Long et al. (1970) measured the absolute ionisation cross section of the helium 2^3S level. We approximate their form of the energy dependence of their cross section by a series of step functions.

FIGURE 10.3

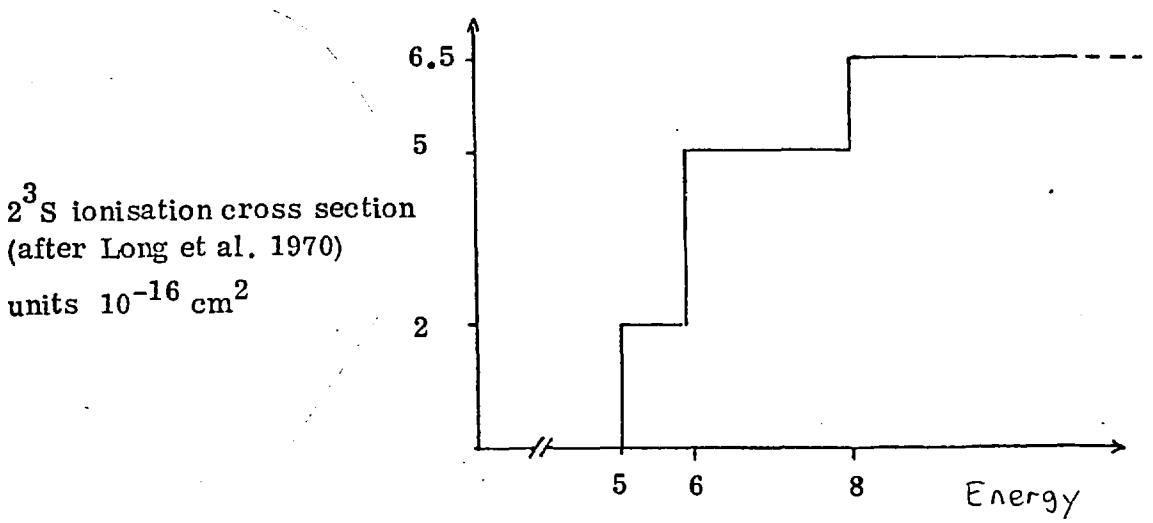

We use Equation 10.2 to obtain an ionisation rate

$$\text{excitation rate} = \frac{2}{(\pi)^{\frac{1}{2}}} N \sigma \left(\frac{2kT}{m}\right)^{\frac{1}{2}} \left(\frac{E_{thresh}}{kT} + 1 \right) \exp -\left(\frac{E_{thresh}}{kT}\right) \qquad (10.2)$$

and sum the contributions from the cross section as given in Fig.10.3.

σ x 10^{-16} cm^2	E_{thresh} eV	ionisation rate sec^{-1}
2	5	5.41×10^5
3	6	3.49×10^5
1.5	8	3.03×10^4

(total 6.5 at 8 eV)

The total ionisation rate of the 2^3S level is 9.20×10^5. Unfortunately, to our knowledge no ionisation cross sections for the $n = 3$ and 4 levels in helium have been published. However, we may use the energy dependence in Equation 10.5 (rate $\propto \frac{1}{E_n} \exp -\frac{E_n}{kT}$) with the above value of the 2^3S ionisation rate to deduce ionisation rates for the $n = 3$ and 4 levels. This gives :

$$\text{ionisation rate} = 2.13 \times 10^7 \quad n = 3$$

$$= 7.68 \times 10^7 \quad n = 4$$

While this procedure is far from satisfactory there is, unfortunately, no rigorous way to obtain these rates. These rates are the same order of magnitude as the observed fluorescence decay rate.

We now calculate the electron temperature and density dependence of the ionisation rate for an arbitrary cross section and compare the results to the observed fluorescence decay rates.

Temperature and Density Dependence of Ionisation Rate

The collisional ionisation rate is highly temperature dependent because the collision rate is a function of the number of electrons with energies above threshold. We use Equation 10.2 to calculate the ionisation rate for an arbitrary cross section with energy dependence :

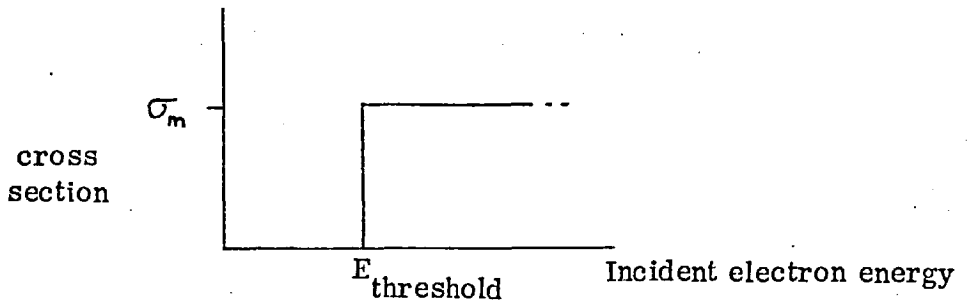

Fig.10.2 shows a plot of the collisional ionisation rate of the n = 3 and 4 levels calculated in this way for an arbitrary cross section taking account of the observed density and temperature behaviour of the linear pinch (Fig.4.1). The graph shows a remarkable similarity to the experimental fluorescence decay results (Fig.5.1) and Fig.10.4 shows a plot of the theoretical n = 3 and 4 level ionisation rates for an arbitrary cross section of 1×10^{-15} cm^2 together with the experimental results. Eqn.6.9 predicts a fluorescence decay rate of $\frac{(g_1/g_2)D_1 + D_2}{1 + (g_1/g_2)}$ where D_1 and D_2 are the loss rates per atom from the lower and upper levels interacting with the laser. In the present case the $\frac{g_1}{g_2} D_1$ term is negligible as $D_1 < D_2$ and the g_1/g_2 factor (0.16 if all the n = 2, and all the n = 3 + 4 levels are grouped together) further reduces the contribution of D_1. Considering the arbitrary form of the cross section the agreement shown in Fig.10.4 is surprisingly good and supports the conclusion that the observed fluorescence decay is due to ionisation of atoms in the n = 3 and 4 levels, and that average ionisation cross section is 10^{-15} cm^2. It is not possible to distinguish between ionisation from particular n = 3 or 4 levels but it is clear from the density and temperature dependence shown in Fig.10.4 that the threshold for the decay process must be close to 1 eV. Multi-step processes, i.e. n = 3 → n = 4 → n = 5 → n = 6 etc. → continuum are likely to have thresholds much less than 1 eV and so are expected to be negligible on the present evidence. To our knowledge no collision cross sections for transitions of this kind in helium have been published.

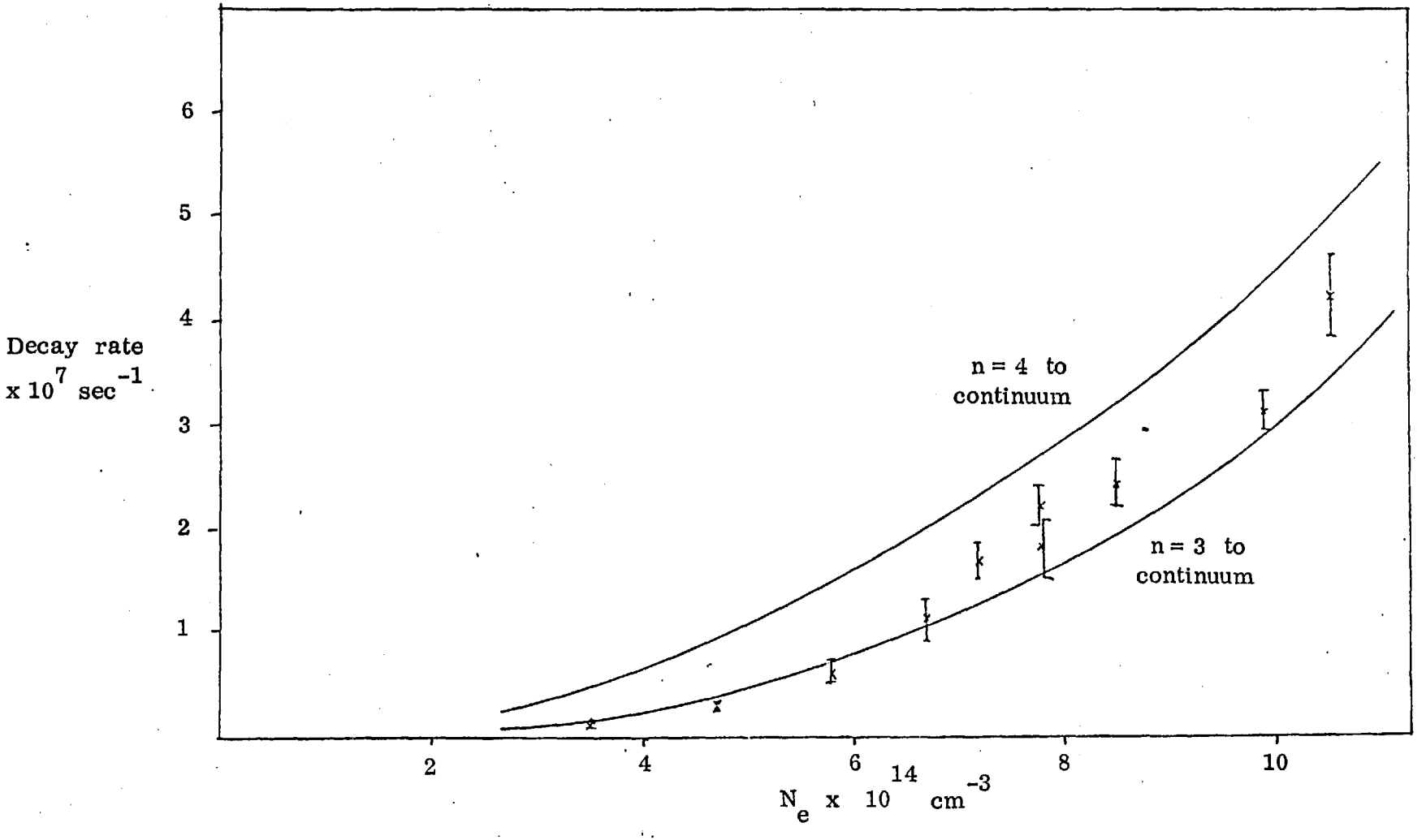

FIGURE 10.4 - Plot of the Collisional Ionisation Rate for the n = 3 and 4 Levels for the Case of a Cross Section = 10^{-15} cm^2 (solid lines), and the experimentally observed fluorescence decay rates (⊥).

Estimation of Populating and Depopulating Rates

The theory described on P.73 also demonstrates new possibilities for deducing the populating and depopulating rates $C_1 + C_2$, $D_1 + D_2$ for a three level atom. In the present case because of the differring enhancements of the n = 3 and 2 levels it is not possible to perform an unambiguous calculation of these quantities. However, using an average value of the enhancement we calculate the $C_1 + C_2$, D_1, D_2 rates for various groupings of the n = 3 and 4 levels. This treatment involves a slightly inconsistent treatment of the g_1/g_2 factor in Eqn.6.9. Eqn.6.7 states that when the laser is on the upper and lower levels have populations in proportion to their statistical weights. However, for n = 2 and 3 levels other than 2^3P and 3^3D this is not the case (Table 8.2), and hence Eqn.6.9 is not strictly valid. In the calculation of the expected decay rate due to ionisation (P.130) we assume the $1 + g_1/g_2$ factor to be approximately one because of this difficulty. Taking first the 2^3P and 3^3D levels alone we have -

$$\frac{(g_1/g_2)\ D_1 + D_2}{1 + (g_1/g_2)} = 3.1 \times 10^7 \text{ (from Fig.5.1)} \qquad (10.6)$$

i.e. $$\frac{9}{15} D_1 + D_2 = 5.0 \times 10^7$$

From Table 8.2

$$\frac{N_{2\ peak}}{N_{20}} = 3.3$$

$$\Rightarrow \quad \frac{N_{10}}{N_{20}} = 4.3$$

also

$$\frac{N_{2\ plateau}}{N_{20}} = 2.0$$

$$= \frac{C_1 + C_2}{N_{20}\left(\frac{g_1}{g_2} D_1 + D_2\right)}$$

i.e. $$\frac{C_1 + C_2}{N_{20}} = 10 \times 10^7$$

Before the laser is turned on we have Eqn.6.6.

$$\frac{C_1 + C_2}{N_{20}} = \frac{N_{10}}{N_{20}} D_1 + D_2 \qquad (10.7)$$

$$10 \times 10^7 = 4.3\ D_1 + D_2$$

combining Eqns.10.6, 10.7 we have

$$D_1 = 1.3 \times 10^7 \text{ sec}^{-1}$$

$$D_2 = 4.2 \times 10^7 \text{ sec}^{-1}$$

We also obtain values for $\frac{C_1 + C_2}{N_{20}}$, D_1 and D_2 by grouping (i) the $3\,^3S, P, D$ levels, (ii) all the $n = 3$ levels (no enhancement is detected in the $n = 4$ levels at 30 μS delay). As the signal/noise ratio in the sensitised fluorescence recorded at 30 μS delay is moderate we obtain the $\frac{N_{2\text{ plateau}}}{N_{20}}$ values for the sensitised fluorescence by comparison with the $\frac{N_{2\text{ peak}}}{N_{2\text{ plateau}}}$ observed for the 5876 Å transition using the fact that the time histories of the sensitised fluorescence are identical to the fluorescence directly excited by the laser. The results are summarised in Table 10.1.

TABLE 10.1

Levels	2^3P 3^3D	2^3S, P 3^3S, P, D	All n = 2 and n = 3
$\frac{g_1}{g_2}$	$\frac{9}{15}$	$\frac{12}{27}$	$\frac{16}{36}$
$\frac{N_{2\ peak}}{N_{20}}$ (average)	3.3	2.5	2.0
$\frac{N_{2\ plateau}}{N_{20}}$ (average)	2.0	1.5	1.2
$\frac{N_{10}}{N_{20}}$	4.3	2.65	1.92
$\frac{C_1 + C_2}{N_{20}}$ ($\times 10^7$ sec^{-1})	10	6.7	5.4
D_1 ($\times 10^7$ sec^{-1})	1.3	1.0	0.61
D_2 ($\times 10^7$ sec^{-1})	4.2	4.0	4.2

For the different groups of levels used the rate coefficients turn out to be approximately the same. However because of the difficulties associated with the g_1/g_2 factor these values should only be regarded as provisional. As a plateau was only observable at high electron densities a study of the variation of $\frac{C_1 + C_2}{N_{20}}$ with electron density is not possible. One possible process corresponding to C_1 and C_2 is three body recombination to the n = 3 and 2 levels, either directly or through intermediate highly excited states.

Roberts (1973) has measured effective three body recombination coefficients by studying the decay of an helium arc plasma. At $T_e = 10^4$ degrees he estimates a recombination coefficient K of 4×10^{-28} cm^6 sec^{-1}. In the absence of doubly ionised helium and associative recombination K is defined by

$$\frac{dN^*}{dt} = -K N_e^2 N^*$$

In the present case, N^*, the ionised helium number density, is equal to the electron density

$$\frac{dN^*}{dt} = -4 \times 10^{-28} \times (10^{15})^3$$

$$= -4 \times 10^{17} \text{ sec}^{-1}$$

The collisional excitation rate from the ground state is (P.124) 2×10^{-2} sec^{-1}. Multiplying this by the ground state number density leads to a value of the net populating rate due to excitation of ground state atoms of 3×10^{14} cm^{-3} sec^{-1}.

In the present case we take

$$\frac{C_1 + C_2}{N_{20}} = 5 \times 10^7 \text{ sec}^{-1}$$

We deduce a value of N_{20} from Fig.8.1, Table 10.1 and the absolute value of the 2^3P population measured by Cairns (1970)

$$N_{20} = 5 \times 10^{11} \text{ cm}^{-3}$$

thus

$$C_1 + C_2 = 1.7 \times 10^{19} \text{ sec}^{-1}$$

Thus it would seem that the process responsible for $C_1 + C_2$ is either atoms cascading from higher excited levels or associative recombination. These problems are further discussed in Chapter XV.

To conclude: the similarity between the observed 5876 Å fluorescence decay rate and the predicted ionisation rate strongly suggests that the observed fluorescence decay is due to collisional ionisation from the $n = 3$ and/or 4 levels with an average cross section of 10^{-15} cm^2.

CHAPTER XI

EXCITATION TRANSFER BETWEEN THE He n = 2, n = 3 AND 4 LEVELS

OPTICAL OPACITY MEASUREMENTS

At the beginning of Chapter IX we made the assumption that all the n = 2 and n = 3 and 4 levels behaved simply as a two level system, fast collisional processes among the levels "locking" the level populations to a fixed ratio. We now examine this assumption in detail. First we discuss collisional processes among the n = 3 and n = 4 levels. Then we describe an experimental investigation into the opacity of the plasma towards radiation arising from transitions from n = 3 and 4 to n = 2. This enables us to estimate the rate at which atoms leave the n = 3 levels. It also reveals changes in the n = 2 (other than 2^3P) level populations during the laser pulse. Finally, we deduce collision rates between the n = 2 levels from some recent cross section calculations and consider the kind of equilibrium established during the laser pulse.

I. Transfer among the n = 3 and n = 4 Levels

The presence of sensitised fluorescence on all the n = 3 and 4 to n = 2 transitions of exactly the same shape as the 5876 Å fluorescence implies a collisional transfer rate between these levels that is faster than the rise time of the fluorescence (20 nS) (see P.104). We compare this rate to the results of Wellenstein and Robertson (1972a). Their cross sections for collisional transfer between singlet and triplet states $3^1D - 3^3D$ are 0.02×10^{-16} cm^2 for atom collisions and $3.0 \pm 1.5 \times 10^{-16}$ cm^2 for electron collisions. In our case this corresponds to a transfer rate of 2×10^4 sec^{-1} and 4.5×10^6 sec^{-1} at a delay of 100 μS; much too slow to account for the sensitised fluorescence.

The alternative of transfer between the n = 3 levels via the continuum would not explain the absence of sensitised fluorescence from n = 5 → n = 2 transitions. As it is most likely that electron collisions are responsible for the transfer we deduce a lower limit on the cross section for transfer among the n = 3 and 4 levels by electron collision of

$$\sigma \geqslant \frac{\text{rate}}{\text{density x velocity}}$$

$$= \frac{1}{20 \times 10^{-9} \times 3 \times 10^{14} \times 5 \times 10^{7}}$$

$$= 4 \times 10^{-15} \text{ cm}^2$$

II. Opacity of the Visible Helium Transitions

In this section we describe studies of the optical opacity of the visible helium transitions in the plasma with and without simultaneous laser excitation.

Experimental Set-Up

A "Garton type" flashtube was used as a continuum source. (Wheaton, 1964). This produced a 2-3 μS pulse of radiation which in the visible region of the spectrum closely corresponded to a blackbody with a temperature of 30,000 ^{o}K. The light was focussed at the centre of the pinch and then collected and dispersed by a monochromator. The optical path was at right angles to the pinch axis (Fig.11.1). Initially a completely independent monochromator was set up so as to permit simultaneous observations of the fluorescence and absorption. However the second monochromator proved to have a very low efficiency and this system was abandoned. Instead the flashtube was arranged so the light from it was collected and dispersed by the monochromator used in the fluorescence measurements. The absorption and fluorescence were then recorded on different shots.

"Garton" type flashtube.

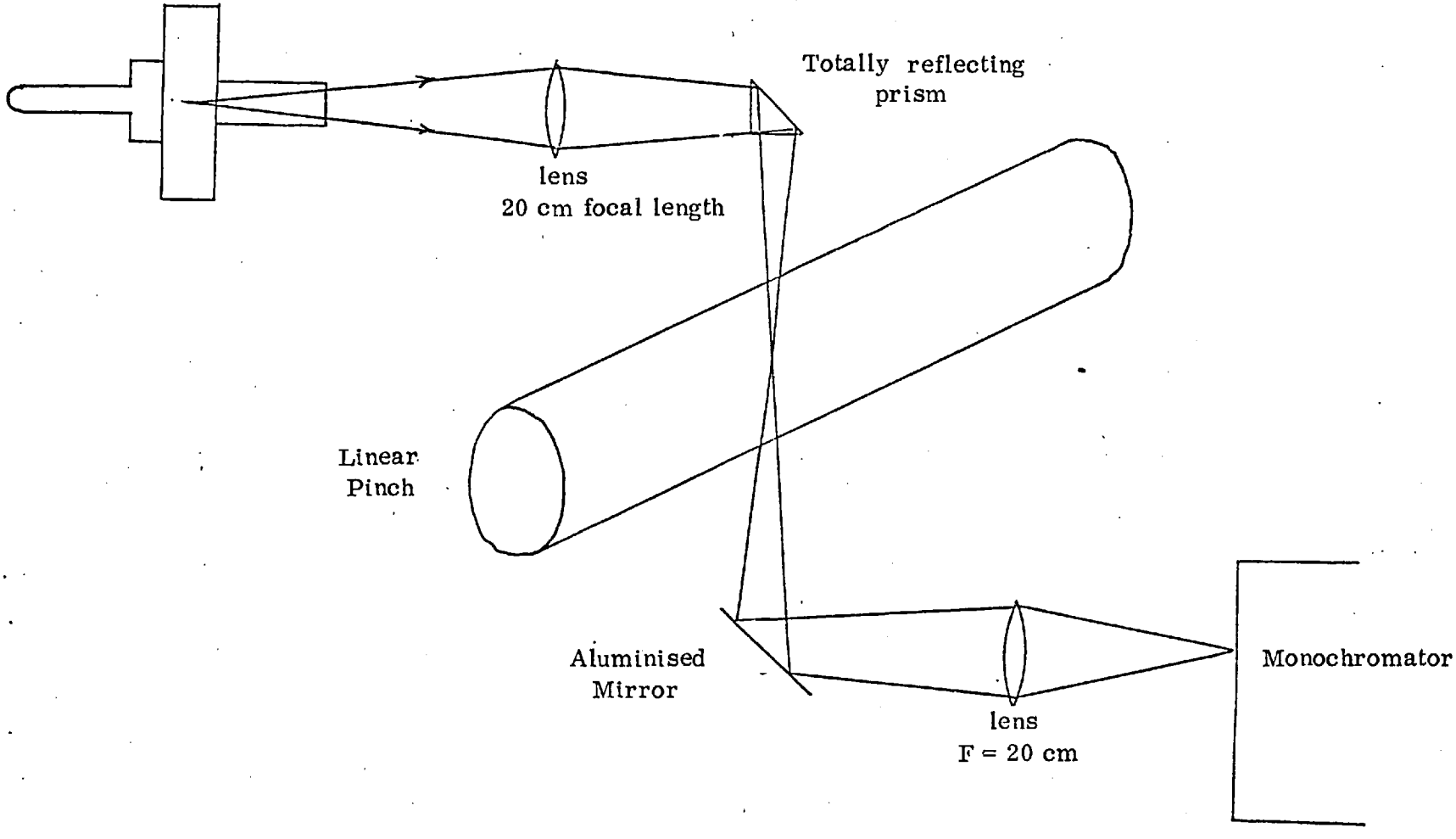

FIGURE 11.1 - OPACITY MEASUREMENTS : EXPERIMENTAL SET-UP

The flashtube was continuously evacuated by a single stage rotary pump with a cold trap. It was powered by a 10 μF capacitor connected to the flashtube by low inductance strip leads. The capacitor voltage was set to 7 kV before each shot. The flashtube was triggered by the same pulse from the external delay unit that triggered the laser as the formative lag between the trigger pulse and the initiation of the discharge was roughly the same in both cases. However, for the best results it was necessary to synchronise the laser with a part of the flashtube time history when the intensity was changing relatively slowly. This was difficult to achieve as the formative lag of the flashlamp was a sensitive function of the capacitor voltage and the pressure, the last being a function of the length of time since the last shot. This synchronisation was achieved through careful manipulation of the flashtube pressure as the difference in time between the laser and flashtube was shorter than the minimum delay available from an electrical delay unit. It was especially important to avoid timing jitter as this would appear as intensity variation on a fast oscilloscope time scale. During a run the flashtube was fired at intervals of exactly 30 seconds, and in this way the timing jitter was reduced to an acceptable level (Plate VI). For each setting, four traces were recorded: (Plate VI) :

(i) The flashtube alone.

(ii) The flashtube with the plasma.

(iii) The flashtube with the plasma and laser.

(iv) The plasma and laser without the flashlamp.

The difference between traces (i) and (ii) is a measure of the absorption. In order to obtain the best signal/noise ratio the absorption was measured as a function of monochromator slit width. Although the proportion of light

PLATE VI - OPTICAL OPACITY RESULTS

Garton Flashtube
Intensity

3 shots

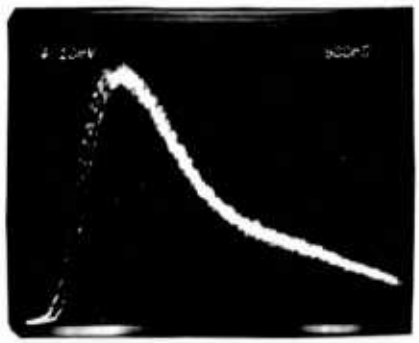

Absorption at 5876 Å
60 μS Delay.

i) Flashtube only

ii) Flashtube with plasma and laser

iii) Flashtube with plasma

iv) Plasma and laser alone on same scale

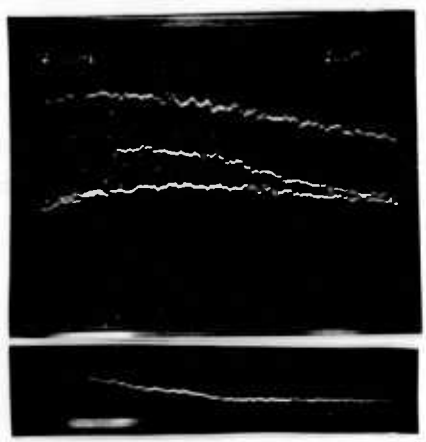

LASER REPRODUCIBILITY AND TIMING JITTER

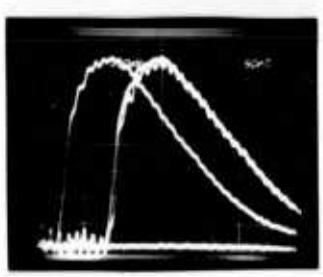

Total laser intensity
3 shots

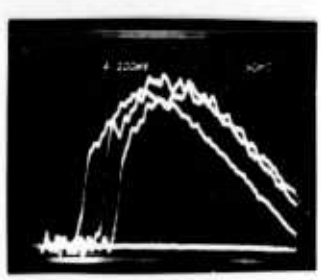

Laser Intensity
(That part producing the fluorescence)
3 shots

LASER FLASHLAMP CURRENT AND LIGHT EMISSION TIME HISTORY

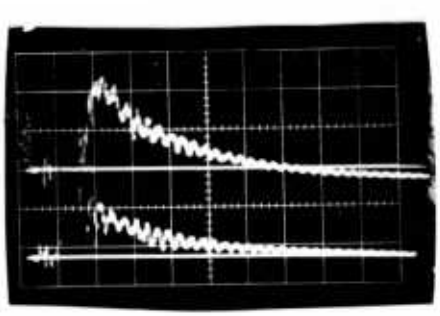

500 nS/cm
Upper: Current
Lower: Light emission
Laser capacitor voltage set to 25 kv
(Fast oscillation is due to electrical pick-up)

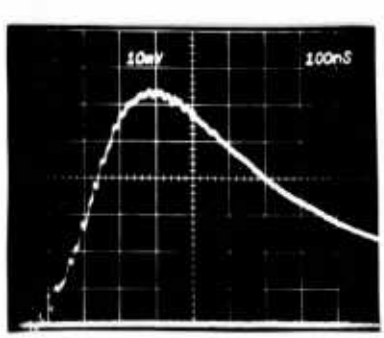

Laser Flashlamp
Light emission.

absorbed decreased with increasing slit width, in absolute terms the amount of absorption increased up to the point where the photomultiplier response became non-linear. The slit width was set at about half this value or less for these experiments (i.e. at 35 μm or 10 μm). The slit height was reduced to 3 mm to exclude as much of the fluorescence as possible.

The monochromator wavelength was set using a helium lamp as the pinch emission intensity was low. This leads to slight errors for lines with appreciable stark shifts (e.g. 4471 Å) but the monochromator instrumental width (0.27 Å) was large enough to make this negligible.

The light intensity of the flashtube was much too small (of the order of milliwatts cm^{-2} Å $^{-1}$) to necessitate any correction due to the excitation of fluorescence by the continuum illumination.

Results : Opacity

No absorption (< 5%) was detected on the following transitions :

$2^1S - 3^1P$
$2^1S - 4^1P$
$2^1P - 3^1S$
$2^1P - 4^1S$
$2^1P - 4^1D$
$2^3P - 3^3S$
$2^3P - 4^3S$

Absorption was detected in the transitions listed in Table 11.1.

The optical depth of the 5876 Å transition as a function of delay time is shown in Fig. 11.2. It can be seen that the degree of optical trapping is small.

We now estimate the decay rate for atoms in the n = 3 and 4 levels to the n = 2 levels. Atoms which decay to the 2^3P level are immediately

FIGURE 11.2 - OPTICAL DEPTH OF 5876 Å TRANSITION

(35 μ slits)

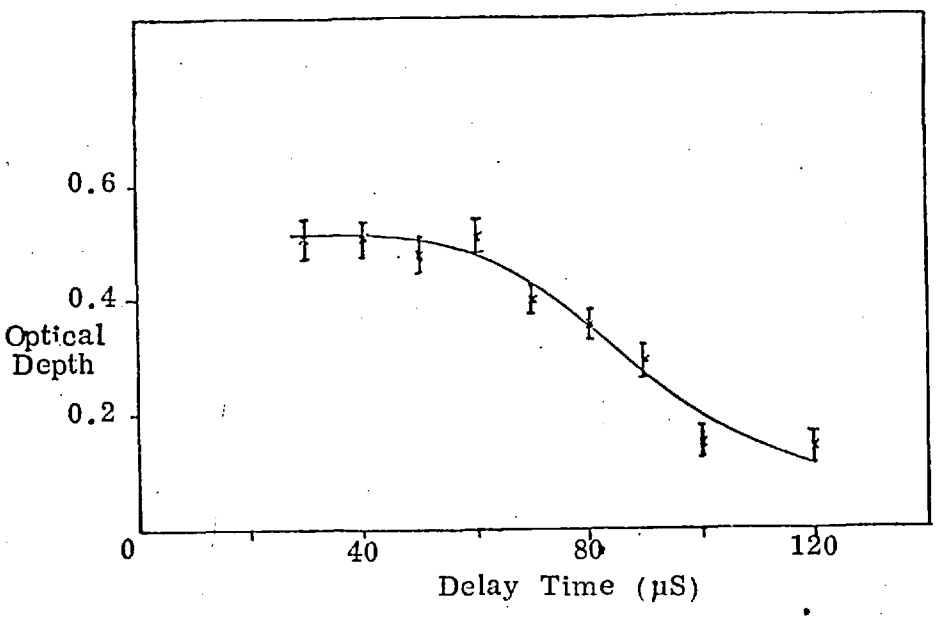

FIGURE 11.3 - DECREASE IN ABSORPTION DUE TO LASER

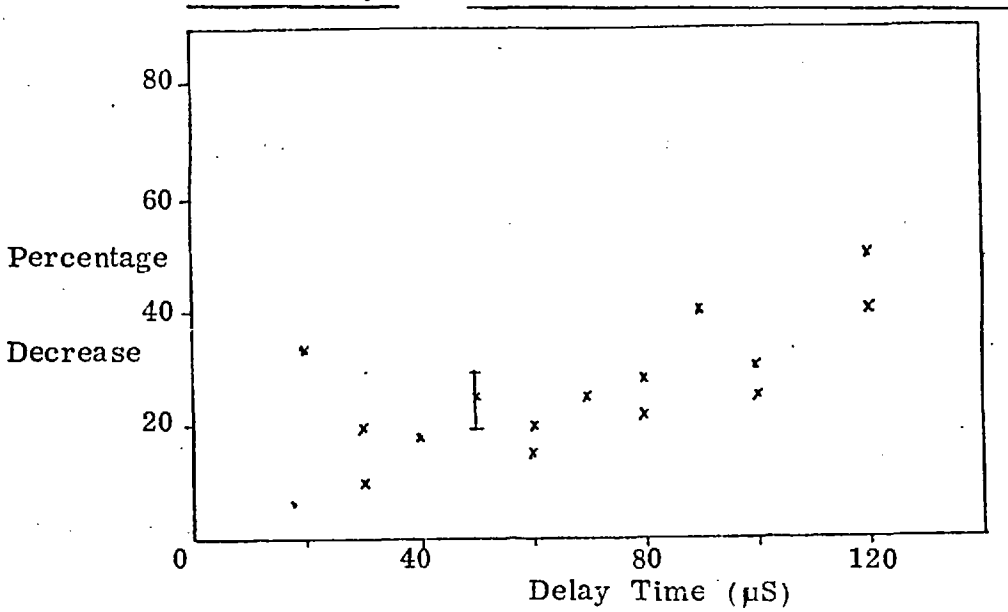

FIGURE 11.4 - ABSORPTION WITH LASER - PULSE LENGTH (P.147)

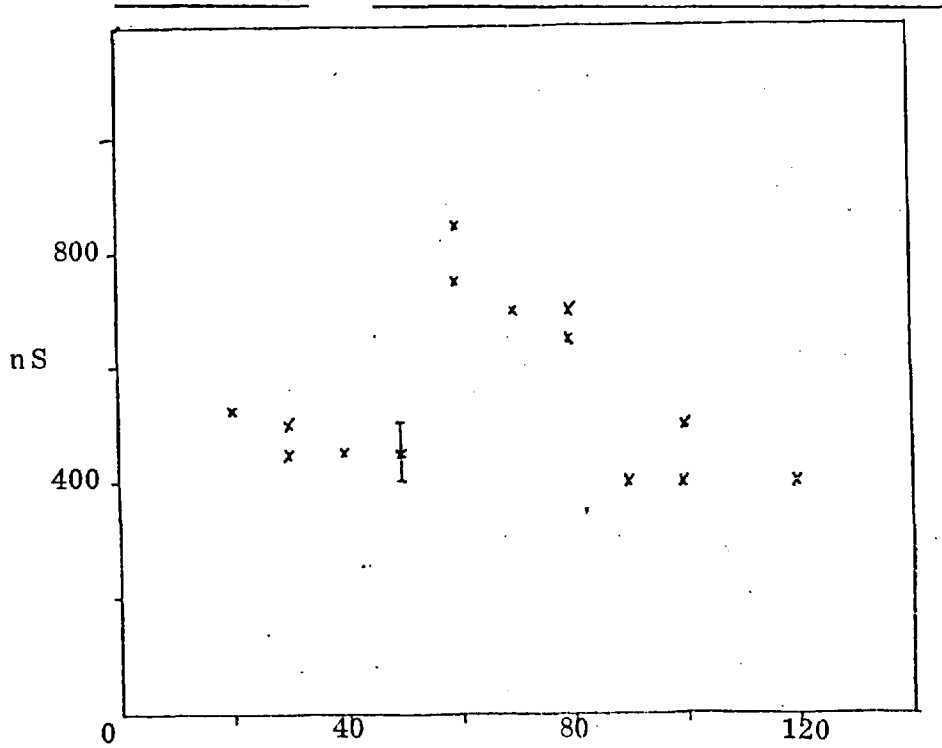

re-excited by the laser so we do not include those transition rates. We also do not take into account radiative decay from n = 4 levels as the n = 4 enhancements are much smaller than in the n = 3 case. The single atom radiative decay rates for the transitions in Table 11.1 will need slight adjustment because of the finite optical depth. Holstein's theory, discussed on P.109, does not apply in the present case as the optical depth is not large. An overestimate of the modification of the radiative decay rate is :

$$A_{effective} = A_{ij} \; e^{-kx}$$

where kx is the optical depth. This only decreases the average radiative decay rate by 5%. Taking the single atom 'A' values then we weight the radiative decay probability for a particular level by the relative probability of finding an atom in that level. In the presence of the laser illumination the latter is given by the product of the statistical weight, the relative sublevel population (P.101) and the fluorescence enhancement (P. 103). The average radiative decay rate calculated in this way for the case of a 30 μS delay time is 2.16×10^{7} sec^{-1} corresponding to a lifetime of 46 nS. As the total duration of the fluorescence is 450 nS it is clear that the 2^3P population at least, will be cycled between the n = 2 and n =3 levels at least 10 times during the fluorescence pulse. This has implications for the collision rates between the n = 2 levels.

n = 2 Level Populations (Without Laser)

Estimates of the relative populations of the n = 2 levels were obtained from the absorption measurements. As the n = 3 to n = 2 transitions are predominantly doppler broadened the line widths are approximately the same. We obtain relative populations by dividing the optical depth by the f-value of the transition. It was only possible to deduce an upper limit for the 2^1S population as no absorption was detected on transitions from this level.

TABLE 11.1

Wavelength Å	Transition	f-Value	Delay Time	Transmission (Spectrometer slits set to 10 μm)	Optical Depth
6678	$2^1P - 3^1D$	.71	20 μS	.9 ± .05	.11 ± .05
			30 μS	.87 ± .05	.14 ± .05
			60 μS	.9 ± .05	.11 ± .05
3888	$2^3S - 3^3P$	.06	30 μS	.75 ± .05	.29 ± .05
			60 μS	.73 ± .05	.31 ± .05
5876	$2^3P - 3^3D$	.61	30 μS	.4 ± .05	.92 ± .08
			60 μS	.4 ± .05	.92 ± .08
4471	$2^3P - 4^3D$	.125	60 μS	.93 ± .05	.07 ± .05

Relative Populations of n = 2 Levels

	30 μS Delay	60 μS Delay
2^3P	1	1
2^3S		3.1 ± 0.5
2^1P	0.1 (± .05)	.1 ± .05
2^1S	0.2 (± .05)	0.2 (± .05)

Cairns (1973) gives a value of 3.7×10^{11} cm^{-3} for the absolute number density of the 2^3P level at 30 μS delay. (He also gives a lower limit of 10^{13} on the 2^3S population from measurements of the optical depth along the pinch axis but later states that this is too high as he could detect no absorption in a transverse direction to the pinch axis.)

n = 2 Populations (With Laser)

The absorption was measured during the laser pulse to record any changes in the n = 2 populations. For the $2^1S - 3^1P$ and $2^1P - 3^1D$ transitions no change was observed. This is not surprising considering the small amount of absorption and the small proportion of the plasma being illuminated by the laser. For the $2^3S - 3^3P$, 3888 Å transition however a very small change was apparent at a delay of 60 μS. Possible changes due to the presence of sensitised fluorescence, or the increased 3^3P population in itself reducing the absorption could not account for this. The decrease in the plasma absorption must have been due to a decrease in the 2^3S population during the laser pulse. After correction by a geometric factor to account for the fact that only a part of the pinch was illuminated by the laser the results revealed a large decrease (50 - 100%) in the local 2^3S population during the laser pulse.

5876 Å Opacity

Typical results are shown in Plate VI. In the second photograph four traces are shown :

(i) The flashtube intensity without the laser or plasma.

(ii) The flashlamp intensity transmitted through the plasma with the laser being fired a short time after the start of the trace.

(iii) The flashlamp intensity transmitted through the plasma in the absence of the laser.

(iv) The fluorescence produced by the plasma and laser alone.

It can be seen that the total intensity detected rises during the laser pulse and that part of this is due to the fluorescence. Similar results were observed over a range of delay times.

An unexpected feature is the continuation of the enhanced transmission of the flashtube light detected after the laser pulse. This was especially apparent for delays from 60 - 80 μS, the enhanced level continuing for about 200 - 300 nS.

Discussion of 5876 Å Opacity

Because the laser is operating above saturation with the 2^3P and 3^3D level populations equalised no absorption takes place in the region of the plasma illuminated by the laser. This, of course, means that no direct measure of the 2^3P population during the laser pulse is possible. The reduction in the observed absorption is a measure of the proportion of the plasma illuminated by the laser. In order to deduce this factor the observed flashtube intensity during the laser pulse needs correction because of the presence of the fluorescence. The optical depth in the absence of the laser is given by

$$\ln \frac{I_{(iii)}}{I_{(i)}}$$

where $I_{(i)}$ is the intensity shown on the (i)th trace as described on P.140. The optical depth with the laser on, after correction for the fluorescence is

$$\ln\left(\frac{I_{(ii)} - I_{(iv)}}{I_{(i)}}\right)$$

We define a quantity, α, by the following relationship -

$$\alpha = 1 - \frac{\ln\left(\frac{I_{(ii)} - I_{(iv)}}{I_{(i)}}\right)}{\ln\left(\frac{I_{(iii)}}{I_{(i)}}\right)}$$

This represents the proportion of the plasma illuminated by the laser. In practice, as the optical depth was small, α was given to a sufficient accuracy by the fractional decrease in absorption with the laser on.

The value of α over a range of plasma conditions is given in Fig.11.2. On average α was about 0.25, close to the factor expected from the ratio of the diameter of the laser beam to the internal diameter of the discharge vessel (0.28).

The continued enhancement of the flashtube transmission after the laser pulse must be due to the relatively slow relaxation of the 2^3P population back to its original value. This is shown by the following model. For convenience the laser is assumed to illuminate the whole plasma and the 2^3P and 3^3D pooulations are assumed to be 24 and zero respectively before the laser is turned on. The laser is a step function in time.

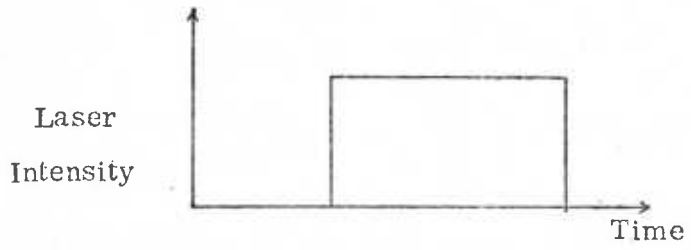

The 3^3D population as a function of time may be obtained from the fluorescence traces as the optical depth is small. Experimentally, at a delay time of 60 μS, the 3^3D population is a third of its peak value just before the end of the laser pulse. While the laser is on the 2^3P and 3^3D populations are in the ratio of their statistical weights.

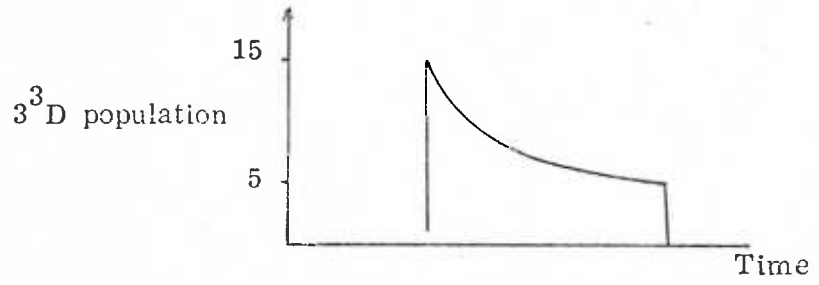

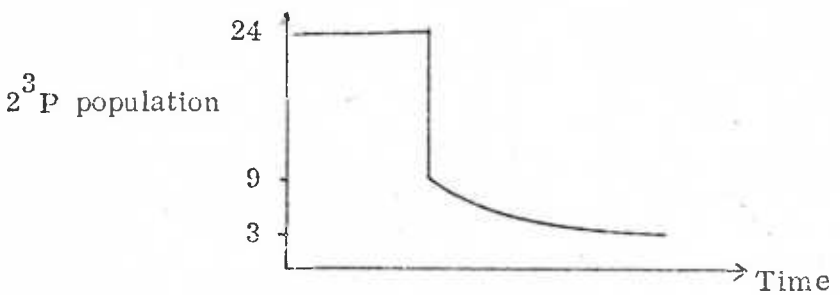

At the end of the laser pulse the 3^3D population decays to the 2^3P level by radiative transition so the 2^3P population is increased to 8. Subsequently it regains its former equilibrium with the rest of the plasma with a time constant given by the decay rate out of the 2^3P state per atom (D_1 in the notation of Chapter VI. See also Appendix 1.)

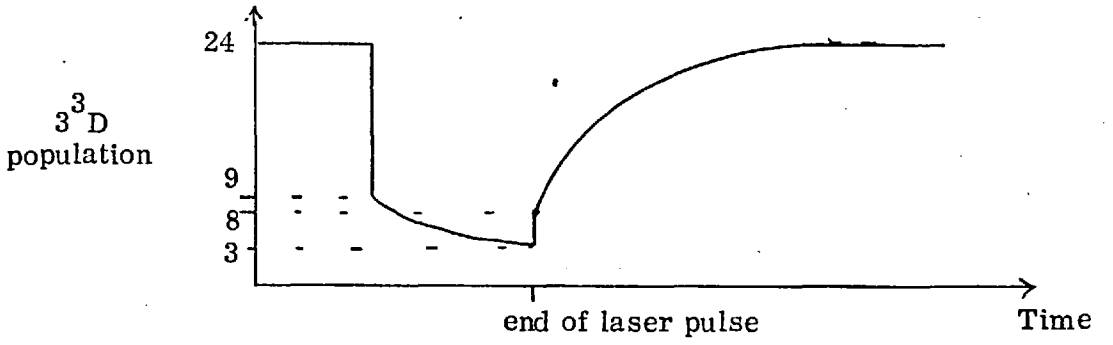

The transmitted flashtube intensity is governed by the 2^3P population and also displays this decay rate.

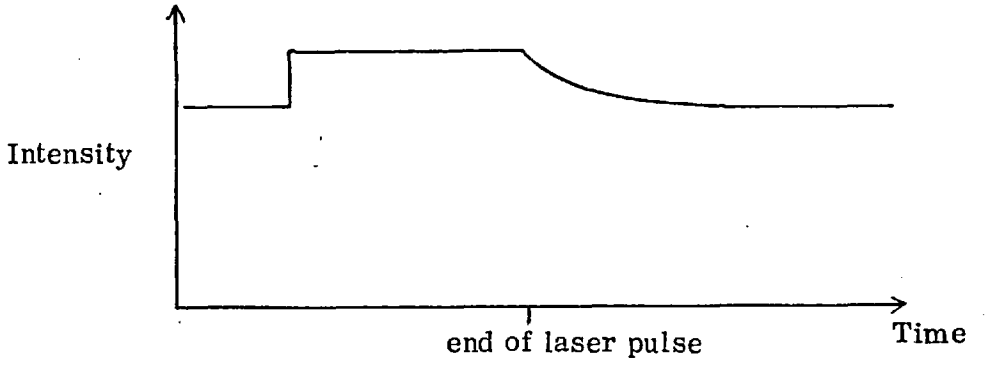

The behaviour of α, with time gives a measure of this decay rate. The pulse length of α is given in Fig.11.4. As α is obtained by considering the differences between four traces it is not possible to estimate this rate to a high accuracy even in the absence of timing jitter. The results at a 60 μS delay show a decay rate similar to the decay rate observed in the fluorescence (approximately 10^7 sec^{-1}). Assuming this similarity also holds at 30 μS and 100 μS delay we explain the apparent lack of relaxation effects in the flashtube intensity at these times as follows. At 30 μS the relaxation is

too fast to be detected. At 100 μS the relaxation is slow but small in amplitude - few atoms have been transferred from the 2^3P-3^3D system - and is hence unobservable in the shot noise.

Fluorescence "After Effects"

The continuation of an enhanced level of plasma emission observed in the fluorescence traces after the end of the laser pulse (P.97) may be understood in exactly the same way.. The delay times at which this is most apparent in the fluorescence correspond exactly to the times when this effect is observed in the flashtube absorption traces. In the absence of the laser the 5876 Å light from the far side of the discharge has to pass through the plasma, of optical depth 0.9, before being detected. When the laser is on the central region becomes transparent and this leads to an increase in the 5876 Å light observed. This increase will last until the 2^3P population relaxes back to its original value.

We conclude -

1) Optical depth measurements show that the radiative decay of n = 3 and 4 states to n = 2 is unimpeded by radiation trapping.
2) Observations of the optical depth of the $2^3S - 2^3P$ transition show that the 2^3S population is reduced during laser excitation of the $2^3P - 3^3D$ transition.
3) Relaxation effects observed in the absorption after the end of the laser pulse provide an independent measure of the decay rate out of the 2^3P level.

We now consider the transfer of atoms among the n = 2 levels necessary to sustain a fluorescence pulse longer than the radiative lifetime of the n = 3 levels.

III. Collisions Between n = 2 Levels

As we have seen, when the laser is turned on about half the 2^3P population is excited to the 3^3D level, transferred among other n = 3 and 4 levels, and then decays down to the n = 2 levels. If there were no transfer between the n = 2 levels the 2^3P population would quickly be exhausted and no further fluorescence would be observed. Theoretical cross sections for transfer between the n = 2 levels have been calculated using the close coupling approximation by Burke et al. (1972). Their cross sections show a complex resonant structure near threshold. We convert these cross sections to collision rates using the formula derived on P. 123 We approximate the complex shape of the theoretical calculations by a series of step functions, the main contribution to the rate coming from the region near to threshold.

We obtain the de-excitation rates from consideration of detailed balance

$$\text{de-excitation rate} = \frac{g_{lower}}{g_{upper}} \times \exp \frac{\Delta E}{kT} \times \text{excitation rate}$$

where the g's are statistical weights and ΔE is the energy difference between the two levels.

$$\text{Excitation rate} = \sum_i \frac{2}{(\pi)^{\frac{1}{2}}} N\sigma_i \left(\frac{2kT}{m}\right)^{\frac{1}{2}} \left\{ \frac{E_i}{kT} + 1 \right\} \exp - \left(\frac{E_i}{kT}\right)$$

where the cross section, σ , is represented by

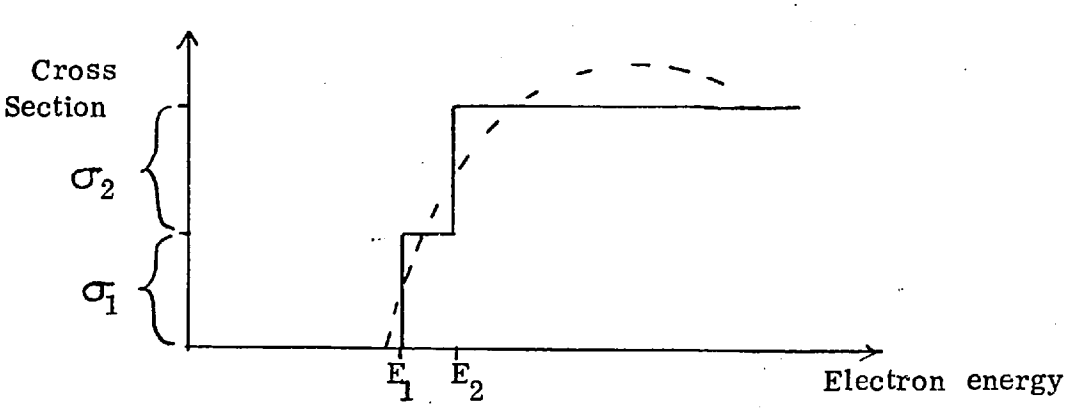

The dashed line represents the theoretical cross section of Burke et al. The excitation and de-excitation rates are calculated for the plasma conditions at 30 μS and 100 μS delay. The results are shown in Table 11.2 and in Figs.11.3 and 11.4. The latter also show radiative and other collisional rates deduced previously and also the observed n = 2 level relative populations. The uncertainties in the (de) excitation rates due to approximating the cross sections is estimated to be 30%.

In general it is hard to visualise the behaviour of all the level populations because of the many simultaneous processes. One important factor is the coupling between the 2^3S and 2^3P populations. If these levels were in LTE the ratio of their populations for kT = 1 eV would be

$$\frac{2^3P}{2^3S} = \frac{g_2}{g_1} \exp\left(-\frac{E}{kT}\right) = 0.96$$

in practice

$$\frac{2^3P}{2^3S} = 0.32$$

so it is clear that 2^3S is overpopulated (or 2^3P is underpopulated) compared to the LTE case. Also comparing the 2^3P and 2^1P populations it is clear that 2^3P is overpopulated compared with 2^1P. The reason for this is not clear as the collision rates between the n = 2 levels are faster than the radiative rates including the effective radiative decay to ground $2^1P - 1^2S$ (P. 154). The observed reduction in the 2^3S population when the laser is on is consistent with a close coupling between the 2^3S and 2^3P levels. At 30 μS delay the n = 2 collisional transfer rates are sufficiently fast to permit the rapid cycling of atoms from $2^3P \rightarrow 3^3D \rightarrow$ other n = 3 levels $\rightarrow$ n = 2 levels $\rightarrow 2^3P$ necessary if the fluorescence is to be sustained throughout the laser pulse.

TABLE 11.2 - CALCULATION OF COLLISIONAL TRANSFER RATE BETWEEN n = 2 LEVELS FROM THE CROSS SECTIONS OF BURKE ET AL. (1972)

Transition	Threshold eV	g_1/g_2	Cross Section (πa_o^2)	Above an Energy of eV	30 μS Delay $N_e = 9.9 \times 10^{14}$ cm^{-3} $T_e = 0.802$ eV Rate Up	30 μS Delay Rate Down	100 μS Delay $N_e = 3.4 \times 10^{14}$ cm^{-3} $T_e = 0.345$ eV Rate Up	100 μS Delay Rate Down
$2^3S - 2^3P$	1.14	1/3	18	1.22	51.8×10^6		2.8×10^6	
			50	1.86	85.3		1.71	
			15	2.72	11.6		5.91	
				Total	149	205×10^6	4.57	41.5×10^6
$2^3S - 2^1P$	1.40	1	2	1.56	4.4	25.2	0.141	8.17
$2^3S - 2^1S$	0.796	3	11	0.9	39.7	321	3.44	104
$2^3P - 2^1P$	0.25	3	2.0	0.33	9.77	40	1.77	11
$2^1S - 2^3P$	.35	1/9	35	.4	166		27.9	
			less 17	1.0	57.3		4.3	
				Total	109	18.5	23.6	7.23
$2^1S - 2^1P$	0.6	1/3	50	.79	194		19.6	
			200	1.54	447		14.8	
				Total	641	451	34.4	65.3

FIGURE 11.3 - HELIUM : POPULATIONS AND COLLISION RATES

30 μS Delay : $N_e = 9.9 \times 10^{14}$. $T_e = 0.8$ eV

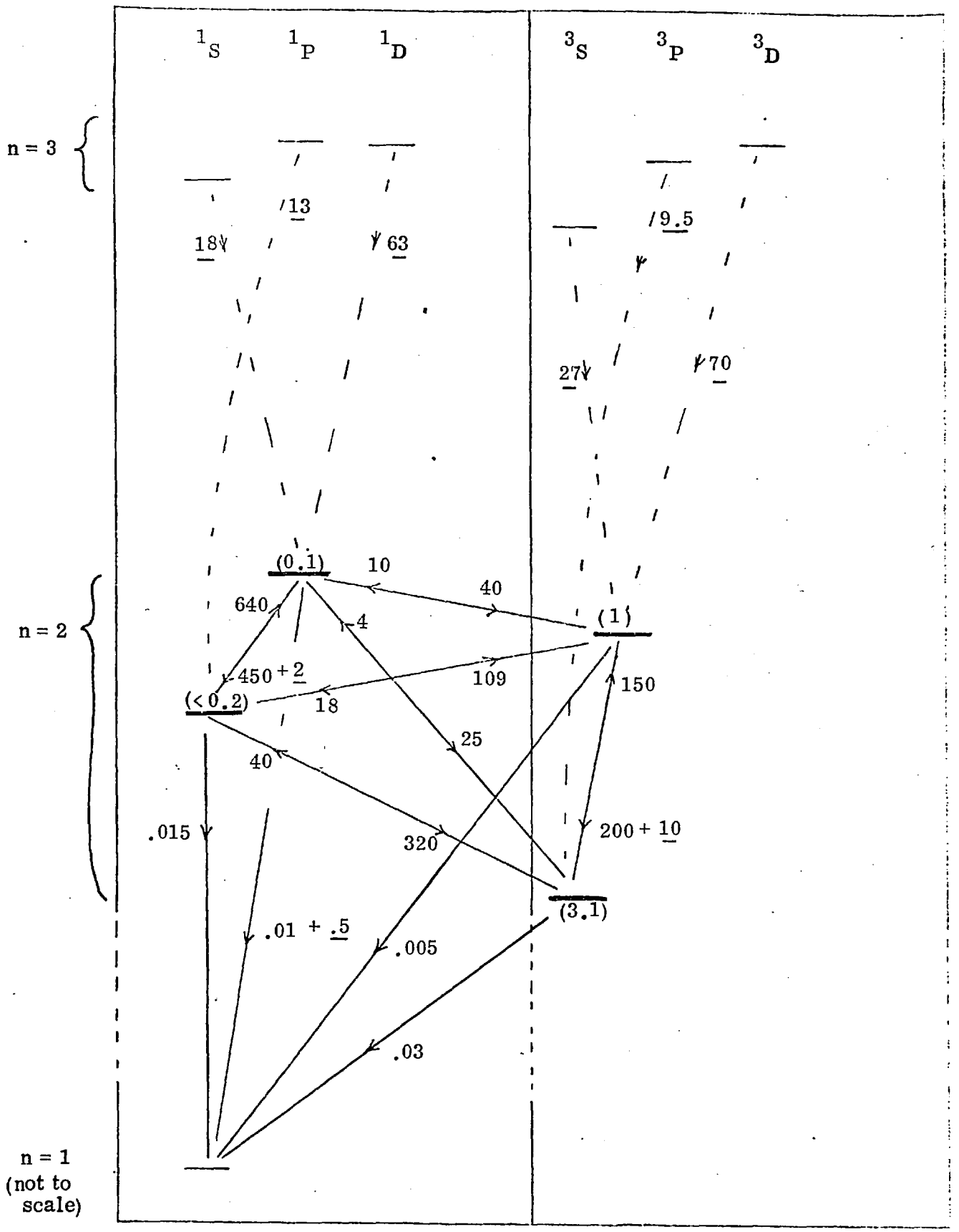

Collision rate $\times 10^6$ sec^{-1}.

Radiative rate shown underlined $\times 10^6$ sec^{-1}
($2^1P \rightarrow 1^1S$ rate corrected for optical trapping).

( ) denotes relative populations.

FIGURE 11.4 - HELIUM : POPULATIONS AND COLLISION RATES

100 μS Delay. $N_e = 3.4 \times 10^{14}$. $T_e = 0.345$ eV.

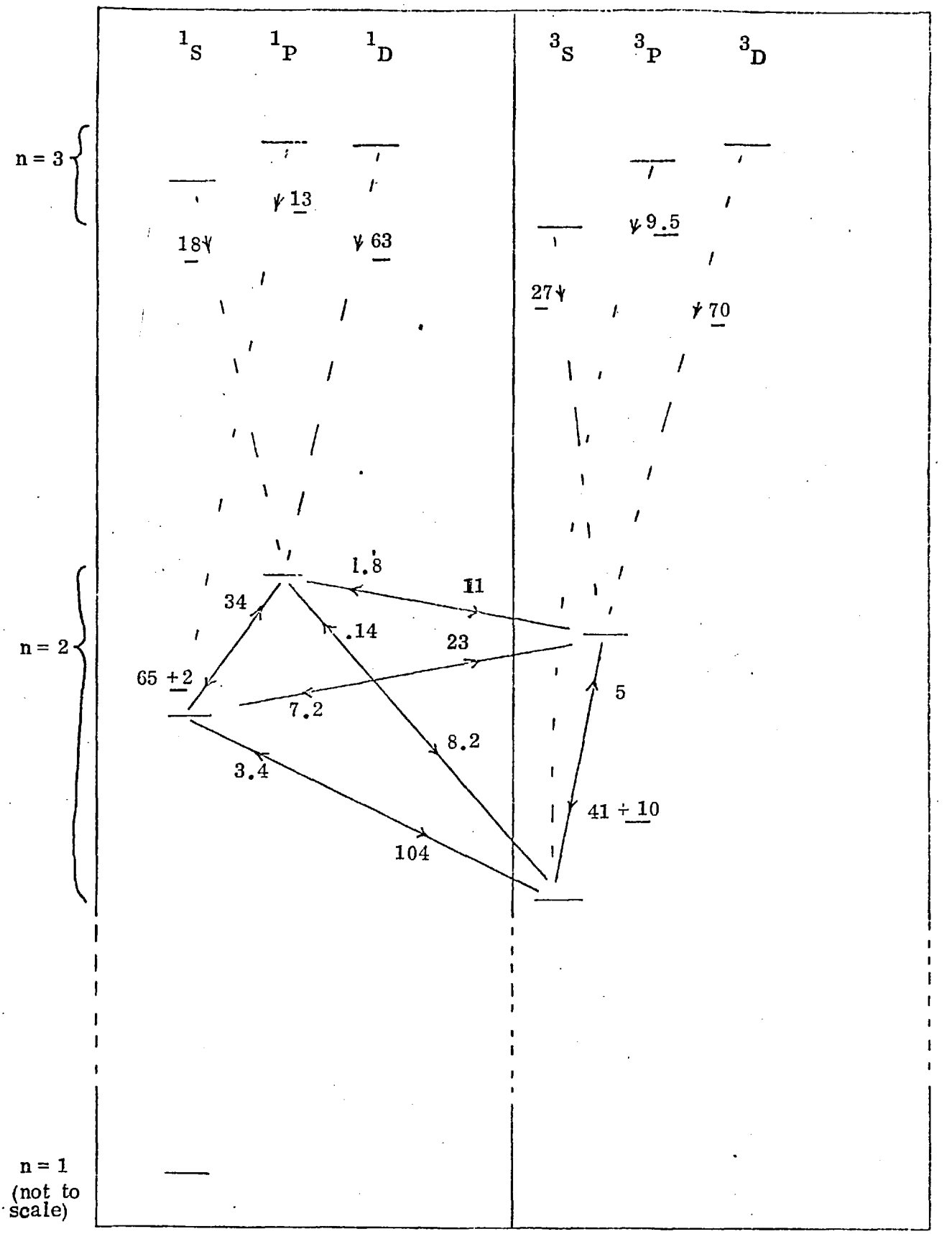

Collision rate x 10^6 sec^{-1}.

Radiative rate shown underlined x 10^6 sec^{-1}.

At 100 μS however the theoretical $2^3S \longrightarrow 2^3P$ rate is slow (5×10^6 sec^{-1}). The de-excitation rate $2^3P \rightarrow 2^3S$ is similar to the rates for other routes of decay for the 2^3P possible when the laser is on, e.g. $2^3P \rightarrow 3^3D$ $3^1D \rightarrow 2^1P \rightarrow 2^1S \rightarrow 2^3S$, and so the slow excitation rate is not necessarily inconsistent with an almost constant intensity fluorescence pulse at 100 μS delay time.

As a further check on the coupling of the n = 2 and 3 levels two experiments were performed. One step taken was to investigate the fluorescence in an atom without these complications - namely hydrogen (see Chapter XIII). Also, the fluorescence produced in helium with the laser wavelength tuned to another n = 3 → n = 2 transition was investigated. The latter is described in the following chapter.

CHAPTER XII

FLUORESCENCE AT 6678 Å

In order to discover whether or not the n = 2 and n = 3 or 4 levels could be regarded as single units in the interpretation of the observed fluorescence, experiments were performed at the equivalent singlet transition to 5876 Å, namely 6678 Å, $2^1P - 3^1D$. The same procedure as for the 5876 Å case was followed. First the laser performance at this wavelength was measured. Then the laser light transmitted by the plasma was examined to discover the time history of the light actually producing the fluorescence and also to estimate the degree of saturation achieved. Finally, the fluorescence was studied over a range of electron densities and laser energies.

Laser Performance at 6678 Å

The wavelength range of rhodamine 6G does not extend to 6678 Å. A mixture of cresyl violet and rhodamine 6G however lases over the range 6350 - 6700 Å with about half the efficiency of rhodamine 6G. The laser was therefore operated with a solution of

128 mg Rhodamine 6G
48 mg Cresyl Violet
} in 1 litre of "Ultrar" methanol.

The dye was filtered through a sintered glass filter (2 μm pore size) before use, as this improved the performance. A dye concentration lower than the above would not lase at 6678 Å.

To offset the lower efficiency of the cresyl violet/rhodamine 6G solution the laser was run at an increased voltage - 20 kV instead of 16 kV. The output energy was typically 30 mJ in a pulse of duration (F.W.H.M.) 200 nS giving an illumination of 32 kW cm^{-2} inside the pinch. As shown

in Fig. 3.6, the spatial characteristics of the laser beam are the same as in the case of rhodamine 6G.

Laser Line Width at 6678 Å

The laser line width,was measured using the arrangement of Fig.4.3. With the intra cavity Fabry Perot at a fixed angle to the laser axis the monochromator was scanned across the laser line and a line profile built up on a shot to shot basis. The wavelength resolved photomultiplier signal was displayed on the 7704 'scope. The scope time base was triggered by the signal from a photodiode monitoring the total laser output. In this way any wavelength change of the laser during the course of a single pulse ("chirp") would be revealed. The same line narrowing during the laser pulse as observed for the 5876 Å transition was apparent and no wavelength shifts were detected. The (whole) half width of the laser line profile at the instant of peak intensity was 5.0 ± 0.5 Å. This compares to 2.2 Å for the 5876 Å case. The difference is due to the lower finesse of the Fabry Perot at 6678 Å. The F.W.H.M. of the transmission band of the Fabry Perot was 32 Å at 5800 Å and 45 Å at 6500 Å.

Saturation at 6678 Å

In comparison to the 5876 Å case the increased laser line width at 6678 Å increases the total laser power needed for saturation. The radiative decay rate of the 6678 Å transition is similar to 5876 Å, Wiese et al (1966). The calculated stark width is 2x larger, Griem (1964). The measured optical depth is 9x lower (P.145).

The transmission of the laser through the plasma was measured over a range of laser intensities and plasma conditions. The results for a 100 μS delay time are shown in Fig.12.1.

FIGURE 12.1 - LASER TRANSMISSION AT 6678 Å

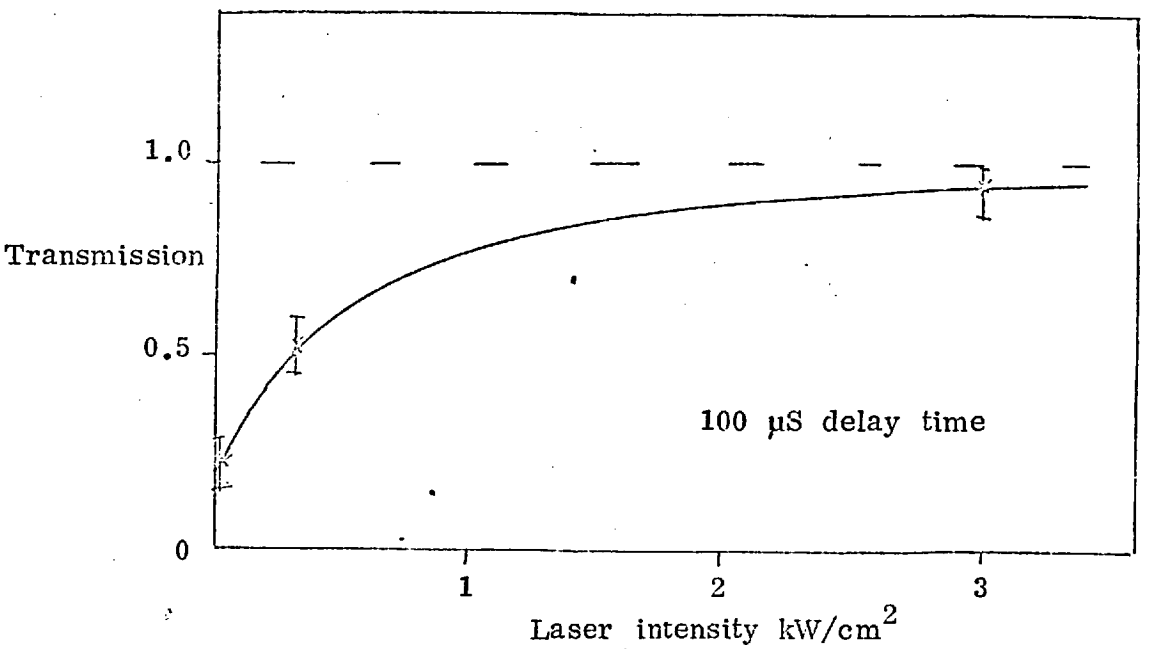

FIGURE 12.2 - 6678 Å FLUORESCENCE DECAY RATE

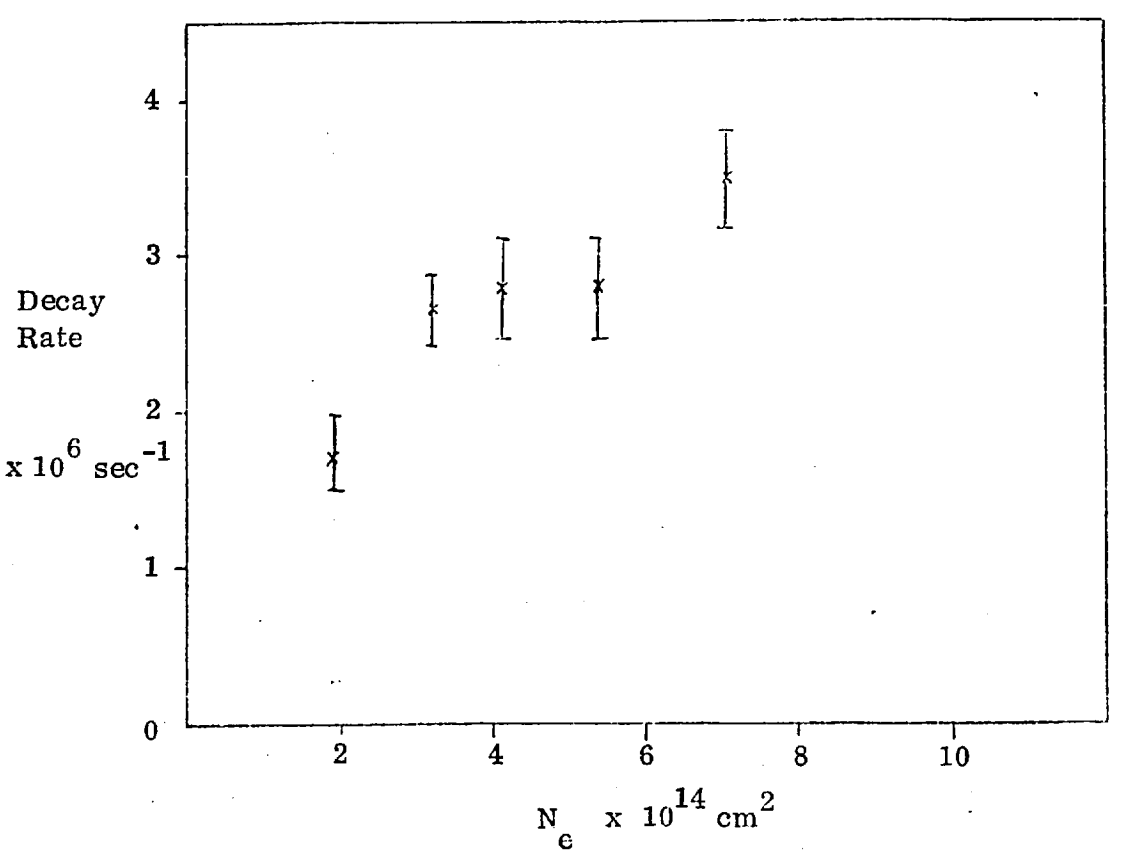

The time history of the laser pulse did not change on transmission through the plasma. This confirms that the changes in the transmitted laser pulse at the 5876 Å wavelength (P. 88) are associated with the high optical depth at 5876 Å. The theoretical estimate of the transmission at different laser powers is shown in Fig.6.6 (P.82; case for optical depth = 1.4). The theoretical and experimental results are similar except that at high laser intensities the observed transmission is higher than predicted, probably because of depletion of the number of atoms interacting with the laser due to relaxation process to other levels. In practice the laser power density inside the pinch had to be reduced below 10 kW/cm^2 before any reduction in the fluorescence was apparent.

At 100 μS delay time the fluorescence intensity is nearly constant with time and the two level model (P.63) is applicable. By comparing Fig.12.1 to Fig.6.6 (optical depth = 1.4) it may be seen that the saturation threshold corresponds to 0.3 kW/cm^2. Thus at typical laser intensities in the plasma of 30 kW/cm^2, the degree of saturation at 100 μS delay time is approximately 100. Assuming the collisional quenching is proportional to the electron density this corresponds to a degree of saturation of 30 at 30 μS delay.

Fluorescence at 6678 Å

Using the methods described in Chapter IV fluorescence traces were recorded over a range of delay times. Typical results are shown in Plate VII. Unexpectedly, they are not similar to the 5876 Å results. As in the 5876 Å case sensitised fluorescence on all other n = 3 and 4 transitions are observed. The sensitised fluorescence closely followed in time the direct fluorescence from the transition excited by the laser. No polarisation was detected in the

fluorescence. Fig.12.2 shows the observed fluorescence decay rate as a function of electron density. As no plateau region was observed the decay rates were calculated assuming an exponential decay process tending towards the initial 6678 Å intensity.

Of course, as the decay rates are measured in slightly different ways an exact comparison is not possible, but it can be seen that the decay rate is about 10 times lower than for the 5876 Å case and shows a different variation with electron density. The time histories of the direct and sensitised fluorescence were identical within experimental error. The enhancement in the emission of the $n = 3$ or 4 to $n = 2$ transitions was recorded. The lower intensity of the enhancement and in addition the increased electrical pickup caused by operating the laser at a higher voltage meant that the experimental uncertainty in the degree of enhancement was higher than the 5876 Å case. The following figures are the average of three experimental runs. With the laser tuned to 6678 Å the enhancement $\left(\frac{\text{Fluorescence}}{\text{previous local emission}} \div 1\right)$ of the 6678 Å transition was 1.6, 3.3, 3.7 ($\pm$ 25%) at delay times of 30, 60, 100 μS respectively. The enhancements of the other singlet transitions was 3/4 → 1 x the 6678 Å enhancement. The enhancement of the triplet transitions was about 0.4 of the 6678 Å enhancement. The lower enhancement in the direct fluorescence compared to the 5876 Å case must be due to a pre-existing population difference between $2^1P - 3^1D$ lower than the $2^3P - 3^3D$ case. In general the sensitised enhancements were a similar proportion of the direct fluorescence enhancement when compared to the 5876 Å case.

We discuss the 6678 Å fluorescence results and their relation to the other fluorescence date in Chapter XV.

PLATE VII

6678 Å FLUORESCENCE

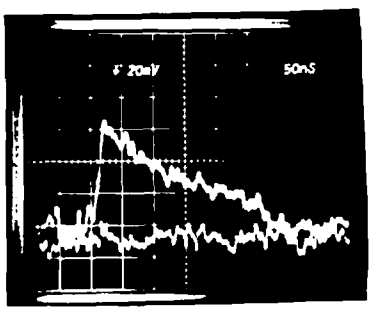

6678 Å Direct Fluorescence
(i) with laser
(ii) without laser
Delay 30 μS

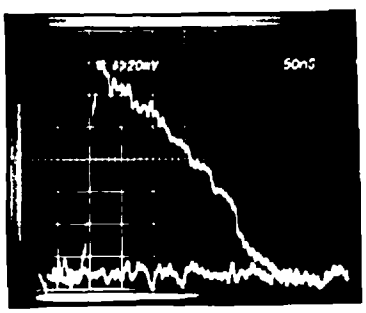

6678 Å Direct Fluorescence
(i) with laser
(ii) without laser
Delay 60 μS

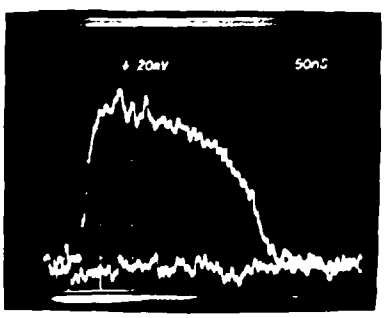

6678 Å Direct Fluorescence
(i) with laser
(ii) without laser
Delay 100 μS

H ∝ FLUORESCENCE

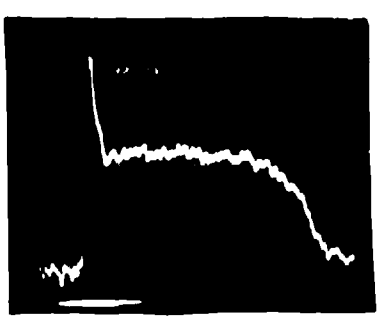

H∝ Fluorescence
Delay 34 μS

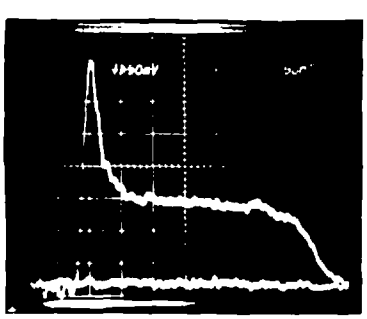

H ∝ Fluorescence
Delay 44 μS

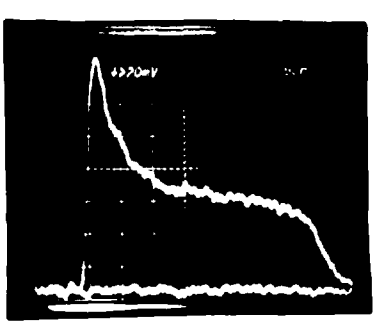

H∝ Fluorescence
Delay 54 μS

CHAPTER XIII

H α FLUORESCENCE

Compared to helium, hydrogen has a very simple atomic structure. Instead of the twelve helium transitions from n = 3 and 4 to n = 2 hydrogen has only two, H α and H β. The fine structure of H α and H β ranges over less than 0.1 Å, all the sublevels of the same principal quantum number interact with the laser. The cross sections for a wide range of collisional processes are well known and the problem of interpreting the fluorescence traces is at once simpler and more susceptible to verification by comparison with published cross sections. The same experimental procedure was followed as for the 6678 Å and 5876 Å cases.

Laser Performance at H α

The mixture of cresyl violet and rhodamine 6G dyes used for 6678 Å also lased at H α (6563 Å). The laser performance at H α was identical to the 6678 Å case described on P. 157.

H α Saturation

The stark width of H α (0.5 Å. Vidal et al. 1973) is larger than the stark width of 6678 Å. However it is difficult to make any statement on the quenching rate compared to helium on this basis alone.

The optical depth of H α (without the laser illumination) was measured using the method described on P.138. Because of the lower flashtube intensity at H α compared to 5876 Å, the signal/noise ratio with the monochromator slits set to 10 μm was poor.

Delay Time μS	Electron Density x 10^{14} cm^{-3}	Monochromator Slit Width μ.m.	Optical Depth
34	4.7	10	1.2 ± 0.2
		20	1.0 ± .05
44	1.5	20	0.78 ± 0.05
54		20	0.49 ± .05

It can be seen that the optical depth of H∝ is similar to that of the 5876 Å transition in a helium plasma.

The laser transmission was measured as a function of laser power and a sharp cut-off was observed at laser powers less than 5kW/cm^2 for a 30 μS delay time. The fluorescence intensity was approximately constant with time at delays exceeding 80 μS. However as no experimental values of the electron density are available for this delay time it was not possible to extrapolate to a value of the degree of saturation at the lower delay times used in the fluorescnece experiment. The laser pulse length was reduced on transmission through the plasma in much the same way as the 5876 Å case. At the intensities used in the fluorescence experiment the laser beam was completely transmitted by the plasma. At a delay of 34 μS, a 50% reduction in the laser intensity from its normal value of 30 kW resulted in a fall in peak fluorescence intensity of only 10%.

The calculated laser transmission is shown in Fig.6.6 (optical depth : 14) and it is clear from this graph that the degree of saturation is at least 20.

Hydrogen Plasma

The discharge vessel was filled with hydrogen to a pressure of 0.45 torr. The plasma conditions were slightly different from the helium case. The electron density decreased faster but from a higher initial value when compared to the case of helium (Fig.14.2). No experimental data is available for the electron temperature. However, theoretical estimates using either a coronal or LTE model both give a temperature of 1×10^4 °K at an electron density of $10^{15} cm^3$ (Mahon 1973).

The technique described on P.100 was used to determine the ratio of the n = 3 to n = 4 populations by measuring the Hα and Hβ emission intensities. The experiment was performed with an instrument function of width (F.W.H.M.) 8 Å and 16 Å. The same ratio was obtained in both cases indicating no correction was necessary due to emission in the far line wings. At a delay time of 30 μS the apparent ratio of the n = 3/n = 4 sublevel populations was 2.7. As no correction was made for the optical depth of Hα the true value is likely to be higher than this. The ratio of the sublevel pooulations expected if the two levels were in LTE is given by the Boltzman factor $\exp(\frac{\Delta E}{k T}) = 1.9$. Thus we conclude that levels 3 and 4 are not in LTE.

Hα Fluorescence Results

Using the same techniques as in the helium case, the Hα emission was recorded with and without laser excitation over a wide range of delay times. Typical results are shown in Plate VII. The fluorescence rises rapidly to a peak then decays exponentially to an enhanced plateau level, subsequently reverting to its original level at the end of the laser pulse. In order to best display the time history of the fluorescence the oscilloscope traces are offset

from zero. The time history of the fluorescence is very similar to the 5876 Å case. A plot of the decay rate (peak to plateau) against electron density is shown in Fig. 13.1. The form of this graph is completely different to the results for 5876 Å (P.60).

No polarisation (< 5%) could be detected in the fluorescence using the method of P.97. The intensity in the plateau region at 34 μS delay was constant in contrast to the 5876 Å results.

Sensitised fluorescence of the same form as the Hα fluorescence was observed on Hβ and Hγ. There was a very small indication of sensitised fluorescence on Hδ but none on Hε.

TABLE 13.1

Hydrogen : Sensitised Fluorescence Enhancements

$$\frac{\text{fluorescence}}{\text{local emission}} + 1$$

Delay Time μS	Hα peak	Hα plateau	Hβ peak	Hβ plateau	Hγ peak	Hγ plateau
34	7.8	4.9	2.1	1.5	1.3	1.3
44	18.4	7.7	4.7	2.3	2.3	1.6
54	21.4	8.9	4.6	2.2	1.9	-

Photomultiplier Temporal Resolution

At the electron densities of 1.6×10^{15} cm^{-3} the total duration of the fluorescence transient spike was only 20 μS. It is important to ensure that the photomultiplier response time is less than this in order to deduce the fluorescence decay rate. The anode rise time quoted by the manufacturers for the RCA C31034 photomultiplier is 2.5 nS. No figures are available

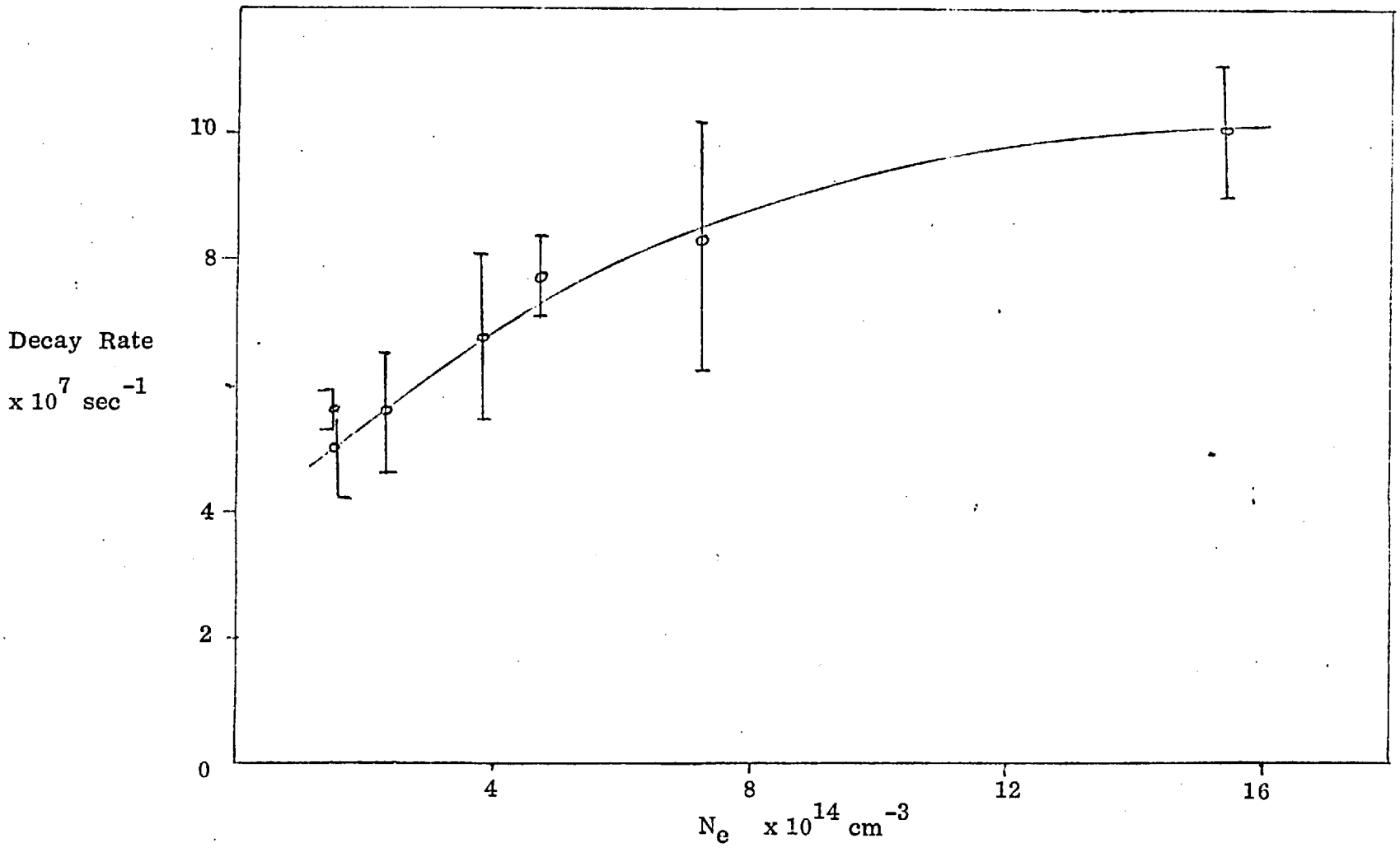

FIGURE 13.1 - H α FLUORESCENCE DECAY RATE

for the transit spread time, i.e. the scatter in time at which electrons simultaneously emitted from the photocathode arrive at the anode due to their different path lengths through the dynode chain. With the co-operation of the Applied Optics group an experiment was arranged in which the same photomultiplier used in the fluorescence experiments was set up to detect a train of pico-second pulses from a modelocked ruby laser. A Tektronix 7904 oscilloscope of 0.8 nS rise time was used to display the photomultiplier signal. The pulses could easily be resolved, the total duration of a single pulse being measured to be 5 nS. Thus, the observed time histories of the fluorescence are not limited in any way by the photomultiplier.

H α Fluorescence : Discussion

The lack of any polarisation in the fluorescence confirms that any coherence effects due to the laser excitation are negligible. The variation of observed decay rate with electron density is somewhat like Fig. 10.1 , where the de-excitation rate to the ground state is plotted. Using the 3-level model of the fluorescence (P.73) we calculate values of the populating and de-populating rates C_1, C_2, D_1, D_2 of levels of principal quantum numbers two and three for the case of $N_e = 10^{15}$ cm^{-3}. We neglect the small enhancement in the n = 4 level.

From Fig .13.1 we have :

$$\frac{(g_1/g_2)\, D_1 + D_2}{1 + (g_1/g_2)} = 9 \times 10^7 \text{ sec}^{-1}$$

i.e.

$$\frac{4}{9} D_1 + D_2 = 13 \times 10^7$$

From Table 13.1 -

$$\frac{N_{2\ peak}}{N_{20}} = 7.8$$

$$\frac{N_{10}}{N_{20}} = 10.3$$

$$\frac{N_{2\ plateau}}{N_{20}} = 4.9$$

$$= \frac{C_1 + C_2}{N_{20}\left(\frac{g_1}{g_2} D_1 + D_2\right)}$$

thus

$$\frac{C_1 + C_2}{N_{20}} = 4.9 \times 13 \times 10^7$$

$$= 6.4 \times 10^8$$

also before the laser is turned on

$$\frac{C_1 + C_2}{N_{20}} = \frac{N_{10}}{N_{20}} D_1 + D_2$$

$$6.4 \times 10^8 = \left(10.3 \times D_1\right) + D_2 \qquad (13.2)$$

solving Eqns.13.1 and 13.2 we have

$$D_1 = 5.1 \times 10^7 \text{ sec}^{-1}$$

$$D_2 = 10.7 \times 10^7 \text{ sec}^{-1}$$

It should be noted that here we are deducing the collisional depopulation rate for the $n=2$ level by observation of the fluorescence from the $n = 3$ level. This is only possible because the laser pulse lasts longer than the relevant decay times. We now estimate the collisional and radiative decay rates using published cross sections in order to compare the predicted decay rates to those deduced above.

Radiative Decay to the Ground State

Here we follow the method of Chapter IX. At a temperature of 1 eV the doppler width is

$$\frac{\Delta\lambda}{\lambda} = \left(\frac{2kT}{m}\right)^{\frac{1}{2}} = 4.62 \times 10^{-5}$$

For Lyman α at 1216 Å $\quad \lambda_D = 0.056$

β 1025 Å $\quad \lambda_D = 0.047$

γ 972 Å $\quad \lambda_D = 0.045$

The stark (half) half width estimated from the tables of Vidal et al (1973) at $T_e = 10^4$ K and $N_e = 10^{15}$ cm^{-3} is:

Ly α .0004 Å

Ly β .03 Å

Ly γ .0075 Å

The theoretical stark profile for Lyβ has a central dip and is not Lorenzian in shape. We take the case of Lyα first. The absorption coefficient for the case of a doppler broadened line is given by

$$k_D(\omega) = C \frac{1}{(\pi)^{\frac{1}{2}} \Delta\omega_D} \exp -\left(\frac{\omega-\omega_o}{\Delta\omega_o}\right)^2$$

ω_o is the angular frequency at line centre and $\Delta\omega_D$ is the doppler width defined by

$$\frac{\Delta\omega_D}{\omega_o} = \left(\frac{2kT}{m}\right)^{\frac{1}{2}}$$

and C is given by the integral absorption relationship

$$C = \int k(\omega)\, d\omega = \frac{\lambda_o^2 N}{8\pi} \left(\frac{g_2}{g_1}\right) \gamma$$

where γ is the radiative emission probability in angular frequency units (2.95×10^9 sec^{-1} for Lyα).

N is the lower state number density (1.5×10^{16} cm^{-3})

g_1, (g_2) the lower (upper) statistical weight; 2 and 8 respectively

for Lyα

For Lα , $C = 1.04 \times 10^{15}$ cm^{-1} radians sec^{-1}

$$\omega_o = \frac{2\pi c}{\lambda} = 1.55 \times 10^{16} \text{ radians sec}^{-1}$$

$$\Delta\omega_D = \omega_o \left(\frac{2kT}{m}\right)^{\frac{1}{2}} = 7.16 \times 10^{11} \text{ rad. sec}^{-1}$$

hence

$$k_D(\omega_o) = \frac{C}{(\pi)^{\frac{1}{2}} \Delta\omega_D} = 819 \text{ cm}^{-1}$$

We now use Holsteins results to calculate the escape factor g for a plasma of cylindrical geometry of radius, R.

In our case R = 2.5 cm.

optical depth $k_D(\omega_o) R = 2.05 \times 10^3$

The point on the line wing where the optical depth = 1 considering doppler broadening alone is given by

$$\exp - \left(\frac{\omega' - \omega_o}{\Delta\omega_D}\right)^2 = \frac{1}{2.05 \times 10^3}$$

$$\omega' - \omega_o = 2.76 \Delta\omega_D$$

$$= 1.98 \times 10^{12} \text{ radians sec}^{-1}$$

$$\lambda' - \lambda_o = 0.155 \text{ Å}$$

On examination of the stark broadening tables of Vidal et al (1973) we find that at this point the doppler and stark contributions to the line profile are comparable. We first calculate the radiation escape factor using Holsteins result for the case of a doppler broadened line.

$$g = \frac{1.6}{k_D(\omega_o)\, R\, (\pi \ln k_D(\omega_o) R)^{\frac{1}{2}}}$$

$$= 1.6 \times 10^{-4}$$

$$\text{radiation lifetime} = \frac{1}{g\, A_{21}} = 13.5\ \mu S$$

For the case of a stark broadened line we need to estimate the absorption coefficient at line centre.

The tables of Vidal et al comprise normalised stark profiles with and without convolution with the appropriate doppler profile. At line centre the absorption coefficient is governed by the doppler profile. We obtain the absorption coefficient for the stark profile at line centre for the case where all the atoms are stationary, by multiplying the doppler absorption coefficient by the ratio of the stark to doppler line profile peak height.

$$k_L(\omega_o) = \frac{\text{stark peak height}}{\text{doppler peak height}} \times k_D(\omega_o)$$

$$R\, k_L(\omega_o) = 3.78 \times 10^4$$

For the next step we need to assume the line profile to be Lorentzian and we use Holsteins relation to calculate the escape factor, g.

$$g = \frac{1.115}{(\pi\, k_L(\omega_o)\, R)^{\frac{1}{2}}}$$

$$= 3.24 \times 10^{-3}$$

The lifetime of a group of excited atoms in the $n = 2$ state is given by

$$\text{Lifetime} = \frac{1}{g\, A_{21}} = 658\ nS$$

$$\text{Decay rate} = 1.52 \times 10^6\ sec^{-1}$$

Thus in both cases the effective radiative decay rate is too slow to account for the observed fluorescence relaxation.

Lyman β

The stark profile of Lyβ is not Lorentzian. The radiative transition rate is 56×10^6 sec^{-1}, too slow by itself to account for the observed fluorescence decay rate even in the absence of radiation trapping. To estimate the decay rate in the presence of radiation trapping we follow the method used for Ly α. The point in the line profile where the optical depth is 1 is outside the central dip. We approximate the line shape to a Lorentzian with a peak height corresponding to the peak height of the stark profile. The decay rate calculated in this way is

$$2.43 \times 10^6 \text{ sec}^{-1}$$

Because of the approximation to the line profile this can only be regarded as a rough estimate. However it seems likely that Ly β radiation is not responsible for the observed fluorescence decay.

Lyman γ, δ, ϵ

The radiative transition rates are

Ly γ	13×10^6 sec^{-1}
Ly δ	4.1×10^6
Ly ϵ	1.6×10^6

The decay rates after taking account of optical trapping are smaller still. Radiative decay by Ly γ, Ly δ and Ly ϵ is much too slow to account for the observed fluorescence.

Although the approximations made in the treatment of the line profile leads to a small degree of uncertainty in the above analysis it seems clear that radiative decay is not an important factor in the observed relaxation of the fluorescence.

Photoionisation

The photoionisation cross section for hydrogen may be obtained from Woolley and Stibbs (1953). Taking the Gaunt factor to be one, the photoionisation cross section of the n = 3 level at 6563 Å is 1.2×10^{-17} cm^2. The total number of photons transmitted through the pinch is 5×10^{16} in a 250 nS pulse. The ionisation rate is therefore 2×10^6 sec^{-1}. This is much slower than the observed fluorescence decay.

Hydrogen Collision Rates

In this section we calculate hydrogen collision rates corresponding to the various published cross sections and compare the predicted collision rates to the decay rate observed in the fluorescence. In Chapter X the experimental values of electron temperature and density were used to scale the predicted collision rates according to the plasma conditions. Although no experimental values of the electron temperature, T_e, are available for hydrogen it seems reasonable to assume the variation of T_e with delay time follows the same pattern as in the case of helium.

n = 1 → n = 2,3,4 Transitions

The electron collision cross section for 1s → n excitation of hydrogen has been investigated experimentally and theoretically by a number of workers, e.g. Fite et al (1959), Kaupilla et al (1970), Johnson (1972), Felden et al (1972), McDowell et al (1973) and Williams et al (1974). The results are in general agreement. We calculate the excitation rate using Equation 10.2 for the case of $N_e = 10^{15}$ cm^{-3}, $kT_e = 1$ eV

$$C_{12} = \frac{2}{(\pi\tau)^{\frac{1}{2}}} N\sigma\left(\frac{2kT}{m}\right)^{\frac{1}{2}} \left(\frac{E_{thresh}}{kT} + 1\right) \exp -\left(\frac{E_{thresh}}{kT}\right) \qquad (10.2)$$

Because of the exponential factor the excitation rate in the present case is governed by the value of the cross section near threshold. We approximate the results of McDowell et al. and Williams by a cross section in the form of a step function for the total 1s → 2s, 2p cross section

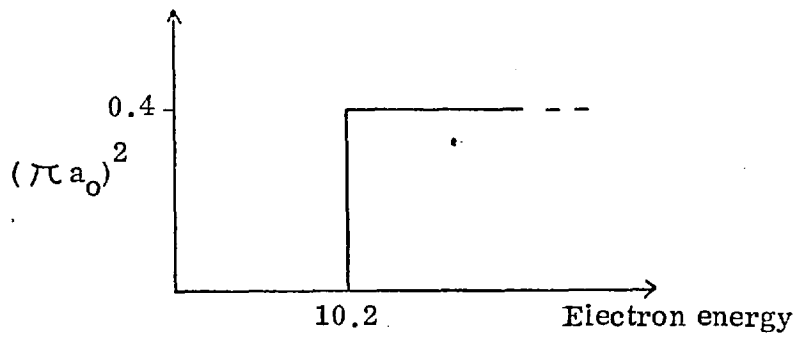

The predicted excitation rate is 9.8×10^2 sec^{-1}. The de-excitation rate is given by detailed balance

$$C_{21} = C_{12} \left(\frac{g_1}{g_2} \right) \exp \left(\frac{E_{thresh}}{kT} \right)$$

$$= 6.6. \times 10^6$$

The excitation cross section for $n = 1 \rightarrow n = 3$ transitions is 0.1 near threshold; lower than the $n = 1 \rightarrow n = 2$ cross section, and the de-excitation rate calculated in the same way as above is 9×10^5 sec^{-1}. We calculate the predicted fluorescence decay rate using the theory of P.73 assuming the fluorescence relaxation is due to de-excitation to the ground state.

$$\text{Decay rate} = \frac{(g_1/g_2)\, D_1 + D_2}{(g_1/g_2) + 1}$$

$$= \frac{(4/9)\ 6.6 \times 10^6 + 9 \times 10^5}{1.44}$$

$$= 3 \times 10^6 \text{ sec}^{-1}$$

This value is approximately twenty times less than the observed fluorescence decay rate. A more fundamental objection to the hypothesis

that the observed fluorescence decay is due to collisions to the ground state is the fact that the observed fluorescence decayed implying by Eqn.6.9 that the depopulating rate out of the upper state is dominant.

Collisional Transfer between Excited Levels

Johnson (1972) has presented semi-empirical electron excitation cross sections for $n = 3 \rightarrow 4$, $n = 6 \rightarrow 7$ and $n = 10 \rightarrow 11$ transitions. The cross sections are in agreement with several other workers including Saraph (1964). The calculations of Saraph show that the cross sections for transitions $n \rightarrow n + 1$ scale roughly as n^4.

For the $n = 3 \rightarrow 4$ transitions the cross section given by Johnson is approximately $100\ \pi a_o^2$ near the threshold energy of 0.66 eV. The excitation rate was calculated using Eqn.10.2 to be $5.05 \times 10^8\ sec^{-1}$. This is consistent with the rapid transfer observed in the $H\beta$ fluorescence. Scaling the $n \rightarrow n + 1$ rate with n^4 this gives rates of $1.6 \times 10^9\ sec^{-1}$ for the $n = 4 \rightarrow 5$ transition; $3.9 \times 10^9\ sec^{-1}$: $n = 5 \rightarrow 6$; $8.1 \times 10^9\ sec^{-1}$: $n = 6 \rightarrow 7$. It is difficult to use the theory of P.73 to calculate the expected fluorescence decay rate on the basis of $n \rightarrow n + 1$ transitions since in practice the level to which the atoms decay does not have a large population and the populating rates $n + 1 \rightarrow n$ are also enhanced when the laser is on. We thus interpret the observed fluorescence decay rate as the net rate at which atoms are transferred to higher excited levels.

For any particular transition we may scale the transition rate with electron density and temperature using Eqn.10.2 by assuming that the time dependence of the electron temperature follows that of the electron density. The results are shown in Fig.13.4. The theoretical curves do not bear any resemblance to the density and temperature dependence of the observed

FIGURE 13.4 - COLLISIONAL EXCITATION RATES FOR HYDROGEN

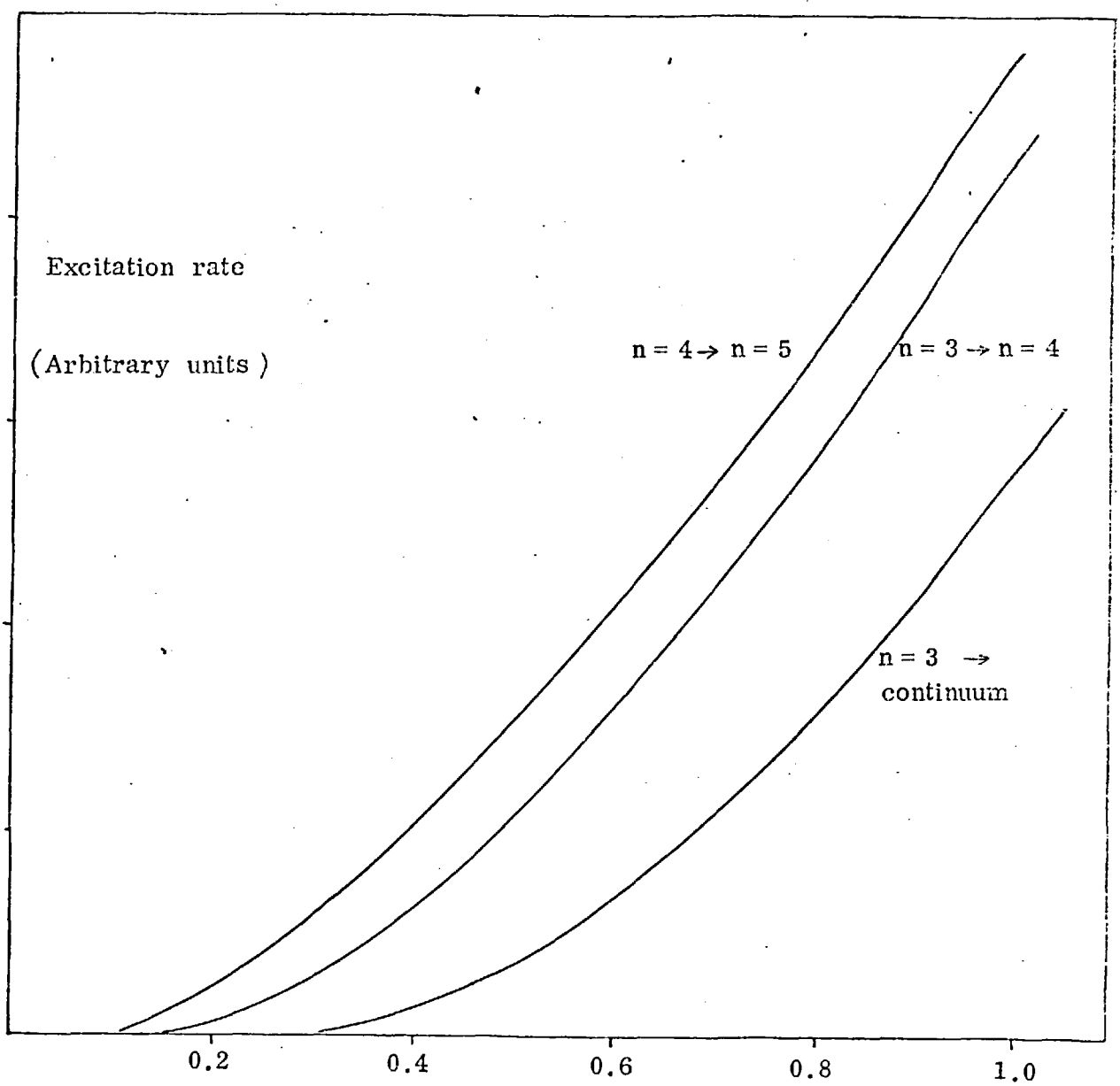

fluorescence decay rates (Fig.13.1) and thus we conclude that either the electron temperature varies as a function of delay time in an unexpected way or that the fluorescence decay rate is not governed by a single process alone but rather by a combination of transitions, e.g. $n \rightarrow n+1 \rightarrow n+2$, etc.

We may estimate the populating rate $C_1 + C_2$ by assuming that the $n = 2$ population is similar to the case of helium at the same electron density (i.e. $\sim 10^{10}$ cm^{-3}). This gives $C_1 + C_2 = 6.4 \times 10^{18}$. From P.171, 175 the excitation rate for ground state atoms to the $n = 1$ level is the density x rate per atom $= 1.6 \times 10^{18}$ cm^{-3} sec^{-1}.

The C_2 rate from ground to the $n = 3$ levels is approximately 0.4×10^{17}. We conclude that excitation of ground state atoms is a major populating process for the $n = 3$ and $n = 2$ levels.

Collisional Ionisation Rates

Omvidar (1965) has used the Born approximation to calculate ionisation cross sections for excited states of hydrogen. He gives an average $n = 3$ ionisation cross section of $56 \pi a_o^2$ for an electron impact energy of 2.2 eV (near threshold). We calculate the ionisation rate using Eqn.10.2 to be 1.17×10^8. This is comparable to the observed fluorescence decay rate. However, if the fluorescence decay was mostly due to ionisation one would expect a variation of decay rate with electron density as shown in Fig.13.4. This is not observed in practice. Cross section calculations near threshold using the Born approximation often overestimate the true cross section. Comparison of the excitation cross sections of Omvidar (1965b) for the $n = 3 \rightarrow 4$ transition with the results of several other workers including Johnson (1972) show that Born approximation near threshold yields a cross section four times too large. Thus the ionisation rate is likely to be lower than that calculated above.

To conclude, it would appear that the observed relaxation in the H α fluorescence cannot be described exactly by a 3-level model. Further discussion of the H α fluorescence results is given in the context of the helium fluorescence results in Chapter XV.

CHAPTER XIV

LONG TERM VARIATION OF PLASMA PARAMETERS

One of the most useful properties of laboratory plasma sources is long term reproducibility. Ten years experience with linear pinch devices by other workers in this Department had fostered the belief that the long term reproducibility of these devices was excellent. The pinch used for the present experiment had reproduced virtually the same electron density over a period of six years. (Cairns 1970; Mahon 1973). During the $H\beta$ line profile measurements described on P.99 a check was made of the $H\beta$ profile at the normal helium filling pressure (0.45 torr). Unexpectedly, repeated measurements at a delay time of 30 μS gave a (whole) half line width of 1.4 Å corresponding to an electron density of 6×10^{14} cm^{-3}. Previous measurements of the electron density at this delay time by Ashby Jephcott interferometric or Thomson scattering methods had given an electron density of 9.5×10^{14} cm^{-3}. Previous measurements of the $H\beta$ line shape had also given an electron density consistent with this figure. At the end of the present experimental work the electron density was remeasured by the interferometric technique and the results confirmed that a change had occurred, the electron density at 30 μS delay time now being 7×10^{14} cm^{-3}, broadly consistent with the latest $H\beta$ results. The pinch capacitor voltage, filling pressure and oscilloscope time bases were checked against other equipment and all found to be functioning as expected although, of course, no cross checks with the previous experimental conditions are possible. The only changes that were made to the apparatus were that the capacitor power supply had been replaced with a more modern unit and the re-entrant windows on the discharge vessel were not used. Previous measurements had

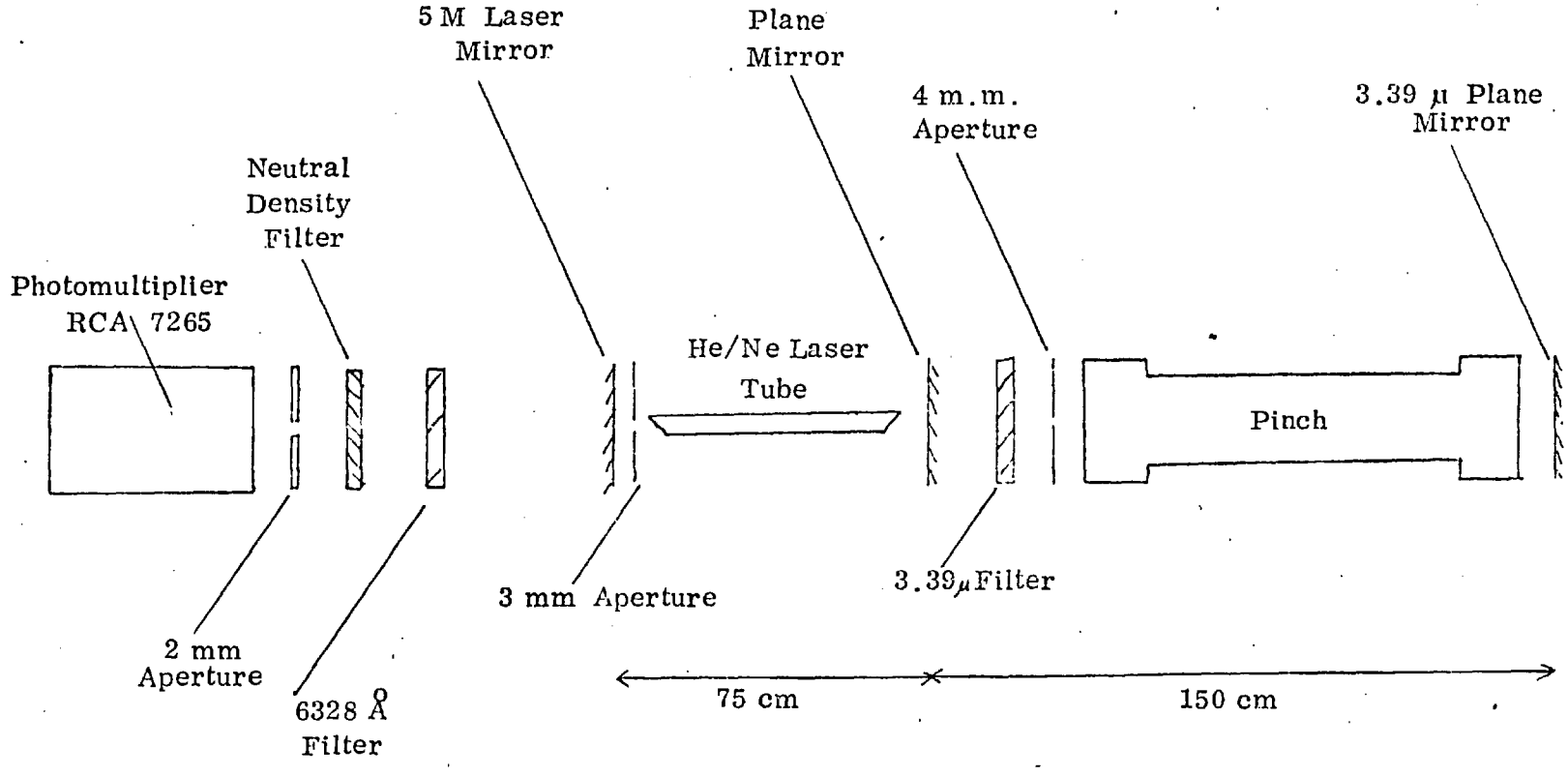

FIGURE 14.1 - EXPERIMENTAL SET-UP OF THE INTERFEROMETRIC EXPERIMENT FOR DETERMINING THE ELECTRON DENSITY IN THE PLASMA

shown that the re-entrant windows had only made a slight (< 10%) difference to the electron density. The discharge vessel was thoroughly cleaned but the original electron density was not regained. The reason for this change in electron density remains unclear. We now describe the electron density measurements in detail.

Electron Density Measurements

The method followed was exactly the same as used by Mahon (1973). A Helium Neon laser operating at both 6328 Å and 3.39 μ simultaneously was set up so that the beam travelled down the axis of the pinch (Fig.14.1). An optical filter prevented the 6328 Å radiation from traversing the pinch, the transmitted 3.39 μ radiation being reflected back along the same axis by a plane mirror. An RCA 7265 photomultiplier, arranged on the opposite side of the laser, detected the 6328 Å radiation. A 6328 Å optical filter (bandpass 10 Å) prevented the plasma light from reaching the photomultiplier. A neutral density (ND2) filter attenuated the beam and prevented saturation of the photomultiplier. The photomultiplier anode current was typically 200 μA. The laser was operated with 5M and plane mirrors, a 3 mm aperture restricting the output to a single traverse mode. The photomultiplier was operated at a cathode voltage of -1·8 kV and the photomultiplier signal lead was terminated by a 1 kΩ resistor and the signal displayed on a Tektronix 551 oscilloscope.

Variations in the phase of the 3.39 μ radiation reflected back to the laser modulated the 6328 Å radiation as both lasing lines have a common upper level. The Fabry Perot type cavity was aligned by observing the fringes due to mechanical vibration on a slow (5 mS) oscilloscope time scale. The changes in electron density produced a variation of the refractive index of

FIGURE 14.2 - ELECTRON DENSITY RESULTS

Initial Filling Pressure 0.45 torr

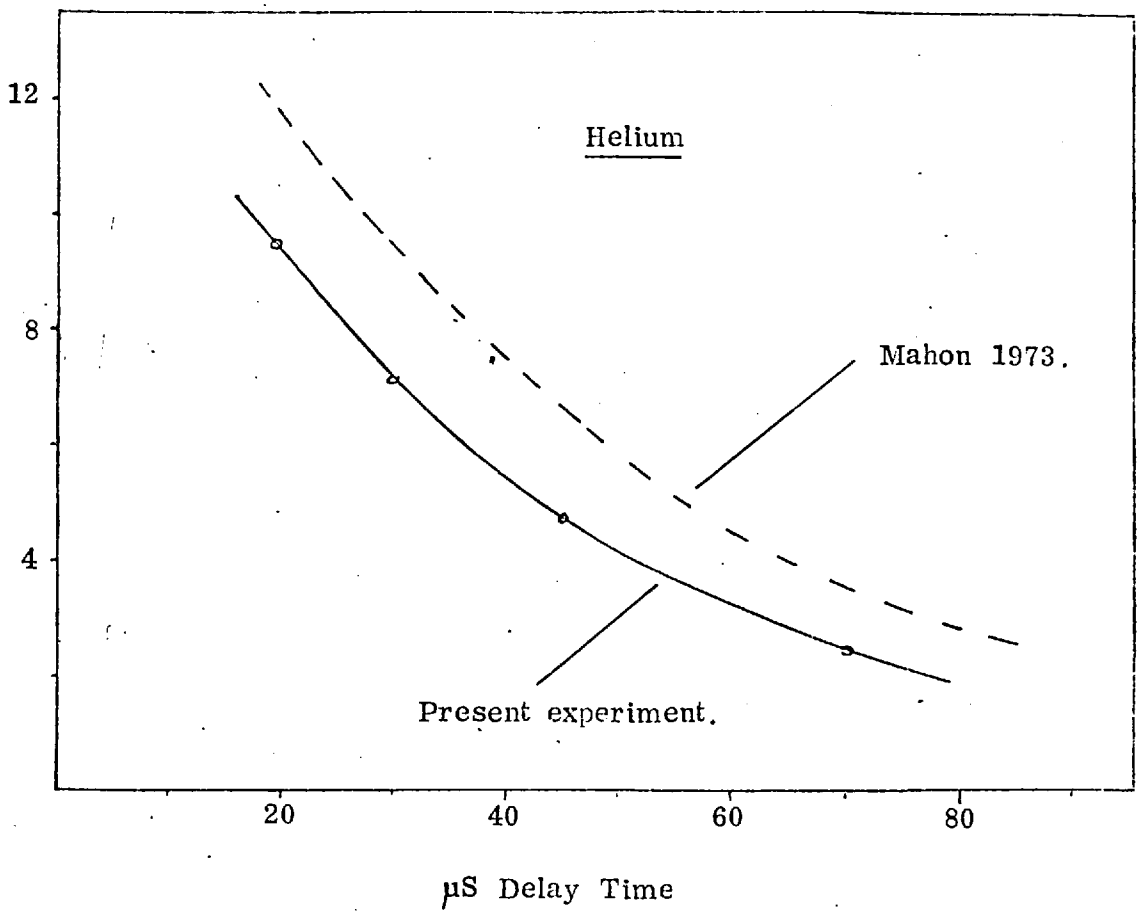

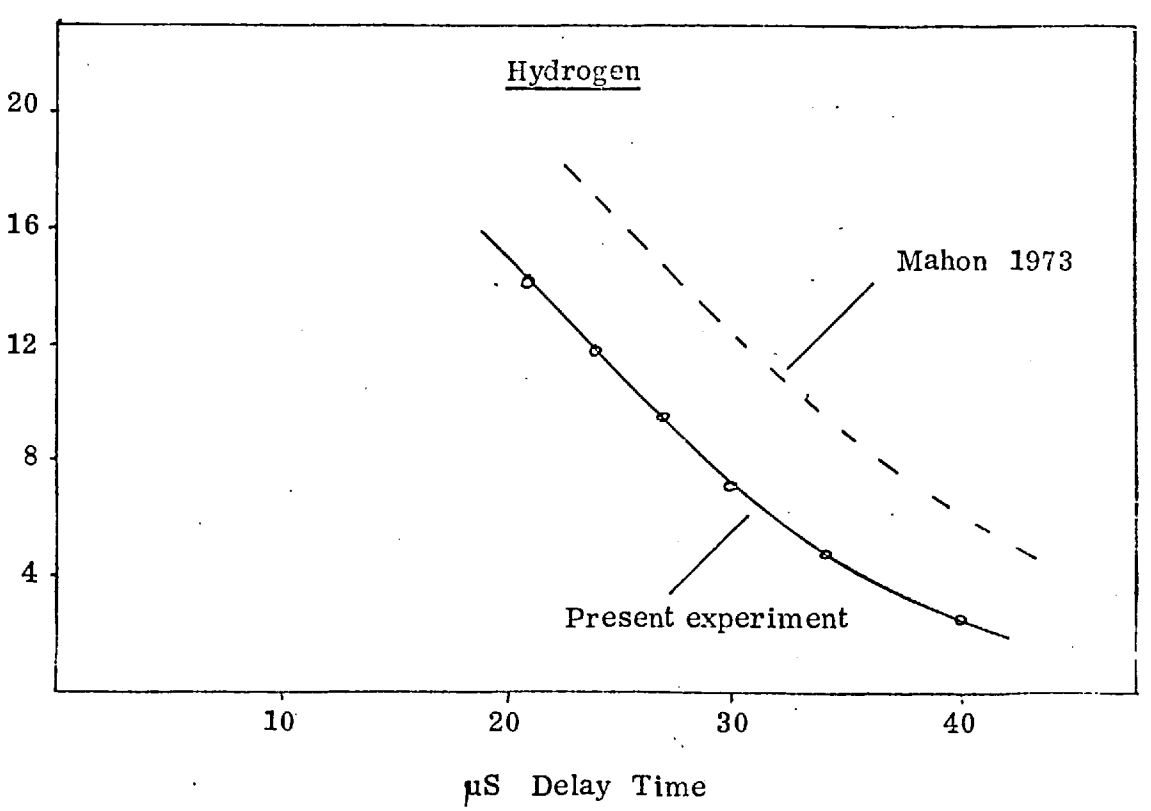

the plasma and hence modulated the laser beam. The use of 3.39 μ probe radiation enabled a x6 increase of sensitivity to be obtained while infra red detection problems were avoided by observation of the visible 6328 Å beam. One fringe is equivalent to a change in electron density of 4.75×10^{14} cm^{-3}.

Fig.14.2 shows electron density results for both helium and hydrogen. There is a substantial (30%) change from the previously recorded figures in terms of the density expected at a given delay time.

Fluorescence Results

The problem remains of estimating the electron density at the time the various fluorescence experiments were performed. The 5876 Å fluorescence results (Fig.5.1) were obtained during the same week as the Thomson scattering measurements of the electron density were made, and so the fluorescence results can be confidently linked to the electron density. Subsequent measurements of the fluorescence showed a decay rate reduced by 15% at a delay time of 30 μS although the functional dependence of fluorescence decay rate on electron density remained unchanged. The fluorescence enhancements presented in Table 8.2 were measured after the $H\beta$ profile had indicated a change in electron density.

The 6678 Å and $H\alpha$ fluorescence measurements were obtained at a time between the $H\beta$ electron density measurements and the latest interferometric results and are presented with the electron density as obtained from the latest interferometric results.

It is clear that in future work on linear pinch devices it would be advisable to check the electron density before and after a set of measurements in order to detect any further changes in electron density, as indeed was done

in the previous line profile work (Cairns 1970; Mahon 1973). The rate of change of electron density with time remains unchanged. All the evidence points to a sudden change due to some undetermined variation in experimental circumstance rather than a gradual drift or general irreproducibility.

CHAPTER XV

CONCLUSIONS

SUGGESTIONS FOR FUTURE WORK

In this chapter we examine all the fluorescence results described in previous chapters. We summarise the experimental work and compare the results to those predicted by the three level theory of P.73. We discuss aspects of the fluorescence which do not readily fit the theoretical model and, finally, we suggest future experiments which should shed some light on these problems.

Firstly we have demonstrated a novel design of coaxial dye laser which has proved to be very reproducible and reliable over three years of intensive use on a plasma fluorescence experiment. We have established that the laser is not subject to any frequency shifts or gross spatial homogeneities that would make it unsuitable for fluorescence experiments. Laser intensities above saturation, even for plasmas of optical depth 14, have been routinely achieved.

Fluorescence has been observed under a range of plasma conditions at three laser wavelengths for helium and hydrogen plasmas of high electron density (10^{15} cm^{-3}). A simple three level theoretical model was devised which qualitatively agreed with the observed time history of the fluorescence and suggested new ways of measuring upper and lower state collision rates from a single fluorescence time history. Observations of the laser beam after transmission through the plasma showed that the time history of the laser pulse was not appreciably affected by the plasma. Opacity experiments in the helium plasma revealed the volume of the plasma illuminated by the laser, and changes in the $n = 2$ populations as a result of the laser pulse. These

changes enable estimates to be made of the collision rates affecting the n = 2 levels. The rates for a wide range of collisional and radiative processes (including collisional excitation from the ground state, transfer between excited levels and optical trapping coefficients) have been calculated from published cross sections and some agreement found between the predicted fluorescence decay rate and the observed decay rate. However, it is clear that some puzzling features remain unexplained.

The most unexpected feature is the dissimilarity of the time history of the fluorescence originating when the laser is tuned to the 5876 Å or 6678 Å transitions in helium. Other features are the slight decay observed in the plateau region of the 5876 Å fluorescence at 30 μS delay and the observation that the enhancements of the sensitised fluorescence are a larger proportion of the 5876 Å fluorescence at conditions of low electron density.

Plasma Equilibrium

In order to understand the changes in the plasma induced by the laser it would seem desirable to fully understand the nature of the pre-existing equilibrium in the plasma. Regarding the n= 3 levels, the 3^1S sublevel population is twice the population of a 3^1P sublevel. This would imply a populating or depopulating process selectively favouring one or other level. Radiative cascades from higher levels are more likely to increase the population of the 3^1D and 3^1P levels. The radiative lifetime of 3^1S (55.2 nS) is very close to that of 3^1P (54.6 nS) when the optical trapping of the 3^1P-1^1S transition is taken into account (impact broadened line P.113). Similar arguments apply to the 3^3S, 3^3P levels. It would appear that either the collisional de-excitation rate for the 3P is larger than the 3S, or recombination processes selectively favour the 3S level. The selective populating or depopulating process must

be comperable to the transfer rate between the n = 3 levels; known to be $\geqslant 50 \times 10^{6}$ sec^{-1} from the identity of the sensitised fluorescence traces.

The 2^3S and 2^3P levels are also overpopulated compared to the 2^1P level even though the calculated transfer rates between the n = 2 levels are much larger than the effective $2^1P - 1^1S$ radiative decay rate. This suggests that the 2^1P radiative decay rate, allowing for optical trapping, may be higher than that predicted on the basis of Holsteins theory (P.109).

Fluorescence

With regard to the fluorescence results, the similarity of the sensitised fluorescence time histories from singlet and triplet transitions implies a collisional transfer cross section (4×10^{-15} cm^2) at least an order of magnitude larger than previous estimates (e.g. Wellenstein et al 1972). Transfer via the continuum would not account for the observed fluorescence as even if the total n = 2 population was ionised the free electron density would only increase by one part in 10^4. However, the differring fluorescence enhancements of the n = 3 → n = 2 transitions indicate that the transfer rates are comparable to the decay rate out of the n = 3 and 4 levels.

The fluorescence time histories observed in the 5876 Å transition in helium at a delay of 30 μS show a slight decay in the plateau region. It is likely that this slow decay reflects photoionisation induced by the intense laser radiation. Another possibility is collisional processes not included in the three level model of P.73. We consider the case where an additional level is loosely coupled by slow collisions to the levels interacting with the laser. If the population of this level is not large the rate at which atoms are supplied to the levels interacting with the laser will change with time, and hence further changes in the fluorescence may occur after the initial transient spike.

The 2^3S level seems the most likely candidate for this additional level. However, the collisional excitation rate $2^3S - 2^3P$ at 30 μS (1.5×10^8 sec^{-1}) seems ample to ensure close coupling between the populations of the 2^3S and 2^3P levels and indeed the decrease in the 2^3S population observed during laser excitation of the 2^3P level confirms this.

We now consider the dissimilarity between the fluorescence observed when a helium plasma is illuminated by laser radiation tuned to the 5876 Å or 6678 Å transitions. This is difficult to explain as the same n = 3 and 4 levels are populated indirectly by the laser in both cases. One difference is that the n = 2 levels in helium are spaced over an energy range of 1 eV and transfer rate of atoms between the other n = 2 levels and the n = 2 level excited by the laser may be slightly different in the two cases. However, the observations that a nearly constant ($\sim$ 25%) fluorescence pulse is observed for both laser wavelengths at low electron densities indicates that efficient circulation of atoms between the n = 2 levels does take place.

The 5876 Å results alone strongly suggest that the observed decay is due to collisional ionisation of the n = 3 and/or n = 4 levels. In considering collisional transfer out of a particular level it should be noted that the collisional transfer rate must be multiplied by the probability of finding an atom in that level in order to deduce the effective fluorescence decay rate of all the n = 3 levels. Thus, in general the fluorescence decay rate is a function of the enhancements in the sensitised fluorescence produced by the laser. If we consider the case where the ionisation cross section of one particular level, e.g. 4^3F, is much larger than for the other n = 3 and 4 levels, the fluorescence decay rate would depend on the enhancement of the 4^3F level. If the enhancement was 10x less when the 6678 Å was excited by the laser this would account for

the much lower fluorescence decay rate observed for this case. As the enhancement of the n = 4 levels is low at high electron densities this is difficult to check experimentally. Also, the 4^3P level is not accessible to visible spectroscop ic techniques. It has been suggested by Lin et al (1961, Am. Phys. 15, 461) that singlet → triplet transfer occurs primarily through nF levels because of substantial singlet/triplet mixing in the nF wave-functions.

This might also explain the increased sensitised fluorescence enhancements (as a proportion of the direct fluorescence enhancement) observed at low electron densities (P.103). The singlet-triplet transfer rate would depend on the 4F enhancement. At low electron densities this may be larger and so the transfer rate increased.

We observe sensitised fluorescence on n = 3 and n = 4 levels but not on n = 5. The collisional rate $n \rightarrow n+1$ scales roughly as n^4 (Saraph 1964) and hence atoms are clearly being supplied to the n = 5 levels at a high rate. The depopulating rate for n = 5 levels must also be high as no increase in the n = 5 level pooulations is observed. If the chief depopulating process for the n = 5 levels was collisions to higher n levels, the 2^3P population excited by laser would quickly be transferred to the continuum raising the free electron density but by an undetectable amount. A fluorescence pulse could not then be sustained for longer than 10 nS or so unless atoms were being supplied to the n = 2 and 3 levels at a rate sufficient to offset this.

Suggestions for Future Work

It can be seen that because of the many simultaneous processes it is not easy to develop a complete model that describes all aspects of the fluorescence observed so far. However, it is straightforward to extend the

work described here in several ways thus leading to a more complete knowledge of the various factors affecting the fluorescence. It would be interesting to see if the fluorescence excited with the laser tuned to transitions other than 5876 Å and 6678 Å displayed the same form as fluorescence from other levels of the same spin quantum number. Fluorescence excited with the laser tuned to the 3888 Å, $2^3S - 3^3P$ transition would be particularly interesting as the large 2^3S population implies that a high degree of enhancement would be produced. Similarly, exciting several lines in the same series, e.g. $3^3D - 2^3P$, $4^3D - 2^3P$, $5^3D - 2^3P$ would lead to conclusions regarding the effects of the levels in LTE on the fluorescence. Lasers with pulse lengths of a microsecond or more would enable the variation of plateau height over a range of electron densities to be determined. A further possibility is the simultaneous excitation of two or more levels using several dye lasers. For instance it would be possible to introduce a short pulse of 5876 Å radiation during a long pulse laser excitation of the 6678 Å transition.

With a laser line width narrower than the atomic line width, fluorescence line shape studies would yield valuable information on radiative redistribution and radiative transfer.

Due to the large optical depth of the 5876 Å transition, opacity studies at 5876 Å in the presence of the laser excitation of the 6678 Å transition would clearly reveal changes in the 2^3P population due to the laser and this would provide additional evidence for the collisional rates between the n = 2 levels.

Because of the intrinsic simplicity of the atomic structure of hydrogen it would seem that further fluorescence studies on hydrogen plasma are most likely to lead to unambiguous conclusions regarding specific collisional processes. The whole Balmer series is accessible to dye lasers and it would

be very interesting to see how the fluorescence varied as a function of the upper principal quantum number. It is possible to run the linear pinch in a gas mixture of hydrogen and helium still exciting the hydrogen (in contrast to the helium, P.98) and thus it is possible to determine if the fluorescence decay rate for a given electron density is independent of the ground state density. This would provide an experimental check on the effects of optical trapping of resonance radiation and on atom-atom collisions. However, in the analysis of the results it should be remembered that the fluorescence decay rate is a function of the sensitised enhancements.

On the theoretical side further consideration could be given to the possibility of collisions between excited atoms and molecules and also three body processes. A Ly α absorption experiment would determine the density of ground state hydrogen atoms and hence the molecular hydrogen number density.

A twenty level numerical model for hydrogen has been devised in order to predict the time history of the fluorescence pulse produced by either Ly α or H α laser radiation (V. Myerscough - private communication). Initial computations for the case of H α show the same general form of the fluorescence pulse as the present results but with approximately 4x lower enhancements and decay times 10x faster than those observed in the present experiment. It is clear that further investigation of these phenomena both by computational studies and experimentally by fluorescence measurements over a wide range of laser wavelengths will yield much valuable information on collision rates between excited states, recombination processes and general problems of plasma equilibrium.

CHAPTER XVI

THE CONFOCAL DYE LASER

Introduction

One of the original aims of the work described in this thesis was to develop new plasma diagnostic techniques made possible by the advent of tuneable lasers. In particular it was hoped to measure the magnetic field direction in a large toroidal plasma machine situated at the United Kingdom Atomic Energy Laboratory at Culham, Berkshire. Although, due to circumstances beyond the author's control, no positive results were obtained on the plasma, much useful information was gained from the preliminary work done in measuring the laser performance and in investigating various optical systems used for the fluorescence experiment. The work is described in the following three chapters. The present chapter contains a description of the laser system used at Culham. In Chapter XVII the fluorescence experiment is described. Chapter XVIII contains a theoretical discussion of a new method of measuring magnetic field directions.

The Confocal Dye Laser

In this section we describe the performance of the commercial dye laser system used at Culham Laboratory.

The dye laser (Model SUA9) was manufactured by Electrophotonics Ltd.* It was of the confocal type with the flashlamp and dye cell placed at the foci of an elliptical cavity. (Fig. 16.1). The flashlamp was a continuously evacuated quartz tube operating in the wall ablative mode. It was powered by a 5 m.f.d. capacitor. The capacitor voltage was normally set at 20 kv.

* The Cutts, Dunmurry, Belfast.

FIGURE 16.1 THE CONFOCAL DYE LASER

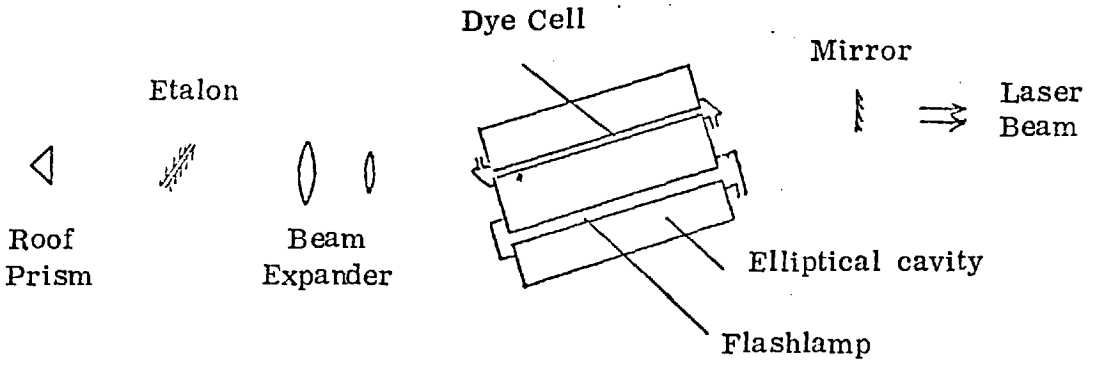

FIGURE 16.2 CONFOCAL LASER EFFICIENCY

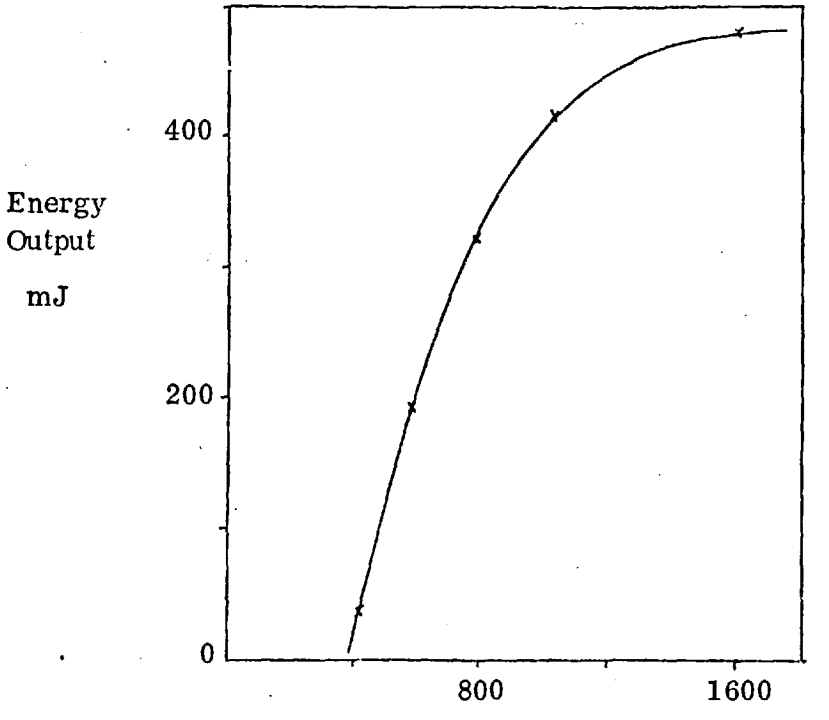

(These results were obtained after the 5 μF laser capacitor had been replaced by a 8 μF capacitor)

The laser was fired by a high voltage pulse applied to a trigger pin set in one of the flashlamp electrodes and the light from the flashlamp was reflected to the dye cell by the polished walls of the elliptical cavity. The dye cell had windows at each end set at Brewster's angle and was surrounded by a jacket of alcohol in order to filter out short wavelength radiation harmful to the dye. The laser cavity was made up of a totally reflecting roof prism and a 30% reflectivity cerium oxide coated mirror. The laser wavelength was controlled by a narrow gap optically contacted Fabry Perot. To prevent damage to the Fabry Perot by the intense radiation inside the laser cavity a 2x beam expander was positioned between the Fabry Perot and the dye cell. The specification of this laser quoted an untuned output of up to 2 joules using rhodamine 6G, and 400 mj using a mixture of cresyl violet and rhodamine 6G with the laser output tuned to a 3 Å band at 6563 Å. This is about 3x the energy of the coaxial dye laser but because of the longer pulse duration the peak laser power is reduced by a factor of 3 compared to the coaxial laser.

Time History of Flashlamp and Laser

The time history of the flashlamp current was measured with a Rogowski coil. The current showed an oscillatory behaviour with a period of 12 μS, there being roughly two cycles in the total pulse length of 24 μS. The second maxima was about 50% of the first. The flashlamp light intensity was recorded with a photodiode The light rose to a peak in a time of 2 μS and slowly decayed. The (F.W.H.M.) duration was 15 μS.

The laser time history was also recorded. A photodiode detected the light scattered when the laser beam was incident on a white card. The signal received was thus averaged over the whole laser beam and was spectrally unresolved. The signal had a 1 μS rise time and duration (F.W.H.M.) of 3 μS.

Laser Efficiency

The laser output energy was recorded over a range of input electrical energy. The results are shown in Fig.16.2. The laser efficiency, expressed as :

$$\frac{\text{increase in output energy}}{\text{increase in input electrical energy}}$$

decreased at input energies above 800 joules. This behaviour was also observed in a confocal dye laser system developed at Imperial College where the limiting factor was found to be the flashlamp efficiency and not any saturation effects in the dye (S.J. Fielding, private communication).

Dye Concentration

The dye concentration recommended by Electrophotonics for operation at $H\alpha$ was 48 mg of each of rhodamine 6G and cresyl violet in 1 litre of "Ultrar" methanol. In practice, a concentration of 70 mg of each per litre gave a 30% higher energy (500 mJ tuned to 6563 Å) and this was used in the subsequent experiments. The dye was filtered through a sintered glass filter (2 μ pore size) before use.

Reproducibility

The shot to shot reproducibility of the laser output was good (approximately 5% variation). However over many shots the performance continuously deteriorated by about 5 mJ per shot (Fig. 16.3). When left unused for a few days the performance partially recovered but the original energy output was only recovered when the dye solution was replaced. This deterioration appears to be due to thermal lensing effects due to the heat absorbed from the flashlamp and/or microscopic air bubbles produced in the dye cell, and also photo-decomposition of the dye (P. 33). The useful life-time of the dye was thus severely limited, the typical dye half life being 60 shots.

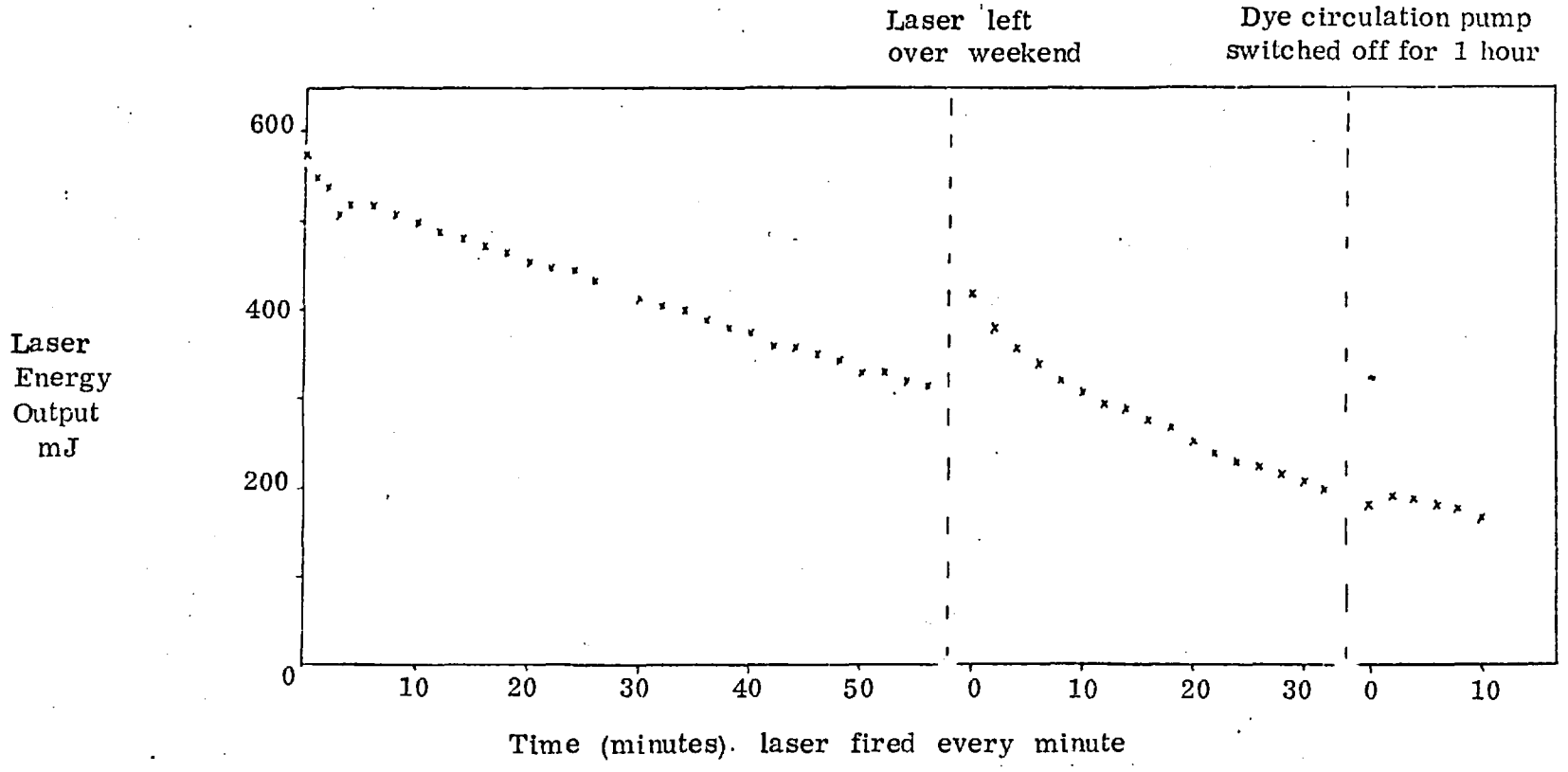

FIGURE 16.3 DYE DETERIORATION

Laser Spectrum

The laser wavelength was monitored by means of a Monospek spectrometer similar to that described on P. 49 . The spectrometer had a poloroid camera attachment. This was used to compare the laser spectrum to the spectrum emitted by a low pressure hydrogen lamp. Using a small aperture slit for the dye laser spectrum and a long slit for the hydrogen lamp it was possible to tune the centre of the laser emission band to well within 1 Å of Hα . Time resolved measurements were then made of the laser spectrum by means of a photomultiplier attached to the spectrometer. A 5 mm diameter fibre optic light guide was placed sc as to transmit part of the laser beam to the monochromator entrance slit. The wavelength setting of the monochromator was scanned across the laser spectrum and a line profile built up on a shot to shot basis. The laser energy deterioration was not corrected for as it was impossible to measure the energy and spectrum simultaneously. However this deterioration was only of the order of 15% during a single scan and did not lead to significant error. A dual beam Tetronix 556 oscilloscope was used to record the wavelength resolved signal from the photomultiplier together with the signal from a photodiode which detected the laser light scattered by the Fabry Perot. The latter enabled the wavelength resolved signals of many shots to be compared on an absolute time scale independent of laser timing jitter. A time resolved laser spectrum was recorded with the laser tuned (i) by a Fabry Perot etalon, and (ii) by an interference filter.

Fig. 16.4 shows the results for the Fabry Perot case. The laser bandwidth is at a maximum at 0.5 μS after onset of lasing action. At 1.0 μS the laser spectrum has contracted from the short wavelength side.

FIGURE 16.4 LASER SPECTRUM AS A FUNCTION OF TIME

(i) Tuned by Fabry Perot etalon.

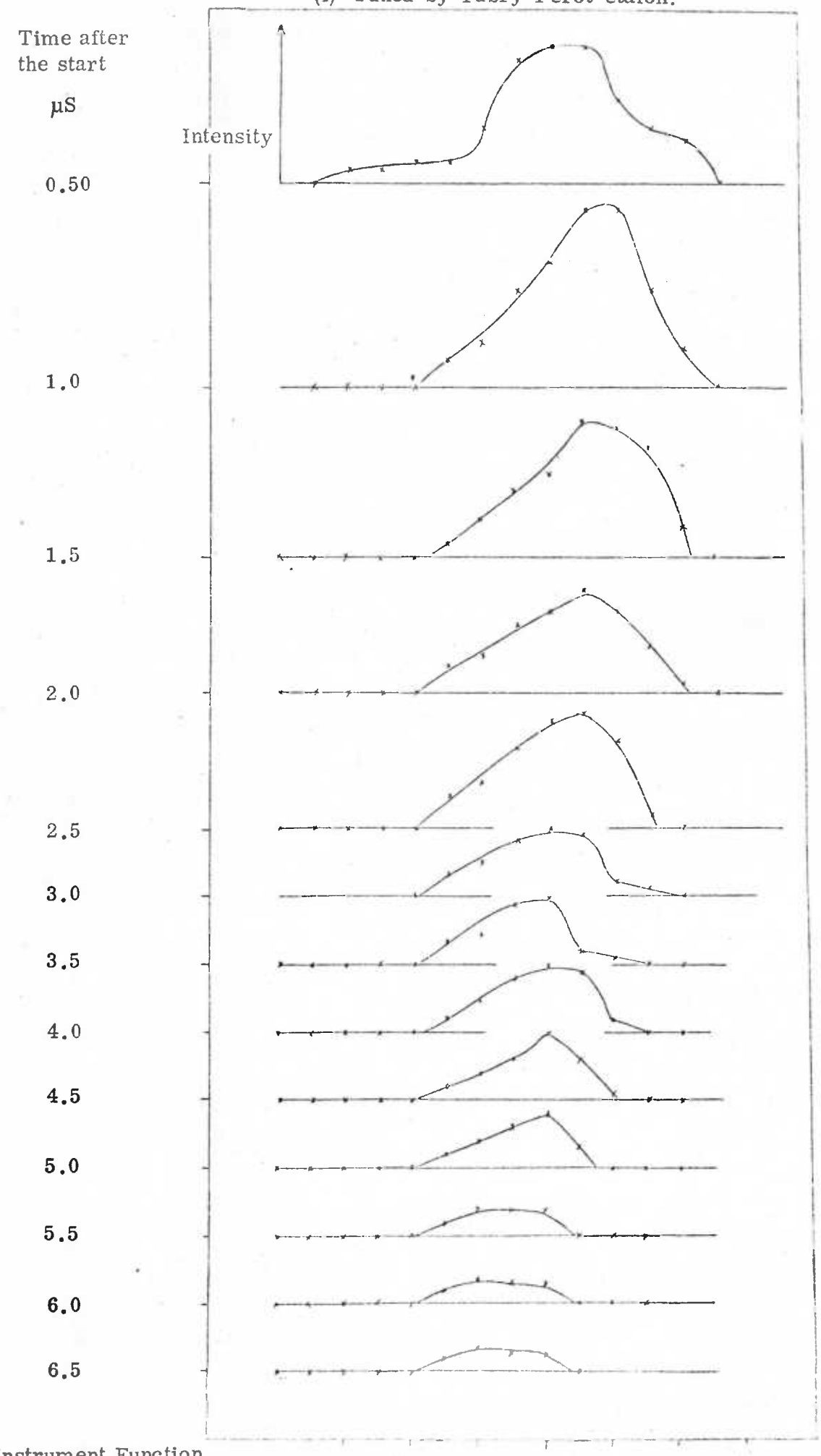

From 1.0 μS to 2 μS the laser spectrum is constant. After 2 μS a gradual shrinkage in width from the long wavelength side is observed. No gross frequency changes during the laser pulse were observed. At the time of peak intensity 1 μS after the start, the (whole) half width of the laser spectrum was 2.1 ($\pm$ 0.1) Å and it was roughly triangular in shape.

Fig. 16.5 shows the results when the interference filter was used as a tuning element instead of the Fabry Perot. For the first 1.5 μS the emission gradually became more intense on the long wavelength side of the spectrum. After 1.5 μS this continued with the emission ceasing completely on the short wavelength side. At 1 μS the (whole) half width of the spectrum was 5.4 Å.

This spectral narrowing during the laser pulse was also observed with the coaxial dye laser (P. 39) but there the wavelength narrowing was symmetrical.

Wavelength Resolved Spatial Scan of Laser Beam

In the above measurements the laser light was transmitted to the monochromator via a fibre optics system which accepted only a small fraction of the laser beam. A check was therefore made on the uniformity of the beam in wavelength as a function of spatial position when tuned by the Fabry Perot etalon. A 1 mm diameter aperture was positioned in front of the fibre optics and this was scanned vertically through the centre of the laser beam with the spectrometer set at 6559 Å and 6561 Å. At 6559 Å a modulation of up to 70% was observed in the time history of the laser intensity In a particular position the modulation was reproducible but the phase and frequency of it showed spatial variation. No such modulation was observed at the 6561 Å wavelength corresponding to the centre of the emission band.

FIGURE 16.5 LASER SPECTRUM AS A FUNCTION OF TIME

(ii) Tuned by interference filter.

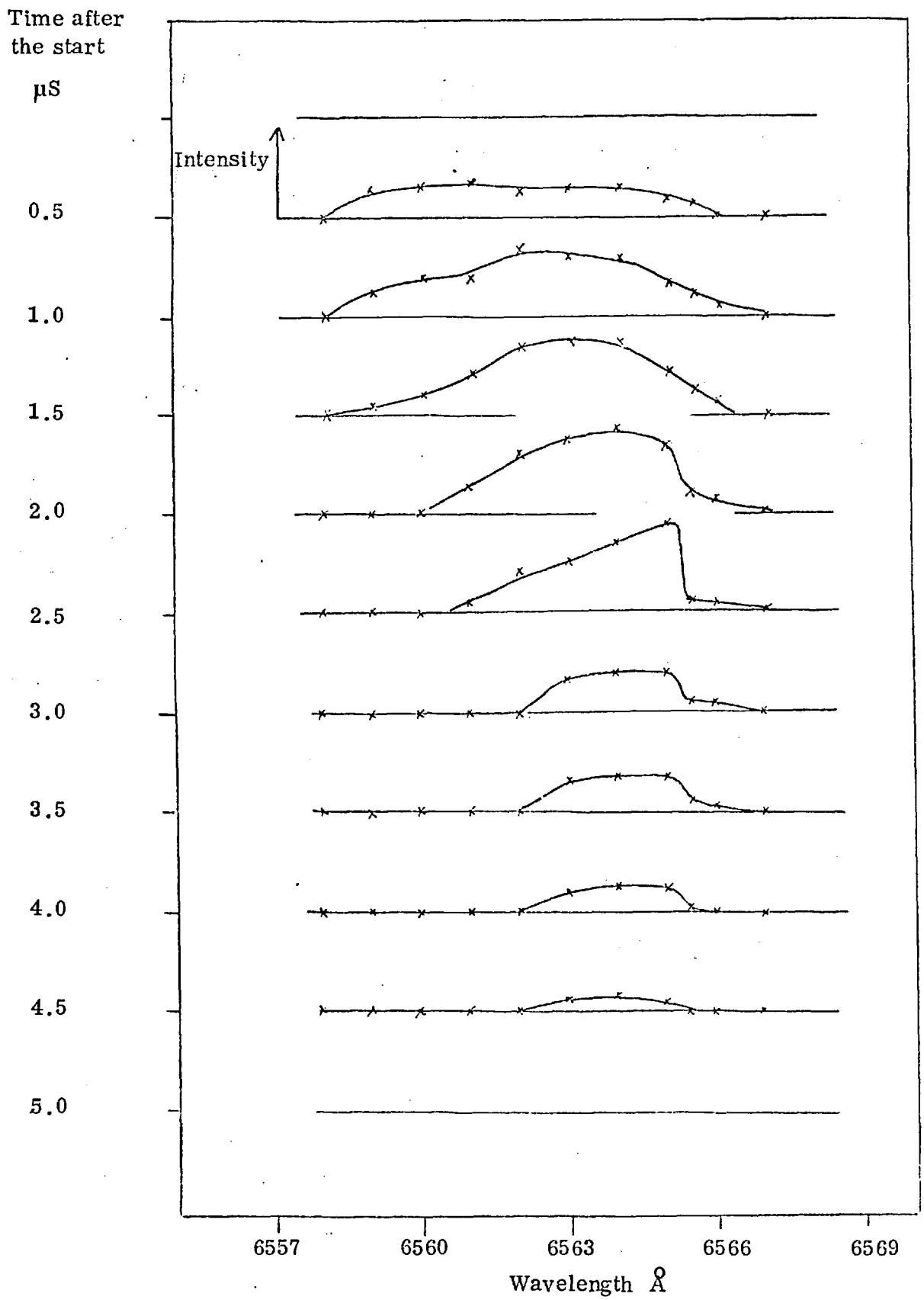

Instrument function 0.5 Å F.W.H.M.
Typical errors 10%

Fig. 16.6 shows a plot of the peak intensity recorded at each position. The two spatial profiles at 6559 Å and 6561 Å have a similar shape.

Divergence

The beam divergence is one of the most important factors of laser performance in plasma diagnostics experiments as it governs the proportion of the beam which may be transferred to the plasma machine. The divergence of the confocal laser was measured using the method described on P. 43. The laser beam was focussed by a 1 M focal length lens. A calorimeter with a variable iris was placed in the focal plane of the lens (Fig 3.8). At a particular setting of the iris diameter the energy incident on the calorimeter was recorded. This was repeated over a range of iris diameters. The divergence was obtained from the angle subtended by the iris when half the total output energy was incident on the calorimeter. The measured divergence was 15 ($\pm$ 1) milliradians half energy full angle. This figure was independent (< 10%) of : the dye temperature, concentration, or slight misalignment of the laser mirrors, the total laser energy output, and the type of dye used whether rhodamine 6G alone or a rhodamine 6G/ cresyl violet mixture. The divergence decreased from 15 to 12 mrad on increasing the laser cavity length from 55 to 80 cm but the total laser energy fell by 30% resulting in a net loss in brightness. The laser was hence operated with a 55 cm cavity.

The measured divergence was double the divergence quoted by Electrophotonics Ltd. Their estimate was obtained by photographing the laser beam and comparing the relative intensities of different parts of the beam close to the laser axis.

FIGURE 16 .6 LASER SPATIAL INTENSITY DISTRIBUTION TUNED BY FABRY PEROT ETALON

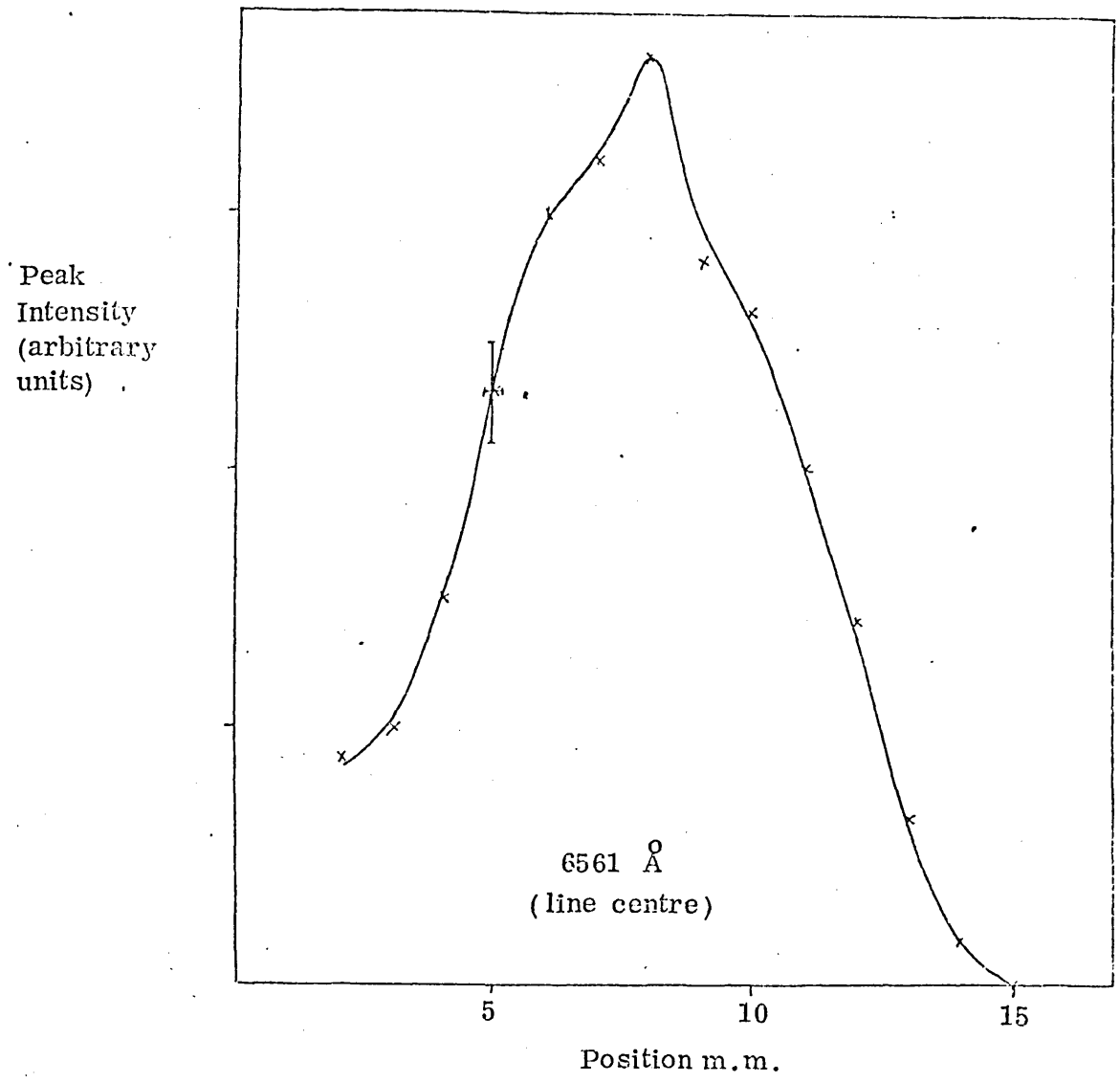

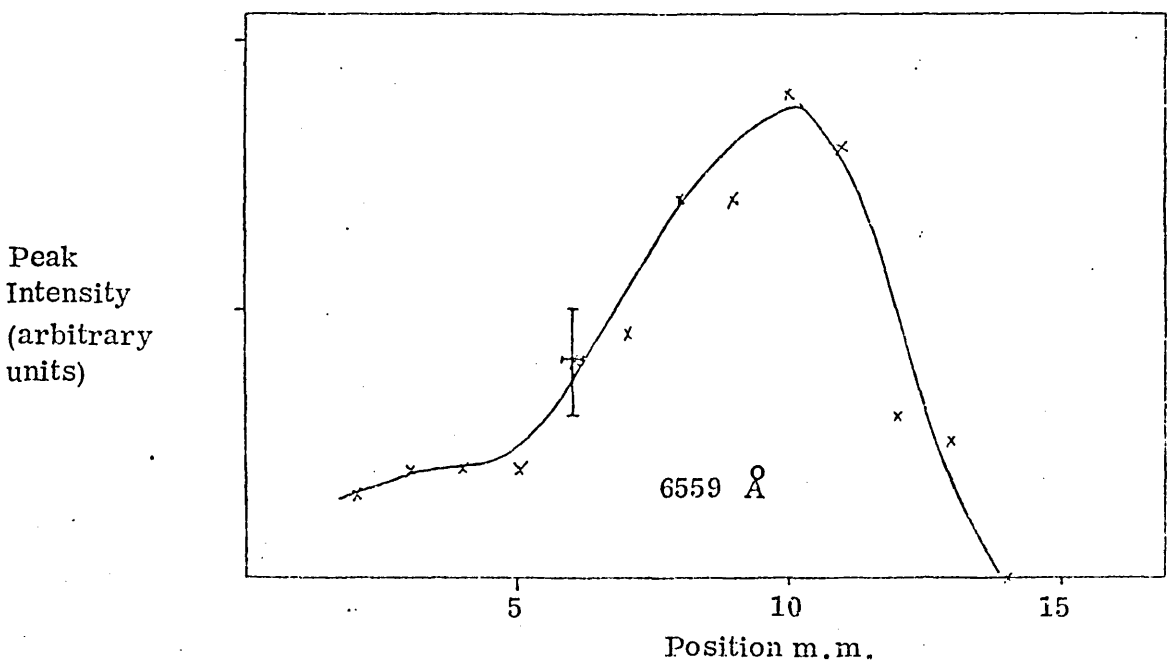

Typical errors shown.
Instrument function 0.5 Å F.W.H.M.
Sampling area 1 mm diameter.

The differing results reveal the importance of measuring laser divergence on an absolute energy scale, for dye lasers at least, as a substantial fraction of the total laser output is emitted at highly divergent angles and is hence not detected in the photographic method.

Polarisation

For optimum fluorescence scattering the polarisation direction of the laser beam must be accurately known. In making measurements of the confocal laser an interesting and unexplained effect in this connection was encountered. The dye cell of the laser was fitted with Brewster end windows and initially it was assumed these would define a horizontally polarised laser beam. However measurements made with sheet polaroid showed that only 70% of the laser output was in the expected polarisation direction. A Glan Thompson prism was then inserted betwen the 100% reflector and the dye cell defining a 100% loss for the vertical polarisation. However, measurement of the polarisation direction, most surprisingly, again showed only 70% horizontal polarisation. Only when the Glan Thompson prism was placed between the dye cell and the output mirror was the beam 100% polarised. The first explanation of this effect was superradiance. However this was not borne out by a subsequent experiment. The 100% reflector was blocked off and no observable laser-like spot occurred. Energy measurements gave only 1/20th of the normal output when lasing, although to explain the polarisation measurements something exceeding 100 mJ would have been expected. This experiment also showed that other reflecting surfaces within the laser cavity were not aligned with the output mirror, and hence forming a resonator giving rise to strange polarisation effects. No positive explanation of this effect has been forthcoming and no means of increasing

the percentage polarisation of the laser output without consequent power loss found. In order to obtain a polarised laser beam the Glan Thompson prism was placed outside the laser cavity directly after the output mirror. This gave just as high a laser energy as with the prism in the laser cavity, i.e. about 30% less than with no polariser.

Anomalous Spectral Output

Before the SUA9 laser described above was purchased some measurements were made of a smaller Electrophotonics laser of similar type but with approximately 1/10th of the energy output. A most peculiar result was discovered in the form of the spectral output of this laser when tuned with a Fabry Perot etalon. The spectrum consisted of either a closely spaced doublet each line 5 Å wide, 15 Å apart or a triplet with lines 5 Å wide, 10 Å apart. The Fabry Perot was checked by the manufacturers and performed normally producing single lines on the coaxial dye laser at Imperial College. As the smaller laser was replaced by the SUA9 which gave single lines as expected, this phenomena was not investigated further.

CHAPTER XVII

FLUORESCENCE EXPERIMENT AT CULHAM LABORATORY

The aim of this experiment was to measure the neutral hydrogen density in a large toroidal plasma machine at Culham Laboratory. The plasma machine, known as CLEO TOKAMAK, was one of the large plasma confinement devices used in the controlled nuclear fusion programme at Culham. (Gibson et al.(1973)). The plasma parameters were approximately as follows :-

Electron density	2×10^{13} cm^{-3}
Electron temperature	200 - 240 eV
Ion temperature	200 eV
Population of n = 4 level (From Hβ emission measurements; (D.D.Summers, private communication)	1.36×10^{6} cm^{-3}
External magnetic field	2×10^{4} gauss
Plasma duration	100 - 200 mS

The torus minor and major radii were 20 cm and 90 cm respectively.

Design of Input Optics System

Because no other ports were available and because a scattering optics system already existed on CLEO for Thomson scattering measurements at the ruby laser wavelength of 6943 Å, it was decided to incorporate the input optics and a section of the collection optics of this system into the chain for the fluorescence experiment, necessarily restricting operation to one or other of these experiments at a time. Because of the close proximity of the ruby and Hα wavelengths the lens blooming and beam dump, optimised at 6943 Å was still adequate at the Hα wavelength of 6563 Å.

This factor was also relevant in the decision to make resonance fluorescence observations at the Hα rather than the Hβ wavelength.

The geometric layout of the high voltage safety screens around CLEO made it necessary to feed the dye laser beam in at an angle of 60^{o}, in the horizontal plane, to that of the ruby laser beam. This meant that if a single reflecting prism was used to reflect the beam vertically up through the plasma, as in the ruby laser experiment, the polarisation direction of the dye laser beam would have been mismatched both for the optimum scattering signal (at least in the absence of a magnetic field) and for efficient dumping of the laser beam. A second reflecting prism was therefore added to deflect the dye laser beam in the horizontal plane into the same direction as the ruby beam.

Fig. (17.1) shows the complete input optics arrangement initially used for fluorescence experiments on CLEO. The two reflecting prisms are positioned between lenses B and C but have not been shown on the diagram for reasons of clarity. The dye cell exit window acts as a self luminous object of 4 mm diameter. Lens A produces an inverted enlarged real image of the dye cell at lens B. Lens B has two functions. It brings originally paraxial rays, diverged by lens A back into parallelism with the axis, and secondly it focusses all rays into the plane of the divergence limiting aperture. Lens C transfers the image of the dye cell at B to the point in the centre of the torus where scattering is to be observed. The acceptance angle of the system with the divergence limiting aperture removed is determined by a series of non-adjustable 1 cm baffles just beyond lens C. The system accepts light of up to 10 milliradians divergence from the laser. Given the existing constraints on the design of the optics system this gives the optimum laser beam brightness inside the plasma.

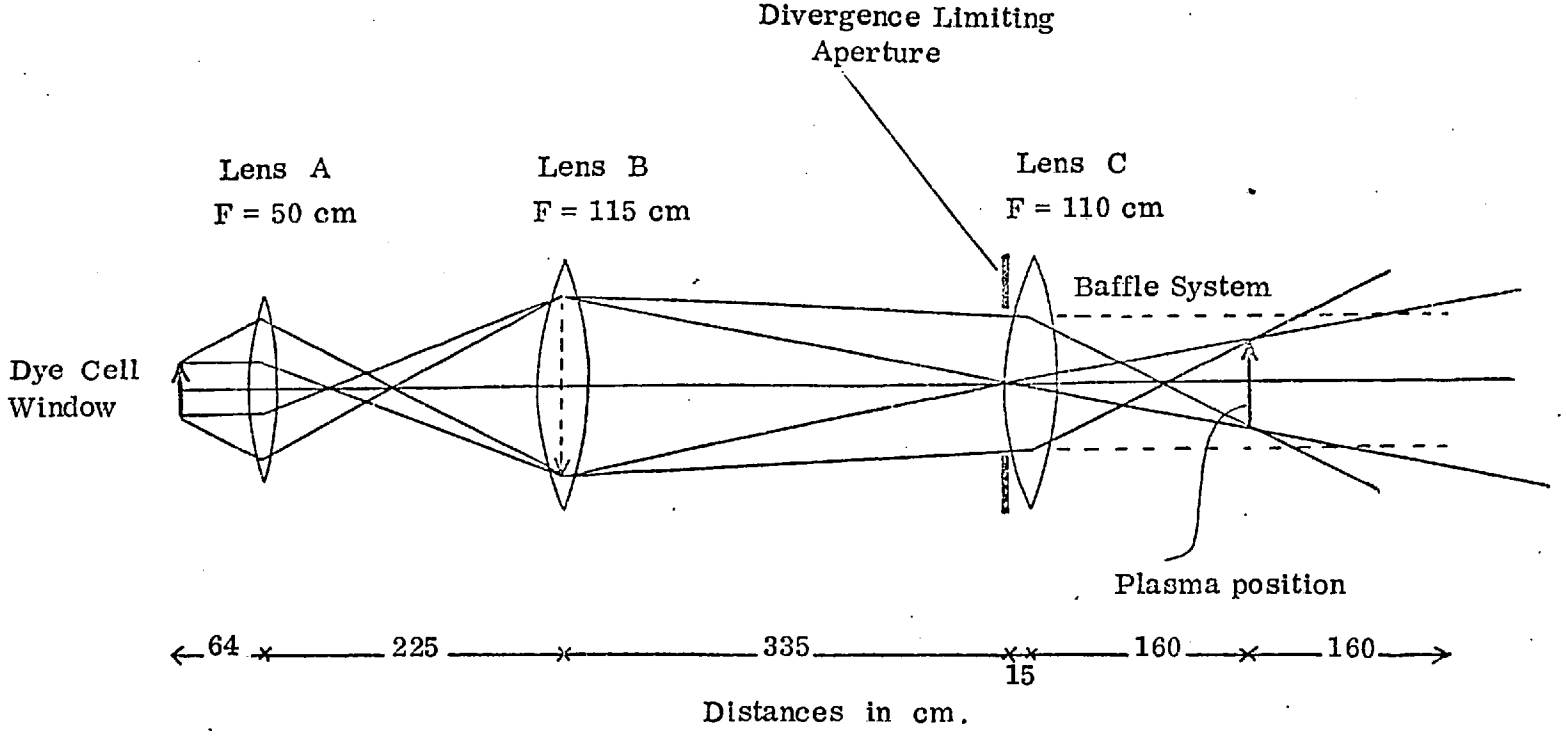

FIGURE 17.1 INPUT OPTICS FOR Hα SCATTERING EXPERIMENT ON CLEO

Due to the limited access time available on CLEO a duplicate of this optics system was set up and the energy transmission of the system measured with a calorimeter. It was found that when a 1 cm aperture diffraction limiter was used 25% of the laser energy reached the plasma position.

Spatial Variation of Energy across the Beam

To ensure the Hα transition is uniformly saturated across the laser beam a rectangular spatial distribution of energy is required within the beam. Measurements of the spatial variation of laser power were made by scanning a pinhole aperture photodiode across the beam at the plasma position in the mock-up of the input optics system. Neutral density filters enabled measurements to be made over a wide range of intensity. The results, Fig.(17.2) show that the laser beam was well collimated to the required aperture of 6 mm.

The oscilloscope traces obtained in this experiment showed up to 70% intensity modulation during the course of the laser pulse. As already mentioned, this was also observed in a wavelength resolved spatial intensity scan across the laser beam. Unless the degree of saturation is very high, this modulation will change the saturation characteristics of the laser beam during a single shot and so affect the fluorescence.

Hα Line Width in CLEO

The fluorescence produced is dependent on the Hα line width compared to the laser line width.

FIGURE 17.2 LASER SPATIAL INTENSITY DISTRIBUTION IN IMAGE PLANE OF INPUT OPTICS.

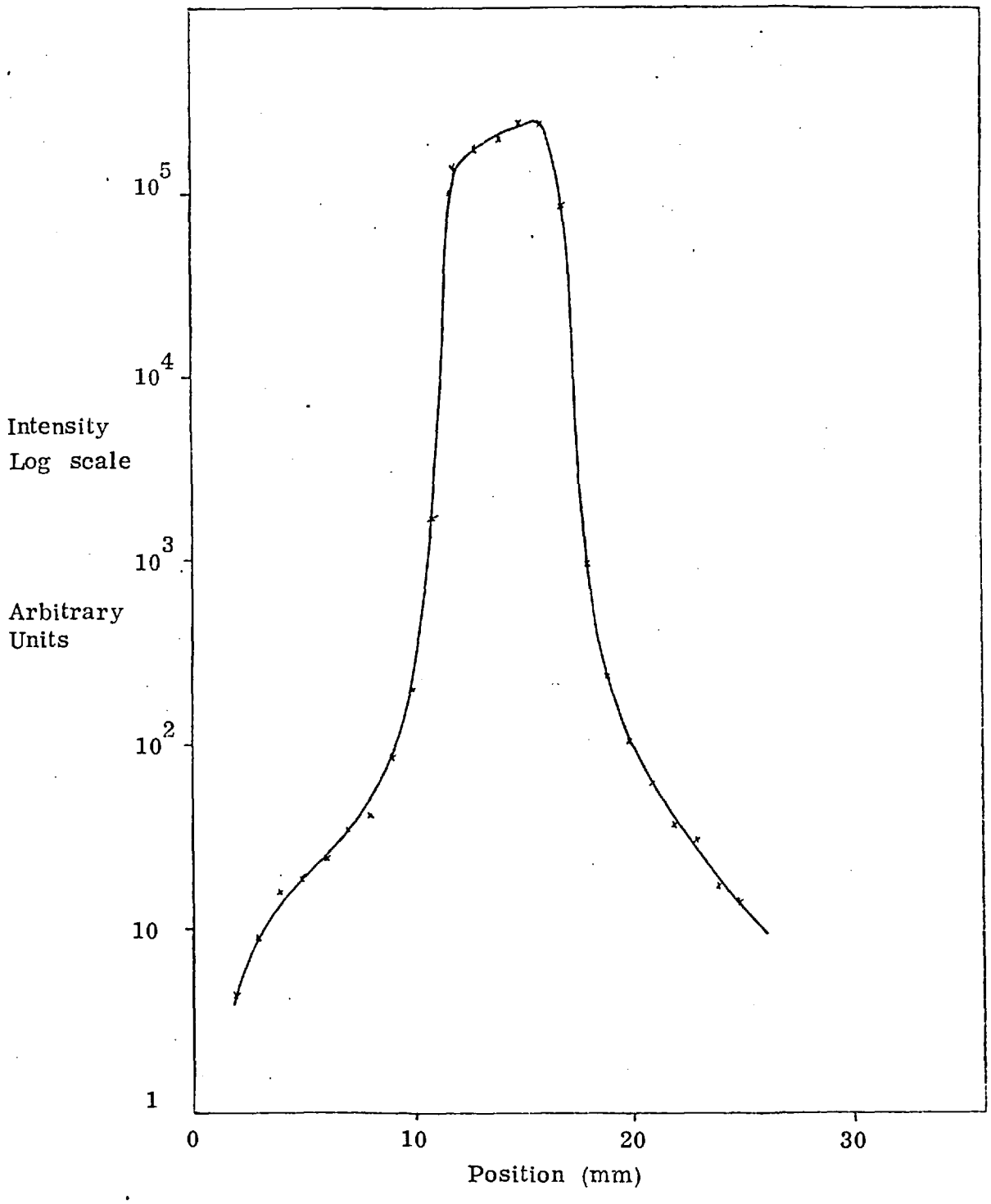

Errors approximately 5%. Area sampled 1 mm dia.

Doppler Width

The doppler (whole) half width is given by

$$2\lambda\left(\ln 2 \times \frac{2kT}{mc^2}\right)^{\frac{1}{2}}$$

working in units of eV

$kT = 200$ eV assuming atom temperature = ion temperature

$mc^2 = 9.38 \times 10^8$ eV

$\lambda = 6563$ Å

doppler (whole) half width = 7.14 Å

Stark Width

The stark (whole) half width of Hα at $N_e = 10^{13}$, $T_e = 4 \times 10^4$ °K is approximately 10^{-3} Å (Vidal et al. 1973). Unfortunately no tabulated values have been published for the case of electron temperature of CLEO. Although the temperature dependence of the stark width is complex it is clear that for the plasma conditions existing in CLEO the stark width is negligible compared to the doppler width.

Fine Structure

The fine structure splitting of the Hα line is approximately 0.4 cm^{-1} (Woodgate 1970) corresponding to 0.17 Å.

Zeeman Splitting

The magnetic field interaction is of the order of $\frac{\mu_B B}{hc}$ where μ_B is the Bohr magneton, B is the field, h Plank's constant and c the velocity of light. At 2×10^4 Gauss the Zeeman splitting is 0.93 cm^{-1}, i.e. 0.4 Å.

Laser Line Width - Broadband Filter

Thus we see that the Hα line is predominantly doppler broadened and laser spectrum is not constant over the whole Hα line whether the laser

was tuned by the Fabry Perot or the interference filter. In this situation the laser beam only interacts with those atoms whose wavelength in the laboratory frame lies within the bandwidth of the laser. As the laser spectrum changes during a single pulse so the proportions of atoms which interact with the laser would also vary. To avoid the interpretive problems this would present, a broad band interference filter (FWHM 160 Å) was purchased. (The untuned laser output (≅ 80 Å wide) lay in the region of 6610 Å and could not be used for Hα fluorescence). This filter was substituted for the Fabry Perot in the laser cavity and the laser wavelength tuned to Hα by adjusting the angle between the filter and the laser axis. The laser bandwidth was 15 Å F.W.H.M. Due to the limited operational life of CLEO there was insufficient time to make any time resolved measurements of the laser spectrum tuned by this filter.

Collection Optics

The collection optics were shared with Thomson scattering experiments. Light emitted at approximately 90° to the laser axis was collected by a system of several lenses and mirrors and directed to a EMI 9558QB photomultiplier via a 40 Å bandwidth 65% transmission interference filter with peak transmission at 6563 Å.

Fluorescence Experiment

The initial aims of the fluorescence experiments were

(i) to measure the signal to noise ratio of the Hα emission from the plasma.

(ii) To measure the stray light level produced by the laser.

(iii) To look for changes in the Hα emission at the time when the plasma was illuminated by the laser.

Signal/Noise of H α Emission

An electrical filter with a bandpass of 20 kHz to 1 MHz was used to remove as much shot noise as possible from the photomultiplier signal. With this filter the signal to noise ratio of the H α emission was measured to be 60 at the time of maximum light emission. A high signal to noise ratio was essential to observe fluorescence as the ratio of the spontaneous emission from the laser illuminated volume observed by the photomultiplier to that seen from the whole plasma was 1 : 100. Since the laser-produced fluorescence was estimated to enhance the local emission by a factor of 3 the fluorescence signal would be detectable above the background noise.

Stray Light

In contrast to Thomson scattering experiments where scattered light may be detected at wavelengths other than the laser wavelength, the fluorescence produced by laser excitation is at the same wavelength as the laser. Consequently the stray light requirements can be more severe than in the case of Thomson scattering.

Initial measurements revealed that the stray light level was high. This was probably due to light back scattered from apertures inside the torus and from the beam dump window which had been damaged by the ruby laser. An additional aperture was used to reduce the stray light to a level about equal to the noise level observed on the H α spontaneous emission. The laser intensity in the plasma under these conditions was not more than 3 kilowatts cm^{-2} which compares to the power density of 300 kW cm^{-2} measured at the laser.

Fluorescence

A change in the H α signal from the plasma at the time the laser was fired was observed. However, stray light measurements made after

the current pulse had been applied to the CLEO magnetic windings but before the initiation of the discharge revealed large variations (up to 300%) in the stray light level and consequently the observations of the change in $H\alpha$ signal could not be attributed to fluorescence. At this point CLEO was taken out of service and no further fluorescence measurements were possible.

Conclusions

This experiment contrasts rather sadly with the fluorescence experiments performed at Imperial College. Part of the problem was unavoidable because operational constraints on a machine of the complexity of CLEO were bound to be more severe. In particular the fact that the machine was only accessible in the evenings and severely limited machine time available for fluorescence experiments coupled to the low plasma repetition rate of once every 30 minutes meant that progress was very slow. In addition during the times the machine was available the various components of the dye laser showed an unexpectedly high failure rate. In all, the laser capacitor failed four times, the rotary vacuum pump broke down, the dye cell windows leaked and needed replacing three times, the laser output mirror suffered damage from the intense radiation field and the entire trigger circuitry needed replacing as it had an 8 millisecond timing jitter. Each time a delay was caused of up to two weeks before replacements could be obtained. This contrasts to the very reliable behaviour of the coaxial laser developed at Imperial College.

The most limiting constraint however was the necessity of sharing the optical system with the Thomson scattering experiment coupled to the fact that the components inside the torus were permanently inaccessible.

The dye laser divergence was much larger than the divergence of the ruby laser, and as the major part of the input optics was designed for the ruby laser it was impossible to transmit the dye laser beam to the plasma in the most efficient manner. As the fluorescence signal was limited by saturation effects it was also desirable to illuminate a larger fraction of the plasma than was arranged for the Thomson scattering experiments. Also, as the fluorescence is observed at the same wavelength as the laser illumination the stray light requirements were more severe and the baffle system designed for the Thomson scattering experiments was not ideal. The alignment of both the input collection optics was quite difficult and needed to be constantly checked as there was a considerable judder of the iron core of CLEO whenever the machine was fired.

In conclusion, there is no reason in principle why a successful fluorescence experiment should not be possible on the plasmas of interest at Culham provided the experimental difficulties mentioned above are avoided. This is confirmed by the successful fluorescence experiment on $H\alpha$ performed at Imperial College with a plasma of higher electron density and lower temperature than found in CLEO establishing that the laser system used is adequate in power to overcome the collision rates and to produce saturation in the plasmas of interest at Culham.

CHAPTER XVIII

MAGNETIC FIELD MEASUREMENTS IN HOT PLASMAS

A plasma parameter important to the theoretical understanding of Tokamak plasma machines and not yet reliably determined is the direction of the magnetic field set up in the plasma. This is governed both by the external magnetic field coils and also by the current generated inside the plasma.

Magnetic field measurements based on Zeeman splitting methods or Faraday rotation studies are severely limited by line of sight integration effects. The Zeeman splitting method is also limited by the large doppler line width of atomic transitions in the plasma. (D.D. Burgess (1970)).

An alternative method was proposed by Sheffield (1972). The method was based on measurements of the shape of the Thomson scattered spectrum for scattering wave numbers close to perpendicular to the magnetic field direction; and uses the result that the spectrum is most heavily modulated when the wavenumber is exactly perpendicular to the field direction. This method poses severe experimental problems, the very low scattered light level necessitating the use of a Fabry Perot interferometer coupled to a gated image intensifier tube to detect the modulation.

A simpler method was proposed by Burgess (to be published). The method was based on measurement of dye laser excited fluorescence and combined the spatial resolution inherent in scattering measurements with the virtual lack of any spectral resolution requirements. The method is independent of the plasma temperature and the number density of scattering centres (apart from the restrictions on the limiting sensitivity if this density is too low). However, in the original proposal no account was taken of the intrinsic atomic angular momentum or the interactions of the levels excited by the laser with the rest of the plasma.

The method is discussed in detail for the particular case of $H\alpha$ fluorescence in the light of the fluorescence results and theoretical models developed in the previous chapters.

Principle

The method is based on Hanle's third effect (Hanle (1924); Mitchell and Zemansky (1934)). Consider the geometrical arrangement in Fig.18.1. A polarised laser beam is incident along the z-axis with polarisation vector in the x-direction. A magnetic field B is present with the field direction lying in the yz plane. We first consider a classical treatment of the problem. The laser excites a classical dipole at the origin, which precesses around the field direction. This produces an oscillating electric field perpendicular to the magnetic field direction. Fluorescence emitted along the x-axis is hence completely polarised, the polarisation vector being perpendicular to the direction of the magnetic field. The magnetic field direction may be determined simply by measurements of the polarisation direction of the fluorescence. This model is exact for a classical atomic dipole excited by electromagnetic radiation but it ignores the effects due to the intrinsic angular momenta of the scattering atoms themselves. Thus 100% polarisation of the scattered radiation is only obtained in cases where the lower state of the pumped transition is $^1S_0$. We consider two simple cases :

I) Helium $2^1S \rightarrow 3^1P$ 5016 Å

In the presence of a magnetic field the 3^1P level is split into three sublevels with magnetic quantum numbers, m_J, of -1, 0, +1 (Fig.18.2). As the polarisation direction of the laser beam is perpendicular to the magnetic field (Fig.18.1) the atom is excited in a " σ " transition in which m_J changes by one. As the lower state 2^1S has an m_J of zero the $m_J = +1$ and -1 sublevels

FIGURE 18.1 - HANLE EFFECT : GEOMETRIC ARRANGEMENT

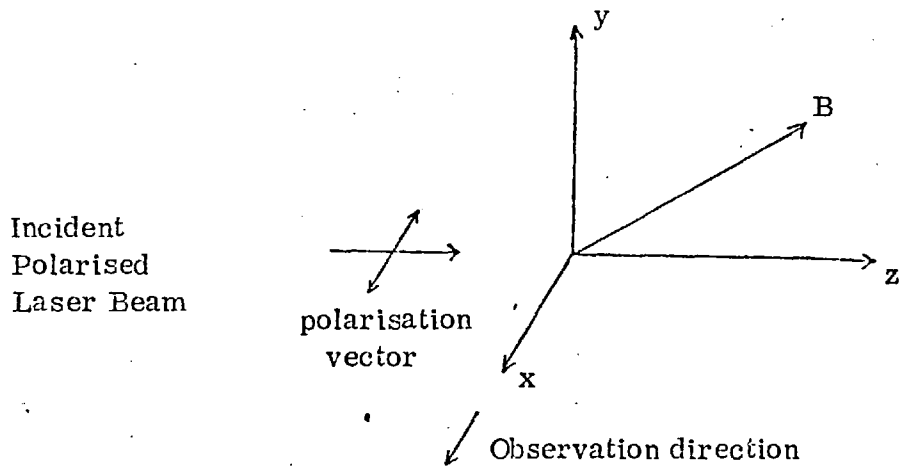

FIGURE 18.2 - FLUORESCENCE POLARISATION He $^1S \longrightarrow {}^1P$

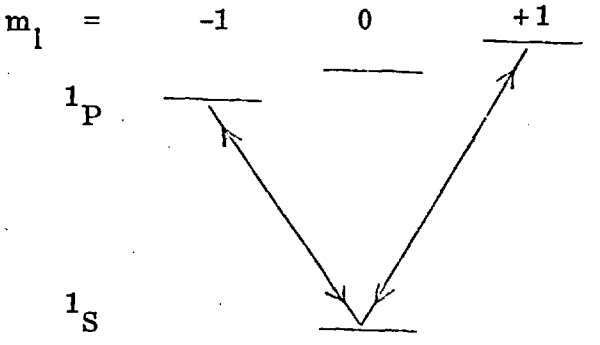

The atoms decay by σ transitions only. The fluorescence is completely polarised.

FIGURE 18.3 - FLUORESCENCE POLARISATION : HYDROGEN

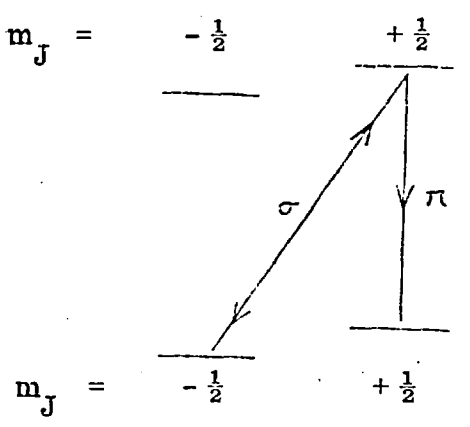

The atoms can decay by σ and π transitions.
The fluorescence is partially polarised.

of 3^1P are excited. In the absence of collisional transfer between sublevels the atom must therefore decay by a σ transition to 2^1S. When observed in the x-direction (Fig.18.1) the σ radiation is polarised perpendicular to the field direction.

Collisional Effects

Collision induced transitions amongst the magnetic sublevels of 3^1P would depolarise the fluorescence signal. As it is the direction of polarisation of the fluorescence that matters, this does not change the principle of the method but only the signal to noise ratio. In the absence of published cross sections for collisional transfer between the 3^1P sublevels we estimate the collision rate from Stark broadening data. The electron impact produced line width, W, for an atom in a plasma is given by Baranger (1962) as

$$W = \langle N_e \sigma v \rangle \qquad (18.1)$$

for the case where the upper state of the line is appreciably broadened, an excellent approximation for He $2^1S - 3^1P$ and also the Balmer lines of hydrogen. σ, is the total electron impact cross section and N_e and v the electron density and velocity. For 5016 Å the electron impact (half) half width is 0.28 Å at $N_e = 10^{16}$ cm^{-3}, $T_e = 8 \times 10^4$ °K (Griem (1964)). We now scale this to conditions in CLEO: $N_e = 2 \times 10^{13}$ cm^{-3}, $kT_e = 200$ eV (2.3×10^6 °K). Far above threshold (i.e. in the Born approximation) cross sections typically scale inversely with the electron energy. The product $\langle N_e \sigma v \rangle$ will therefore scale proportionally with N_e and inversely with $(T)^{\frac{1}{2}}$. This yields:

$$0.28 \times \frac{2 \times 10^{13}}{10^{16}} \times \left(\frac{8 \times 10^{4}}{2.3 \times 10^{6}} \right)^{\frac{1}{2}}$$

$$= 1.04 \times 10^{-4} \text{ Å}$$

collision frequency $= 7.82 \times 10^{7} \text{ sec}^{-1}$

This is an estimate of the total collision rate including elastic transitions, and inelastic transitions other than those between magnetic sublevels. The frequency of collisional transitions between sublevels is likely to be considerably smaller than the above figures. The radiative transition probability for the 5016 Å transition is $1.34 \times 10^{7} \text{ sec}^{-1}$ (Weise et al. 1966).

Thus, if collisional transitions between the 3^1P sublevels only accounts for 10% or less of the total collision frequency, collisional transfer between the sublevels may be neglected and to a first approximation the fluorescence is completely polarised.

II) Magnetic Field Measurements in Hydrogen

Even in the absence of a magnetic field each level in hydrogen is split into at least two sublevels by the spin orbit interaction. An atom, excited by σ radiation can thus re-radiate by transitions in which m_J changes either by ± 1 or zero producing σ and π radiation respectively (Fig.18.3). In the geometry of Fig.18.1, π transitions produce fluorescence polarised parallel to the magnetic field direction when observed in the x-direction and hence in general the fluorescence is <u>not</u> completely polarised. We consider the case of Hα in detail.

<u>Hα - Collisions Between n = 3 Sublevels</u>

We follow the procedure outlined on P 219 . For Hα the line (half) half width is 0.6 Å at $N_e = 10^{16} \text{ cm}^{-3}$, $kT_e = 20{,}000\ ^{\circ}\text{K}$ (Hill, 1964).

The majority of this line width is not due to electron impacts but is due to the stark splitting produced by the static electric field of nearby ions (irrelevant in the present situation). Taking 0.25 Å as an overestimate of the electron impact width at the above conditions and scaling the equivalent transition rate to the conditions in CLEO (P.206), we get a total effective collision rate of 2.0×10^{7} sec^{-1}. This compares with the H α transition probability of 4.4×10^{7} sec^{-1}. Radiative decay is therefore more likely than collisional transfer by a factor of two and to a first approximation collisional effects may be ignored.

Atom Coupling Scheme

The atom - magnetic field interaction is of the order of μ_B B where μ_B is the Bohr magneton and B the field strength. In the 20 kilogauss field of CLEO this is 0.93 cm^{-1} compared to the largest case of the fine structure splitting of H α by the spin orbit interaction of 0.36 cm^{-1} (Woodgate 1970). Hence the magnetic field can be considered to have de-coupled the spin orbit interaction and the appropriate representation for the description of the atomic states is an l, s representation. As the spin does not change in electric dipole transitions in the absence of spin-orbit interactions the calculations can therefore be done with complete generality by treating the case of $m_S = +\frac{1}{2}$ only.

Initially the polarisation of the fluorescence was calculated by assuming all the n = 2 sublevels were equal before the laser pulse. The n = 3 sublevel populations were calculated by balancing spontaneous and stimulated decay rates and the degree of polarisation of the fluorescence deduced from the n = 3 sublevel populations and the radiative decay rates. This approach is described in Appendix 3. However the fluorescence results described in the

previous chapters prompted a reconsideration of the whole problem and a much improved calculation is described below.

Equilibrium Considerations

In order to determine the change in the various level populations in the presence of the laser illumination we must first establish the nature of the pre-existing equilibrium in the plasma. On P. 220 we deduced that the collision rate for transfer between the $n = 3$ sublevels was lower than the $H\alpha$ radiative decay rate so clearly local thermodynamic equilibrium is not present in the lower excited levels. We therefore consider the criteria for coronal equilibrium considering in the first case a steady state plasma. In a coronal plasma the populations of the bound levels (n_p) relative to the population of the ground state (n_1), are controlled by the collisional excitation rate S_{1p} and radiative transition probability A_p

$$\frac{n_p}{n_1} = \frac{S_{1p}}{A_p} \qquad (18.2)$$

However at a sufficiently high excited level the collisional de-excitation rate will be greater than the radiative transition probability and the level populations will be in LTE with the free electrons. Wilson (1963) discussed the concept of a "thermal limit" : a level in the atom above which collisional processes predominate and the level populations are approximately thermal and below which the level populations are approximately coronal. The thermal limit is defined as the level at which upward and downward transitions are equally probable. In the following table we list the radiative decay rate for level n, $\sum A_{n,\,n-1} + A_{n,\,n-2} + \ldots$ (Wiese 1966), together with the collision rates $C_{n,\,n-1}$ and $C_{n,\,n+1}$ obtained (P. 121) from the cross sections of Johnson (1972).

n	$C_{n,\,n-1}$	$A_{n,\,n-1}$	$C_{n,\,n+1}$
2	0.01	47	0.44
3	0.2	10	1.48
4	0.83	3	4.6
5	3	1.2	36

All rates $\times 10^{7}$ sec^{-1}

The collision rates $C_{n,\,n+2}$, $C_{n,\,n+3}$, etc., are smaller than the rates in which the principal quantum number changes by one (see e.g. Felden et al. 1972). It can be seen that the thermal limit corresponds approximately to $n = 4$.

Time Dependent Effects

The plasma lifetime in CLEO was 100 - 200 mS. McWhirter (1965) has given an order of magnitude criteria for the atomic relaxation time in a coronal plasma:

$$\tau \simeq \frac{10^{12}}{N_e} \text{ sec}$$

In the present case τ is 50 mS, less than the plasma lifetime and so coronal equilibrium was reasonably well established.

Level Populations

Johnson and Hinnov (1973) have calculated excited state populations in terms of the ground state population for hydrogen plasmas over a wide range of density and temperature. They include a term proportional to the rate of change of the ground state population density

$$n(p) = r_o(p)\ n_E(p) + r_1(p).\ p^2 - \tau(p)\ \frac{d\,n_{(1)}}{dt} \qquad (18.3)$$

$n(p)$ is the population density of the p^{th} level.

$n_E(p)$ is the Saha equilibrium population of the p^{th} level.

r_o, r_1, $\gamma(p)$ are coefficients listed by Johnson et al.

$$n_E(p) = n_e \; n(H^+) \; p^2 \left(\frac{h^2}{2\pi m kT}\right)^{3/2} \exp -\frac{E_p}{kT}$$

$$= 12\, p^2 \text{ cm}^{-3} \text{ in the present case.}$$

We assume a steady state has been reached in the plasma and use Eqn.(18.3) in conjunction with the coefficients of Johnson et al. to deduce the populations of levels $1 \rightarrow 3$ from the observed $n = 4$ population. We use the coefficients for the optically thin case.

$$n(1) = 3.86 \times 10^9 \text{ cm}^{-3}$$

$$n(2) = 3.24 \times 10^6 \text{ cm}^{-3}$$

$$n(3) = 2.26 \times 10^6 \text{ cm}^{-3}$$

$$n(4) = 1.36 \times 10^6 \text{ cm}^{-3} \text{ (experimental)}$$

The absorption coefficient for Ly α calculated (P.109) with the above value of the $n(1)$ population is 10^{-4} cm^{-1}. The absorption coefficient calculated with the $n(1)$ population obtained by using the r_o, r_1 coefficients for the optically thick case is smaller still, so clearly the assumption of low optical depth is justified.

A point not explicitly taken into account by Johnson et al. is that the 2s level in hydrogen is metastable. In most cases this does not affect the 2s population appreciably as it can decay by fast collisional transfer to the 2p levels followed by radiative decay to ground state. However, as we have seen in the high temperature, low density conditions of CLEO, the collisional transfer rates between the $n = 3$ levels are slower than the H α radiative transition rate.

We calculate the populations of the 2s, 2p, 3s, 3p, 3d levels separately by balancing (Eqn. 18.2) the collisional excitation rate from ground to the radiative decay rate. We take the figure of the ground state population deduced on P. 224, i.e. 3.86×10^{9} cm^{-3}. As this is estimated from the observed $n = 4$ level population, problems due to metastable levels do not arise. We use the collisional excitation cross sections for the 2s, 2p, 3s, 3p levels of Felden et al. (1962). We estimate the 3d excitation cross section by comparing the sum of the 3s, 3p cross sections to the total $n = 3$ cross section of Johnson (1972).

The most likely de-excitation route for the 2s level is by collisional transfer to the 2p level. No cross sections for this collision process have been published but from the arguments of P.220 we estimate a collisional transfer rate of 10^{7} sec^{-1}. For this level only we calculate the population by balancing collisional excitation from ground to collisional transfer to the 2p level.

The calculated 3s population turns out to be almost equal to the total 2p population. This is clearly unphysical, considering the statistical weights of the two levels and may indicate that the transfer rate 3s - 3p is larger than expected. We assume the 3s population is reduced by stimulated emission to 2p so that the populations of the 3s, 2p sublevels are equal.

Table 18.1 shows the excitation and radiative decay rates and the 2s - 3d populations.

Time Variation of the $n = 3$ Levels in the Presence of the Laser

In the presence of the laser illumination we divide the $n = 2$ and 3 levels into two systems unconnected by optical transitions 2s - 3p and 2p - 3s, 3d.

TABLE 18.1

Level	Excitation Cross Section for Electron Impact Energy of 300 eV ($E = {}^{3}/_{2}\ kT$) Units of πa_o^2	Excitation Rate sec^{-1}	Radiative Decay Rate sec^{-1}	Population cm^{-3}
2s	.03	4.44×10^{4}	10^{7}	1.71×10^{7}
2p	.3	4.44×10^{5}	6.2×10^{8}	2.76×10^{6}
3s	.003	4.44×10^{3}	6.3×10^{6}	(2.72×10^{6}) see 0.92×10^{6} text
3p	.05	7.4×10^{4}	1.89×10^{8}	1.51×10^{6}
3d	.01	1.48×10^{4}	6.46×10^{7}	8.84×10^{5}
3s, 3d			5.49×10^{7} (avr.)	1.8×10^{6} (sum)

Using the theory developed on P.73 we calculate the time variation of the $n = 3$ populations for the case of the laser intensity being a step function in time.

The difficulties found in interpreting the $H\alpha$ fluorescence results described in Chapter XIII in terms of this model are not likely to be significant in the present case. The $n = 2$ and 3 levels are populated only by the ground state and as this has a large population the populating rates are not likely to be disturbed by the laser. The basic equation may be written -

$$n_u(t) = \frac{(n_{lo} - g\, n_{uo})\ (D_u - D_l)}{(1 + g)\ (g.\, D_l + D_u)} \quad \exp -\left(\frac{g.\, D_l + D_d}{1 + g} \right) + \frac{C_l + C_u}{g.D_l + D_u} \tag{18.4}$$

n_l , n_u are the lower and upper state populations, g is the ratio of the statistical weights $(\frac{g_l}{g_u})$, D_l , D_u are the depopulating rates and C_l, C_u are the populating rates given on Table 18.1. 'o' refers to initial conditions.

2s - 3p System

The laser excites only the $m_l = \pm 1$ sublevels of the 3p level. The initial population of 3p $m_l = \pm 1$ is taken to be 2/3 the total 3p population, i.e. 1.0×10^6. The g factor in Eqn.18.4 is 1/2. The time variation of the 3p, $m_l = \pm 1$ sublevels is given by

$$n_{3p, m_l = \pm 1} = 10 \times 10^6 \quad \exp \quad -(1.3 \times 10^8)\, t + 2.36 \times 10^6 \quad cm^{-3}$$

There is a transient x 12 increase in the 3p $m_l = \pm 1$ population lasting for approximately 10 nS. Subsequently the population remains enhanced by a factor of two. The time dependence of the 3p $m_l = \pm 1$ population is shown in Fig.18.4.

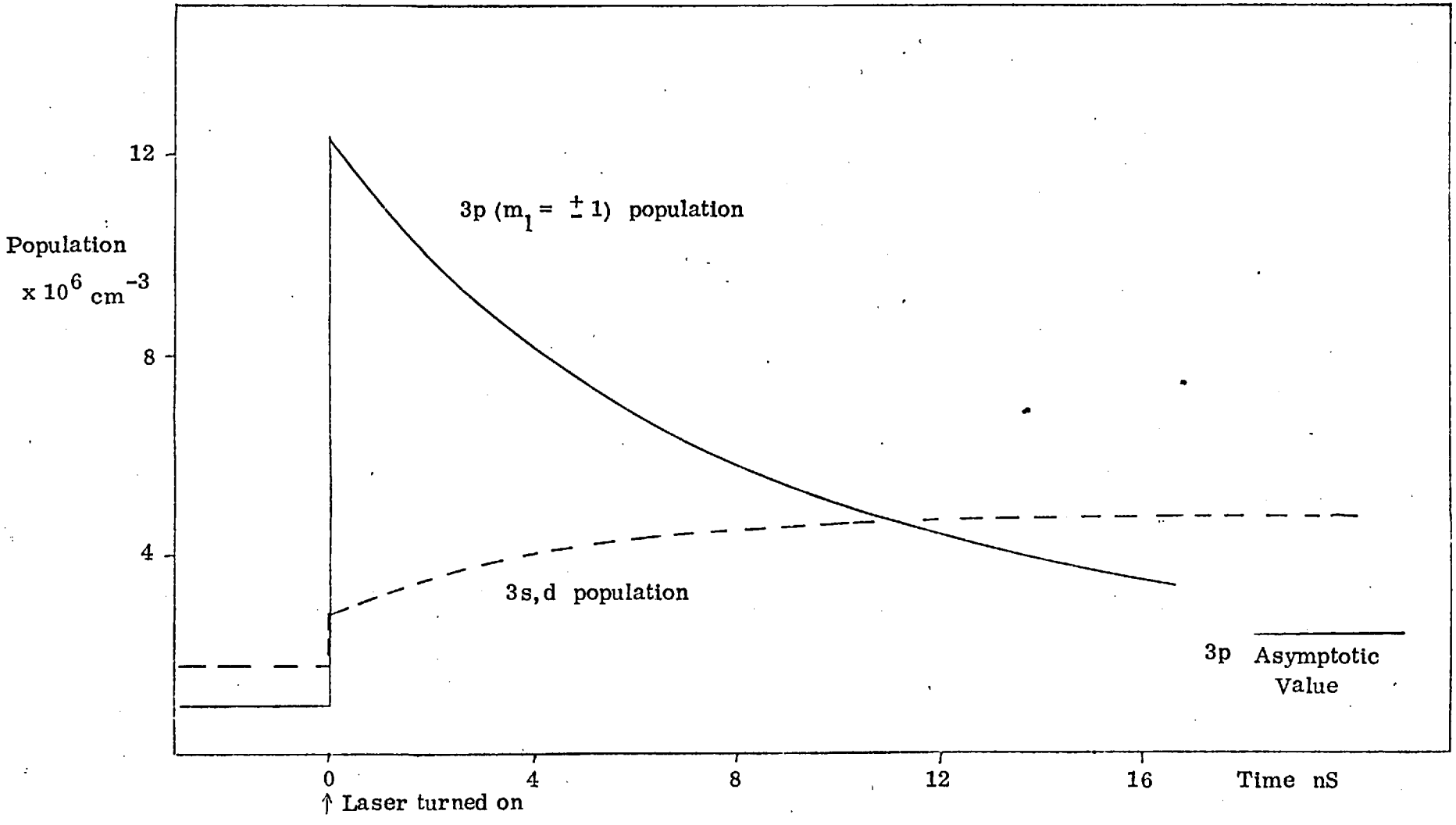

FIGURE 18.4 - 3p AND 3s POPULATIONS DURING A Hα LASER PULSE

2p - 3s, 3d System

In this case we sum the populating and depopulating rates of the 3s and 3d levels to obtain the C_u, D_u coefficients. The initial 3s, d population is 1.8×10^6 cm^{-3}. For D_u we take the average (weighted by statistical weight) decay rate for the 3s and 3d levels. With the laser on the time variation of the 3s,d population is

$$n_{3s,d}(t) = -1.92 \times 10^6 \exp -(2.43 \times 10^8)\, t + 4.82 \times 10^6 \text{ cm}^{-3}$$

The 3s,d population shows a fast initial rise followed by an exponential rise to an enhanced value. The time dependence of the n = 3 populations are shown in Fig.18.4. The 3p and 3s,d levels thus illustrate the two possible forms of the fluorescence time history as predicted by Eqn.18.4, producing an exponential rise or fall respectively.

Fluorescence Polarisation

Atoms which decay from the 3p $m_l = \pm 1$ sublevels produce only σ polarised radiation. Atoms decaying from the 3s,3d levels will produce σ and π radiation. Initially, as the laser intensity is above saturation all the 3s and 3d sublevels will share the same equal population of the 2p sublevels. Radiative processes between the 3s,d and 2p levels of the kind discussed in Appendix 3 wil not change this as the 2p sublevel populations are kept equal by the fast populating and depopulating rates from the ground state. Thus, in general the 3s and 3d levels will emit an unpolarised background. The 3p $m_l = 0$ level continues to emit π radiation. We estimate the intensity of the 3p $m_l = \pm 1$ polarised radiation to the 3p $m_l = 0$, 3d,3s background by multiplying the level populations by the appropriate radiative

transition probability. It is necessary to multiply the total σ radiation emitted by a geometric factor of 1/2 in order to estimate the amount of σ radiation observed in a transverse direction (Woodgate, 1970).

At the instant the laser is turned on the 3p $m_l = \pm 1$ population is 12.36×10^6. The radiative transition probability is 2.2×10^7. The intensity of σ radiation emitted in the x-direction is proportional to

$$\frac{1}{2} \times 2.2 \times 10^7 \times 12.36 \times 10^6$$

$$= 1.36 \times 10^{14}$$

TABLE 18.2

Polarisation of Hα Fluorescence

Level	Polarisation	Intensity Observed (arbitrary units)	
		t = 0	t = ∞
3p $m_l = \pm 1$	σ	1.4	0.26
3p $m_l = 0$	π	0.11	0.11
3d	σ	0.78	1.3
"	π	0.78	1.3
3s	σ	.02	.025
"	π	.02	.025

Degree of Polarisation of the Fluorescence

	t = 0	t = ∞
$\frac{\sigma}{\sigma + \pi}$	71%	52%
$\frac{\sigma - \pi}{\sigma + \pi}$	41%	5%

After the exponential decay the observed 3p $m_l = \pm 1$ intensity is given by

$$\frac{1}{2} \times 2.36 \times 10^{6} \times 2.2 \times 10^{7}$$

$$= 2.6 \times 10^{13}$$

The 3p $m_l = 0$ sublevel continues emitting π radiation at the same level as before. The observed intensities from the various $n = 3 \rightarrow n = 2$ transitions are shown in Table 18.2. At the instant the laser is turned on ($t = 0$) there is a substantial degree of polarisation of the fluorescence.

Signal/Noise Ratio

This will depend on the particular experimental setup used. In the H α fluorescence experiment on CLEO described in Chapter XVII the signal/noise ratio in the absence of the laser illumination was measured to be 60. The ratio of the laser illuminated volume observed by the photomultiplier to that seen from the whole plasma was 1 : 100. Thus the x3 enhancement of the H α emission predicted after the laser has been turned on and after the initial transient should be detectable. However, it would be impossible to detect the small (5%) degree of polarisation as the fluorescence signal is only approximately twice the amplitude of the noise already present. However in the initial transient period just after the laser is turned on, the situation is different. The enhancement is approximately x5 and the σ polarised signal corresponds to 70% of this. The angle through which a polarising filter would have to be turned before the σ polarised signal was reduced by an amount equivalent to the noise is of the order of 40^{o}. Thus for the case of CLEO we would expect to measure the magnetic field angle to that order of accuracy. This illustrates very clearly that, in contrast to Thomson scattering, it is essential in fluorescence studies to illuminate as large a proportion of the total

plasma volume as possible in order to measure the fluorescence accurately above the noise in the background emission. With a higher illuminated volume ratio the accuracy with which the magnetic field could be determined would be substantially improved.

The degree of polarisation produced with the laser intensity below saturation may be higher than the above value, especially if the laser intensity is sufficiently low so as the 2s population was unperturbed. However, in view of the limits imposed by the existing signal/noise ratio it is unlikely that the polarisation of the fluorescence would be detectable above the background noise if the laser was below saturation intensity.

Compared to the above analysis, the polarisation model described in Appendix 3 assumes that the interactions of levels two and three with the rest of the plasma are negligible. The $n = 2$ sublevel populations are calculated from the spontaneous decay rates from $n = 3 \rightarrow n = 2$. In the model described in this chapter the main factor controlling the $n = 2$ sublevel pooulations is shown to be the interactions with the ground state atoms and the polarisation is calculated taking full account of the interactions between levels two and three, and the rest of the plasma.

An alternative to H α fluorescence would be to seed the plasma with a small amount of helium atoms and perform fluorescence experiments using the $2^1S - 3^1P$ transition. This would combine a high initial population of metastable 2^1S atoms with (assuming collisional processes between the 3^1P sublevels to be negligible) 100% polarisation of the fluorescence.

The Lyα radiation produced when hydrogen is excited with an electron beam is up to 25% polarised (Ott et al 1970). However, it is not possible to apply this to Tokamaks as the electron beam would be deflected by the magnetic fields present. A more speculative possibility is Lyα fluorescence, but this awaits the advent of a polarised Lyα laser.

APPENDICES

APPENDIX 1

Single Level Plus Infinite Reservoir

We take the case of a level of population, n, and an infinite reservoir. Atoms are supplied to the level at a constant rate, C, and atoms are lost at a rate, D, per atom.

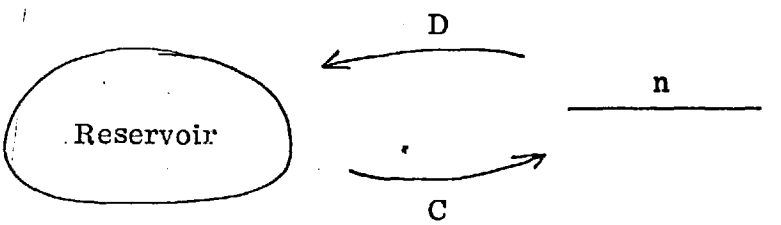

n initially has an arbitrary value n(0). We calculate the variation of n in time.

$$\frac{d\,n(t)}{dt} = C - n(t)D$$

$$\frac{d}{dt}\left[n(t)e^{Dt}\right] = \left[\frac{d\,n(t)}{dt} + n(t)D\right] e^{Dt} = C\,e^{Dt}$$

$$n(t)\,e^{Dt} = \int C\,e^{Dt}$$

$$= \frac{C}{D}\,e^{Dt} + K$$

where K is a constant. $n(t) = n(0)$ when $t = 0$

$$n(t) = \frac{C}{D} + K\,e^{-Dt}$$

$$K = n(0) - \frac{C}{D}$$

Solution

$$n(t) = \left(n(0) - \frac{C}{D}\right) e^{-Dt} + \frac{C}{D}$$

thus n(t) relaxes to a value given by $\frac{C}{D}$ with a time constant given by D. The supply rate, C, to the level has no effect on the rate at which equilibrium is established.

APPENDIX 2

We solve the general case of laser induced fluorescence in a three level atom with arbitrary laser intensity.

A_{21} = spontaneous emission rate.

W_{12}, W_{21} = stimulated emission rate.

C_1, C_2 = total supply rates from level 3 to levels 1 and 2.

D_1, D_2 = transfer rates per atom from levels 1 and 2 to level 3.

E_{12}, E_{21} = collision rates between levels 1 and 2.

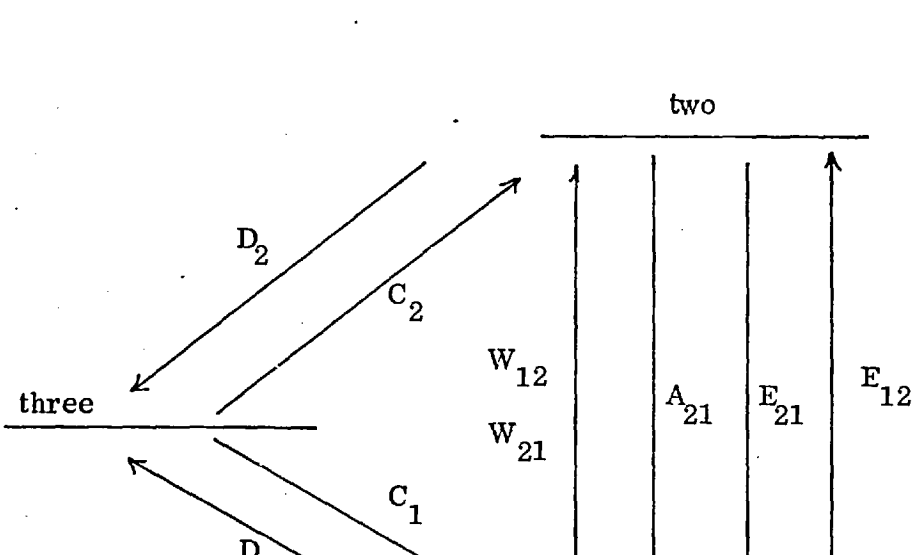

The value of all these rates are constant with one exception : W_{12}, W_{21} is zero for $t < 0$ and constant and positive for $t > 0$. For $t < 0$ we assume equilibrium :

$$\frac{d n_1}{dt} = 0 = C_1 - n_1 D_1 + n_2 (A_{21} + E_{21}) - n_1 E_{12}$$

$$\frac{d n_1}{dt} = 0 = C_2 - n_2 D_2 + n_1 E_1 - n_2 (A_{21} + E_{21})$$

$t > 0$

$$\frac{d\,n_1}{dt} = -(D_1 + E_{12} + W_{12})\,n_1 + (A_{21} + E_{21} + W_{21})\,n_2 + C_1$$

$$= I\,n_1 + J\,n_2 + K$$

where I, J, K are defined by the above equation,

similarly

$$\frac{d\,n_2}{dt} = (W_{12} + E_{12})\,n_1 - (D_2 + A_{21} + E_{21} + W_{21})\,n_2 + C_2$$

$$= F\,n_1 + G\,n_2 + H$$

solve for n_2

$$(\frac{d}{dt} - I)\,n_1 = J\,n_2 + K$$

$$(\frac{d}{dt} - G)\,n_2 = F\,n_1 + H$$

$$(\frac{d}{dt} - I)\,(\frac{d}{dt} - G)\,n_2 - F\,(J\,n_2 + K) - I\,H$$

$$\frac{d^2}{dt^2}\,n_2 - (G + I)\,\frac{dn_2}{dt} + (I\,G - F\,J)\,n_2 = F\,K - I\,H$$

Complimentary function;

$$(\frac{d}{dt} - L)\,(\frac{d}{dt} - M)\,n_2 = 0$$

where L, M are defined by

$$L\,M = I\,G - FJ$$

$$L + M = G + I$$

Particular Integral

$$n_2 = \frac{FK - IH}{\left(\frac{d}{dt} - L\right)\left(\frac{d}{dt} - M\right)}$$

$$= \frac{FK - IH}{LM} \quad \frac{1}{\left(1 - \frac{1}{C}\frac{d}{dt}\right)\left(1 - \frac{1}{M}\frac{d}{dt}\right)}$$

$$= \frac{FK - IH}{LM} \quad \left(1 + \frac{1}{L}\frac{d}{dt} - \cdots\right)\left(1 + \frac{1}{M}\frac{d}{dt} - \cdots\right)$$

$$= \frac{FK - IH}{LM}$$

We define

$$R = \frac{FK - IH}{LM}$$

The complete solution is, therefore -

$$n_2(t) = P\ e^{Lt} + Q\ e^{Mt} + R$$

Similarly

$$n_1(t) = S\ e^{Lt} + U\ e^{Mt} + V$$

APPENDIX 3

Magnetic Field Measurements on Hot Plasmas

In Chapter XVIII we described the expected results of a fluorescence experiment on a coronal plasma designed to measure the magnetic field direction. In this appendix we present, for reference, the results of an earlier calculation of the expected degree of polarisation of $H\alpha$ fluorescence. We take the hypothetical case where initially all the 2s, 2p sublevels are equally populated, the $n = 3$ sublevels have a negligible initial population. With the exception of $Ly\alpha$ fluorescence we neglect interactions between levels 3 and 2 and the rest of the plasma.

The transition probabilities between the individual sublevels of the $n = 2$ and 3 levels were calculated from first principles as tabulated values were not available in the form required. Matrix elements for the various possible $|\, nlm \,\rangle$ to $|\, n'l'm' \,\rangle$ transitions were calculated for electric dipole transitions and the results are shown on P. 239 . The polarisation was then calculated by

1) solving a steady state rate equation to determine the populations of the excited sublevels,

2) multiplying the enhanced sublevel populations by the appropriate transition probability,

3) summing the fluorescence from the σ and π transitions separately.

Unfortunately, whilst the fluorescence from the 3p to 2s transition is completely polarised this contribution is greatly reduced by Lyman fluorescence. This effect varies with the laser intensity. Two cases were treated.

FIGURE A3.1 - Complete Transition Probabilities for the Transitions in Hydrogen

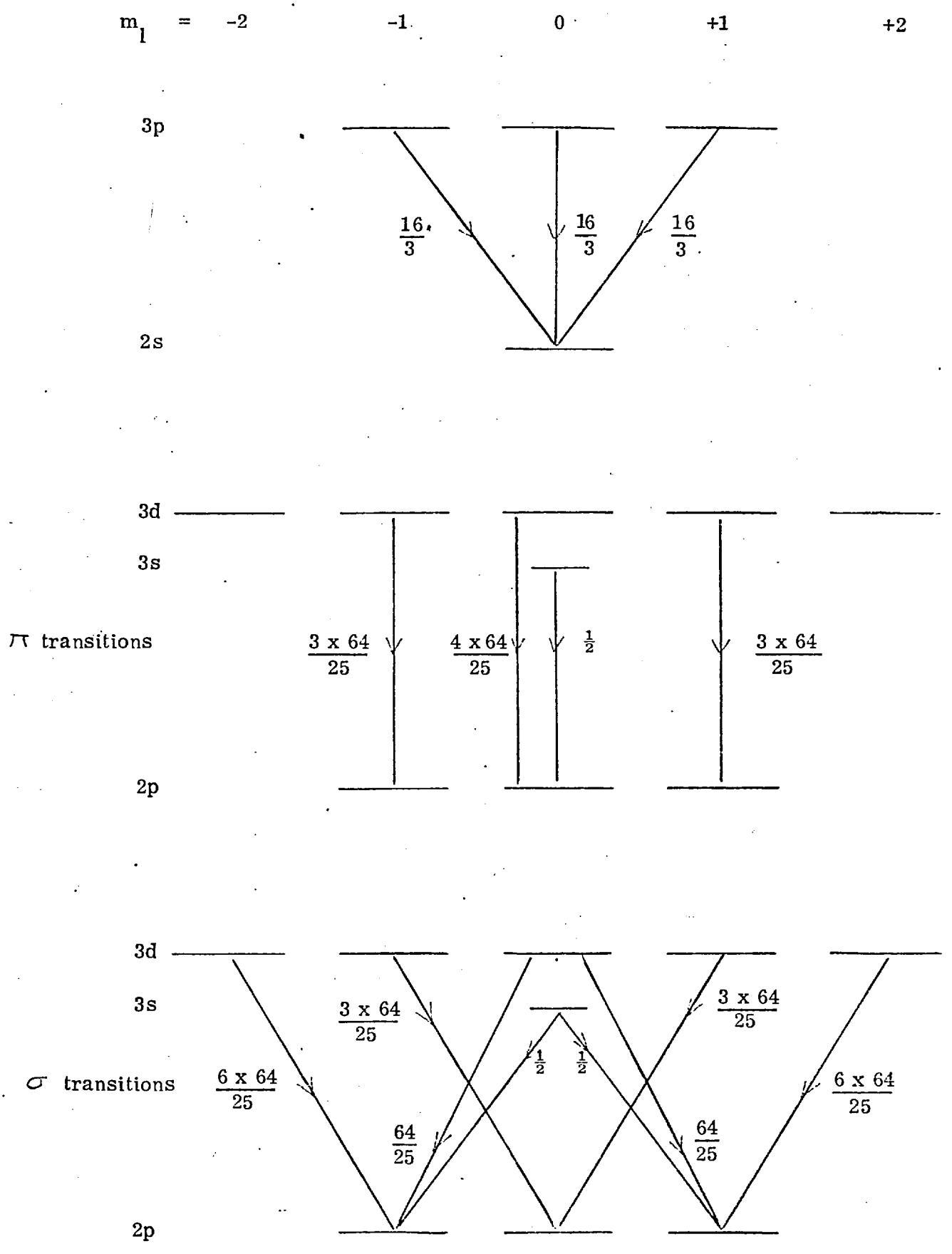

Laser Intensity below Saturation

For low laser powers the stimulated transition probabilities are much less than the saturated values. The sublevel populations are found by balancing the rates of absorption and spontaneous emission. Detailed results are shown on P. 241. Ly β fluorescence reduces the 3p sublevel enhancement but the net population of the 2s level is assumed to be unperturbed.

It should be noted that it is necessary to multiply the total σ fluorescence emitted by a geometric factor of 1/2 to determine the σ fluorescence observed in a transverse direction. Fig. A3.2 shows that at low intensities the polarisation of the fluorescence is quite high, 30%, most of the polarisation being due to the $m_l = \pm 2$ sublevels of the 3d state.

Laser Intensities above Saturation

At high laser powers the situation changes. The 2s, 3p system is assumed to be depleted by Ly β radiation and no H α fluorescence from the 3p sublevels is included. The 3d, 3s, 2p levels form two systems interconnected only by spontaneous emission. For convenience because of the shape of the transition array these will be referred to as the V and W systems (see P. 239). For laser powers above saturation the high stimulated emission probability means that within each system all the sublevels have equal populations. However, a sublevel in the V system does not necessarily have the same population as one in W. Atoms transfer between the V and W systems by spontaneous π radiation. The relative V and W populations were obtained by balancing the rate of spontaneous transitions in and out of each system. The relative amounts of σ and π fluorescence was then calculated by multiplying the sublevel populations by the appropriate transition rates. Above saturation the laser mixes the 3d $m_l = \pm 2$ sublevels with the other 3d sublevels and so reduces the major source of polarisation. The

FIGURE A3.2

FLUORESCENCE POLARISATION OF Hα

(i) Laser Power below Saturation Level

Transition	Population Enhancement (relative units)	Relative Transition Probability	Fluorescence intensity (arb.units)
3p-2s	0.107	$\frac{2 \times 16}{3}$	1.14
3s-2p	2/3	1	0.66
3d-2p $l = 2$ $m_l = \pm 2$	1	$\frac{12 \times 64}{25}$	30.7
$m_l = 1$	1/2	$\frac{6 \times 64}{25}$	7.68
$m_l = 0$	1/3	$\frac{2 \times 64}{25}$	1.70
		Total σ radiation emitted =	41.8
		Total σ radiation observed =	20.9
3p-2s	0.107	0.0	-
3s-2p	2/3	1/2	0.33
3d-2p $m_l = \pm 2$	1	0.0	-
$m_l = \pm 1$	1/2	$\frac{3 \times 64}{25}$	7.7
$m_l = 0$	1/3	$\frac{4 \times 64}{25}$	3.41
		Total π radiation emitted and observed =	11.44

Degree of Polarisation $\frac{20.9 - 11.44}{20.9 + 11.44} = 30\%$

(ii) Laser Power above Saturation Level

Transition		Relative Population	Transition Probability (un-normalised)	Fluorescence intensity (arb. units)
3p-2s		Negligible	$\frac{2 \times 16}{3}$	-
3d, 3s – 2p	V system	0.259	$\frac{64}{25} \times 6$	3.98
	W system	0.370	$(\frac{64}{25} \times 14) + 1$	13.66

Total σ radiation emitted = 17.63

Total σ radiation observed = 8.81

3p-2s		0.04	0.0	-
3d, 3s – 2p	V system	0.259	$\frac{64}{25} \times 6$	3.971
	W system	0.370	$(\frac{64}{25} \times 4) + \frac{1}{2}$	3.982

Total π radiation observed = 7.953

$$\text{Degree of Polarisation} = \frac{8.814 - 7.953}{8.814 + 7.953} = 5\%$$

results is that for laser powers above saturation the degree of polarisation drops to 5%.

It would appear that for the case where this model is a good description of the fluorescence process a high signal/noise ratio in the H α emission is required before the fluorescence polarisation may be detected.

REFERENCES

Alekseev, V.A., Antonov, I.V., Mikhnov, S.A. and Prokudin, V.S. 1972. Sov.J. of Quant.Elec. 2, 52.

Arecchi, F.T. and Courtens, E. 1970. Phys.Rev. A2, 1730.

Atkinson, J.B. and Pace, F.P. 1973. I.E.E.E. J. of Quant.Elec. 9, 569.

Avizonis, P.V., Doss, T.T. and Heimlich, R. 1967. Rev.Sci.Inst. 38, 311.

Bakos, J. and Szigeti, J. 1968. J.Phys.B. 1; 1115.

Ballakov, F.N., Barikhin, B.A., Kornilov, V.G., Mickhnov, S.S., Rubinov, A.N. and Sukhanov, L.V. 1973. Sov.Phy.Tech.Phys. 17, 1161.

Bieberman, L.M. and Gourevitch, I.M. 1950. J.E.T.P. 20, 108.

Bradley, D.J. 1969. App.Opt. 8, 1957.

Bradley, D.J., Gaughey, W.G. and Vukusik, J.I. 1971. Opt.Comm.4, 150.

Bradley, D.J., Ewart, P., Nicholas, J.V. and Shaw, J.R.D. 1973. J.Phys.B. 6, 1594.

Brongesma, H.H., Boerboom, A.J. and Kistemaker, J. 1969. Physics 44, 449.

Brongesma, H.H., Koop, F.W. and Backx, C. 1972. Chem.Phy.Lett. 13, 16.

Bunkenberg, J. 1972. Rev.Sci.I. 43, 1611.

Burell, C.F. and Kunze, H.J. 1972a. Phy.Rev.Lett. 28, 1.

Burell, C.F. and Kunze, H.J. 1972b. Phy.Rev.Lett. 29, 1445.

Burke, P.G., Cooper, J.W. and Ormonde, S. 1969. Phy.Rev. 183, 245.

Burgess, D.D. 1970. UKAEA Culham Memorandum "Zeeman Magnetometry in Hot Plasmas".

Burgess, D.D. 1972. Space Science Review. 13, 493.

Burgess, D.D. and Cairns, C.J. 1970. J.Phys.B. 3, L67.

Burgess, D.D. and Cairns, C.J. 1971. J.Phy.B. 4, 1364.

Burgess, D.D., Richards, A.G. and Mahon, R. 1971. J.Phys.B. 4, L76.

Burgess, D.D. and Mahon, R. 1972. J.Phys.B. 5, 1756.

Cairns, C.J. 1970. Ph.D. Thesis. Univ. of London.

Carlsten, J.L., McIlrath, T.J. and Parkinson, W.H. 1974. J.Phys.B, 7, L244.

Colles, M.J., Pidgeon, C.R. and Smith, S.D. 1973. Phy.Bull. 24, 419.

Collins, C.B., Johnston, B.W. and Shaw, M.J. 1972a. J.Chem.Phys.57, 5310.

Collins, B.W. and Johnston, B.W. 1972b. J.Chem.Phys. 57, 5317.

Cooper, J. 1966. Repts.Prog.Phys. 29, 1, 40.

De Michelis, C. 1971. "A Survey of Organic Dye Laser Research" EUR-CEA-FC-617 Association Euratom 92 Fontenay-aux-Roses, France.

Demtröder, W. 1973. Phys.Rep. 7, 223.

Dennis, R.B., Pidgeon, C.R. and Smith, S.D. 1972. Proc.Roy.Soc. A331, 203.

Dewey, C.F. and Hocker, L.O. 1971. App.Phy.Lett. 18, 58.

Dicke, R.H. 1954. Phys.Rev. 93, 99.

Dienes, A., Ippen, E.P. and Shank, C.V. 1971. App.Phy.Lett. 19, 258.

Dimcock, D., Hinnov, E. and Johnson, L.C. 1969. Phy.Fluids, 12, 1730.

Drexhage, K.H. 1973. Laser Focus, 9, (3), 35.

Drexhage, K.H. 1974. Laser Focus, 10, (8), 18.

Dunning, F.B. and Stebbing, R.F. 1974. Phy.Rev.Lett. 32, 1286.

Evans, S.A. and Neal, F.L. 1969. Bull.Am.Phy.Soc. Series 11, 14, 262.

Ewansky, T.F., Wright, R.H. and Thessing, H.H. 1973. App.Phy.Lett.22, 250.

Felden, M.M. and Felden, M.A. 1972. Astrophy.J., 174 , 219.

Ferrar, C.M. 1969. Rev.Sci.Inst. 40, 1436.

Fielding, S.J. 1974. J.Phys.E. 7, 252.

Fite, W.L., Stebbing, R.F. and Brackman, R.T. 1959. Phy.Rev. 116, 356.

Fleming, R.J. and Higginson, G.S. 1964. Proc.Phy.Soc., 84, 531.

Fünfer, E., Kronast, B. and Kunze, H.J. 1963. Phy.Lett. 5, 125.

Furomoto, H.W. and Ceccon, H.L. 1969. App.Opt. 8, 1613.

Gabriel, A.H. and Heddle, D.W.O. 1960. Proc.Roy.Soc. 258, 124.

Gale, G.M. 1973. Opt.Comm. 7, 86.

Geltman, S. and Teague, M.R. 1974. J.Phys.B. 7, L22.

Gibson, A., Bickerton, R.J., Cole, H.C., Haegi, M., Reynolds, P., Sheffield, J., Speth, E. and Stott, P.E. 1973. Culham Report CLM-R122.

Gibson, A.J. and Sandford, M.C. 1972. Nature, 239, 511.

Griem, H.R. 1964. Plasma Spectroscopy, McGraw Hill.

Griem, H.R., Barranger, M., Kolb, A.C. and Oertel, G. 1962. Phy.Rev.125, 177.

Hanle, W. 1924. Z.Phy. 29, 93.

Hanna, D.C., Luther Davies, B. and Smith, R.C. 1973. App.Phy.Lett.22, 440.

Hansch. T.W.1972. Atomic Physics 3, 579. Ed. Smith, S.J. and Walters, G.K. Plenum Press.

Hansch, T.W., Shanin, I.S. and Schawlow, A.L. 1971. Phy.Rev.Lett. 27, 707.

Harris, S.E., Kung, A.H., Stappaerts, A.E. and Young, J.F. 1973. App.Phy.Lett. 23, 232.

Hill, R.A. 1964. JQSRT. 4, 857.

Hinnov, E. and Hirschberg, J.G. 1962. Phy.Rev. 125, 795.

Hirth, A., Vollrath, K. and Fouassien, J.P. 1973. Opt.Comm. 9, 139.

Hodgson, R.T., Sorokin, P.P. and Wynne, J.J. 1974. Phy.Rev.Lett. 32, 343.

Hodgson, R.T., Sorokin, P.P. and Wynne, J.J. 1974. Laser Focus, 10(3), 24.

Holritzer, J.F. and Schawlow, A.L. 1970. Anal.New York Acad.Sci., 168, 383.

Holstein, T. 1947. Phy.Rev. 72, 1212.

Holstein, T. 1951. Phy.Rev. 83, 1159.

Johnson, L.C. 1972. Astrophy.J. 174, 227.

Johnson, L.C. and Hinnov, E. 1973. JQSRT. 13, 333.

Kauppila, W.E., Ott, W.R. and Fite, W.L. 1970. Phy.Rev. A1, 1099.

Kuhl, J. and Spitschan, H. 1972. Opt.Comm. 5, 382.

Kunze, H.J. 1968. "Plasma Diagnostics". Ed. Lochte Holtgraven, P.550.

Lankard, J.R. and Von Gutfield, R.J. 1969. IEEEJ. of Quant.Elec. 5, 625.

Lees, J.H. 1932. Proc.Roy.Soc. 137, 173.

Lees, J.H. and Skinner, H.W.B. 1932. Proc.Roy.Soc. 137, 186.

Long, D.R. and Geballe, R. 1970. Phy.Rev. A1, 260.

Magyar, G. 1972. Opt.Comm. 6, 388.

Magyar, G. 1974. App.Opt. 13, 25.

Mahon, R. 1973. Ph.D. Thesis. Univ. of London.

Mahon, R., Lee, R.W. and Burgess, D.D. 1973. J.Phys.B. 6, 354.

Maier-Leibnitz, H. 1935. Z.Phy. 95, 499.

Marling, J.B., Hawley, J.G., Liston, E.M. and Grant, W.B. Oct. 1974. App.Opt. 13, 2317.

Martin, W.C. 1973. J.Phys.Chem.Ref.Data. 2, (2), 257.

Mathur, K.C. and Rudge, M.R.H. 1974. J.Phy.B., 7, 1033.

Maurer, W. and Wolf,R. 1934. Z.Phy. 92, 100.

(Wolf, R. and Maurer, W. 1940. Z.Phy. 115, 410.)

McDowell, M.R.C., Morgan, L.A. and Myerscough, V.P. 1973. J.Phy.B.6, 1435.

McIlrath, T.J. and Carlsten, J.L. 1972. Phy.Rev. A6, 1091.

McWhirter, R.W.P. 1965. Plasma Diagnostics Techniques, P.216. Ed. Huddlestone and Leonard.

Measures, R.M. 1968. J.App.Phy. 39, 5232.

Mitchell, A.G. and Zemansky, M.W. 1934. Resonance Radiation and Excited Atoms C.U.P.

Neynaber, R.H., Trujillo, S.M., Marino, L.L. and Rothe, E.W. 1964. Atomic Collision Processes. Ed. McDowell M.R.C. P.1089.

Oberoi, R.S. and Nesbet, R.K. 1973. Phy.Rev. A8, 2969.

Omvidar, K. 1965a. Phy.Rev. 140, A26.

Omvidar, K. 1965b. Phy.Rev. 140, A38.

Ott, W.R., Kauppila, W.E. and Fite, W.L. 1970. Phy.Rev. 1A, 1089.

Peacock, N.J., Robinson, D.C., Forrest, M.J., Wilcock, P.D. and Sannikov, V.V. 1969. Nature, 224, 488.

Peacock, N.J., Hobby, M.G. and Galanti, M. 1973. J.Phy.B. 6, L298.

Peterson, O.G., Tuccio, S.A. and Snavely, B.B. 1970. App.Phys.Lett. 17, 245.

Phelps, A.V. 1958. Phy.Rev. 110, 1363.

Roberts, D.E. 1973. J.Phys.B. 6, 929.

Rodrigo, A.B. and Measures, R.M. 1973. IEEJ of Quant.Elec. 9, 972.

Runze, K.P. 1971. Opt.Comm. 4, 195.

Saraph, H.E. 1964. Proc.Phy.Soc. 83, 763.

Schaefer, F.P. 1973. Dye Lasers. Springer Verlag.

Schaefer, F.P., Schmidt, W. and Volze, J. 1967. Phy.Lett. 24A, 280.

Schmidt, W., Schaefer, F.P. 1968. Phy.Lett. 26A, 558.

Schulz, G.J. and Fox, R.E. 1957. Phy.Rev. 106, 1179.

Sears, F.W. 1952. Thermodynamics. Addison Wesley.

Seaton, M.J. 1964. Planet Space Sci. 12, 55.

Seigman, A.E. 1971. An Introduction to Lasers and Masers. McGraw Hill.

Shanin, I.S. and Hansch, T.W. 1973. Opt.Comm. 8, 312.

Shearer-Izumi, W. and Botler, R. 1974. J.Phy.B. 7, L125.

Sheffield, J. 1972. Plasma Physics, 14, 385.

Snavely, B.B. 1969. Proc.I.E.E.E. 57, 1374.

Sobelman, I.I. 1972. An Introduction to the Theory of Atomic Spectra. Pergammon.

Sorokin, P.P. 1969. Sci.Am. 220, (2), 30.

Sorokin, P.P. and Lankard, J.R. 1966. IBM.J. of Res.Dev. 10, 162.

Sorokin, P.P., Lankard, J.R., Moruzzi, V.L. and Hammond, E.C. 1968. J.Chem.Phy. 48, 4726.

Teter, M.P. and Robertson, W.W. 1966. J.Chem.Phy. 45, 2167.

Thieme, O. 1932. Z.Phy. 78, 412.

Thomson, J.J. 1924. Phil.Mag. 47, 337.

Van Raan, A.F.J. and Heideman, H.G.M. 1974. J.Phy.B. 7, L216.

Vidal, C.R., Cooper, J. and Smith, E.W. 1973. Astrophy.J.Supp. No.214, 25, 37.

Vriens, L., Bonsen, T.F.M. and Smit, J.A. 1968. Physica. 40, 229.

Weise, W.L., Smith, M.W. and Glennon, B.M. 1966. Atomic Transition Probabilities. N.B.S.

Wellerstein, H.F. and Robertson, W.W. 1972a. J.Chem.Phy. 56, 1072.

Wellerstein, H.F. and Robertson, W.W. 1972b. J.Chem.Phy. 56, 1077.

Wellerstein, H.F. and Robertson, W.W. 1972c. J.Chem.Phy. 56, 1411.

Wheaton, J.E.G. 1964. App.Opt. 3, 1247.

Williams, J.F. and Willis, B.A. 1974. J.Phy.B. 7, L61.

Wilson, R. 1963. JQSRT. 2, 477.

Wolf, R. and Maurer, W. 1940. Z.Phy. 115, 410.

Woodgate, G.K. 1970. Elementary Atomic Structure. McGraw Hill.

Woolley, R.R. and Stibbs, D.W.N. 1953. The Outer Layers of a Star. P.61. Clarendon.

Yarborough, J.M. 1974. App.Phy.Lett. 24, 629.

J. Phys. B: Atom. Molec. Phys., Vol. 7, No. 9, 1974. Printed in Great Britain.

LETTER TO THE EDITOR

Dye laser induced fluorescence of plasmas and its application to measurement of lower state decay rates

D D Burgess and C H Skinner
Department of Physics, Imperial College, London SW7

Received 16 April 1974

Abstract. A simple but powerful extension of fluorescence scattering methods for the measurement of decay rates is described together with results of an experiment on a helium plasma. The technique should allow measurements of A-values and excitation rates for vacuum UV transitions from observations of visible fluorescence, and reduces the need for short pulse lasers for decay rate measurements.

The decay of fluorescence radiation has long been used to measure total decay rates whether collisional or radiative, for the upper state of the fluorescing transition and with the advent of high-power tuneable dye lasers such measurements have become possible on relatively hot, dense plasmas (eg Kunze and Burrell 1971). The classical use of fluorescence relies on a short excitation pulse, and therefore dye laser systems pumped by ruby, neodymium or N_2 lasers or mode-locked flash-lamp pumped dye lasers have attracted much attention. We wish to make the following simple, but powerful and previously unnoticed point. With laser powers exceeding those required to saturate the pumped transition, it is *unnecessary* to use a short pulse since decay rates can be deduced just as easily from the relaxation of the fluorescence *with the laser illumination still on* and, indeed, much more information is then obtained, since the fluorescence also yields the decay rate of the *lower* state of the pumped transition. The effects of illumination with a long laser pulse have been discussed explicitly but in the context of localized plasma diagnostics by Measures (1968), and relaxation effects under laser illumination have been observed by Collins *et al* (1972). Our very simple mathematical derivation below yields the same form of fluorescence pulse as derived by Measures. However, as far as we can ascertain, no discussion of the use and advantages of this technique for determination of *atomic* parameters, as opposed to localized plasma diagnostics, has been given previously, the most important consequence being the possibility of applying *lower* state decay measurements from visible fluorescence to the determination of atomic parameters for vacuum UV transitions.

Consider the following very simple model. Let the laser illumination correspond to a transition between two levels 1 and 2, with populations small enough that the fluorescence process does not materially alter the populations of all the other levels in the system from which these two states are populated. Let the laser illumination be turned on at time $t = 0$, and instantaneously rise to a value sufficient to saturate the transition (ie such that the ratio of the two level populations become essentially the ratios of their statistical weights). Note that this does not require a very carefully shaped laser pulse, since provided the saturation intensity is reached rapidly, further variations in intensity

do not alter the relative populations of the two levels concerned. Note also one important distinction from other pulse-excitation methods, whether optical, beam-foil, or otherwise in that, so long as the laser remains on, excitation and decay rates directly between the levels 1 and 2 themselves do not enter the analysis, thus simplifying interpretative problems. Let now the rate at which level 1 is populated from all other levels in the plasma except level 2 be C_1 and the corresponding decay rate (per atom) be D_1, and similarly the corresponding rates for level 2 by C_2 and D_2. Let the level populations before the laser is turned on be n_{10} and n_{20}. Then consider the equilibrium situation under laser illumination for the *joint* system of the two levels 1 and 2.

$$t < 0 \qquad C_1 + C_2 = n_{10}D_1 + n_{20}D_2 \tag{1}$$

$$t > 0 \qquad n_1(t) = \frac{g_1}{g_2} n_2(t) \tag{2}$$

$$n_1(t) + n_2(t) = n^+(t)$$

$$\frac{\mathrm{d}n^+}{\mathrm{d}t} = (C_1 + C_2) - n_1 D_1 - n_2 D_2$$

$$n^+(0) = n_{10} + n_{20}.$$

Thus, the equation governing the population of the upper level, and hence the observed fluorescence intensity is

$$\frac{\mathrm{d}n_2(t)}{\mathrm{d}t}\left(1 + \frac{g_1}{g_2}\right) = (C_1 + C_2) - n_2\left(\frac{g_1}{g_2}D_1 + D_2\right) \tag{3}$$

with the solution

$$n_2(t) = \left(\frac{n_{10} + n_{20}}{1 + g_1/g_2} - \frac{C_1 + C_2}{g_1/g_2 D_1 + D_2}\right) \exp\left[-\left(\frac{g_1/g_2 D_1 + D_2}{1 + g_1/g_2}\right)t\right] + \frac{C_1 + C_2}{g_1/g_2 D_1 + D_2}. \tag{4}$$

Hence the fluorescence has two possible forms. Either the intensity rises very rapidly from the initial background level corresponding to n_{20} to a peak value and then decays exponentially with a time constant determined by both D_1 and D_2, levelling out at a new steady (enhanced) value for as long as the laser remains on, or if the sign of the first term in (4) is appropriate after the initial rapid rise the fluorescent intensity continues rising to a new equilibrium plateau value. In either case the following information is available from a single time-history of the fluorescence. The height of the initial spike against the background level gives the ratio of the initial populations, n_{20}/n_{10}. The exponential decay gives the combined decay rates of the two levels, weighted by their statistical weights, since with the laser still on decays out of one level affect the population of the other level. The final equilibrium plateau gives the ratio of the decay rates determined from the exponential decay to $(C_1 + C_2)/n_{20}$. Combination of these values with the initial equilibrium equation (1) then yields *separately* D_1, D_2, n_{20}/n_{10} and $(C_1 + C_2)/n_{20}$.

The major difference with established fluorescence decay techniques is the presence of the lower state decay rate, combined with the removal of effects of decays of level 2 due to transitions down to level 1. In many cases it should be possible to determine eg the A-values of a vacuum UV resonance line, for instance of a high ionization stage in a coronal plasma, by pumping on a visible transition out of the first excited state and thus determining D_1. The method would have the advantage over eg beam-foil spectroscopy

of greatly reduced problems due to cascades. Note also that previous plasma measurements have not permitted the determination of A-values as opposed to collisional excitation rates for high ionization states (for which coronal equilibrium normally applies). Conversely, the technique allows determination of collisional de-excitation rates from first excited states to ground in high-density LTE plasmas where spectroscopic measurements normally yield only A-values. The technique also provides information on collisional excitation rates via $C_1 + C_2$.

We have observed such relaxation effects during long-pulse laser illumination. The experiment used a recombination plasma source much-discussed previously (eg Burgess and Cairns 1970, 1971, Burgess and Mahon 1972, Mahon *et al* 1973). The electron density n_e, and temperature T_e, are extremely accurately known both from the measurements in the papers cited and now from spatially-resolved Thomson scattering measurements along the discharge axis (Mahon R, *PhD thesis*, University of London 1973 and Smith C, unpublished), the Thomson scattering data confirming all original conclusions about n_e, T_e and the plasma homogeneity. For the present experiments the optics developed for the Thomson scattering measurement were used, giving a very low stray light level. A co-axial flash-lamp pumped dye laser similar in general design to that of Furamoto and Ceccon (1969), but made to be fully demountable, provided a peak power of up to 1 MW in a 2·2 Å bandwidth centred on the 5876 Å He I 2^3P–3^3D transition, the laser operating on a solution of rhodamine 6G in alcohol. The peak illumination in the plasma was 30 kilowatts cm^{-2}, and the shot-to-shot reproducibility of the laser was excellent ($\pm 5\%$). The fluorescence produced from the plasma in a direction at right angles to that of illumination was observed using a monospek 1000 monochromator and an RCA C31034 quantacon photomultiplier. Figure 1 shows (i) the laser pulse, (ii) the fluorescence produced and (iii) the background emission level. Under these conditions the laser pulse is a modest approximation to a step function, saturation being reached within a few nanoseconds of the laser firing and this illumination retained for about 300 nanoseconds. As can be seen, the fluorescence pulse observed

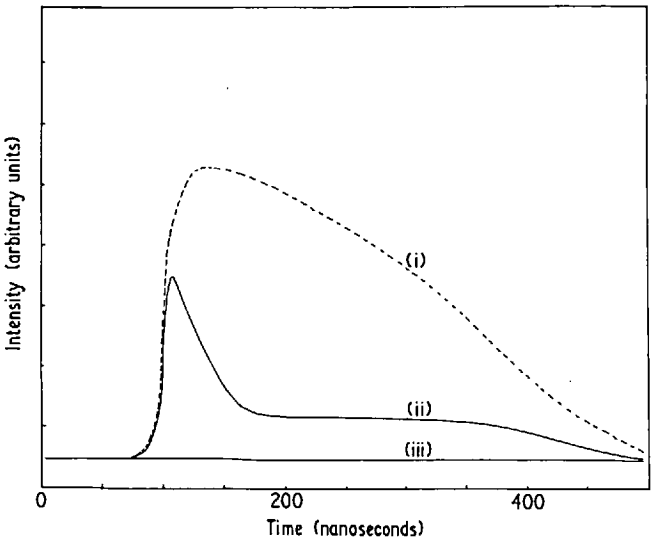

Figure 1. Time histories of (i) the laser intensity (broken line), (ii) the observed fluorescence, and (iii) the plasma emission without laser excitation.

behaves essentially as predicted from equation (4) above. The density dependence of the decay was investigated by varying the delay of laser-firing between about 20–100 microseconds after plasma formation, corresponding to $5\times10^{15}\ \mathrm{cm}^{-3} > n_e > 10^{14}\ \mathrm{cm}^{-3}$. The decay constant observed proved to be essentially proportional to n_e. Experiments at much reduced laser power showed a fluorescence pulse simply following the form of the laser illumination, as expected. Observations of 'sensitized fluorescence' on other He I transitions whilst pumping on 5876 Å showed signals of identical form for all transitions to $n = 2$ (singlets and triplets) from $n = 3$ and $n = 4$ but no observable signal for $n = 5$ or higher transitions. The identity of these time histories demonstrated that the decay of the observed fluorescence was not due simply to collisional transitions out of 3^3D to other nearby levels, since relaxation times for these processes are much faster, as expected from theoretical estimates and from observed pressure-broadened line widths. The dependence of the decay rate on n_e is shown in figure 2. Error bars became large at high density, when the decay time is extremely short and comparable to the rise time of the laser illumination, and at low densities when the decay time is comparable to the length of the available laser pulse. The decay observed is much too long to be due to radiative depopulation of the $n = 3$ levels (in collisional equilibrium with 3^3D). This is not surprising since in the pure helium plasma resonance lines are very optically thick, and the corresponding radiative contributions to D_1 and D_2 thereby greatly reduced. However the 2^1P–3^1D transition was expected from other data to be optically thin. Investigations of the optical depth of this transition during laser illumination are now under way. A tentative analysis suggests that the levels with $n = 3$ and those with $n = 2$ are so tightly coupled by collisions as to behave as a single pair of levels and that the decay constant involved in the relaxation of the fluorescence is possibly collisional de-excitation of levels of $n = 2$ to ground.

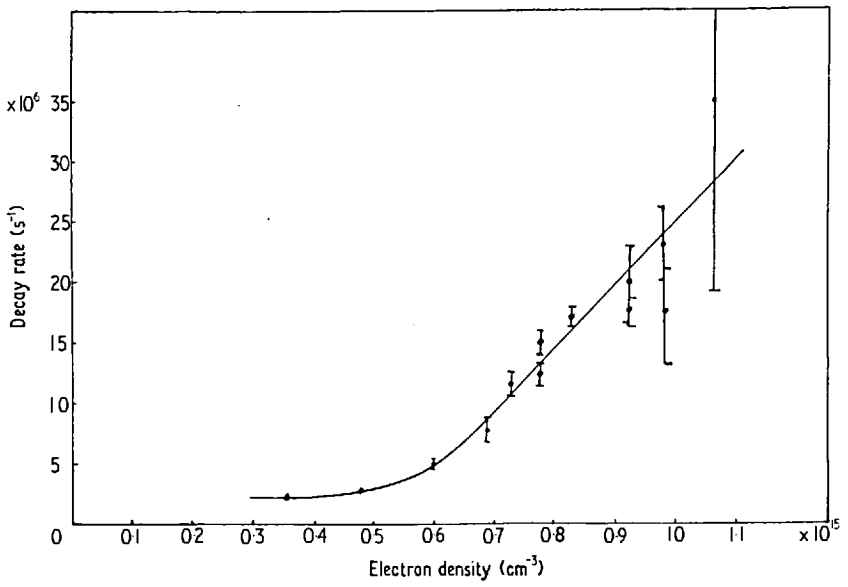

Figure 2. Fluorescence decay rate. Based on Thomson scattering electron densities measurements to be compared with collision rate based on line width = $10^{10}\ \mathrm{s}^{-1}$. Radiative transition probability $70\times10^6\ \mathrm{s}^{-1}$.

Detailed analysis of the helium results will be reported in a forthcoming paper, and studies of the relaxation under long-laser pulse illumination for the Hα transition are also under way. However, whilst the particular case of He I 5876 is complex, in simpler systems it is clear that measurements of lower state decay rates should allow many interesting determinations of parameters for vacuum ultra-violet resonance lines without the need for absolute intensity calibration in the VUV region. An interesting prospect seems to be that of pumping 2^1S to 2^1P transitions in helium-like ions in coronal plasmas, thus obtaining information on the 1^1S to 2^1P A-value, and on the 1^1S–2^1S collisional excitation rate, and a new method of measuring fast decay rates in such experiments is being studied. What is already clear is that once power levels above saturation are available, in many cases it may be disadvantageous to use short or ultra-short pulses for fluorescence experiments and better to use pulses with lengths *exceeding* decay times of interest.

The experimental work described was partially supported under the terms of a contract from UKAEA Culham Laboratory.

References

Burrell C F, Kunze H J 1972 *Phys. Rev. Lett.* **28** 1–4
Burgess D D, Cairns C J 1970 *J. Phys.* B: *Atom. molec. Phys.* **3** L67–70
—— 1971 *J. Phys.* B: *Atom. molec. Phys.* **4** 1364–76
Burgess D D, Mahon R 1972 *J. Phys.* B: *Atom. molec. Phys.* **5** 1756–61
Collins C B, Johnson B W 1972 *J. chem. Phys.* **57** 5317–21
Mahon R, Lee R W and Burgess D D 1973 *J. Phys.* B: *Atom. molec. Phys.* **6** 354–63
Measures R M 1968 *J. appl. Phys.* **39** 5232–45